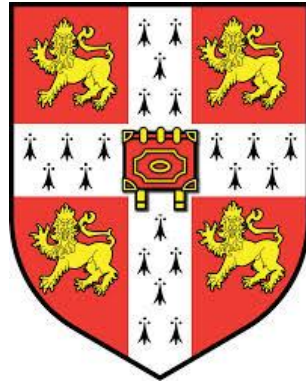


# **THE USE OF REDUCED-MODERATION LIGHT WATER REACTORS FOR TRANSURANIC ISOTOPE BURNING IN THORIUM FUEL**

Benjamin Andrew Lindley



St Catharine's College  
Department of Engineering  
University of Cambridge

A thesis submitted to the University of Cambridge for the degree of Doctor  
of Philosophy

November 2014

*To my family*

## **Declaration**

No component of this thesis has nor will be submitted by myself or any other individual for admission to any other degree. This thesis is primarily my work as an individual research project. However, it contains several contributions from collaborators which are clearly indicated in the text. Any reference to the work of others is clearly indicated in the text.

This thesis contains a total of 71 489 words and 93 figures. Prior permission has been received for a 10% word limit extension, and therefore this thesis does not exceed the limits prescribed by the Degree Committee for the Faculty of Engineering as stated in the Memorandum to Graduate Students.

Benjamin Andrew Lindley

## **The Use of Reduced-moderation Light Water Reactors for Transuranic Isotope Burning in Thorium Fuel**

B. A. Lindley

Light water reactors (LWRs) are the world's dominant nuclear reactor system. Uranium (U)-fuelled LWRs produce long-lived transuranic (TRU) isotopes. TRUs can be recycled in LWRs or fast reactors. The thermal neutron spectrum in LWRs is less suitable for burning TRUs as this causes a build-up of TRU isotopes with low fission probability. This increases the fissile feed requirements, which tends to result in a positive void coefficient (VC) and hence the reactor is unsafe to operate. Use of reduced-moderation LWRs can improve TRU transmutation performance, but the VC is still severely limiting for these designs. Reduced-moderation pressurized water reactors (RMPWRs) and boiling water reactors (RBWRs) are considered in this study.

Using thorium (Th) instead of U as the fertile fuel component can greatly improve the VC. However, Th-based transmutation is a much less developed technology than U-based transmutation. In this thesis, the feasibility and fuel cycle performance of full TRU recycle in Th-fuelled RMPWRs and RBWRs are evaluated. Neutronic performance is greatly improved by spatial separation of TRU and  $^{233-6}\text{U}$ , primarily implemented here using heterogeneous RMPWR and RBWR assembly designs.

In a RMPWR, the water to fuel ratio must be reduced to around 50% of the normal value to allow full actinide recycle. If implemented by retrofitting an existing PWR, steady-state thermal-hydraulic constraints can still be satisfied. However, in a large break loss-of-coolant accident, the emergency core cooling system may not be able to provide water to the core quickly enough to prevent fuel cladding failure. A discharge burn-up of ~40 GWd/t is possible in RMPWRs. Reactivity control is a challenge due to the reduced worth of neutron absorbers in the hard neutron spectrum, and their detrimental effect on the VC, especially when diluted, as for soluble boron. Control rods are instead used to control the core. It appears possible to achieve adequate power peaking, shutdown margin and rod-ejection accident response.

In RBWRs, it appears neutronicly feasible to achieve very high burn-ups (~120 GWd/t) but the maximum achievable incineration rate is less than in RMPWRs. The reprocessing and fuel fabrication requirements of RBWRs are less than RMPWRs but more than fast reactors. A two-stage TRU burning cycle, where the first stage is Th-Pu MOX in a conventional PWR feeding a second stage continuous burn in a RBWR, is technically reasonable. It is possible to limit the core area to that of an ABWR with acceptable thermal-hydraulic performance. In this case, it appears that RBWRs are of similar cost to inert matrix incineration in LWRs, and lower cost than RMPWRs and Th- and U-based fast reactor recycle schemes.

## **Acknowledgements**

I am particularly grateful to my PhD supervisor Dr Geoff Parks for his constant support and encouragement, detailed feedback and enthusiasm for this project. I have also received much advice from Prof. William Nuttall, Tony Roulstone and Dr Eugene Shwageraus at Cambridge, and am also grateful for all the help and discussion from my colleagues, notably: Dr Ali Ahmad, Dr Stephen Ashley, Dr David Coates, Andrew Flintham and, in particular, Zara Zainuddin for her help with full-core modelling of PWRs.

My particular thanks must also go to Dr Fausto Franceschini of Westinghouse Electric Company, LLC. He has been a great source of advice, direction and information across a range of topics. Dr Paolo Ferroni and Prof. Edward Lahoda of Westinghouse have also provided invaluable advice on thermal-hydraulics and fuel fabrication respectively.

I am very grateful to Dr Julian Kelly and his colleagues at Thor Energy for supporting collaborative work with Westinghouse and many other helpful discussions and useful ideas. I would also like to thank Prof. Thomas J. Downar and his group at the University of Michigan (in particular, Andrew Hall) for hosting me as a visiting student and helping me model the RBWR. Without them, this would not have been possible.

I am extremely grateful to Prof. Paul Smith and the rest of the ANSWERS team at AMEC for providing access to and extensive guidance on the use of WIMS, MONK and FISPIN. WIMS in particular has proved absolutely integral to performing the analyses in this thesis. I am also grateful to Dr Paul Bryce of EDF Energy for providing advice on using PANTHER and guidance on PWR core analysis. I would also like to thank EDF Energy for providing access to PANTHER.

I would like to thank: the EPSRC for funding this research; the Institution of Mechanical Engineers for awarding me with a postgraduate scholarship; and the Roy G Post foundation for their award of a scholarship related to the Waste Management Conference in Phoenix.

I have had numerous helpful discussions and collaborations with many others over the past 3 years, in many cases indicated in the text. These include: Dr Matthew Eaton and his colleagues at Imperial College London; Robert Gregg and his colleagues at NNL; and Dr Carlo Fiorina, now of PSI.

On a personal note, I would like to thank my awesome Mum & Dad for always being there for me. I'd also like to thank my lovely wife Ting-Ray for putting up with my constant ramblings about void coefficients and always brightening my day, and our amazing baby daughter Amy who always provides a welcome distraction from working (eating, sleeping...). I am extremely grateful to my Mum & Dad in-law for their incredible support of our young family. Since I've acknowledged just about every person I can think of, I should probably also acknowledge May (the dog).

## **Contents**

<b>List of Abbreviations</b>	<b>3</b>
<b>Chapter 1 – Introduction</b>	<b>6</b>
1.1. The Nuclear Fuel Cycle	6
1.2. Plutonium and TRU Recycling Options	9
1.3. Thorium	16
1.4. Reprocessing	21
1.5. Thesis Motivation and Objectives	22
1.6. Thesis Organisation	24
<b>Chapter 2 – Assembly Analysis</b>	<b>25</b>
2.1. Rationale	25
2.2. Fuel Cycle Schemes	27
2.3. Lattice Calculations	29
2.4. Results	44
2.5. Concluding Remarks	57
<b>Chapter 3 – Void Reactivity Feedback Analysis</b>	<b>58</b>
3.1. Introduction	58
3.2. Method	58
3.3. Results	61
3.4. Discussion	67
3.5. Heterogeneous Recycle	71
3.6. Concluding Remarks	78
<b>Chapter 4 – Thermal-hydraulic Study of RMPWRs</b>	<b>79</b>
4.1. Introduction	79
4.2. Analysis	80
4.3. Concluding Remarks	101
<b>Chapter 5 – RMPWR Full-core Analysis</b>	<b>102</b>
5.1. In-core Fuel Management	102
5.2. Core Analysis	117
5.3. Rod Ejection Accident Analysis	133
5.4. Concluding Remarks	142
<b>Chapter 6 – RBWR Full-core Analysis</b>	<b>144</b>
6.1. Full-core Analysis of RBWR with Homogeneous Fuel	144
6.2. Radially Heterogeneous Fuel in RBWRs	152

6.3. Implementation of a Multi-tier Fuel Cycle in RBWRs	156
6.4. Variable Pin Diameter Fuel	158
6.5. Cold Shutdown Margin	161
6.6. Preliminary Assessment of Axially Heterogeneous Fuel	162
6.7. Concluding Remarks	169
<b>Chapter 7 – Fuel Cycle Performance</b>	<b>171</b>
7.1. Description of Fuel Cycle Cases	171
7.2. Fuel Cycle Performance	179
7.3. Comparison with Other Incineration Schemes	186
7.4. Economics	189
7.5. Repository Radiotoxicity and Decay Heat	191
7.6. Decay Heat and Radiation Field Affecting Fuel Fabrication	194
7.7. Concluding Remarks	198
<b>Chapter 8 – Conclusions</b>	<b>200</b>
8.1. Recommendations for Future Work	203
<b>References</b>	<b>206</b>

## List of Abbreviations

Elements are commonly abbreviated to their symbols (e.g. Th = thorium)

ABWR	Advanced boiling water reactor
ADSR	Accelerator-driven subcritical reactor
AFF	Axial form factor
AGR	Advanced gas-cooled reactor
AHWR	Advanced heavy water reactor
APA	Advanced plutonium assembly
BP	Burnable poison
BWR	Boiling water reactor
CHF	Critical heat flux
CR	Conversion ratio
CRP	Control rod program
CSDM	Cold shutdown margin
DC	Doppler coefficient
DDH	Dalle Donne-Hame
DNB	Departure from nucleate boiling
DNF	Delayed neutron fraction
EOC	End of cycle
EPR	European Pressurized Reactor
Eta	Ratio of neutron productions to absorptions (see also $\eta$ )
FdH	Normalized hot pin rise in enthalpy (see also $F\Delta H$ )
FLWR	Flexible light water reactor
FP	Fission product
FR	Fast reactor
FVR	Fully voided reactivity – reactivity when core is filled with saturated steam
GFR	Gas-cooled fast reactor
H/HM	Hydrogen to heavy metal [ratio]
HC	High conversion
HFP	Hot full power
HWR	Heavy water reactor
HZP	Hot zero power
JAEA	Japanese Atomic Energy Agency
LBLOCA	Large-break loss-of-coolant accident
LEU	Low enriched uranium

LOCA	Loss-of-coolant accident
LP	Loading pattern
LWR	Light water reactor
MA	Minor actinides (Pa, Np, Am, Cm, Cf – sometimes a relevant subset is specified)
MCPR	Minimum critical power ratio
MDC	Moderator density coefficient
MDNBR	Minimum departure from nuclear boiling ratio
MOX	Mixed oxide fuel
MSR	Molten salt reactor
MT	Multi-tier
MTC	Moderator temperature coefficient
NNL	The UK National Nuclear Laboratory
OD	Outer diameter
O&M	Operations & Maintenance
PWR	Pressurised water reactor
RBWR	Reduced-moderation boiling water reactor
RCCA	Rod cluster control assembly
RCP	Reactor coolant pump
REA	Rod ejection accident
RFF	Radial form factor
RIA	Reactivity initiated accident
RM	Reduced-moderation
RMPWR	Reduced-moderation pressurised water reactor
RMWR	Reduced-moderation water reactor
SCWR	Supercritical water reactor
SDM	Shutdown margin
SFR	Sodium-cooled fast reactor
SN	Spontaneous neutron
SOC	Start of cycle
ST	Single-tier
TCUP	Heterogeneous assembly design with Th-TRU at Centre and Th-U3 at Periphery
TD	Theoretical density; e.g. 85% TD means ‘fuel with a density of 85% of theoretical’
tiHM	Tonnes initial heavy metal
TPUC	Heterogeneous assembly design with Th-TRU at Periphery and Th-U3 at Centre
TRU	Transuranic

UNF	Used nuclear fuel
U3	U bred from Th, i.e. $^{233-236}\text{U}$
VC	Void coefficient
VF	Void fraction
VHTR	Very high temperature reactor
WABA	Wet annular burnable absorber
WATU	LWR loading scheme with Whole Assembly heterogeneity of Th-TRU and Th-U3
ZCR	Zero coolant reactivity – reactivity when coolant density is set to zero

### **List of Symbols**

Where not defined, symbols adhere to standard mathematical notation. Symbols used exclusively in derivations are defined in the text and are not reproduced here.

$A$	Absorptions
$D$	Pin diameter
$F\Delta H$	Normalized hot pin rise in enthalpy (see also FdH)
$H$	Wire-wrap pitch
$k$	Neutron multiplication factor
$k_{\text{eff}}$	Effective neutron multiplication factor (including leakage)
$k_{\infty}$	Infinite neutron multiplication factor
$P$	Productions
$T_{\text{in}}$	Core inlet temperature
$T_{\text{out}}$	Core outlet temperature
$\beta_{\text{eff}}$	Effective delayed neutron fraction
$\eta$	Ratio of neutron productions to absorptions (see also eta)
$\rho$	Reactivity (except Chapter 4: where it is coolant density)
$\rho_d$	Coolant density (Chapter 3)

## **Chapter 1 – Introduction**

Extensive research has been performed on transuranic (TRU) transmutation and full actinide recycle across a range of candidate fuel cycles and reactor platforms. In this thesis, conventional light water reactors (LWRs) are preferred as they are cheaper, lower risk and the technology already exists. TRU recycle in LWRs is limited by the moderator temperature coefficient (MTC) and/or void coefficient (VC), although feasibility is improved by using reduced-moderation LWRs. The thorium (Th) fuel cycle is chosen as it has superior MTC/VC performance. This introduces additional fuel fabrication and reprocessing challenges, but full recycle of TRU is, in any case, expensive and requires the development of new technology. While some studies of closed Th-TRU cycles in LWRs have been performed, these are mostly limited to single assembly analyses and/or do not consider full TRU recycle. This thesis presents a more comprehensive analysis of the design, operation and fuel cycle of Th-TRU-fuelled LWRs operating with full actinide recycle.

### **1.1. The Nuclear Fuel Cycle**

The overwhelming majority of operating nuclear power plants use uranium (U) fuel. In most reactors, this is enriched to increase the proportion of fissile  $^{235}\text{U}$  in the fuel to produce low enriched uranium (LEU). Thermal reactors are used, which employ a moderator to slow down the neutrons from ‘fast’ to ‘thermal’ energies, at which the fission cross-section of  $^{235}\text{U}$  is larger. Most reactors use water as a moderator – these are LWRs and comprise Pressurized Water Reactors (PWRs) and Boiling Water Reactors (BWRs). Graphite and heavy water are also used as moderators, notably in Advanced Gas-cooled Reactors (AGRs) and CANDU reactors respectively.

At the end of the fuel cycle, the spent fuel may be disposed directly, or it can be reprocessed to separate depleted U, TRU waste and fission products (FPs). FPs are highly radioactive, but only take around 1000 years to decay to safe levels. TRU waste takes around 100 000 years to decay to safe levels, and therefore requires a geological storage repository. Depleted U is much less radioactive. The TRU waste is mostly plutonium (Pu) and also contains americium (Am), curium (Cm), neptunium (Np) and a tiny quantity of californium (Cf), which are collectively referred to as minor actinides (MAs). The Pu is by far the most significant contributor to radiotoxicity in the actinide waste (e.g. see (Salvatores, 2005)).

The Pu can be reused in mixed oxide fuel (MOX), but only part of the waste is incinerated. Even if this is done, only a small proportion of the available energy in the U is converted into power. The importance of using fuel efficiently is debatable as U is currently relatively cheap, and while the sustainability of U resources is contested, reserves are judged to be sufficient in the medium term (Bunn et al., 2003; Kazimi et al., 2010; WNA, 2011).

Approaching 100% of the energy can be extracted from U by retaining all actinides within the fuel cycle in a 'breeder' reactor. All actinides have a finite fission probability, and will fission or absorb a neutron or decay into a daughter isotope. Therefore by continued presence in the reactor, virtually all actinide nuclei will ultimately fission and provide energy. The relative probability of fission to capture of most isotopes is greater at higher neutron energies and therefore fast reactors (FRs) are usually favoured for this strategy (e.g. see (Rubbia et al., 1995)). FRs are therefore seen as being the best long-term option due to their vastly improved fuel utilization (OECD, 2003; ANS, 2005). This fuel cycle can be described as 'self-sustaining' as it can be fuelled using natural or depleted U, or Th (Fig. 1.1).

A breeder reactor operating a closed fuel cycle produces very little actinide waste. Some breeder concepts recycle Pu and not MAs, and therefore still produce some actinide waste despite greatly improving the nuclear fuel efficiency. For example, France currently recycles Pu in MOX (IAEA, 2005a) and envisages full recycle in FRs (Behar, 2013), with the potential for MA recycle dependent on feasibility and economics (Rouault et al., 2009).

Alternatively, it is possible to pursue a strategy of full actinide recycle, without full utilization of U. This strategy is motivated by a cheap source of U, and an environmental, political and/or economic incentive to limit high level nuclear waste storage time and repository size (OECD, 2002). The TRU from a conventional fleet of LEU-fuelled LWRs is burned in a fleet of incinerators. It is typically desired to limit the number of incinerator reactors required, as they are assumed to be more expensive than the LWRs (OECD, 2002). It is also desirable to limit the amount of fuel reprocessing required. FRs are typically also preferred for this strategy, again because the TRU is more fissile at fast neutron energies.

While greatly increasing the size and required life-time of a high level waste/used nuclear fuel disposal facility, a once-through nuclear fuel cycle is cheaper than full actinide recycle strategies, due to the high cost of reprocessing (OECD, 1994) and the need to fabricate recycled fuel, which is highly radioactive, remotely (Franceschini et al., 2012), which increases the fuel fabrication cost (Sease et al., 1966). This has led many countries to pursue direct disposal of nuclear fuel assemblies in preference to recycle strategies. In particular, this strategy is often favoured in countries with large areas of disused land – e.g. Finland and Sweden (Rempe, 2007).

In the UK, nuclear fuel was reprocessed as the precursor to a FR programme, which was ultimately not implemented. This has led to the production of a large stockpile of separated Pu (DECC, 2011). Disposal of this stockpile is complicated by proliferation concerns, as the Pu is fissile and is therefore a potential weapons risk (DECC, 2011). The currently favoured strategy is to implement one or more passes of the Pu through an LWR as MOX fuel, such that the fissile quality of the Pu is

reduced and it is mixed with U and fission products, which form proliferation barriers (King, 2011). Similarly, Pu from decommissioned nuclear warheads can be disposed of using MOX fuel (NNSA, 2011).

Some different fuel cycle concepts are summarized in Fig. 1.1.

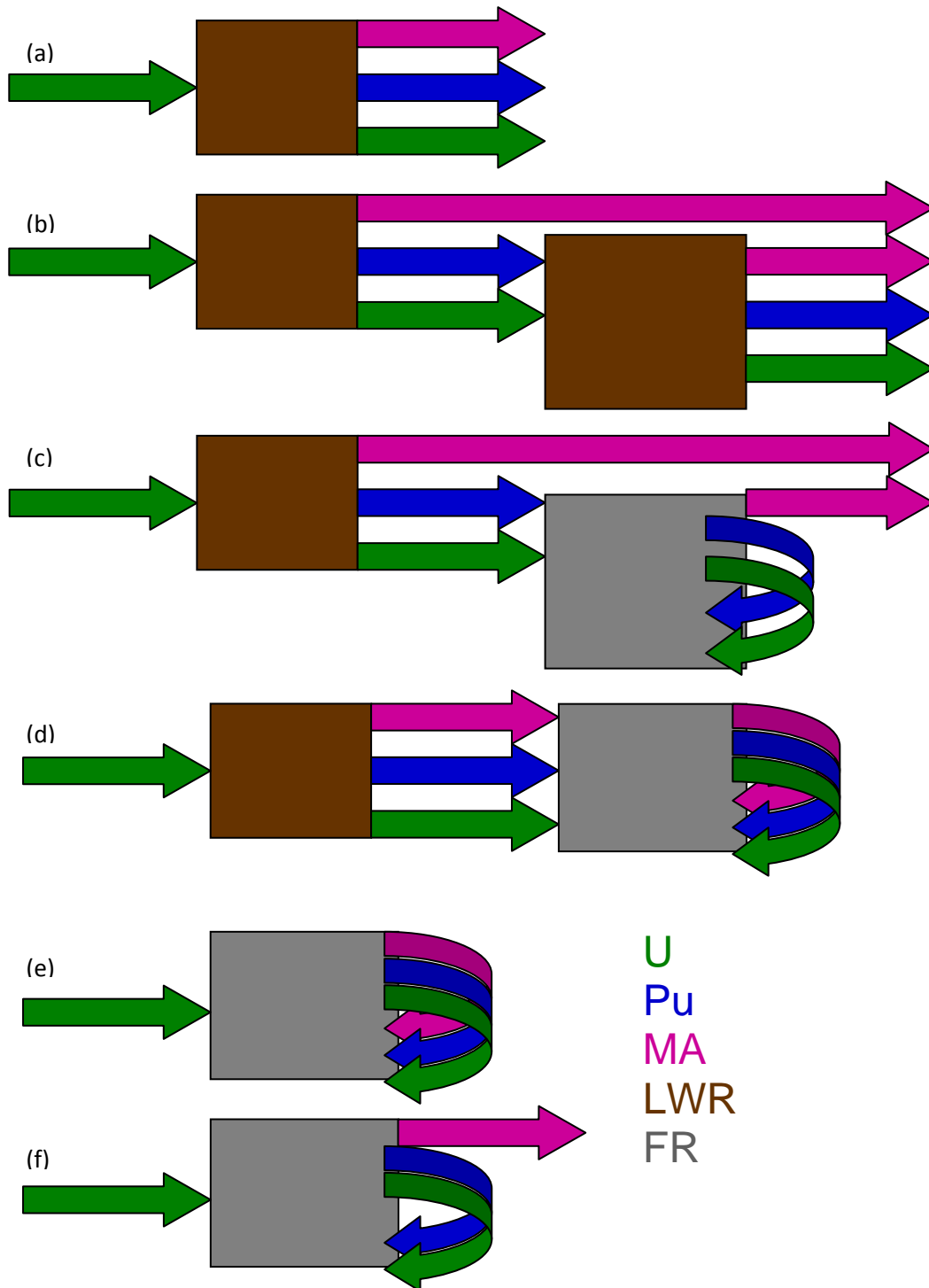


**Fig. 1.1** Fuel cycle concepts: (a) Once-through LWR; (b) LWR then single Pu pass in LWR; (c) LWR then Pu recycle in FR; (d) LWR then full recycle in FR; (e) Full recycle in self-sustaining FR; (f) Pu recycle in self-sustaining FR

*The motivation for this thesis is the TRU waste incineration problem, with the aim of reducing high level waste volume and storage time.* An increase in U utilization efficiency is not considered as an objective. The approach to managing the separated Pu stockpile in the UK is of particular interest.

## **1.2. Plutonium and TRU Recycling Options**

### **1.2.1. Overview**

Recycling of Pu and TRU has been extensively researched in a range of reactor systems. These include FRs (typically liquid-metal cooled), molten salt reactors (MSRs), LWRs, heavy-water-cooled reactors, accelerator-driven subcritical reactors and graphite-moderated reactors. The characteristics and objectives of different schemes vary between full and partial recycle (e.g. a single pass through the reactor), and between maximising TRU destruction rates to achieving a self-sustaining fuel cycle. TRU recycle schemes typically envisage decades to centuries of operation and require extensive research and development, so a significant long-term commitment is required to implement a meaningful strategy.

### **1.2.2. FRs and MSRs**

OECD (2002) contained a detailed comparison of thermal and fast transmutation strategies using the same analysis framework. Low reprocessing losses were identified as crucial to reducing radiotoxicity and it was acknowledged that significant R&D work is required.

Full TRU recycle is generally considered to require an FR. Sodium-cooled FRs (SFRs) are most commonly considered. Other liquid metal coolants, notably Pb, Pb-Bi and Na-K have been considered or proposed. Gas-cooled fast reactors (GFRs) are also being studied (e.g. Hejzlar et al., 2009). Fast-spectrum designs of the MSR (i.e. without a graphite moderator) are also gaining increased interest because of their favourable closed fuel cycle performance. MSR designs have been proposed with no fertile isotope, leading to rapid TRU destruction (e.g. Ignatiev et al., 2007). This is possible because heating of the fuel salt leads to voiding of the fuel and therefore increased leakage, so a fertile isotope is not necessary to ensure negative reactivity feedback.

From a reactor physics perspective, it is feasible to recycle all actinides in a fast-spectrum reactor. This has been confirmed in multiple studies (e.g. Kim et al., 2009). Most actinides have higher  $\eta$  (ratio of neutron productions to absorptions) in the fast spectrum, which directly improves neutron economy and reduces build-up of MAs.

In LWRs, it is necessary for the MTC and/or VC to be negative at nominal power to ensure safe operation (Westinghouse Electric Company LLC, 2009). In sodium-cooled FRs, the VC can be positive due to the other reactivity effects ensuring overall passive feedback (Hill, 2007), although

this is not desirable. With a complicated core design, it is possible to keep the VC negative (Devictor et al., 2012). In GFRs, it is desirable to keep the VC negative, which can be accomplished by reducing the coolant volume fraction and adding BeO (a moderator) to the fuel (Pope et al., 2009).

There are practical challenges in the implementation of all of the FR concepts which could delay their deployment even in the case of sizable investment. For example, the chemical reactivity of Na with air and water is a significant safety challenge for SFRs (Denman et al., 2012), while Pb, Pb-Bi (e.g. Zhang, 2009) and molten salt (Abram and Ion, 2008) coolants present corrosion problems. GFRs experience high temperatures and have lower thermal inertia than graphite-moderated gas-cooled reactors, making it difficult to cool the core in the event of a loss-of-coolant accident (LOCA) (Pope et al., 2009; Abram and Ion, 2008). Conversely, it is also claimed that FR concepts can result in various safety advantages over LWRs (Wade et al., 1997).

The SFR is the most advanced FR concept with prototype and demonstration reactors currently or previously operated in many countries (IAEA, 2006). GE Hitachi advocate a SFR (PRISM) to perform a single Pu recycle in the UK to address the proliferation concerns associated with the separated Pu stockpile, but this also provides the capability for complete actinide recycle (GE, 2011).

### ***1.2.3. Accelerator-driven Systems***

Accelerator-driven subcritical reactors (ADSRs), where the reaction is sustained by an external neutron source, are sometimes claimed to improve FR safety and neutron economy (Nifenecker et al., 2001). ADSRs have been proposed as part of Pu + MA (Rubbia et al., 1995) and dedicated MA (OECD, 2002) recycle schemes. In the latter case, subcritical operation may allow the use of fuels with poor neutron economy and otherwise unacceptable kinetic behaviour and fuel and coolant reactivity feedback coefficients. The principal disadvantage of an ADSR is the high cost of building and operating an accelerator (Cardin et al., 2011), especially given the necessity of high accelerator reliability to limit clad fatigue (Ahmad et al., 2012). The technology also requires significant further research and is unsuitable for implementation in the medium term. ADSRs have also been proposed as a means of improving the neutron economy in thermal reactor systems which may be otherwise unsuitable for TRU incineration (Coates and Parks, 2011).

### ***1.2.4. LWRs***

A comprehensive report on Pu recycling options was performed by (OECD, 2003). Multiple recycle of LWR MOX was considered to lead to impractically high Pu enrichments after multiple recycles and the build-up of MAs with high radiotoxicity was also highlighted as a problem. This report was

generally favourable to the long-term deployment of FRs: the report covers the period “up to the point at which a fully sustainable fuel cycle is eventually established, which the WPPR [Working Party on the Physics of Innovative Power Reactors] takes as a FR fuel cycle with multiple recycle.” It was considered preferable to manage the Pu in a way that does not foreclose future options – i.e. if direct disposal is pursued, then it is desirable to be able to recover the Pu later, or if thermal recycle strategies are pursued, then the Pu isotope vector should not be degraded to the point where it cannot be used in FRs. Within this framework, it is possible to pursue strategies of Pu preservation or Pu destruction, similar to the overall fuel strategy strategies of breeding and incineration. A recent analysis by Worrall (2013) indicates that Pu from future LWR used nuclear fuel (UNF) is sufficient to start a FR program in the USA, such that existing UNF can be disposed of. The timing of the FR program influences when Pu must be stockpiled in advance of fuelling future FRs.

Many LWRs in Europe are currently part-loaded with U-MOX fuel, leading to significant operating experience in using this fuel (OECD, 2003). Fully MOX-fuelled cores require further research due to reductions in soluble boron worth, and delayed neutron fraction (DNF) compared to LEU fuel.

Partly loaded cores typically use some MOX assemblies and some LEU assemblies. The Pu fraction in the MOX assembly is lower in the peripheral pins, due to variation in the thermal flux across the assembly. Pu is a strong thermal absorber, resulting in a much lower thermal flux in the Pu assemblies than the LEU assemblies. This means that the pins at the edge of the MOX assemblies experience a higher thermal flux than those at the centre, due to thermal neutron diffusion from the LEU assemblies. The thermal neutron diffusion length is of the order of one pin pitch. Variable enrichments in different pins increase the fabrication cost.

An alternative to different fuels in different assemblies is to utilize heterogeneous ‘CORAIL’ assemblies with different fuels in different pins (Kim, 2002; Ganda et al., 2007). The design contains some LEU pins and some MOX pins. More MOX pins neighbour LEU pins, such that the thermal flux is generally higher in the MOX pins – although variable Pu fractions in the MOX pins are still desirable. Multiple recycle of the Pu or TRU in the assembly at equilibrium (i.e. when cycle  $n+1$  has the same Pu composition as cycle  $n$ ) is possible with zero-net production of Pu/TRU at equilibrium. Seven years were allowed for reprocessing and fabrication between recycles. 45 GWd/t average discharge burn-up was possible with 4.8% enriched LEU. For Am and Cm recycling with a given burn-up, the required LEU enrichment is higher than if only LEU fuel were used. This can increase costs by ~\$5.6M per 18 month reload (OECD, 2013). An additional cost penalty to the utility of at least ~\$4M per reload (and potentially substantially higher) is anticipated due to additional licensing costs, transport and storage of highly reactive fuels, reprocessing costs and

potentially higher costs for discharge, storage, transport and spent fuel management of TRU fuels (OECD, 2013).

The reactivity optimal moderation for Pu is somewhat higher than for LEU. Increasing the moderation in Pu-bearing pins increases the degradation of the Pu isotope vector. Annular pins can be used to increase the local moderation around Pu pins in a CORAIL-style assembly. This design was considered by (Puill and Bergeron, 1997) in the ‘Advanced Plutonium Assembly’ (APA).

Kloostermann (1998) modelled the multiple recycling of U-Pu MOX in PWRs with unmodified and increased moderation over 4 recycle stages. Increasing moderation reduced the required Pu enrichment. The increase in moderation also reduced the tendency of the MTC to go positive after multiple recycles. However, MAs are not recycled at each stage. In all cases, the Pu enrichment significantly increased with each recycle stage. Indeed, increased moderation increases the rate at which the fissile Pu fraction is reduced, which has previously been noted to reduce the practicality of multiple recycle (OECD, 2003).

It is also possible to use U-MOX in CANDUs. An additional option is to directly utilize spent PWR fuel in CANDUs, such that the bred Pu and remaining  $^{235}\text{U}$  can be burned without reprocessing (OECD, 2003).

Multi-tier strategies with thermal cycles followed by fast recycle are often considered. There is a strong economic incentive to minimise the number of transmuting reactors per LWR as LWRs are considered to be cheaper (OECD, 2002).

If MAs are recycled multiple times in thermal reactors,  $^{252}\text{Cf}$  is ultimately produced. This is a strong spontaneous neutron (SN) source which takes several years to decay. Remote fuel fabrication or long cooling times are necessary (Shwageraus, 2003). In FRs, this source is essentially zero due to the much higher fission probability of TRU isotopes, and the long chain of captures required to produce  $^{252}\text{Cf}$ .  $^{244}\text{Cm}$  also contributes to the neutron source. OECD (2002) reported neutron sources at fabrication of around  $10^{10}$  and  $10^{11}$  n/s/tiHM for a fast breeder reactor and a fast TRU incinerator respectively.

### ***1.2.5. Reduced-moderation Water Reactors***

In LWRs, water is necessary to cool the reactor, and is also deliberately introduced to moderate the reactor at an optimal level for use of LEU in the open cycle. For TRU recycle, it is desirable to have a low moderation reactor. It is possible to design LWRs which contain less water while still providing adequate cooling. The reduced moderation results in a much harder neutron spectrum in the reactor, allowing the LWR to behave somewhat like a fast reactor. The reactor can function as a breeder and/or pursue a strategy of full actinide recycle, due to the increased fission to capture

probability of most TRU isotopes in the hard spectrum, which allows a superior neutron economy to be achieved.

Extensive studies have been conducted by the Japan Atomic Energy Agency (JAEA) to develop a flexible light water reactor (FLWR) concept. This is a reduced-moderation BWR. They propose reactors designed to recycle Pu, and potentially MAs, and to breed fissile Pu from  $^{238}\text{U}$  (Uchikawa et al., 2007). Designs are designated the high conversion (HC) FLWR and the reduced-moderation water reactor (RMWR). In these designs, the gap between fuel pins was reduced and the void fraction (VF) was increased (Fukaya et al., 2008), resulting in a faster neutron spectrum. PWR configurations have also been considered. Hitachi are also developing reduced-moderation BWR designs (RBWRs) to achieve a high conversion ratio (CR) and/or burn TRU waste (Takeda et al., 2007; IAEA, 2004). The assemblies are typically hexagonal with triangular pin pitch. The JAEA and Hitachi designs contain 2 seed regions, with an internal axial blanket between them, and usually external axial blankets above and below the seed. The core height is much lower than conventional LWRs, which results in reduced pressure drop despite the tight lattice pitch (Ishikawa and Okubo, 2009) and increases neutron leakage. The fast spectrum can also lead to higher power excursions during overcooling transients. The reduced core height (~1.25m) limits the coolant volume and speeds up the transient response, which along with the low magnitude VC decreases the reactivity excursion due to overcooling (Hu, 2010).

Around zero net  $^{237}\text{Np}$  and  $^{241}\text{Am}$  production was found to be possible in the HC-FLWR when MAs were loaded into the core (Fukaya et al., 2009a). Doping the internal blanket of the RMWR with  $^{237}\text{Np}$  or  $^{241}\text{Am}$  can also greatly increase the achievable cycle length (Hamase et al., 2013). However, Pu and MA loading tends to increase the VC, and Fukaya et al. (2009b) found that reducing the core height was necessary to increase neutron leakage to mitigate this. Even so, the need to keep the VC negative is extremely limiting, and it is difficult to evaluate the VC accurately due to the feedback between void and power distributions in the core and the importance of neutron leakage. The complicated seed-blanket structure of the RMWR/ RBWR core improves the VC but adds to the difficulty of modelling the core accurately. Downar et al. (2012) calculated a significantly positive VC for the RBWR, whereas the JAEA and Hitachi generally calculate it to be slightly negative. In addition, the high TRU content and low moderation tends to make the core reactivity increase as the VF approaches 100% (Fukaya et al., 2009b).

Thermal-hydraulic analysis indicates that the RBWR has generally satisfactory transient performance provided that the VC is negative. However, the relatively low minimum critical power ratio (MCPR) compared to an ABWR can lead to dry-out following a pump trip (Shirvan et al., 2014).

The VC can be made more negative by including ‘axial streaming channels’ – voids in the centre of the fuel assemblies, to increase neutron leakage (e.g. Feng and Ganda, 2013).

As of 2004, a commercial plant was targeted by the 2020s (IAEA, 2004).

To further reduce moderation, heavy water variants of the RMWR have been considered (Hibi et al., 2001). In BWRs, this has the severe disadvantage of the potential for tritium leakage in the steam generators of the primary circuit. A hard spectrum, heavy water-cooled PWR breeder was considered by (Hiruta and Youinou, 2013).

In this thesis, the reduced-moderation BWR is referred to as an ‘RBWR’, while a reduced-moderation PWR is referred to as an ‘RMPWR’. Reduced-moderation BWRs have variously been abbreviated to RMWR and RBWR in previous studies. RMBWR is also a logical choice. Here, RBWR is selected for consistency with other recent published research, and to differentiate from a PWR.

#### ***1.2.6. Super-critical Water Reactors (SCWRs)***

Heavy and light super-critical water have been proposed as an advanced reactor coolant. This increases the plant thermal efficiency, but also results in corrosion problems (Abram and Ion, 2008). Similar to the RBWR, a hard spectrum can be achieved in an SCWR using a tight pitch lattice (Cao et al., 2008). Thermal designs can utilize solid moderator or water rods and operate an open LEU cycle (e.g. Bae et al., 2007). Hybrid designs have been proposed which combine both concepts in different regions of the same core (e.g. Kim et al., 2004). U-MOX-fuelled SCWRs may require intricate blanket designs to achieve a negative VC (Mukohara et al., 1999).

#### ***1.2.7. Heterogeneous Recycle***

Currently, Pu and MAs are extracted separately, which allows thermal recycle of Pu and subsequent incineration of MAs in a dedicated FR. This approach is flexible but leads to proliferation concerns from holding separated Pu. Fuel containing MAs needs to be fabricated using remote handling, which is expensive. It is possible to fabricate U-MOX fuel using glove-boxed lines (e.g. Uematsu et al., 2002), which is an incentive for either direct disposal of MAs (i.e. recycle of Pu only) or recycling MAs in dedicated ‘target’ pins or assemblies. In this manner, the remote fuel fabrication requirements can be minimised. In FRs, heterogeneous recycle of MAs has been considered using U-MOX fuel in the seed assemblies and (Am,U)O<sub>2</sub> fuel in the blanket assemblies or MA targets in a fertile-free matrix (Bonnerot et al., 2010; Varaine et al., 2010). This requires further research on fabrication of MA-bearing pins,<sup>1</sup> including irradiation experiments, to demonstrate that remote

---

<sup>1</sup> Irradiation testing may be required in any case for pins containing a small amount of MA, but the extensive data available for MOX fuels is more likely to be applicable (OECD, 2013).

fabrication of a fuel that can meet licensing criteria (e.g. fission product retention) (IAEA, 2009). Development of MA-bearing fuel fabrication technology is estimated to require 10-15 years (OECD 2013). While heterogeneous fuel design can lead to increased scope for optimising fuel loading schemes, it also complicates the nuclear and thermal-hydraulic design (OECD, 2013).

(Hyland et al., 2011) considered using MA pins in a CANDU fuel element. The MA pins also contained the lanthanides from the waste as these may be difficult to separate from the MAs (see Section 1.4).

With large quantities of MAs in a fuel cycle, and/or dedicated MA targets, uncertainty in the MA cross-section data (OECD, 1999a) may become an issue, with more accurate nuclear data being required.

### ***1.2.8. Fertile-free Fuels***

It is usually considered necessary to mix the TRU with a fertile isotope. This reduces the incineration rate (as more TRU is bred from the fertile isotope), but improves the fuel and coolant reactivity feedback coefficients and kinetic parameters. Mixing the TRU with  $^{238}\text{U}$  is the most studied case, but mixing with  $^{232}\text{Th}$  is also often considered. As well as resulting in unacceptable reactivity feedback coefficients, use of pure TRU typically would result in a large reactivity swing over the cycle. Making the reactor very small severely limits the reactor power. The TRU can also be mixed with a ‘fertile-free’ material, such as ceramic or metal matrix (Porta and Pulil, 1998). For an LWR, Baldi and Porta (2001) found that it was necessary to use fertile-free fuels in conjunction with  $\text{UO}_2$  fuel.

This strategy is pursued in the CEA-designed APA and APA-DUPLEX assemblies, which contain  $(\text{Pu,Ce})\text{O}_2$  and LEU pins. The absence of  $^{238}\text{U}$  in the Pu pins helps increase the net Pu destruction rate (OECD, 2003).

Shwageraus (2003) considered combining fertile-free fuels with conventional enriched U pins in a single heterogeneous LWR assembly. This was found to allow zero net TRU production with multiple recycling of the TRU. Increasing the U enrichment was necessary to compensate for the decreased fissile content of the TRU after multiple reprocessing stages. A build-up of  $^{252}\text{Cf}$ , which can decay by spontaneous fission, was found to present problems when reprocessing and fabricating the fuel. Long cooling times were recommended to circumvent this problem. Zhang (2003) considered using  $\text{ThO}_2$  fuel in conjunction with fertile-free fuel.

***In this thesis, LWRs are selected as the platform for full TRU recycle as they are a well understood, commercially mature technology with reduced cost and time to deployment compared to FRs.***

## 1.3 Thorium

### 1.3.1. Overview

Th occurs naturally as  $^{232}\text{Th}$ , a fertile isotope. When  $^{232}\text{Th}$  absorbs a neutron, fissile  $^{233}\text{U}$  is produced through two beta decays via  $^{233}\text{Pa}$  – which has a 27 day half-life. Higher isotopes of U are produced through subsequent captures. In this thesis, U bred from Th is designated U3 to distinguish it from LEU and U-Pu-based fuel cycles.

Th is more abundant than U. Thus far, it has never been used as a nuclear fuel on a commercial scale. The relative merits of using Th with regard to proliferation resistance and waste toxicity are the subject of much debate and a summary of potential advantages and disadvantages can be found in (IAEA, 2005b).

Proliferation resistance, in particular, is a contentious issue. The Th fuel cycle is often cited as having superior proliferation resistance due to the presence of  $^{232}\text{U}$  (which has strong gamma emitters, notably  $^{212}\text{Bi}$  and  $^{208}\text{Tl}$ , in its decay chain) in the bred  $^{233}\text{U}$ , which makes the  $^{233}\text{U}$  difficult to handle or conceal (IAEA, 2005b). However, closed fuel cycles involving the separation of fissile materials are unlikely to be more proliferation resistant than open cycles (Kang and von Hippel, 2001) and there are concerns about separation of the intermediate isotope,  $^{233}\text{Pa}$ , to allow production of pure  $^{233}\text{U}$  (Kang and von Hippel, 2001; Ashley et al., 2012). The UK National Nuclear Laboratory (NNL)'s view is that “thorium systems are no more proliferation resistant than U-Pu systems, though may offer limited benefits in some circumstances” (NNL, 2010). (IAEA, 2012) reached similar conclusions.

Th has been advocated, in particular, as a fuel for MSR (e.g. by the Weinberg Foundation in the UK) and ADSRs (e.g. (Rubbia et al., 1995)).

One of the main issues with reprocessing Th fuel is the high energy gamma source. This necessitates remote fuel fabrication, which is expensive. The  $^{232}\text{U}$  gamma source of a Th-fuelled FR is 40 times greater than the SN source (Wenner et al., 2012) and therefore is the most significant factor for remote fuel fabrication. In U-fuelled systems it can be argued that it is not worthwhile to reprocess MAs, i.e. Pu recycle only should be performed. In Th-fuelled systems, this argument is less relevant because the MA source is less significant by comparison.

### 1.3.2. Fuel Cycle

In fast breeder reactors, the U-Pu cycle can generally achieve a higher breeding ratio due to the high value of  $\eta$  for Pu in the fast spectrum (Fiorina et al., 2013a) and the relatively high fast fission cross-section of  $^{238}\text{U}$  relative to  $^{232}\text{Th}$ . Th is therefore not generally preferred for fast breeders. In incinerators, the intrinsically lower conversion ratio of Th-based FR cycles can lead to slightly

higher incineration rates than with U-based cycles.  $^{232}\text{Th}$  intrinsically generates very little TRU in an open or closed fuel cycle as it is a lighter isotope than  $^{238}\text{U}$ . This is often claimed to greatly improve the TRU burning potential of Th-based fuel cycles. While this is true for a single pass (Ghrayeb et al., 2009), U3 is bred instead of TRU. U3 is itself a potential proliferation risk, and, if disposed of directly, would require long-term storage, similar to TRU. In the closed cycle, where U3 is retained in the fuel cycle, the TRU incineration rate is comparable to the U-Pu cycle, as U3 behaves similarly to the TRU bred in-situ in the U-Pu cycle. The principal fuel cycle advantages of the closed Th cycle in FRs are therefore lower waste radiotoxicity and lower actinide decay heat in incineration cycles (Franceschini et al., 2011) and breeder cycles (Fiorina et al., 2013a).

In thermal reactors, the large TRU destruction rate in a single pass is often used to advocate use of Th-Pu MOX fuel for reactor-grade and weapons-grade Pu destruction in PWRs (e.g. Galperin, 1995; Weaver and Herring, 2003; Shwageraus et al., 2004; Tsige-Tamirat, 2011), BWRs (e.g. Bjork et al., 2011) and also in SCWRs (Weaver and MacDonald, 2002). These studies are predominantly at the assembly level, but include analyses of partly Th-Pu-fuelled cores (Mittag and Kliem, 2011) and fully Th-Pu-fuelled cores (Fridman and Kliem, 2011; Downar et al., 2008). Similar constraints apply to Th-Pu-fuelled cores as U-MOX cores. In PWRs the main problems for the full Th-Pu MOX cores are reduced shutdown margin (SDM) caused by lower control rod worth, reduced soluble boron worth and reduced DNF (Fridman and Kliem, 2011). The reduced SDM can be addressed by using different control materials (Dziadosz et al., 2004), while the reduced control rod worth mitigates the reduced DNF in a rod ejection accident (REA) (Dziadosz et al., 2004). The SDM and response to a REA cannot be improved simultaneously by changing the control rod worth. There may therefore be deterioration in reactivity initiated accident (RIA) performance which should be investigated (Fridman and Kliem, 2011). Despite this, (Long et al., 2004) found that maximum fuel and cladding temperature increases for Th-Pu oxide fuel were similar to those for  $\text{UO}_2$  fuel in transient events, although use of weapons-grade Pu reduced the required Pu content in the fuel relative to reactor-grade Pu.

Ratises and Todosow (2010) and Sorensen et al. (2006) performed assembly-level studies of Th-TRU multi-recycle in PWRs, analysing cases containing reprocessed U3 in the fresh fuel, but without full recycle of TRU.

Th has favourable material properties compared to U which make it well suited for MOX fuel, including higher thermal conductivity, higher melting point and higher chemical stability (summarized in (Kelly and Franceschini, 2013)). However, much superior operational experience is available for U-MOX fuel, which means further materials tests are needed before Th-Pu MOX could be deployed (Kelly and Franceschini, 2013). The materials behaviour of  $\text{ThO}_2$ -based fuels

was considered by (Long et al., 2004) and Th-U and Th-Pu fuels were generally found to have the same or improved safety performance over UO<sub>2</sub> fuels. Experimental programs on Th-based fuels are also described in (Thor Energy, 2010; Schram and Klaassen, 2007; IAEA, 2012).

IAEA (2012) performed a detailed study of closed Th-based fuel cycles with thermal reactors. Full recycle of U3 and Pu was simulated using a mixture of LWRs and heavy water reactors (HWRs), with full reprocessing allowing the volume of discharged waste to be substantially reduced. MAs remained with the FPs and were not recycled. Full Pu recycle was also considered for U-based fuel cycles. Th-based cycles can reduce the MA discharge relative to U-based cycles, depending on how the Pu is recycled (i.e. which reactors it is located in).

Pu-Th-fuelled HWRs were projected to become economically competitive by around 2030, with closed Th cycles in HWRs and LWRs becoming competitive around 2070-2080, due to exhaustion of U resources under \$130/kg. With deployment of FRs, use of the Th and U3 was not economically competitive, i.e. a pure U-Pu cycle was favoured.

Gas-cooled, graphite-moderated Very High Temperature Reactors (VHTRs) may have the capability to achieve very high burn-up due to their use of TRISO fuel with carbide cladding (Brossard et al., 2009). This makes it a candidate reactor for achieving high Pu burn-ups, and, as a result, Th fuels have been proposed to achieve this in a once-through cycle (e.g. Chang et al., 2006).

### ***1.3.3. Neutronic Considerations in Thermal Reactors***

Th is often proposed as a fuel for thermal and epithermal reactor systems due to its superior breeding characteristics in the thermal spectrum (e.g. (Yun et al., 2010)) and notably the high  $\eta$  of <sup>233</sup>U over a wide range of energies, including resonance energies (IAEA, 2005b). Breeding of <sup>233</sup>U from <sup>232</sup>Th, and subsequent burning of <sup>233</sup>U, was successfully performed at the Shippingport Light Water Breeder Reactor (Hecker, 1979).

The neutronic properties of Th fuel allow it to maintain relatively flat reactivity with burn-up once sufficient <sup>233</sup>U has been bred, in a relatively thermal neutron spectrum. This makes it well suited to high burn-up open-cycle schemes, where it is useful in limiting the reactivity swing over the cycle and increasing the proliferation resistance of the spent fuel. However, a high burn-up has to be achieved before use of Th becomes worthwhile, as a ‘seed’ fuel is necessary to start and sustain the reactor. In open-cycle schemes, this is typically LEU. LEU seed and Th blanket fuels can be loaded separately and refuelled on different batch schemes. Significant reductions in U consumption cannot be realised due to the need for much higher (up to 20%) U enrichment to sustain reactivity, and high burn-up is necessary for the cycle to be worthwhile, which results in materials challenges. There are also thermal-hydraulic challenges resulting from spatial separation of U and Th.

Homogeneous mixing of U and Th was found to decrease burn-up relative to enriched U, but some denaturing of Th with U was necessary to improve proliferation resistance, and in some cases to produce sufficient power in the blanket at start-of-cycle (SOC) to reduce power peaking (NERI, 2002; Todosow and Kazimi, 2004; Todosow et al., 2005). IAEA (2012) found that open-cycle use of Th can lead to an increase in U consumption, and the higher LEU enrichment required negates proliferation resistance advantages, such that the only advantage is the reduced Pu and MA production.

Heavy-water-moderated reactors (notably CANDUs) can achieve economic advantages from Th in the open cycle at much lower burn-ups (Zhongsheng and Boczar, 1999; IAEA, 2012). The burn-ups are still significantly lower than in LWRs as the uranium is only slightly enriched, such that the proliferation resistance is worse.

For closed-cycle applications, CANDUs can operate at a higher CR than LWRs (Nuttin et al., 2012). CANDUs may have the potential to achieve a self-sufficient Th cycle, or breed fissile fuel to start a FR programme (Zhongsheng and Boczar, 1999). Closed Th cycles in CANDUs and advanced-CANDUs (ACRs) require some external Pu feed (IAEA, 2012). A Th-fuelled heavy-water-moderated SCWR has been proposed by Canada (NSERC, 2011).

The option of breeding U<sup>233</sup> in FRs and burning it in thermal reactors has been studied (IAEA, 2012). Here, Pu is bred in LEU-fuelled LWRs and burned in a FR to breed U<sup>233</sup>.

The Indian nuclear power programme envisages a 3-stage strategy, with: (1) Pu breeding in U-fuelled CANDUs; (2) mixing this Pu with Th to breed U<sup>233</sup> in FRs; (3) use of Th-U<sup>233</sup> in the light-water-cooled, heavy-water-moderated Advanced Heavy Water Reactors (AHWRs) (WNA, 2013). The objective is to utilize India's significant Th resources in a closed nuclear fuel cycle, and take advantage of the high thermal  $\eta$  of U<sup>233</sup> (Sinha and Kakodkar, 2006). The AHWR is not quite self-sustaining in U<sup>233</sup>, but does have a negative VC (unlike a U-fuelled CANDU) (IAEA, 2012).

Nuttin et al. (2012) performed a detailed study of the trade-off between CR and burn-up of Th-based fuels in PWRs of different moderations and CANDU reactors. Using D<sub>2</sub>O in PWR geometries as a reduced moderation coolant was considered. This contrasts with the very thermalized neutron spectrum of a CANDU. D<sub>2</sub>O provides two advantages in this case: reduced neutron absorption in the coolant and reduced moderation without reduced cooling. A Th PWR, D<sub>2</sub>O-cooled breeder concept was also considered by (Takaki and Mardiansah, 2012).

Graphite-moderated MSR are often considered as they reduce the core fissile inventory (Forsberg, 2007). For self-sustaining MSRs, Th is frequently considered as a MSR fuel (Forsberg, 2007; Nagy, 2012; Krepel et al., 2013). The Th fuel cycle can improve the CR of MSRs (IAEA, 2012) as the

spectrum is often softer than FRs due to the moderation of the salt, and graphite, if it is present. It is often proposed to allow the  $^{233}\text{Pa}$  in the salt to decay into  $^{233}\text{U}$  outside of the reactor to improve the neutron economy (e.g. Nagy, 2012), although this can cause proliferation concerns due to extraction of an almost pure stream of  $^{233}\text{U}$  (Kang and von Hippel, 2001). Removing the graphite moderator can improve breeding performance (e.g. (Krepel et al., 2013)).

#### ***1.3.4. Moderator Temperature Feedback***

The main obstacle to TRU multi-recycle burning schemes in thermal reactors is that the degradation of the fissile proportion of the recycled fuel leads to increasing Pu feed requirements to sustain criticality and, accordingly, to a growth of the TRU inventory in the recycled fuel, ultimately resulting in a positive MTC and/or VC for typical LWR designs. The harder spectrum of reduced-moderation (RM) water reactors, i.e. RMPWRs and RBWRs, can improve TRU transmutation performance by mitigating their increase in the recycled fuel, but, as discussed, the VC is still severely limiting for these designs (IAEA, 2004).

Using Th instead of U as the fertile fuel component can greatly improve the VC. This is due to the relatively high probability of fission for neutrons of resonance energies and relatively low fast fission probability of the U3 and increased resonance capture in Th with increased voiding and high fast fission threshold (Xu et al., 2002). In RBWRs using Th can improve the VC and therefore allow the core height to be increased (therefore reducing the neutron leakage). A single recycle stage of weapons-grade Pu was considered by (Downar and Xu, 2001). Higher Pu loading is required for Th-Pu fuel than U-Pu fuel to achieve the same burn-up (Kim and Downar, 2002).

The improved VC is also one of the motivations for considering Th in fast reactors (Fiorina et al., 2013a).

Ganda et al. (2011) demonstrated that multi-recycle of Th in RBWRs can allow a self-sustaining cycle to be achieved, with a very negative VC. Indeed the VC is too negative, and adding some Pu may be necessary to make it less negative (Ganda et al., 2012), in particular to allow a sufficient SDM. The core height was around 2m in this study, compared to ~1.25m for U-Pu RBWRs. In conjunction with the more negative VC than the U-Pu RBWR, this could lead to a less stable response to overcooling transients.

Similarly, self-sustaining Th fuel cycles appear possible in fast SCWRs (Csom et al., 2012).

Rahman et al. (2012) investigated Th-TRU incineration in conventional and RMPWRs, finding that the VC could be improved with RM operation (including use of nitride fuel, which increases the heavy metal density) and that spatial separation of U3 and TRU was neutronicly advantageous.

Zakova and Wallenius (2013) investigated TRU multi-recycling in Th- and U-fuelled BWRs using single assembly and full-core models. They found that multi-recycling of TRU was possible, with 5 year cooling between recycles. Th gave superior VC performance due to a reduction in Pu inventory after multiple recycles relative to U. However, maintaining criticality was found to be difficult without enrichment of Th with an external supply of U3. Np was not recycled due to its detrimental effect on the neutron economy, which resulted in higher fissile enrichment in the feed fuel and therefore a more positive VC.

*In this thesis, Th is considered as a fertile isotope for full TRU recycle. The argument for using Th in multi-recycle LWRs is essentially an MTC/VC based feasibility argument.*

#### **1.4. Reprocessing**

Several countries currently reprocess nuclear fuel using the PUREX process, separating it into U, Pu and everything else, i.e. FPs + MAs. This is performed by aqueous reprocessing, i.e. a solvent extraction method. Spent fuel is typically cooled for several years before it is reprocessed. This reduces the radioactivity and therefore the degradation of the organic solvent. A 5-year cooling time was selected for the British reprocessing plant THORP and the French reprocessing plants UP3 and UP2-800; the Japanese Rokkasho-Mura reprocessing plant was based on French technology.<sup>2</sup>

Reprocessing times of under 1 year (highly desirable for some envisaged breeder programs to speed up Pu production for additional FRs) have been accomplished on a tonne scale for ~100 GWd/t burn-up fuels<sup>3</sup> (270 days at Dounreay – (Pugh, 1978)) using mixer-settlers to speed up solvent mixing and therefore limit its exposure to radiation. The throughput at Dounreay is much lower than the LWR and AFR reprocessing plant THORP, making it easier to design the plant for short cooling times. THORP used pulse columns rather than centrifugal contractors (which would speed up mixing and therefore reduce solvent degradation) for solvent mixing as the centrifugal contractors were not sufficiently developed when the plant was designed. In addition, some short-lived FPs could be problematic (e.g. Ru-106 which has a half-life of 1 yr and extracts to some extent, and gaseous isotopes of iodine), and in general the technical challenges of short cooling times would need to be addressed.<sup>4</sup>

There was also little incentive to reprocess the fuel quickly at THORP, as there was no pressing demand for additional MOX fuel. Also, if there is no intention of recycling the MAs, it is better to reprocess immediately before fuel fabrication and use, to limit <sup>241</sup>Am content in the MOX fuel.<sup>5</sup> Therefore, it may be difficult to perform PUREX reprocessing on a larger scale than Dounreay with

---

<sup>2</sup> Private communication with Dr Chris Phillips, Energy Solutions, May 2013

<sup>3</sup> Private communication with Tony Roulstone, University of Cambridge, April 2013

<sup>4</sup> Private communication with Dr Chris Phillips, Energy Solutions, May 2013

<sup>5</sup> Private communication with Prof. Bruce Hanson, University of Leeds, April 2013

a short cooling time while meeting modern environmental and regulatory requirements,<sup>6</sup> although it is feasible.

Separation of MAs from FPs requires modification of the PUREX process. In particular, it is difficult to separate Am and Cm from the lanthanides. Several processes have been proposed to accomplish this (OECD, 1999b). In general, the processes under consideration for MA extraction are not yet feasible on an industrial scale (Forschungszentrum Juelich, 2008). Low reprocessing losses are necessary to limit the actinides being disposed of with the FPs, else the multi-recycling is of limited benefit.

An alternative to aqueous reprocessing is pyroreprocessing, which is suitable for coextraction of all TRU isotopes. Long cooling times are not required (IAEA, 2008). The process has not been performed on an industrial scale and therefore requires significant development.

Th is difficult to reprocess as it cannot be dissolved with pure nitric acid (HNO<sub>3</sub>), which is typically performed for U fuels. Some hydrofluoric acid (HF) is necessary, which is highly corrosive. The THOREX process is proposed for the reprocessing of Th-based fuel. This has so far only been performed on a small scale. Extraction of Pa from FPs is problematic, and this is a concern because the long half-life of <sup>231</sup>Pa makes it highly desirable to recycle it.<sup>7</sup> Non-aqueous reprocessing methods are significantly less advanced for Th-based fuel compared to U-Pu-based fuel (IAEA, 2005b).

If U-Pu reprocessing can be performed more quickly than Th reprocessing then this may impact the relative neutronic performance of the Th fuel cycle.

One problem with fast reprocessing is that the high level waste that is produced contains more short-lived FPs and therefore has a higher decay power. It is highly desirable to vitrify this waste immediately, as there are safety concerns from storing liquid high level waste (it may leak).<sup>8</sup> As the heat load limits the packing density of vitrified waste, this leads to increased waste volumes.

## 1.5. Thesis Motivation and Objectives

Extensive research has been performed on TRU transmutation and full actinide recycle across a range of candidate fuel cycles and reactor platforms. In this thesis, conventional LWRs are preferred as they are cheaper, lower risk and the technology currently exists. TRU recycle in LWRs is limited by the MTC/VC, although feasibility is improved by using RM LWRs. The Th fuel cycle is chosen as it has superior MTC/VC performance. This introduces additional fabrication and

---

<sup>6</sup> Private communications with Dr Robin Taylor, National Nuclear Laboratory, February 2013

<sup>7</sup> It must be noted that Pa recycling increases the quantity of <sup>232</sup>U in the recycled fuel, which results in an increased high energy gamma source from the <sup>232</sup>U decay chain which further complicates fuel fabrication.

<sup>8</sup> Although liquid high level waste is currently stored in the UK, it is highly desirable to limit this. See for example (Office for Nuclear Regulation, 2011)

reprocessing challenges, but full recycle of TRU is in any case expensive and requires the development of new technology.

While some studies of closed Th-TRU cycles in LWRs have been performed, these are mostly limited to single assembly analyses and/or do not consider full TRU recycle. While the potential of Th fuel for addressing the potentially positive VC in RM LWRs has previously been identified, there is little or no previous work on the use of Th fuel for the full recycle of TRU in RM LWRs, in particular in RBWRs. Given strong interest in fuel cycles that consider full recycle of TRU, and the potential for RM LWRs to provide a relatively near-term platform for performing this role, the feasibility and performance of this design therefore requires assessment, to widen the scope of fuel cycles that LWRs can perform and gain an understanding of their performance in this context. This thesis contains a comprehensive analysis of the design, operation and fuel cycle of Th-TRU-fuelled LWRs operating with full actinide recycle.

The objectives of this thesis are to:

- Consider the neutronic feasibility of this fuel cycle in retrofit and non-retrofit designs of RMPWR using lattice calculations and full-core analysis.
- Consider the neutronic feasibility of this fuel cycle in RBWRs using lattice calculations and full-core analysis.
- Perform a quantitative comparison of using  $^{232}\text{Th}$  instead of  $^{238}\text{U}$  as a fertile fuel.
- Determine whether it is possible to retrofit an existing PWR with tight-lattice assemblies without violating thermal-hydraulic constraints.
- Determine whether it is possible to employ a multi-tier fuel cycle, where full recycle in RM LWRs is preceded by a single pass of Th-Pu MOX in an unmodified PWR.
- Compare the fuel cycle performance of the RMPWR and RBWR and discuss their performance relative to other TRU incineration options.

An alternative to a tight-lattice LWR is to utilize a regular lattice but replace the light water coolant with heavy water, again with Th-TRU fuel. A PWR design should be considered instead of a BWR to limit tritium leakage from the primary circuit. (Harris, 2013) performed a feasibility study on this concept, parallel to the work in this thesis, and found that the neutron spectrum from use of mixes of  $\text{H}_2\text{O}$  and  $\text{D}_2\text{O}$  coolant in a PWR was unfavourable for TRU burning. This was due to increased resonance flux relative to fast and thermal flux, increasing the detrimental resonance capture effects on neutron economy and void reactivity.

## **1.6. Thesis Organisation**

Chapter 2 outlines the proposed fuel cycle scheme and investigates the feasibility of full TRU recycle in RMPWRs and RBWRs using single assembly models; it is based on (Lindley et al., 2014a). Chapter 3 contains an analysis of the void reactivity feedback effects in Th-fuelled and U-fuelled TRU incineration cycles in conventional PWRs, RMPWRs and RBWRs; it is based on (Lindley et al., 2013a). Chapter 4 contains a thermal-hydraulic feasibility analysis of RMPWRs; it is based on the first section of (Lindley et al., 2014b). Chapter 5 contains a detailed RMPWR neutronic analysis based on (Lindley et al., 2013b) and (Lindley et al., 2014c). Chapter 6 contains a detailed RBWR neutronic analysis with coupled thermal-hydraulic feedback, partly based on the third section of (Lindley et al., 2014b) and on (Lindley et al., 2014d; 2014e). Chapter 7 assesses the fuel cycle performance, based on (Lindley et al., 2014f) and some content from (Lindley et al., 2014g). Chapter 8 concludes.

This thesis considers fuel cycles operating at equilibrium. This is a common but major assumption. Analysis of time-dependent scenarios is ongoing.

## **Chapter 2 – Assembly Analysis**

In this chapter, a single assembly analysis is used to assess the feasibility of RMPWRs and RBWRs to sustain an equilibrium cycle, where the feed to the reactor is a mixture of Th and TRU, and all actinides are returned to the reactor after reprocessing. The focus of this chapter is a single-tier fuel cycle, where the TRU feed to the RMPWR or RBWR is the discharged TRU from conventional LWRs. However, it is also worth considering a multi-tier fuel cycle, where the first stage is a Th-Pu fuelled ‘reference’ PWR. Spatial separation of TRU from bred uranium is found to greatly improve neutronic performance. This will pose thermal-hydraulic challenges, which are discussed in Chapter 4. In addition, the harder neutron spectrum resulting from the reduced moderation also reduces the control rod worth, while there is a neutronic incentive to use increased mechanical shim to maintain a negative MTC. It may therefore be desirable to increase the number of rod cluster control assemblies. Superior burn-up is achievable in a reduced-moderation BWR as a larger reduction in moderation is feasible, although the incineration rate is reduced relative to a PWR due to a higher conversion ratio. The fuel design for RMPWRs and RBWRs is further refined in Chapters 5 and 6, based on the conclusions of this chapter.

### **2.1. Rationale**

A TRU incinerator uses an external feed of TRU isotopes to sustain criticality and continue incineration. When fuel is discharged from the core, it contains a mixture of actinides and FPs. The FPs are removed, and are replaced by Th and TRU, which are used to ‘make up’ the fuel. At equilibrium, the resultant fresh fuel has identical composition for successive cycles. The TRU incineration rate can be altered by altering the TRU reload or ‘make up’ fraction in the feed. At equilibrium, the TRU used to make up the fuel is equal to the TRU incinerated, and therefore the TRU reload fraction directly influences the TRU incineration rate – here it is considered to be a key parameter as it is a ‘design’ parameter, rather than a measured output. A higher TRU reload fraction generally leads to a higher TRU inventory in the core, increasing the incineration rate by reducing  $^{232}\text{Th}$  capture relative to TR and  $\text{U}3$  fission. This process is shown diagrammatically in Fig. 2.1.

It is desirable to increase the TRU reload fraction to maximize burn-up and incineration performance, within the fuel and cladding material limits, and thus minimize reprocessing and manufacturing requirements. Particularly for thermal reactors, the TRU reload fraction is limited by the degradation in the MTC, or VC, which becomes less negative as the proportion of TRU in the recycled fuel inventory increases (OECD, 2003, reconfirmed in this chapter). The MTC is roughly proportional to the TRU content of the fuel, but the isotopic composition also influences the MTC, and a less fissile TRU vector means that a higher TRU loading is necessary to sustain criticality.

Reducing moderation changes the trade-off between the various figures of merit, as will be discussed.



**Fig. 2.1.** Illustration of TRU reload fraction. At equilibrium, the discharged fuel contains 5 kg fission products (FPs). The fresh and burned fuel contains the same amount of U3 as this is at equilibrium, however 2 kg of TRU and 3 kg of Th has been burned relative to the fresh fuel. Therefore, for cycle n+1 to have the same fuel as cycle n, the FPs must be replaced with 3 kg Th and 2 kg TRU, giving  $72 + 3 = 75$  kg Th and  $18 + 2 = 20$  kg TRU for the next cycle. The TRU reload (or ‘make up’) fraction is therefore  $2/(2+3) = 2/5 = 40\%$ .

In principle, the MTC and VC can also be improved by increasing the reactivity worth of neutron leakage and, consequently, the negative reactivity insertion in case of voiding. This can be achieved by shortening the core and/or using internal blankets. However, for a given power rating and reactor vessel diameter, the core size is limited by thermal-hydraulic constraints, while the adoption of internal axial blankets acts to decouple the fluxes in the seed regions. This can make the power peaking very sensitive to local changes in reactivity, such as during transients (Hibi et al., 2001). For example, it is possible that a negative reactivity insertion into one region of the core could increase reactivity in a different region (Kawashima et al., 1992). In addition, axial heterogeneities are especially undesirable for fuel with remote fuel manufacturing requirements, as is the case in this study. Therefore an axially homogeneous reactor is the preferred choice adopted for this study.

For the RMPWR, a core design that can be retrofitted into a current PWR design is highly desirable to minimize the time to and cost of deployment. However, retrofitting often results in a deviation from the plant’s original operating conditions, and the impact of such a deviation must be thoroughly assessed before claiming viability. Also, practical constraints imposed by the existing plant structures should be considered and accounted for, since these determine whether retrofitting is economically more attractive than designing a new plant. These considerations and, specifically, avoiding replacement of the reactor vessel top head and internals, lead to the choice of a 17×17 square lattice assembly, with the same footprint as a typical PWR assembly but with larger pin

diameter, as the logical starting point for this investigation. Changes in plant operating conditions, such as core inlet/outlet temperature and coolant flow rate, have been considered, and their impact on thermal-hydraulic constraints, such as minimum departure from nucleate boiling ratio (MDNBR) and pressure drop, have been assessed.

The RBWR design is not fixed at this point, but a reference design with hexagonal assemblies, 120 or 200 cm core height and 53% average VF was selected for comparison with the RMPWR. The 120 cm core is similar to current U-Pu RBWR designs (Downar et al., 2012), while a taller core has been considered for Th designs where axial leakage is a less important mechanism for ensuring a negative VC than in U designs (Ganda et al., 2011). The reduction in moderation fostered by the tight pitch and relatively high VF of the RBWR leads to a significantly harder neutron spectrum than in retrofit RMPWR designs. The RBWR designs considered have a large reduction in moderation compared to conventional BWRs. This may result in a design that cannot be retrofitted into an existing core, but the plant is the same as the ABWR plant (IAEA, 2004).

## **2.2. Fuel Cycles Schemes**

The TRU feed is assumed to be UO<sub>2</sub> 4.4 wt% enriched PWR discharge, burned to 52 GWd/t and cooled for 10 years. This is the ‘single-tier’ fuel cycle. It is also worth considering a ‘multi-tier’ fuel cycle, where the first stage is a Th-Pu-fuelled ‘reference’ PWR. The feed to the RMPWR or RBWR is the discharge from the previous stage, reprocessed with 5 years cooling between stages, with the MAs from the initial UO<sub>2</sub> LWR stage added back to the actinide feed, so that the overall actinide balance across stages is preserved with only reprocessing losses and fission products being disposed of. This multi-tier implementation may allow more rapid implementation than straight full TRU recycle: the first stage homogeneous Th-Pu fuel could be implemented with existing Pu stockpiles and glove-box fuel fabrication (Fig. 2.2). However, it also introduces specific challenges, including increased higher actinide content in the RMPWR fuel inventory and separate management requirements for the Pu and MAs from the UO<sub>2</sub> LWR stage. The equilibrium cycle inventory contains more U3 than with a single-tier fuel cycle as the feed contains U3 from the discharge of the intermediate Th-Pu PWR stage.

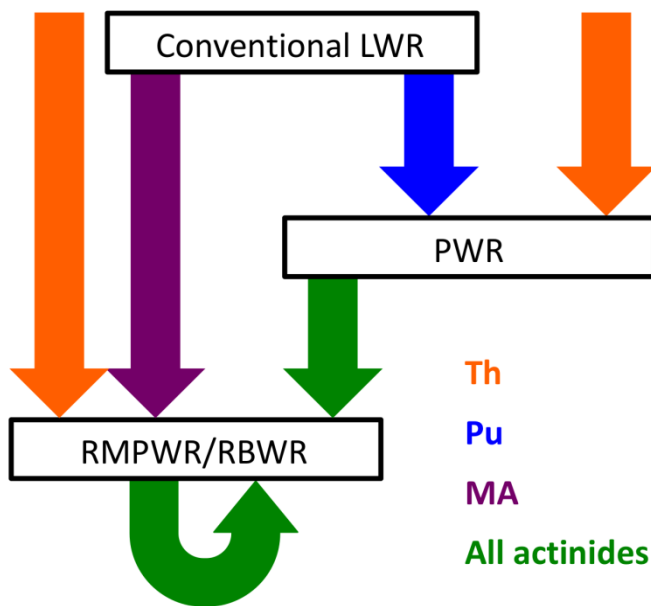


**Fig. 2.2.** Multi-tier fuel cycle scheme.

The Th-Pu first stage of the multi-tier scheme is burned to 50 GWd/t in most cases, corresponding to an initial loading of 10 at% Pu in the fuel. This level of Pu content has been considered in a previous full-core analysis (Fridman and Kliem, 2011). Th-Pu fuel is often advocated for a single irradiation pass through the core, e.g. (Galperin, 1995; Shwageraus et al., 2004), to reduce the Pu fissile quality and place the TRU waste in a proliferation-resistant form. It is therefore possible that a higher discharge burn-up may be desirable in the first stage, e.g. to minimize spent fuel volume or increase proliferation resistance, particularly if a final decision on full recycle has not been taken, or a single-pass strategy is enacted and a later decision is taken on full recycle. An additional multi-tier, high burn-up case with 15 at% Pu and an assembly average discharge burn-up of 84 GWd/t is also considered. This is thought to be the upper neutronic limit of what is reasonably achievable (Zainuddin et al., 2013) and the peak burn-up is likely beyond the maximum achievable with Zircaloy-based clad (~70–80 GWd/t) (OECD, 2006a). The isotope vectors for single- and multi-tier fuel cycles were calculated using lattice calculations in WIMS 10 (see Section 2.3), and are given in Table 2.1. The percentage reduction in Pu during the first stage is 46.3% and 51.8% for 50 GWd/t and 84 GWd/t respectively, i.e. the proportion incinerated is relatively insensitive to discharge burn-up. Including the bred U3 and recovered MAs as part of the legacy, the proportion of waste incinerated during the first pass is 22.6% and 28.5% for 50 GWd/t and 84 GWd/t respectively.

**Table 2.1.** Feed isotope vectors (at%).

Isotope	Single Tier	Multi-Tier	Multi-Tier, high burn-up
<sup>241</sup> Am	5.77	10.22	11.02
<sup>242m</sup> Am	7.15E-03	3.70E-02	5.04E-02
<sup>243</sup> Am	1.60	4.39	4.88
<sup>242</sup> Cm	2.99E-07	3.30E-04	3.43E-04
<sup>243</sup> Cm	5.73E-03	1.79E-02	2.16E-02
<sup>244</sup> Cm	0.50	1.53	1.98
<sup>245</sup> Cm	0.06	0.24	0.40
<sup>246</sup> Cm	6.46E-03	2.06E-02	3.89E-02
<sup>247</sup> Cm	9.34E-05	3.45E-04	9.36E-04
<sup>248</sup> Cm	7.04E-06	2.09E-05	6.56E-05
<sup>237</sup> Np	4.94	6.38	6.91
<sup>238</sup> Pu	2.74	3.42	3.91
<sup>239</sup> Pu	48.45	14.64	12.68
<sup>240</sup> Pu	21.03	21.41	21.41
<sup>241</sup> Pu	8.45	9.59	9.12
<sup>242</sup> Pu	6.46	9.21	9.68
<sup>233</sup> U	0.00	16.83	15.40
<sup>234</sup> U	0.00	1.76	2.04
<sup>235</sup> U	0.00	0.27	0.40
<sup>236</sup> U	0.00	2.21E-02	4.30E-02

The remainder of this chapter focuses on the single-tier fuel cycle.

## 2.3. Lattice Calculations

### 2.3.1. Implementation of Assembly Calculations in WIMS

Lattice calculations were performed using WIMS 9 and a development version of the UK deterministic reactor physics code WIMS 10 (Newton et al., 2008). A 172-group calculation with geometric approximations was first performed using the collision probability method to generate 11- and 12-group cross-sections for the RMPWR and RBWR respectively. A few-group solution in detailed geometry was then performed using the method of characteristics. Table 2.2 gives the geometric characteristics of the assembly designs under consideration, including the reference PWR assembly used to generate the TRU feed isotope vector.

**Table 2.2.** Reference fuel assembly parameters.

Parameter	PWR	RMPWR	BWR*	RBWR
Pellet radius (cm)	0.4095	0.4845, 0.5095	0.424	0.5865
Gap (cm)	0.0085	Same	0.0075	0.0125
Clad thickness (cm)	0.057	Same	0.0605	0.086
Pin radius (cm)	0.475	0.55, 0.575	0.492	0.685
Lattice type	Square	Square	Square	Triangular
Pitch (cm)	1.26	Same	1.295	1.5
Fuel height (cm)	366	366	399	120, 200
Power density in fuel (W/cm <sup>3</sup> )	400	285, 258	232	194, 116
Fuel temperature (K)	900	900	800**	900
Moderator density (g/cc)	0.707	0.707	0.456**	0.3655

\* Westinghouse Sweden SVEA-96 Optima 2 (Nuclear Engineering International, 2004)

\*\* Taken from (Bjork et al., 2011)

For the RMPWR the pin diameter was increased from the reference value of 9.5 mm to 11.5 mm, with the gap and clad thickness, as well as the pin pitch, unchanged with respect to the reference assembly values. A thicker clad may be necessary to limit the clad stress of the larger pin. A larger gap size or plenum may also be necessary, depending on the fission gas release relative to the reference case. This will slightly affect the minimum required pin diameter. The RMPWR model is run with rods out, as although some use of mechanical shim is considered later, this is not usual for a PWR, and, in any case, rods-out is thought an acceptable approximation.

Historically, various RBWR assembly designs have been investigated, which differ in geometry (and therefore fuel volume fraction) and power to flow ratio (and therefore core-average VF) (IAEA, 2004). For the purposes of this study, a relatively low hydrogen to heavy metal (H/HM) ratio design was selected so that conclusions could be drawn about a relatively bounding case (Table 2.3). The RBWR model consisted of 1/6<sup>th</sup> of a hexagonal 217 pin assembly based on the JAEA design from (IAEA, 2004). The pin pitch was 15 mm, the pin outside diameter (OD) 13.7 mm and the pellet radius 5.865 mm. The core-average VF was 53%. This is one of the best documented designs, and has a relatively low H/HM ratio.

Typically, RBWR designs have Y-shaped control blades which are asymmetrically positioned between assemblies (Fig. 2.3). As a consequence of this, the unit cell for the problem is large. However, it was deemed acceptable as a first approximation to smear the control material around the assembly such that a 1/6<sup>th</sup> hexagonal model could be used as pin powers are not calculated. The impact on the shim rod worth (calculated in Chapter 6) is not thought to be significant. The lattice

calculations were run with rods out, which is an acceptable approximation, as the rods will not significantly affect the achievable discharge burn-up and a minority of the fuel assemblies are rodded at power. A graphite follower was added to the control rod, such that the graphite rod is present when the rod is out. This reduces the moderation from bypass flow. This is typical for RBWRs (Nakano et al., 2007).

**Table 2.3.** H/HM ratio of considered cases.

Reactor type	Lattice type	Pin outer diameter (OD) (mm)	Pin pitch (mm)	H/HM*
PWR	Square	9.5	12.6	1.98
RMPWR	Square	11.0	12.6	1.09
RMPWR	Square	11.5	12.6	0.87
RBWR	Triangular	13.7	15.0	0.26

\* The H/HM for the PWR and RMPWR is calculated as the coolant/fuel area ratio. The H/HM ratio for the RBWR is relative to the PWR coolant density, i.e. it is calculated as the RBWR coolant/fuel area ratio multiplied by the ratio of the PWR coolant density, 0.707 g/cc, and BWR coolant density, 0.3655 g/cc at 53% VF.

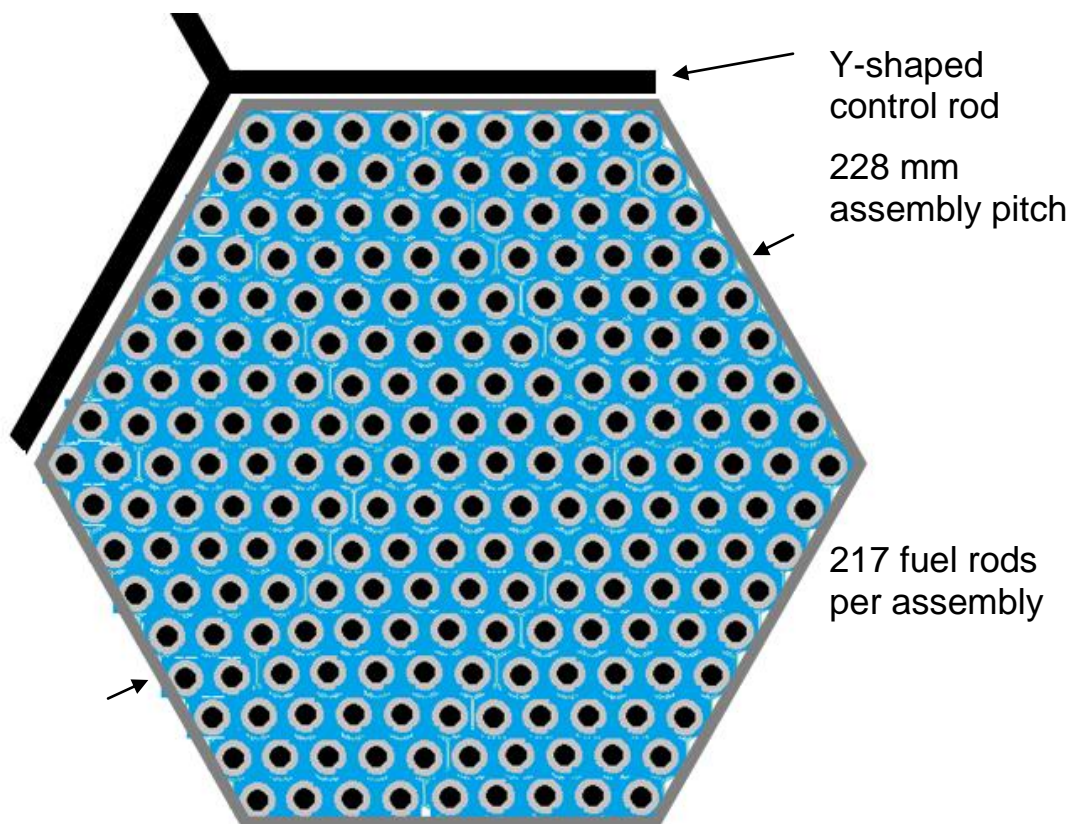


**Fig. 2.3.** Fuel assembly design considered for the RBWR case.

The H/HM ratio is considerably reduced for the RMPWR relative to an unmodified LEU-fuelled PWR. The RBWR has a large further decrease in moderation relative to the RMPWR (Table 2.3). Fig. 2.4 shows the neutron flux per unit lethargy for the PWR, 11 mm pin RMPWR, RBWR and a representative SFR, normalized to unit total flux. The LWR spectra are plotted in the WIMS 172-group energy structure, while the SFR spectrum is plotted in the 33-group structure used in the cell code ECCO within the fast reactor physics code ERANOS-2.2N (Rimpault et al., 2002).<sup>9</sup>

There is a large reduction in thermal flux for both RMPWR and RBWR concepts relative to the unmodified PWR, although the spectrum is still significantly softer than the SFR, with a significantly higher resonance and thermal flux.

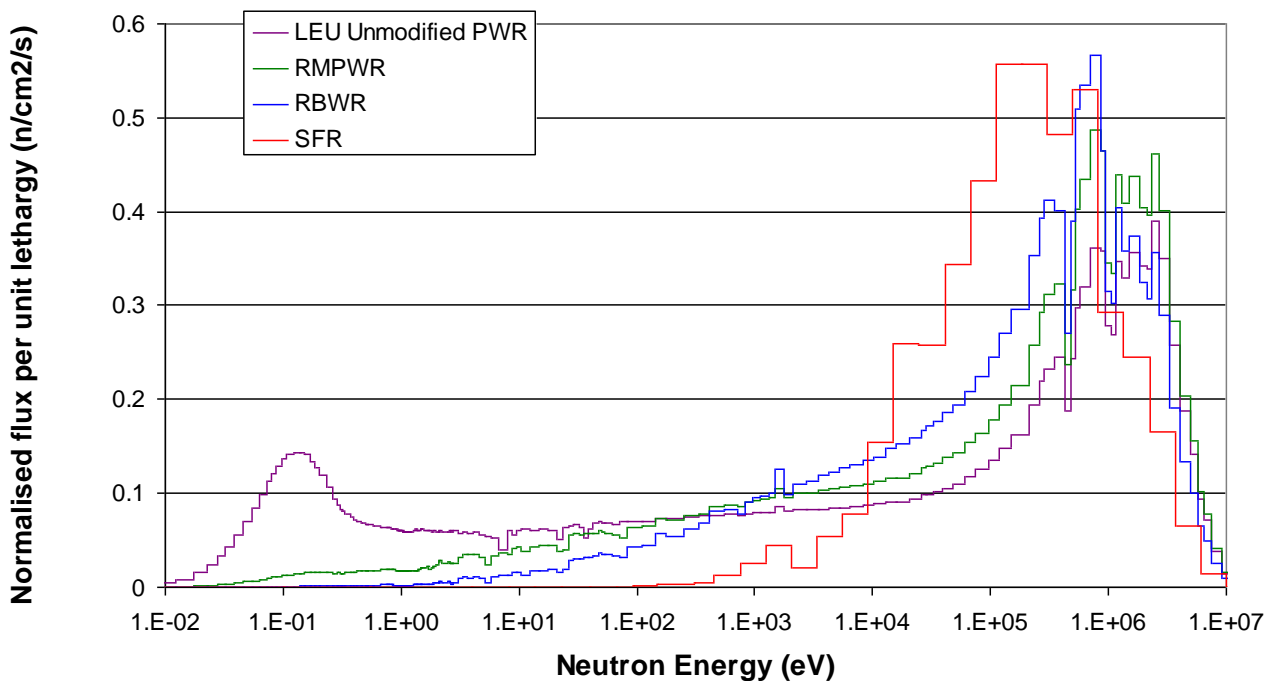


**Fig. 2.4.** Neutron spectra normalized per unit flux. For radially heterogeneous fuel assembly designs, i.e. assemblies having different fuel types in different lattice locations, the subgroup method was used to generate 172-group cross-sections for  $^{232}\text{Th}$ ,  $^{233}\text{U}$ ,  $^{239}\text{Pu}$  and  $^{240}\text{Pu}$  to properly treat resonance interaction. This method is computationally expensive with factorial complexity so only the most important isotopes are considered. Other isotopes are treated using equivalence theory (Powney and Newton, 2004).

In all the cases analysed, the equilibrium cycle composition was determined by running the models for a sufficient number of recycles at an assumed equilibrium cycle burn-up, with full actinide recycle assuming no losses and 5-year cooling time between irradiation cycles. This procedure was chosen as it is easy to automate. This means that the burn-up during the transient may be incorrect,

<sup>9</sup> The SFR spectrum was calculated by Dr C. Fiorina, PSI, Zurich, Switzerland.

but this is irrelevant as the transient is not being analysed. It was found that after about 20 recycles the isotope vector was practically converged.<sup>10</sup> The equilibrium isotope vectors for representative single-tier cases are given in Table 2.4.

**Table 2.4.** Start-of-Cycle (SOC) equilibrium isotope vector (at/barn cm) for selected cases.

	RBWR homogeneous 26% TRU reload	RMPWR 11.5 mm pin OD homogeneous 45% TRU reload	RMPWR 11 mm pin OD heterogeneous 50% TRU reload 132 Th-TRU pins	RMPWR 11 mm pin OD heterogeneous 52.5% TRU reload 152 Th- TRU pins	RMPWR 11.5 mm pin OD heterogeneous 40% TRU reload 132 Th-TRU pins
<sup>241</sup> Am	1.391E-04	1.957E-04	3.158E-04	3.226E-04	2.643E-04
<sup>242m</sup> Am	5.374E-06	5.079E-06	8.525E-06	8.573E-06	7.780E-06
<sup>243</sup> Am	7.251E-05	1.359E-04	1.708E-04	1.838E-04	1.488E-04
<sup>242</sup> Cm	3.548E-09	1.285E-08	1.467E-08	1.468E-08	1.190E-08
<sup>243</sup> Cm	4.353E-07	1.077E-06	1.108E-06	1.194E-06	9.815E-07
<sup>244</sup> Cm	4.029E-05	1.005E-04	1.143E-04	1.317E-04	1.012E-04
<sup>245</sup> Cm	2.237E-05	5.154E-05	4.847E-05	5.630E-05	4.482E-05
<sup>246</sup> Cm	1.667E-05	4.322E-05	4.586E-05	5.031E-05	4.171E-05
<sup>247</sup> Cm	3.824E-06	8.047E-06	1.068E-05	1.137E-05	1.014E-05
<sup>248</sup> Cm	1.492E-06	3.947E-06	5.010E-06	5.327E-06	4.633E-06
<sup>237</sup> Np	7.273E-05	9.483E-05	1.293E-04	1.290E-04	1.081E-04
<sup>238</sup> Pu	2.210E-04	3.867E-04	5.345E-04	5.567E-04	4.569E-04
<sup>239</sup> Pu	3.567E-04	5.097E-04	7.810E-04	8.412E-04	6.180E-04
<sup>240</sup> Pu	4.588E-04	6.281E-04	1.204E-03	1.247E-03	1.039E-03
<sup>241</sup> Pu	1.018E-04	1.958E-04	2.380E-04	2.707E-04	2.011E-04
<sup>242</sup> Pu	1.918E-04	3.745E-04	6.370E-04	6.713E-04	5.460E-04
<sup>232</sup> Th	1.639E-02	1.788E-02	1.660E-02	1.627E-02	1.712E-02
<sup>233</sup> U	1.109E-03	8.439E-04	5.667E-04	6.331E-04	6.697E-04
<sup>234</sup> U	3.935E-04	4.293E-04	4.906E-04	5.099E-04	5.094E-04
<sup>235</sup> U	1.433E-04	1.843E-04	1.421E-04	1.467E-04	1.514E-04
<sup>236</sup> U	1.067E-04	1.133E-04	1.460E-04	1.426E-04	1.453E-04
O	3.970E-02	4.437E-02	4.437E-02	4.437E-02	4.437E-02

The <sup>232</sup>Th content varies between 73% and 83%, and is lower when the TRU reload fraction is larger. The U3 content is in the range 6–9% and the TRU content is in the range 9–20%. The

<sup>10</sup> <sup>246</sup>Cm and above isotopes are not fully converged to equilibrium due to the impractically long time required for convergence. The impact on reactor physics is negligible.

RBWR has the highest U3 content as the hard neutron spectrum due to reduced moderation encourages breeding. It also has the lowest TRU content due to the low TRU reload fraction. The softer neutron spectrum also has an effect as this increases the build-up of heavier isotopes through successive captures, e.g. higher isotopes of Cm.

The TRU is ~78% Pu, although this varies slightly between cases. The RMPWR fuel contains ~2% Am and ~1% Cm, while the RBWR Am and Cm content is about half this, again due to the lower TRU reload fraction. In all cases the fuel contains ~0.5% Np. Some  $^{237}\text{Np}$  is produced from  $^{236}\text{U}$  neutron capture. The Pu fissile fraction ( $^{239}\text{Pu}$  and  $^{241}\text{Pu}$ ) is 30–35% in each case, while the U3 fissile fraction ranges from ~54% for the 11 mm RMPWR to 71% for the RBWR.

The heterogeneous RMPWR fuels have higher TRU content and lower U3 content than homogeneous designs due to the harder spectrum in the Th-TRU region and the thermal spectrum in the Th-U3 region (see Section 2.4.4). The fuel isotope vectors are discussed in more detail in Chapter 7 and are further compared to FR incineration cycles in (Franceschini et al., 2013).

### ***2.3.2. Data Library Uncertainty and Treatment of Reduced Moderation***

WIMS was applied to the benchmark problem for Th-Pu MOX fuel in a standard PWR lattice (IAEA, 2003). The results from WIMS with JEF-2.2 and ENDF/B7.0 agreed very well with the results of the benchmark, with results either within the range of submitted solutions or exhibiting very minor deviations.

WIMS is capable of modelling thermal and fast systems, the latter through using ECCO within WIMS (Newton et al., 2008). RMPWRs and RBWRs have a significant thermal neutron flux, and hence a thermal reactor flux was assumed when deriving 172-group cross-sections. This capability uses a limited number of fast energy groups (31 groups above 183.2 keV) compared to fast reactor lattice physics analysis methods (Newton et al., 2008). Therefore some errors are incurred when it is applied to RM designs. Future work could consider whether assuming an epithermal or fast spectrum is more appropriate. To quantify some of these errors, a single 1.26 cm square pincell was modelled. The pin diameter was 9.5 mm and the pellet radius was 4.095 mm. The water density was varied between 0.707 g/cc, the nominal PWR operating conditions, and 0.0365 g/cc, full void in a BWR.  $k_{\infty}$  was calculated in WIMS and the Monte Carlo code MONK (Answers, 2001). MONK is used in UK licensing criticality applications. The WIMS 172-group data library was used in MONK to isolate errors from WIMS equivalence theory rather than the data library group structure. For data library availability reasons (in MONK), the JEFF-3.1 library was used in both cases. This data

library is not thought appropriate for Th applications,<sup>11</sup> but this is not a problem when testing the WIMS methodology, as opposed to the data library.

WIMS uses a two-stage procedure to solve the transport equation. First, a 172-group calculation is carried out in approximate geometry. This solution is used to condense to few (usually 6 or 11) energy groups (although a higher number of groups – e.g. 22 – is often used for MOX fuel), and then the problem is solved in detailed geometry. In this study, for the RBWR a 12-group scheme derived by Hitachi is used, which contains relatively high fidelity in the fast and epithermal neutron energy range (Downar et al., 2012). This group scheme was selected as it was specifically derived for the RBWR and hence is highly likely to provide a reasonable trade-off between accuracy and computational cost. For the RMPWR, an 11-group scheme from (Answers, 2004) is used, as this was found to give lower group condensation errors for the RMPWR than the 12-group scheme used for the RBWR and the 6-group scheme usually employed for LEU-fuelled PWR calculations in WIMS. The 11-group scheme gives more fidelity in the thermal energy range than the 12-group scheme used for the RBWR. For the RMPWR, it must be noted that the 22 group scheme typically used for MOX fuel is likely to give reduced condensation error, but for this study 11 groups was deemed to be a reasonable trade-off between accuracy and computational cost. Deriving an optimal group scheme is beyond the scope of this study.

For the single pincell, a detailed geometry solution in 172 groups is also evaluated. This is relatively computationally expensive, but allows isolation of errors from equivalence theory and the group condensation procedure. Ultimately, an epithermal reactor must either be analysed by Monte Carlo methods (computationally prohibitive for broad scoping studies such as this), or a careful study of the lattice code (and group structure) is required to minimize errors.

Four fuel isotope vectors were investigated: Th-Pu MOX, Th-U3-TRU typical of the composition in this study, U-Pu MOX and U-TRU derived in a similar manner to the Th-U3-TRU composition (see Section 2.4.1) (Table 2.5).

---

<sup>11</sup> Private communication with ANSWERS team, AMEC, Winfrith, United Kingdom, 2011.

**Table 2.5.** Fuel isotope vectors investigated (at/barn cm).

Isotope	Th-Pu	Th-U3-TRU	U-Pu	U-TRU
<sup>241</sup> Am		1.989E-04		3.507E-04
<sup>242m</sup> Am		5.218E-06		1.134E-05
<sup>243</sup> Am		1.364E-04		1.509E-04
<sup>242</sup> Cm		1.300E-08		1.905E-08
<sup>243</sup> Cm		1.087E-06		1.488E-06
<sup>244</sup> Cm		1.007E-04		1.165E-04
<sup>245</sup> Cm		5.162E-05		5.462E-05
<sup>246</sup> Cm		4.294E-05		4.110E-05
<sup>247</sup> Cm		8.072E-06		8.951E-06
<sup>248</sup> Cm		3.940E-06		4.103E-06
<sup>237</sup> Np		8.997E-05		7.145E-05
<sup>238</sup> Pu	2.290E-05	4.521E-04	2.290E-05	5.646E-04
<sup>239</sup> Pu	7.478E-04	5.269E-04	7.478E-04	1.752E-03
<sup>240</sup> Pu	2.903E-04	6.440E-04	2.903E-04	1.527E-03
<sup>241</sup> Pu	1.534E-04	1.981E-04	1.534E-04	3.105E-04
<sup>242</sup> Pu	5.010E-05	3.777E-04	5.010E-05	4.636E-04
<sup>232</sup> Th	2.059E-02	1.792E-02		0.000E+00
<sup>233</sup> U		8.457E-04		2.309E-09
<sup>234</sup> U		3.339E-04		4.631E-05
<sup>235</sup> U		1.582E-04		3.552E-05
<sup>236</sup> U		9.407E-05		2.079E-05
<sup>237</sup> U		1.216E-07		5.407E-08
<sup>238</sup> U		1.340E-07	2.059E-02	1.665E-02
O	4.371E-02	4.437E-02	4.371E-02	4.437E-02

The statistical error in MONK was 10 pcm. The discrepancy in  $k_{\infty}$  between WIMS and MONK for different group condensation schemes, and the direct errors from the condensation schemes are given in Tables 2.6(a)–(c).

**Table 2.6. (a)** Discrepancies (in pcm) in  $k_{\infty}$  between WIMS (172 group) and MONK.

Water density (g/cc)	Th-Pu	Th-U3-TRU	U-Pu	U-TRU
0.707	89	83	19	85
0.3535	529	347	566	371
0.17675	1244	643	1321	590
0.0365	2374	640	2139	511

**(b)** Errors (in pcm) in RMPWR and RBWR group condensation schemes in WIMS relative to no condensation.

Water density (g/cc)	Th-Pu		Th-U3-TRU		U-Pu		U-TRU	
	RMPWR	RBWR	RMPWR	RBWR	RMPWR	RBWR	RMPWR	RBWR
0.707	-170	-345	-252	-435	-292	-470	-429	-609
0.3535	-233	-488	-181	-314	-359	-593	-217	-355
0.17675	-216	-409	-88	-130	-265	-421	-56	-107
0.0365 <sup>12</sup>	-45	-37	-9	-5	-22	-26	-1	-2

**(c)** Discrepancies (in pcm) in  $k_{\infty}$  between WIMS with RMPWR and RBWR group condensation schemes and MONK.

Water density (g/cc)	Th-Pu		Th-U3-TRU		U-Pu		U-TRU	
	RMPWR	RBWR	RMPWR	RBWR	RMPWR	RBWR	RMPWR	RBWR
0.707	-80	-256	-169	-352	-273	-451	-344	-525
0.3535	295	41	167	34	208	-26	154	16
0.17675	1028	835	555	514	1056	901	534	484
0.0365	2329	2337	631	634	2117	2113	510	509

Errors up to 634 pcm are observed for Th-U3-TRU in the fully voided case with 11- or 12-group condensation schemes. These errors are relatively good, given a thermal spectrum was assumed, but there is some error cancellation at higher moderation between group condensation and equivalence treatment. The 11-group scheme generally performs better than the 12-group scheme, in particular for a water density of 0.3535g/cc and above, which suggests it is suitable for the RMPWR.

As expected, the error incurred in the 172-group calculations increases as the water density decreases. This is particularly true for the fully voided and 0.17675 g/cc cases. WIMS tends to

<sup>12</sup> The condensation error at low water density is extremely low. This is likely to be the result of low errors in the approximations in the collision probability method used for group condensation, itself likely the result of the hard neutron spectrum acting to limit the impact of fuel assembly heterogeneity.

overestimate  $k_{\infty}$  and this effect increases at lower moderation. In particular, this has the effect of increasing the difference in reactivity between fully voided and operating conditions by ~900 pcm. This is a ‘conservative’ error but should be considered when drawing conclusions about the viability of a given design based on a negative MTC/VC criterion. Errors in the cross-section preparation for burn-up obviously propagate into the evaluated isotope vector over multiple recycles, so their effect is difficult to estimate.

The code performs worse for the relatively ‘pure’ MOX fuels at low VFs. This is thought to be due to the relatively high significance of errors in the treatment of  $^{232}\text{Th}$  and  $^{238}\text{U}$  due to the higher fertile proportion relative to the Th-U3-TRU and U-TRU fuels. To gain some understanding behind these errors, the discrepancies in microscopic cross-sections of the actinides for the Th-U3-TRU and U-TRU cases were investigated. The discrepancies in  $\eta = \nu\sigma_f/\sigma_a$  are tabulated for the actinides in Table 2.7.

As the H/HM ratio is reduced, the discrepancy in  $\eta$  becomes more positive for the fertile isotope ( $^{232}\text{Th}$  and  $^{238}\text{U}$  for Th-U3-TRU and U-TRU respectively – highlighted in bold). This correlates with the larger discrepancy of the Th-MOX and U-MOX cases, where  $^{232}\text{Th}$  and  $^{238}\text{U}$  captures and fissions at high VFs are more significant. The ~2% error in  $^{232}\text{Th}$  and  $^{238}\text{U}$   $\eta$  is a combination of ~1% errors in capture and fission cross-sections in both cases.

It should also be noted that as the spectrum becomes harder, the importance of the  $^{232}\text{Th}$  and  $^{238}\text{U}$  fast fission increases. This results in errors due to the group structure. Many groups are required in the vicinity of the fission thresholds to accurately capture the flux gradients in this region.<sup>13</sup> The fast reactor cell code ECCO (Rimpault et al., 2002), which is available in WIMS 10, (Newton et al., 2008), could be used to model these geometries, as it utilizes a much higher number of energy groups in the fast energy region. However, this is thought to be unsuitable to model the significant thermal neutron flux and hydrogen scatter still present in an RMPWR or RBWR.

The same cases (Table 2.5) were run with a 172-group calculation in WIMS with the JEF-2.2, JEFF-3.1 (for completeness) and ENDF/B7.0 data libraries to investigate the effect of data library differences. The differences between the data libraries are plotted in Fig. 2.5, with the differences plotted relative to JEF-2.2, which is the library used for the RBWR/RMPWR reactor physics calculations in the remainder of this chapter.

---

<sup>13</sup> Private communication with ANSWERS team, AMEC, Winfrith, United Kingdom, 2013.

**Table 2.7.** Discrepancies (%) in  $\eta$  for actinides for WIMS 11-group condensation relative to MONK.

	Th-U3-TRU				U-TRU			
Water density (g/cc)	0.707	0.3535	0.17675	0.0365	0.707	0.3535	0.17675	0.0365
H/HM (area ratio for 0.707 g/cc, relative to this for other cases)	1.67	0.83	0.42	0.09	1.67	0.83	0.42	0.09
<sup>241</sup> Am	0.51	1.28	1.69	0.80	1.09	1.45	1.68	0.99
<sup>242m</sup> Am	0.01	0.02	0.02	0.00	0.00	0.01	0.02	0.02
<sup>243</sup> Am	-1.10	-0.55	-0.20	0.44	0.14	0.09	0.09	0.70
<sup>242</sup> Cm	-0.51	-0.39	-0.37	-0.04	0.07	0.10	0.09	0.19
<sup>243</sup> Cm	0.01	0.00	-0.02	-0.03	0.00	0.00	-0.01	-0.01
<sup>244</sup> Cm	-1.27	-1.10	-1.31	-0.14	-1.21	-1.80	-2.10	-0.37
<sup>245</sup> Cm	-0.02	-0.02	-0.02	-0.03	0.05	0.07	0.06	-0.01
<sup>246</sup> Cm	-0.30	-0.05	0.02	0.21	-0.25	-0.14	0.02	0.34
<sup>247</sup> Cm	-0.14	-0.10	-0.03	0.04	0.03	-0.02	0.00	0.07
<sup>248</sup> Cm	-0.53	-0.64	-0.87	-0.23	-0.25	-0.78	-1.29	-0.59
<sup>237</sup> Np	-0.16	-0.13	-0.03	0.27	1.19	1.44	1.49	0.96
<sup>238</sup> Pu	-0.01	-0.15	-0.33	-0.17	-0.25	-0.28	-0.27	-0.03
<sup>239</sup> Pu	0.09	0.13	0.13	0.02	0.21	0.25	0.14	0.02
<sup>240</sup> Pu	-0.17	0.07	0.47	0.69	0.94	1.12	1.11	0.18
<sup>241</sup> Pu	-0.03	-0.09	-0.11	-0.04	0.13	0.14	0.10	0.03
<sup>242</sup> Pu	-1.33	-0.77	-0.13	0.56	0.67	0.44	0.49	0.51
<sup>232</sup> Th	<b>-0.49</b>	<b>1.11</b>	<b>2.17</b>	<b>2.30</b>				
<sup>233</sup> U	-0.01	0.00	-0.01	-0.01	-0.01	-0.04		
<sup>234</sup> U	1.03	1.78	2.35	1.29	0.46	1.07	1.20	0.96
<sup>235</sup> U	0.07	0.08	0.06	-0.01	0.08	0.05	-0.03	-0.01
<sup>236</sup> U	1.68	1.24	1.69	0.99	4.37	3.32	3.33	1.56
<sup>238</sup> U					<b>-0.47</b>	<b>1.26</b>	<b>2.51</b>	<b>2.59</b>

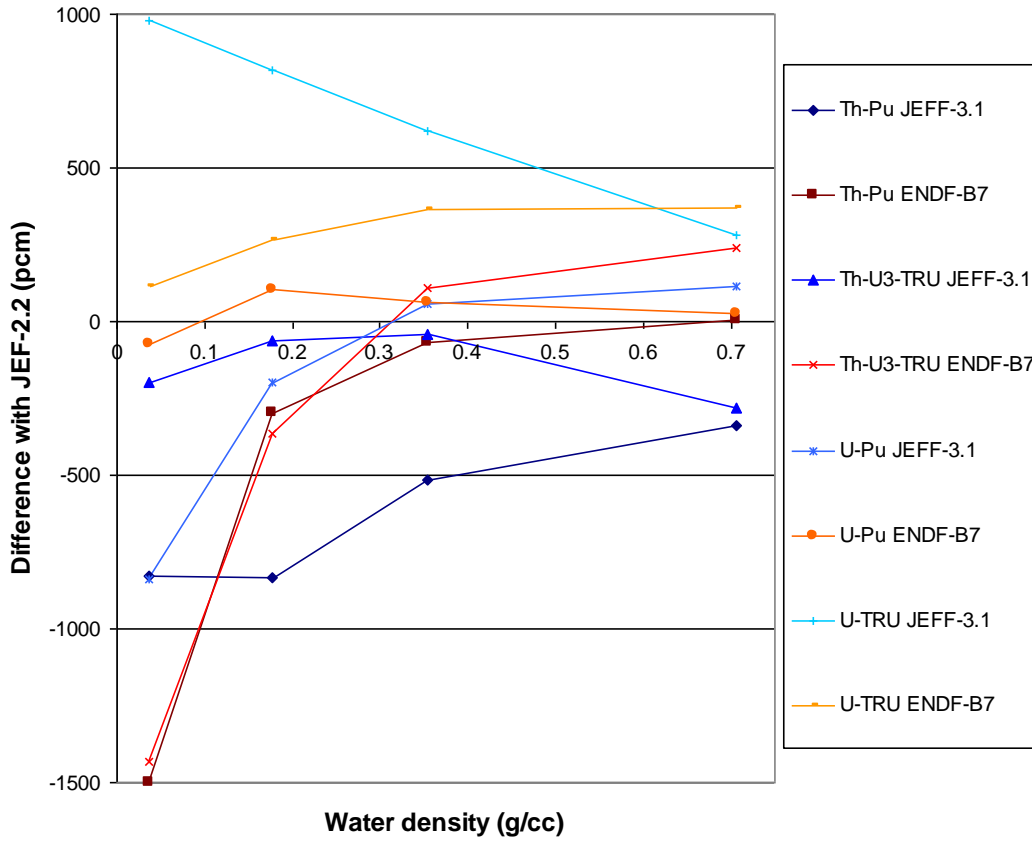


**Fig. 2.5.** Data library discrepancies.

While all libraries tend to agree relatively well at high density, larger discrepancies are observed at low water densities. At low water density, there is a large (up to 1500 pcm) difference between the ENDF/B7.0 and JEF-2.2 data libraries, and for the Th-U3-TRU case the difference between nominal and fully voided reactivity (FVR) is even greater. This will have a relatively small impact on equilibrium cycle calculations, but will lead to a much more pessimistic calculation of FVR in JEF-2.2. In Th-Pu, this effect is due to a higher resonance capture rate in  $^{232}\text{Th}$  in ENDF/B7.0 (Table 2.8). This is itself due to a higher resonance capture cross-section in the region 4–48 keV, so the most appropriate data library for these conditions is likely to depend on the accuracy of the  $^{232}\text{Th}$  capture cross-section in this region. The JEFF-3.1 library with Th fuel is generally offset from JEF-2.2, but will give a similar FVR.

**Table 2.8.** Capture rates in  $^{232}\text{Th}$  for Th-Pu fuel, 0.0365 g/cc, normalized per 1000 productions in pincell.

	Fast (20 MeV to 9119 eV)	Resonance (9119 eV to 0.625 eV)	Thermal (0.625 eV to 0 eV)
JEF-2.2	401.68	448.38	0.82
ENDF/B7.0	402.12	430.92	0.85

In the Th-U3-TRU case, also at 0.0365 g/cc, it is also worth noting the slightly higher  $\eta$  for  $^{233}\text{U}$  in JEF-2.2 compared to ENDF/B7.0, but the slightly lower  $\eta$  for  $^{239}\text{Pu}$  (Table 2.9). Differences in  $\eta$  between isotopes will lead to slight differences in the fuel cycle performance calculated using different data libraries.

**Table 2.9.**  $\eta$  for selected fissile isotopes, Th-U3-TRU fuel, 0.0365 g/cc.

	$^{233}\text{U}$		$^{239}\text{Pu}$	
	ENDF/B7.0	JEF-2.2	ENDF/B7.0	JEF-2.2
Fast	2.33	2.35	2.62	2.59
Resonance	2.14	2.22	1.63	1.61
Thermal	2.28	2.29	1.80	1.80

As already mentioned, any data library uncertainties will propagate through multiple recycles in a manner that is difficult to predict. The selected approach is therefore to derive and analyse an equilibrium cycle in JEF-2.2 and ENDF/B7.0. The “RMPWR 11.5 mm pin OD homogeneous 45% TRU reload” case from Table 2.4 was selected for this comparison. The equilibrium isotope vectors are compared in Table 2.10.

**Table 2.10.** Equilibrium isotope vectors for the RMPWR 11.5 mm pin OD homogeneous 45% TRU reload case.

Isotope	JEF-2.2	ENDF/B7.0	% difference
<sup>241</sup> Am	1.957E-04	2.001E-04	2.2
<sup>242m</sup> Am	5.079E-06	5.456E-06	7.4
<sup>243</sup> Am	1.359E-04	1.402E-04	3.2
<sup>242</sup> Cm	1.285E-08	1.297E-08	0.9
<sup>243</sup> Cm	1.077E-06	1.116E-06	3.6
<sup>244</sup> Cm	1.005E-04	9.933E-05	-1.2
<sup>245</sup> Cm	5.154E-05	5.397E-05	4.7
<sup>246</sup> Cm	4.322E-05	3.718E-05	-14.0
<sup>247</sup> Cm	8.047E-06	5.324E-06	-33.8
<sup>248</sup> Cm	3.947E-06	4.018E-06	1.8
<sup>237</sup> Np	9.483E-05	9.483E-05	0.0
<sup>238</sup> Pu	3.867E-04	3.739E-04	-3.3
<sup>239</sup> Pu	5.097E-04	5.112E-04	0.3
<sup>240</sup> Pu	6.281E-04	6.360E-04	1.3
<sup>241</sup> Pu	1.958E-04	1.958E-04	0.0
<sup>242</sup> Pu	3.745E-04	3.879E-04	3.6
<sup>232</sup> Th	1.788E-02	1.779E-02	-0.5
<sup>233</sup> U	8.439E-04	8.262E-04	-2.1
<sup>234</sup> U	4.293E-04	5.144E-04	19.8
<sup>235</sup> U	1.843E-04	1.811E-04	-1.7
<sup>236</sup> U	1.133E-04	1.316E-04	16.2

The most significant differences are the much larger <sup>234</sup>U and <sup>236</sup>U equilibrium populations for the ENDF/B7.0 case. The other differences are relatively minor.

The equilibrium cycle burn-up dependent  $k_{\infty}$ , MTC and FVR are compared in Fig. 2.6(a)–(c).

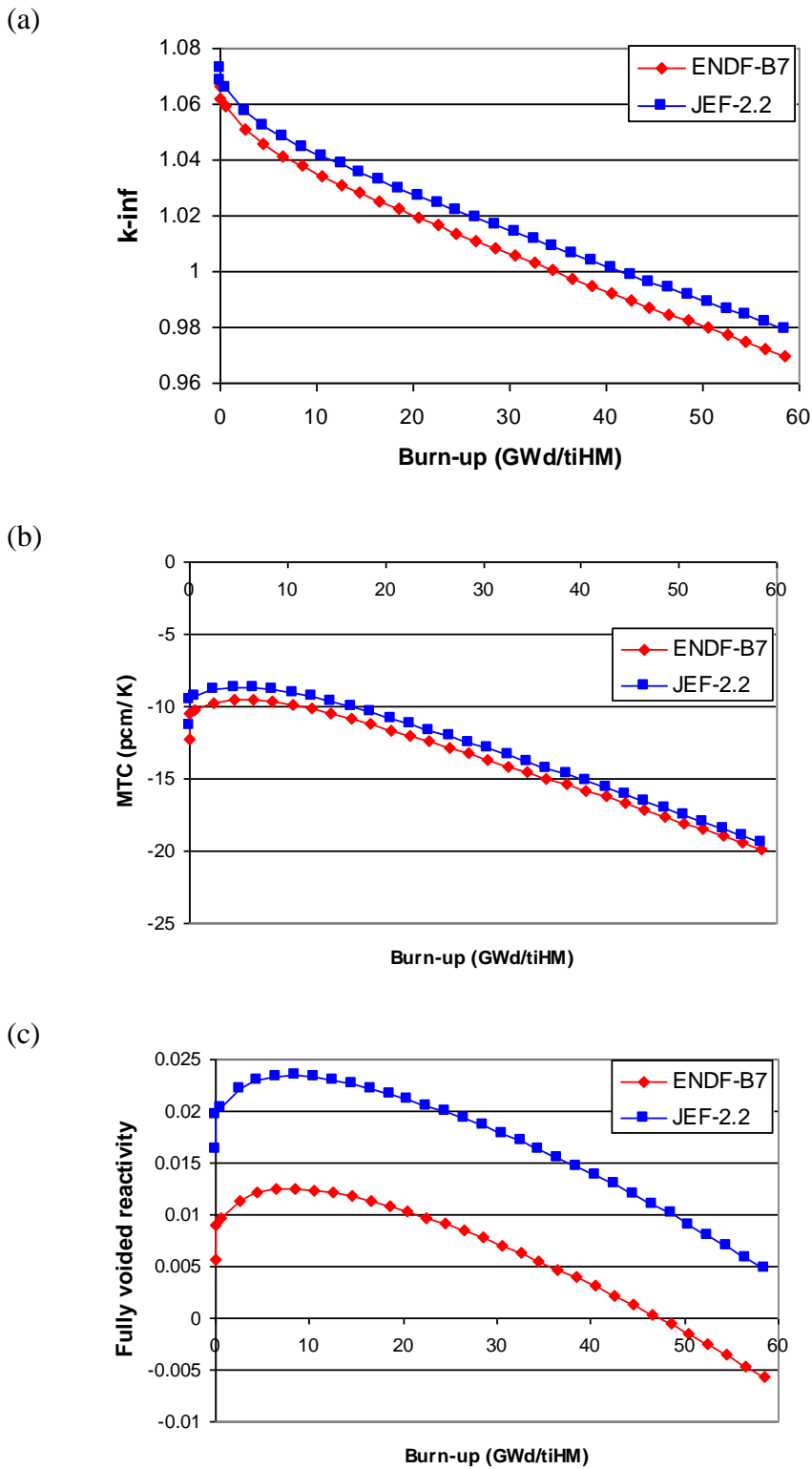


**Fig. 2.6.** (a)  $k_{\infty}$ , (b) MTC, (c) FVR variation without leakage for equilibrium cycles derived and analysed with ENDF/B7.0 and JEF-2.2.

JEF-2.2 predicts a higher  $k_{\infty}$  by  $\sim 0.01$  over the equilibrium cycle, which results in a longer equilibrium cycle (in this case  $\sim 5$  GWd/t difference in the one-batch burn-up), potentially due to lower equilibrium  $^{234}\text{U}$  and  $^{236}\text{U}$  populations. The MTC is very similar for both equilibrium cycles,

but is  $\sim 1$  pcm/K more negative for ENDF/B7.0. As expected, ENDF/B7.0 predicts lower FVR by  $\sim 1000$  pcm.

The choice of the JEF-2.2 data library therefore appears to result in a longer equilibrium cycle but a significantly higher FVR. This is preferable because it is likely to lead to the most conservative results for the FVR, for which there is a great degree of uncertainty.

## 2.4. Results

### 2.4.1. RMPWR Homogeneous Assembly

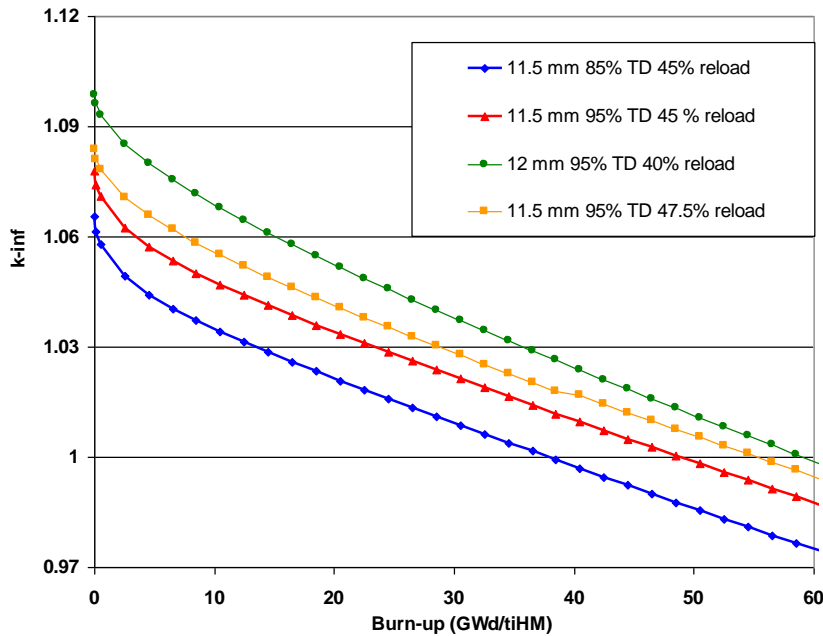
A sensitivity study with perturbed pin diameter and various TRU reload fractions was undertaken to assess the impact on hot-full-power MTC and  $k_{\infty}$ . For simplicity, a homogeneous assembly configuration was assumed. More specifically, the pin diameter within a standard  $17 \times 17$  PWR assembly was varied between 9.5 mm (current PWR fuel) and 12 mm. The TRU reload fraction in the feed was also varied. In addition, fuel smeared densities between 85% and 95% have been investigated, assuming that the lower range may be applicable for fuel with remote manufacturing requirements. The MTC was calculated without leakage, i.e. with 2D unit assembly geometry and reflective axial conditions. Leakage was estimated to improve the MTC by  $\sim 3$  pcm/K using a critical mode calculation. Reactivity control (e.g. burnable poisons (BPs)) generally makes the MTC substantially worse. The impact of control rods on MTC is beneficial (this is discussed in Section 2.4.2.1). The relative magnitude of these effects will be discussed later on.

The burn-up was calculated assuming a 3-batch fuel management scheme using the linear reactivity model (Driscoll et al., 1991) and  $k_{\infty} = 1.03$  to determine the end-of-cycle (EOC) length. A higher TRU reload fraction improves the burn-up capability but makes the MTC worse. A larger pin diameter improves the burn-up-MTC trade-off due to increased U3 breeding and improved fission to capture probability of TRU isotopes, but makes the incineration rate worse due to the increased conversion ratio.

The upper bound fuel density of 95% theoretical (95% TD) was used to try to identify a neutronically acceptable design (negative MTC and 3-batch burn-up  $> \sim 35$  GWd/t) as a fast enough neutron spectrum does not appear achievable with 85% TD fuel. Reducing the density of the fuel has the undesirable effect of increasing the H/HM ratio and therefore requiring a larger pin diameter for a given H/HM ratio. 95% TD may be difficult to achieve with a remote fuel manufacturing technique suitable for production of industrial amounts. With this optimistic assumption, a pin diameter of  $\sim 11.5$  mm was found to be the minimum. The corresponding 3-batch discharge burn-up was found to be  $\sim 35$  GWd/t for 45% TRU reload fraction, with the most positive MTC over the cycle being  $\sim -2$  pcm/K. Since the multi-recycle equilibrium vector was determined with an

estimated burn-up of 40 GWd/t, the start-of-cycle (SOC) equilibrium isotope vector used for the reactor physics calculation is optimistic, as reduced burn-up results in more  $^{241}\text{Pu}$  decay to  $^{241}\text{Am}$ , making the actual reactor performance worse. Further increase of the pin diameter improves the feasible cycle length (Fig. 2.7).

(a)



(b)

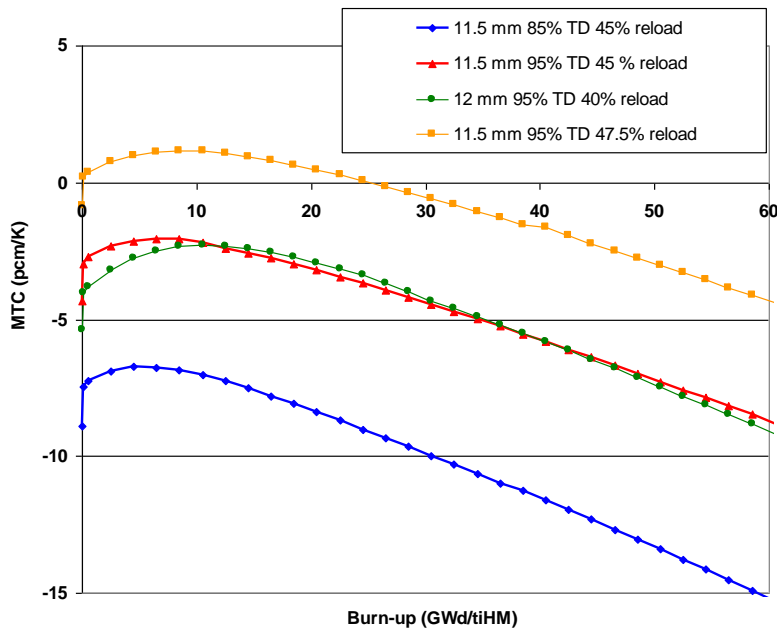


**Fig. 2.7.** (a)  $k_{\infty}$ , (b) MTC variation with burn-up for selected RMPWR cases.

As the burn-up is relatively low and increasing it results in a more positive MTC, it is desirable to take the maximum MTC as close to zero as possible. Fig. 2.7 shows the  $k_{\infty}$ -MTC trade-off for different pin diameters, TRU reload fractions ('reload') and fuel densities. With 11.5 mm pin

diameter, a change in TRU reload fraction from 45% to 47.5% (red to yellow) changes the MTC by  $\sim 3.5$  pcm/K but increases the one-batch burn-up by  $\sim 6$  GWd/t, showing that increased TRU reload fraction improves discharge burn-up but makes the MTC worse. The burn-up for 11.5 mm, 85% TD fuel is clearly unacceptable, especially in consideration of the very high fuel handling, manufacturing and reprocessing requirements and associated costs (blue compared to red). Increasing the pin diameter to 12 mm yields a large increase in burn-up at approximately the same MTC, hence delivering improved feasibility, although this is at the expense of lower TRU incineration rate. This is observed by comparing 11.5 mm 95% TD 45% TRU reload fraction (red) with 12 mm 95% TD 40% TRU reload fraction (green).

In all cases, the Doppler coefficient (DC) was around  $-3.5$  pcm/K for a uniform perturbation of fuel temperature from 900 K to 1000 K, which is slightly more negative than that of existing U cores, which typically exhibit a DC of between  $-2.6$  pcm/K and  $-3.4$  pcm/K with typical design limits of  $-2.0$  pcm/K and  $-3.5$  pcm/K (AREVA/EDF, 2011). The high resonance flux and use of Th in the reactor improves the DC, although this can be somewhat offset by higher fissile loading.

#### **2.4.2. Reactivity Control**

It has been shown that meeting the MTC constraint in a RMPWR while maintaining acceptable performance is a key challenge in core design. Typical neutron absorbers used for reactivity hold-down are predominantly thermal absorbers and thus make the MTC worse. It is therefore essential to control the reactor while minimizing the increase in MTC. Reactivity control is now investigated for the 11.5 mm pin diameter homogeneous assembly design.

Soluble boron is one of the main ways reactivity is controlled in PWRs. It does, however, make the MTC significantly more positive. As the coolant expands, the boron absorption cross-section decreases and the boron content of the core reduces. It is therefore essential to minimize the soluble boron concentration. In addition, the soluble boron worth is significantly reduced, from  $\sim -6.0$  pcm/ppm (unmodified 4.4 wt% LEU PWR SOC calculated for 1000 ppm) to  $\sim -0.6$  pcm/ppm, due to reduced coolant volume and the harder neutron spectrum. The MTC gets worse by  $\sim 0.007$  pcm/K/(pcm controlled). So, for every 1000 pcm of excess reactivity to be suppressed,  $\sim 1780$  ppm of unenriched boron is required, and this makes the MTC worse by 7 pcm/K. For comparison, the MTC gets worse by  $\sim 0.004$  pcm/K/(pcm controlled) in the unmodified LEU PWR. There are also operational and safety issues associated with high boron content and enrichment.

Stationary BPs (used here to describe also solid fixed poisons in the core including Gd mixed in the fuel, integral fuel burnable absorbers (IFBAs) and fixed burnable absorbers) are also very commonly used for power shaping and reactivity control. Black absorbers (which absorb a large proportion of incident neutrons and cause a large flux depression) or grey absorbers (which absorb

some incident neutrons) can be placed in some or all of the pins. The RMPWR has a harder neutron spectrum than a PWR which makes BPs less effective. They absorb fewer neutrons initially and also burn out more slowly, making it difficult to design them such that they burn out by the end of the first cycle.

Evenly distributing the BPs in the fuel increases the rate at which they burn out, but also makes their overall effect on the MTC worse. However, a localized heavy-worth BP (e.g. within a fuel pin or guide tube) will create a local flux dip, which mitigates the MTC by making the number of neutrons absorbed less sensitive to changes in the BP absorption cross-section following spectral changes.

The use of  $^{167}\text{Er}$  to improve the MTC by acting as a resonance absorber was proposed for similar configurations in (Rahman et al., 2012). This was found not to be effective as the 0.4 eV  $^{167}\text{Er}$  resonance was at too low an energy. The normalized flux at 0.4 eV increases with coolant temperature for a conventional LWR, but decreases for an RMPWR. In addition, due to the relatively low cross-section of  $^{167}\text{Er}$  and the presence of other mild absorbers in its depletion chain, it does not burn out sufficiently fast to make it an effective BP (Fig. 2.8).

Dispersed BPs can be implemented by mixing  $\text{Gd}_2\text{O}_3$  or  $\text{Er}_2\text{O}_3$  with the fuel or by applying a thin coating of  $\text{ZrB}_2$  (IFBA) respectively. IFBA coatings are typically 1.5 mg/inch, and 3–4.5 mg/inch may be possible. Distributed Er and Gd loadings can be selected based on the initial required reactivity worth of the poison, but must be configured such that they burn out within the first cycle. For the poison to burn out sufficiently quickly, only Gd appears to have a sufficiently high absorption cross-section. This absorber would need to be added to a large number of pins in the RM designs to ensure burn-out within one cycle (Fig. 2.8). This is in contrast to  $\text{UO}_2$  fuel where Gd is only placed in a minority of pins to prevent burn-out over too short a time. Putting Gd in a small number of pins or concentrating  $^{10}\text{B}$  in burnable absorbers (i.e. fixed absorbers in the guide tubes) is not effective.

$\text{Gd}_2\text{O}_3$  is most effective in this spectrum as the capture cross-sections of  $^{155}\text{Gd}$  and  $^{157}\text{Gd}$  (~37 and 98 barns in this spectrum) are higher than the capture cross-section of  $^{10}\text{B}$  (~28 barns) and  $^{167}\text{Er}$  (~26 barns) leading to sufficiently rapid burn-out. It is potentially easier to mix Gd or Er into a radioactive pellet than to apply an IFBA coating to a radioactive rod. One issue is that Gd and Er are lanthanides, which makes them tend to stay with minor actinides (MAs) during reprocessing. However, in Section 2.4.4, a heterogeneous assembly is shown to be neutronically favourable, which does not require mixing of Gd or Er with MAs.

Gd distributed over a large number of pins deteriorates the MTC by ~0.004 pcm/K /(pcm controlled) which is just over half the figure for soluble boron.

### 2.4.2.1. Control Rods

One advantage of the Th-TRU fuelled RMPWR (or indeed a U-TRU fuelled RMPWR) is the relatively low reactivity swing over the cycle at equilibrium. Due to the high MA content of the feed, this low reactivity swing may also be true of transition cycles, but to determine this requires further analysis. From the linear reactivity model, it is estimated that without control rods or BPs, this could be as little as 2500 pcm for the homogeneous case and less than 5000 pcm for heterogeneous fuel assembly designs (see Section 4.4). Provided there is sufficient rod worth, this is sufficiently low to make mechanical shim an option for short- and long-term reactivity control in place of some or all of the soluble boron.

Highly enriched (95 at%  $^{10}\text{B}$  in the B considered here)  $\text{B}_4\text{C}$  rods are necessary for the RMPWR. The hard neutron spectrum necessitates  $^{10}\text{B}$  enriched  $\text{B}_4\text{C}$  rods to provide a sufficient shutdown margin. The same rod poison is also assumed for the RBWR, which is consistent with previous studies (Downar et al., 2012). The production and depletion of  $^{10}\text{B}$  will limit the rod life and result in a reduced control worth.

In contrast to other reactivity control mechanisms, the control rods improve the MTC. This is because the reduction in  $^{10}\text{B}$  absorption cross-section ensuing from the reduction in moderator density is outweighed by the increase in neutron flux on the control rod, so the overall number of captures increases. Essentially, if the control element is large enough, then it behaves more like a black absorber and the increase in flux (due to the decrease in absorption cross-section in the rest of the fuel assembly) becomes more significant than the decrease in the rod poison absorption cross-section.

A rod is a sufficiently high worth control element to improve the MTC. When the rod worth is reduced (by artificially reducing the  $\text{B}_4\text{C}$  density without changing the volume of displaced water in this case), the beneficial effect reduces. In this manner, it is possible to quantify how big a control element needs to be to improve the MTC (Fig. 2.9), and it is apparent that while a control rod has sufficient worth to make the MTC more negative, integral burnable absorbers do not.

While wet annular burnable absorbers (WABAs) have already been ruled out as they do not deplete sufficiently rapidly, the WABA worth is expected to be substantially less than  $-0.2$ , which from Fig. 2.9 is insufficient to improve the MTC. It is worth noting that replacing the coolant in the guide tubes by void (i.e. the act of displacing the coolant) makes the MTC worse by 2–3 pcm. There is therefore a significant MTC advantage in using mechanical shim to control reactivity.

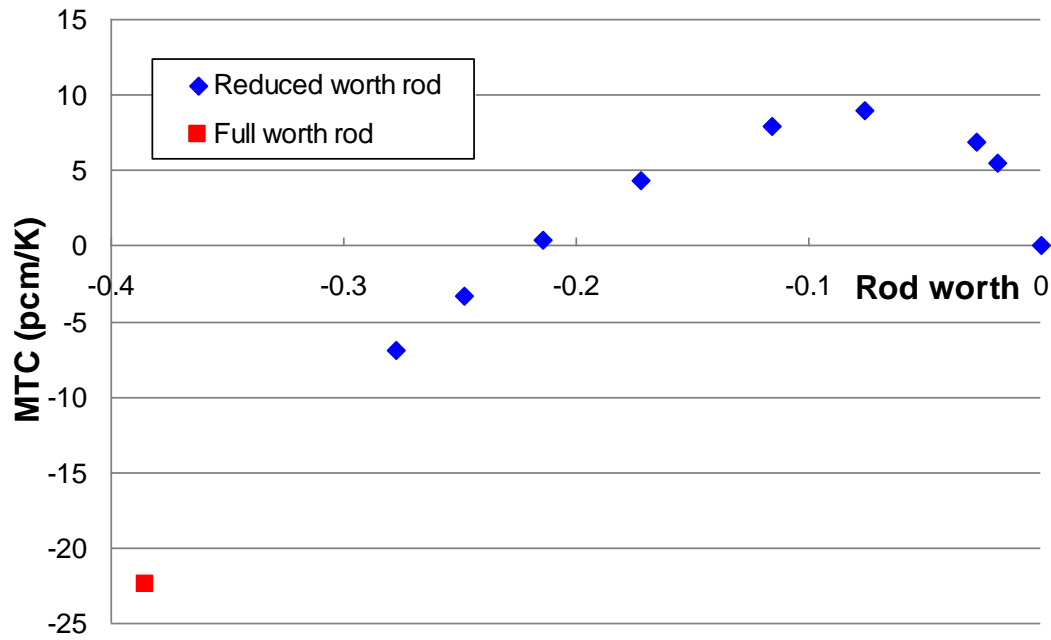


**Fig. 2.9.** Rod worth vs MTC (for a case with 0.0 pcm/K MTC when unrodded).

### 2.4.3. RBWR Homogeneous Assembly

125 cm and 200 cm core heights were considered, as reference ‘small’ and ‘large’ cores. 200 cm is similar to the height considered in (Ganda et al., 2011) for a Th breeder RBWR, and 125 cm is comparable to the U-Pu RBWR (Downar et al., 2012). Axially homogeneous RBWR fuel will be easier to manufacture remotely while enabling better thermal-hydraulic performance (from the reduced axial form factor) compared to the U-Pu RBWR fuel with an internal axial blanket. The assumed equilibrium cycle burn-up for generating the equilibrium isotope vector was 64 GWd/t with ratings of 15 MW/t (large core) and 24 MW/t (small core) and 5-year cooling times between cycles. Unlike for the RMPWR, the performance is relatively insensitive to these assumptions as the conversion ratio (and therefore the TRU reload fraction) is much closer to unity (as a result of the harder spectrum) and the  $^{241}\text{Pu}$  population is significantly smaller.

The RBWR equilibrium cycle is largely feasible from a reactivity feedback standpoint with homogeneous 85% TD fuel, although the TRU reload fraction is significantly lower resulting in a lower incineration rate but also a reduced build-up of higher actinides. As the neutron diffusion length is significantly larger in an RBWR than an RMPWR, and the core is shorter, leakage is a significant and useful mechanism to ensure a negative VC. Fig. 2.10 gives the performance of the equilibrium cycle for 26% and 30% reload fraction cases. These approximately correspond to the large and small cores. Leakage is estimated for each case using geometric bucklings of  $0.0004\text{ cm}^{-2}$  and  $0.0006\text{ cm}^{-2}$ , corresponding to 4.3% and 6.3% neutron leakage. The 2% increase in leakage approximately balances the 4% absolute increase in reload fraction, i.e. their influences on  $k_{\text{eff}}$  and

the VC approximately cancel at all fuel burn-ups. Both cases appear to have excellent discharge burn-up potential (with these leakage estimates the one-batch discharge burn-up, i.e. the burn-up at which  $k_{\text{eff}}$  is estimated to be 1, exceeds 40 GWd/t: see Fig. 2.10). The large low-leakage core does, however, have a slightly better  $k_{\infty}$  and VC at a given burn-up than the small high-leakage core, i.e. leakage is a less effective mechanism than reduced TRU reload fraction when optimizing the burn-up-VC trade-off.

The reactivity at 100% VF was also considered, i.e. the reactivity from operating conditions to a core filled with 100% steam at the operating pressure. The constraint on VC is that the global VC must be kept negative when the power and/or flow rate are perturbed. Here it is termed the ‘fully voided reactivity’ or FVR.<sup>14</sup> The FVR is useful for RBWRs because the VC is sensitive to how it is calculated. VCs based on 100% VF are often found to be a more limiting case (e.g. (Fukaya et al., 2009b)) and are the extreme (although non-physical) case of increased power or reduced flow. In particular, it is possible for the fully voided core to have positive reactivity if it contains a large amount of TRU. Therefore considering this condition as well as a VC based on flow rate perturbation is more conservative. The case of a single voided assembly is not considered physical or particularly relevant for a RBWR, although as axial leakage is the principal leakage mechanism, if these constraints are satisfied then it is probable that a single voided assembly also results in a negative VC.

The reactivity with zero water in the core, termed the zero coolant reactivity (ZCR), is also calculated. The ZCR and the FVR may be relevant in severe accidents, such as a large-break loss-of-coolant accident (LBLOCA) without scram. In this instance, the core depressurizes, and is partially or fully uncovered before reflood.

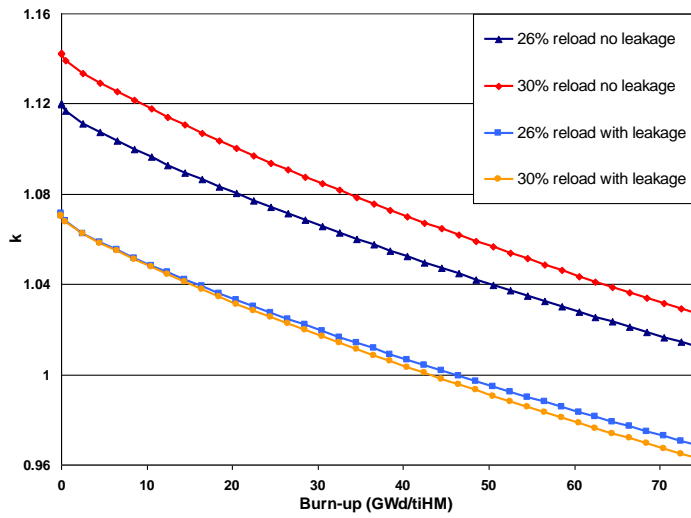
A full-core analysis is necessary to determine the FVR and ZCR accurately, but a 2D calculation with these buckling assumptions indicates that these parameters are negative for both cores when axially homogeneous Th-TRU fuel is used (Fig. 2.10c). For the RBWR, the FVR and the ZCR are essentially equal, with leakage. Hence in the RBWR core analysis (Chapter 6) it is deemed sufficient to consider the FVR.

The FVR and ZCR of the RMPWR are discussed in Chapter 5.

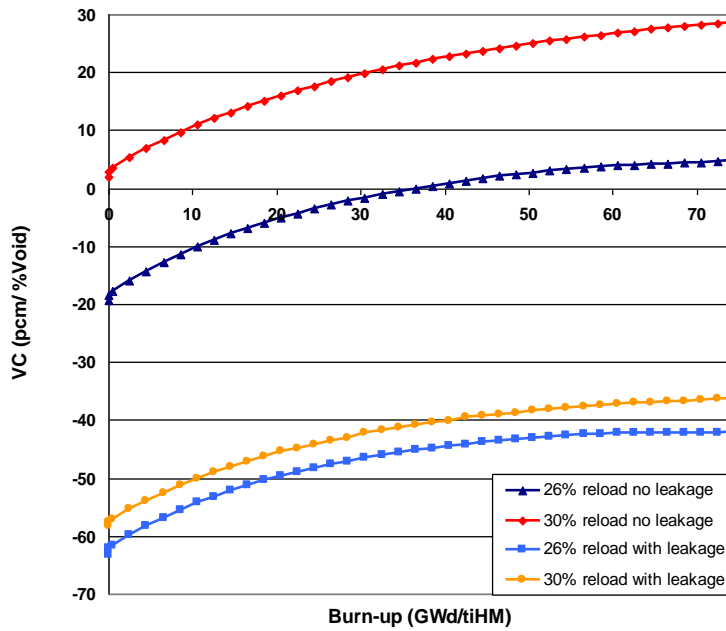
---

<sup>14</sup> This term is selected for consistency with published papers based on this work. Depending on the relevant core condition, FVR could reasonably be used to mean reactivity at zero coolant density or 100% VF.

(a)



(b)



(c)

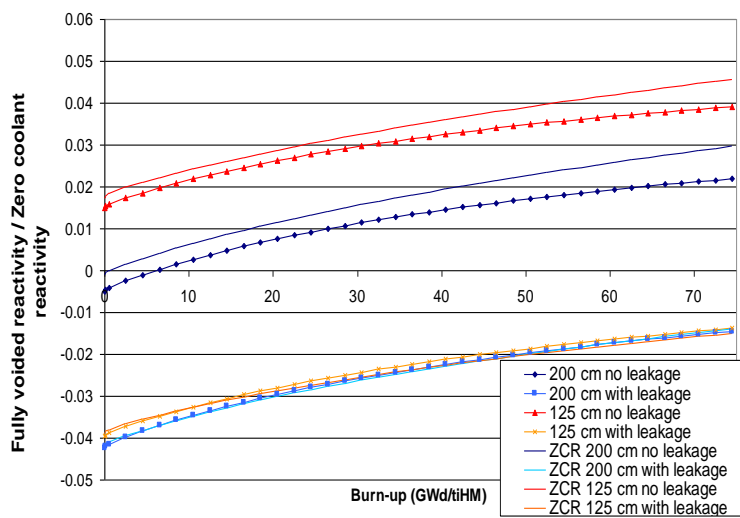


**Fig. 2.10.** (a)  $k_{\infty}$ , (b) VC variation, (c) FVR and ZCR with burn-up for selected RBWR cases.

#### 2.4.4. RMPWR Heterogeneous Assembly

Spatial separation of U3 and TRU has been shown to improve neutronic performance (Rahman et al., 2012) but would require a suitable elemental partition at the reprocessing stage. Both discharge burn-up and MTC are improved using this fuel configuration, and this can be attributed to an increase in thermal neutron flux in the U3-bearing pins and a decrease in thermal neutron flux in the TRU-bearing pins relative to the homogeneous fuel assembly configuration. These effects are caused by the high thermal absorption cross-section of TRU. The heterogeneous loading implemented here consists of placing Th-TRU pins in the Centre of the assembly and Th-U3 pins in the Periphery (TCUP) (Fig. 2.11).

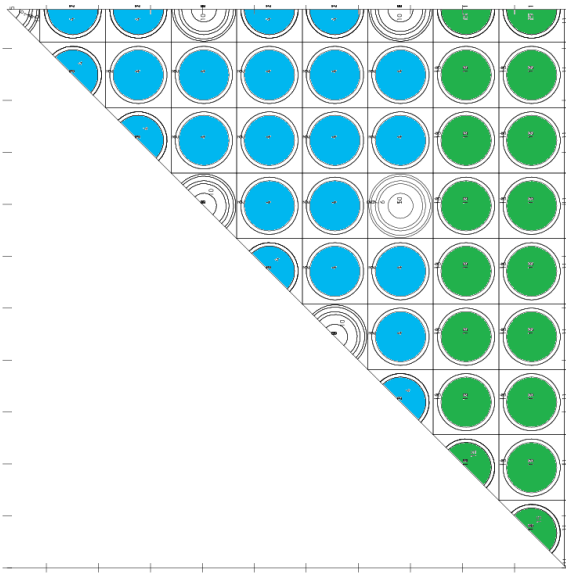


**Fig. 2.11.** 144 Th-TRU pin (blue) 120 Th-U3 pin (green) TCUP assembly design (WIMS model), one octant.

By concentrating the TRU in about half the pins, the TRU content for the Th-TRU pins is doubled. This leads to a significantly harder spectrum in this region (Fig. 2.12) and therefore larger fast fission contribution and improved neutron economy. By removing the TRU from the pins containing U3, the spectrum is made more thermal, increasing the thermal fission of U3. Overall, this leads to a decrease in resonance capture and an increase in  $\eta$ . The advantages of this design are quantified and analysed in detail in Chapter 3. A heterogeneous RBWR assembly is considered in Chapter 6.

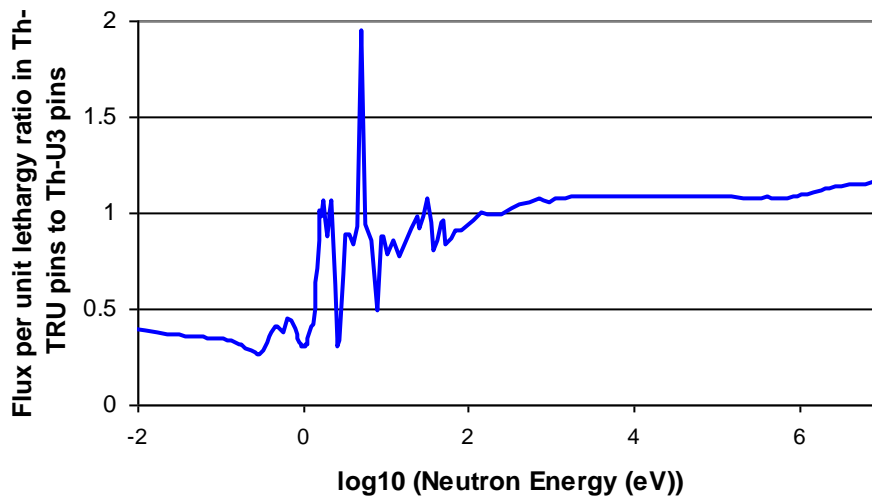


**Fig. 2.12.** Relative flux in Th-TRU pins compared Th-U3 pins in a TCUP assembly.

It must be noted that inverting this design (i.e. placing the Th-U3 in the centre and the Th-TRU pins at the periphery) to place the ‘thermal’ region near the guide tube holes leads to a slightly improved burn-up-MTC trade-off. However, the TCUP design is preferable if MAs are partitioned and placed as targets in the guide tubes positions (see Chapter 7) as they are then burned in a harder spectrum.

As a result of the more favourable neutronic properties, an 11 mm pin diameter was sufficient to obtain an equilibrium cycle with burn-up > 35 GWd/t and negative MTC, compared to 11.5 mm for the homogeneous assembly.

The reactivity is plotted against the burn-up for an uncontrolled heterogeneous assembly with the equilibrium fuel composition in Fig. 2.13. The relatively low reactivity swing is due to the harder spectrum and larger content of TRU isotopes with even mass-number, which effectively behave as fertile neutron absorbers. By suppressing reactivity and enhancing the conversion to fissile isotopes, they promote a flatter reactivity profile with irradiation. The thermal flux in the Th-U3 pins was found to be sufficiently high for Gd to be an effective BP (Fig. 2.13). Placing Gd in the Th-TRU pins was much less effective. While the number of Gd-bearing pins would be significantly increased with respect to the current configurations, the dominant factor increasing manufacturing costs is the requirement to remotely fabricate pins due to the presence of  $^{232}\text{U}$  in the fuel. Lighter absorbers such as  $^{167}\text{Er}$  do not burn out quickly enough and therefore appear to be unsuitable for RM designs.

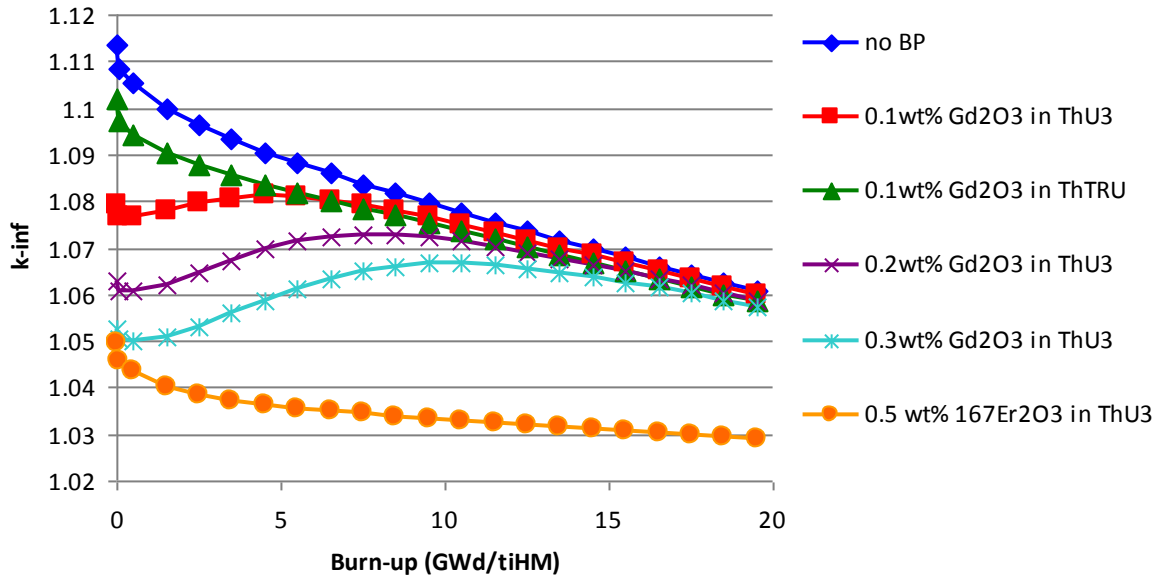


**Fig. 2.13.** Gd and Er BP burn-out for a typical TCUP equilibrium cycle.

Approximately 144 Th-TRU pins per assembly appears sensible to allow as even a power distribution as possible (Fig. 2.11; this is discussed in more detail in Chapter 5), and the performance of this design at different reload fractions is presented in Table 2.11. 3-batch burn-ups were estimated by multiplying the one-batch burn-up by 1.5 in accordance with the linear reactivity model.

**Table 2.11.** Performance of 144 Th-TRU pin TCUP assembly.

Reload fraction TRU (at%)	Equilibrium TRU at% in TRU pins	Discharge burn-up (GWd/t)	Maximum HFP MTC over cycle (pcm/K)	Assumed BU in convergence calculation (GWd/t)
45	28.3	27.1	-18.4	40
50	34.0	40.7	-10.8	40
52.5	36.8	51	-7.5	40
55	37.8	53.2	-5.9	40
52.5	37.2	56.2	-7.5	50
55	40.5	65.1	-3.8	50

As previously discussed, the assumed burn-up used when converging the equilibrium isotope vector affects results, and therefore a good estimate of this burn-up is required. From Table 2.11, it can be seen that an increase in the assumed burn-up for the isotopic convergence significantly affects the estimated discharge burn-up, TRU fraction and MTC. The overall effect of this is that underestimating the burn-up leads to pessimistic results.

The introduction of Gd BP in the fresh fuel results in a severe penalty to the MTC (Fig. 2.14). The full-core MTC can still be negative due to the negative MTC of the burned fuel assemblies but a

full-core evaluation is required to ascertain this (see Chapter 5). As previously discussed, high worth control rods have a beneficial effect on the MTC. With a marginally negative MTC, it is necessary to use control rods to suppress at least some of the remaining excess reactivity given that soluble boron has low worth and is highly disadvantageous to MTC. The reactivity swing over the cycle can be reduced to  $\sim 2000$  pcm using Gd BP, so it is conceivable to eliminate soluble boron for reactivity control (but it may not be possible to eliminate it altogether, e.g. it may be required to achieve cold shutdown).

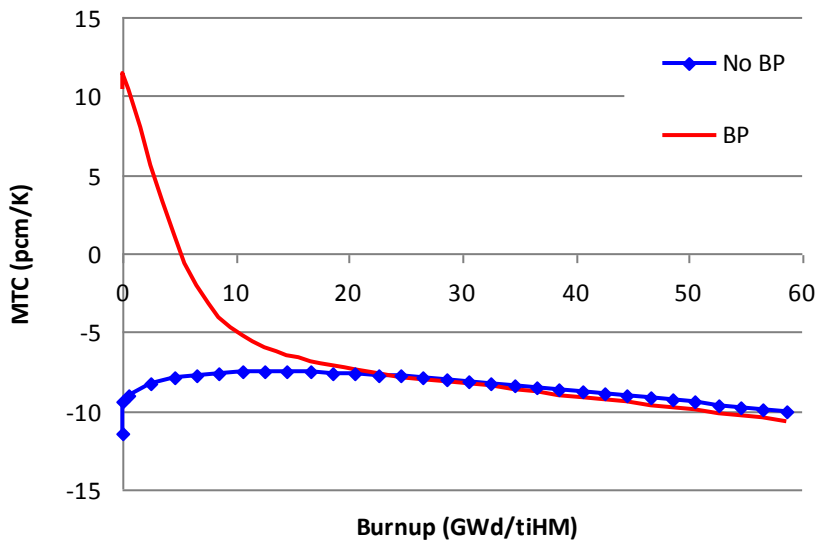


**Fig. 2.14.** TCUP assembly MTC over the core residence time.

#### 2.4.4.1. Non-uniform Temperature Perturbations over the Assembly

The heterogeneous design has an additional secondary effect on the MTC. It was found that when the coolant density was reduced, the reaction rate in the Th-TRU pins increased. Therefore it is not valid to calculate the MTC by uniformly perturbing the coolant density. The coolant density distribution should be obtained coupling the lattice calculation with a subchannel analysis. However, it is a sufficiently good approximation to calculate the density variation with an assumed power shape. Using WIMS, a uniform change in coolant density from 0.707 g/cc to 0.655 g/cc was found to perturb the power distribution between Th-TRU and Th-U3 by  $\sim 1\%$ . This change in power shape was used in a COBRA model (Basile et al., 1987, updated 1999). The relative change in coolant density between Th-TRU and Th-U3 channels was  $\sim 0.1\%$ . The MTC was then recalculated using coolant densities calculated from the power distributions in the subchannel model. This made the MTC worse by  $\sim 1$  pcm/K by reducing the negative feedback effect of Th-U3 and increasing the positive feedback effect of Th-TRU.

The variable moderator density within the assembly itself affects the power distribution in the assembly (i.e. the power distribution and moderator density are coupled). The power distribution

was recalculated using variable moderator density and was essentially unchanged (a 0.04% negative feedback effect was observed, where the reduced moderator density around the Th-TRU pins very marginally reduced their power under perturbed conditions), so the above calculation can be regarded as being ‘converged.’

The DC is  $\sim -3.5$  pcm/K for perturbations to the fuel temperature in both the Th-TRU and Th-U pins so differential heating during rapid transients should not be an issue.

#### *2.4.4.2. Power Distribution within Assembly*

Careful enrichment balancing is required to maintain adequate power peaking over the core residence time. This is due to the large spectral difference across the assembly and the different variations of  $k_{\infty}$  with burn-up in the Th-TRU and Th-U3 regions of the assembly.

As a result of the higher thermal flux and fission cross-section, the U3 burns out much faster than the TRU, leading to large power redistributions and high power peaking over the core residence time. This can be limited during the first irradiation cycle by using BPs and fissile zoning. Power peaking may become problematic for subsequent cycles, although the hot assembly is likely to be in either the first or second batch, which acts to mitigate this.

BPs can help balance the power peaking over the first cycle by keeping an even power sharing between the Th-U3 and Th-TRU regions (Fig. 2.15). In subsequent cycles, the assembly power peaking becomes significantly worse, but by ensuring the ‘hot’ assembly has an adequate form factor, the overall core form factor should be acceptable.

To minimize the power peaking of the hot pin, fissile zoning is required. In particular, since the flux on the Th-TRU pins close to the Th-U3 pins is relatively thermalized, a reduction of their fissile content can be adopted to avoid power spikes. For the 152 Th-TRU pin assembly of Fig. 2.15. with no fissile zoning, the power peaking at SOC is 1.16 (Fig. 2.16) increasing to 1.21 at 20 GWd/t. Fissile zoning is considered in Chapter 5.

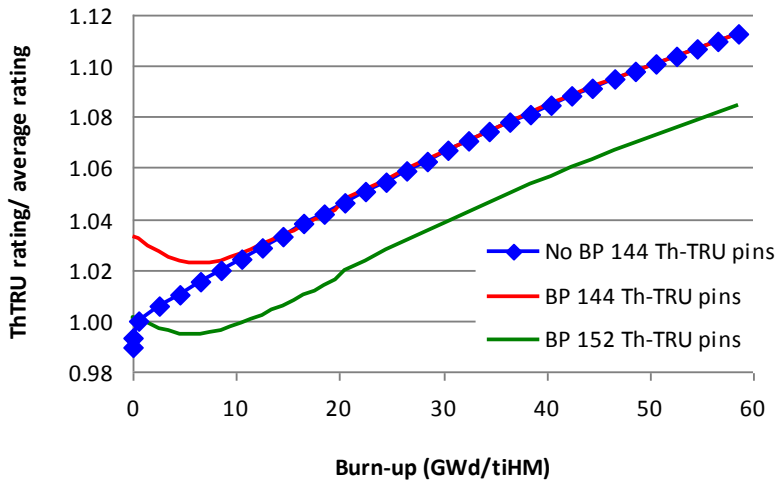


**Fig. 2.15.** Power share of Th-TRU region for 52.5% reload TCUP assembly (1) without BPs, (2) with Gd BPs, which reduces power redistribution over first cycle, (3) appropriate adjustment of the number of Th-TRU pins from 144 to 152 to minimize initial power imbalance.

IT									
0.95	0.91								
0.95	0.91	0.92							
GT	0.96	0.97	GT						
0.96	0.93	0.94	0.99	1.00					
0.99	0.94	0.96	1.04	1.09	GT				
GT	1.02	1.08	GT	1.16	1.16	0.97			
1.08	1.07	0.93	1.01	0.98	0.97	1.00	1.02		
0.92	0.94	0.97	1.00	1.01	1.02	1.03	1.05	1.07	

Th-U3
Th-TRU
GT/IT

**Fig. 2.16.** Power peaking for 152 Th-TRU pin TCUP assembly with no fissile content variation.

### 2.5. Concluding Remarks

With sufficiently reduced moderation, a Th-fuelled LWR can operate on full TRU recycle while burning an external supply of TRU, e.g. recovered from reprocessing used fuel discharged from once-through LWR operation. A Westinghouse 17x17 PWR assembly with 12.6 mm pin pitch can achieve sufficiently low moderation to perform full TRU recycle if the pin diameter is increased from 9.5 mm to 11–11.5 mm. This requires fuel of 95% theoretical density to sufficiently reduce the H/HM ratio, and spatial separation of TRU from U3 is also necessary to improve neutronic performance. However, an RBWR has a sufficiently fast neutron spectrum to comfortably maintain a high burn-up equilibrium fuel cycle even with homogeneous 85% TD fuel. This is not possible if  $^{238}\text{U}$  is used as a fertile isotope. This reactor and fuel designs introduced in this chapter will be used as a basis for further design and analysis in the subsequent chapters.

## **Chapter 3 – Void Reactivity Feedback Analysis**

In Chapter 2, it was established that the TRU incineration performance of RM LWRs is limited by coolant reactivity feedback. Generalizing for RMPWRs and RBWRs, the moderator density coefficient (MDC) must be kept negative. The MDC is worse when more TRU is loaded, but TRU feed is also needed to maintain criticality.  $^{232}\text{Th}$  has been selected as a fertile isotope to improve the MDC. To establish its performance advantage over  $^{238}\text{U}$  in LWRs, TRU incineration in three systems is compared: ‘reference’ PWRs, RMPWRs and RBWRs. The MDC of the equilibrium cycle is analysed by reactivity decomposition with perturbed coolant density by isotope and neutron energy. The results show that using  $^{232}\text{Th}$  as a fertile isotope yields superior performance to  $^{238}\text{U}$ . This is due essentially to the high resonance  $\eta$  (neutrons produced/neutrons absorbed) of U3, which increases the fissibility of the U3-TRU isotope vector in the Th-fuelled system relative to the U-fuelled system, and also improves the MDC in a sufficiently hard spectrum. The advantage of spatial separation of TRU and U3 in the Th-fuelled system renders further improvement by hardening the neutron spectrum in the TRU and softening it in the U3. This improves the TRU  $\eta$  and increases the negative MDC contribution from reduced thermal fission in U3.

### **3.1. Introduction**

As discussed in Chapter 1, the favourable  $^{232}\text{Th}$  void reactivity effect compared to  $^{238}\text{U}$  has resulted in recent interest in use of Th fuel across a range of reactor platforms. The beneficial effect of Th on the MDC is well known, and the mechanisms for this have previously been studied for single-pass Th-Pu designs (Xu et al., 2002) and fast reactors (Fiorina et al., 2013b). Notably,  $^{232}\text{Th}$  has a much lower fast fission cross-section than  $^{238}\text{U}$ , and  $^{233}\text{U}$  has a higher resonance  $\eta$  and lower fast  $\eta$  than  $^{239}\text{Pu}$  with the fission cross-section decreasing steeply with neutron energy at high energies (Fiorina et al., 2013b).

In this chapter, the contributions to the reactivity change with moderator density are decomposed by energy and isotope for U- and Th-fuelled PWRs, RMPWRs and RBWRs.

### **3.2. Method**

#### ***3.2.1. Reactivity Decomposition***

Reactivity ( $\rho$ ) can be expressed in terms of the sum of absorptions ( $A_i$  using suffix notation) and productions ( $P_i$ ) within the reactor, where (n, 2n) reactions are treated as negative absorption:

$$\rho = \frac{k-1}{k} = 1 - \frac{A_i}{P_i} \quad (3.1)$$

where  $k$  is the neutron multiplication factor. The reactivity change with respect to coolant density can therefore be expressed as:

$$\Delta\rho = \frac{d\rho}{d\rho_d} \Delta\rho_d = -\frac{d}{d\rho_d} \left( \frac{A_{ii}}{P_{ii}} \right) \Delta\rho = \frac{1}{P_{ii}} \left( -\frac{\partial A_{ii}}{\partial \rho_d} + \frac{A_{ii}}{P_{ii}} \frac{\partial P_{ii}}{\partial \rho_d} \right) \Delta\rho_d \quad (3.2)$$

where  $\rho_d$  is the coolant density.

For a small perturbation in coolant density, with reaction rates normalized relative to the production rate, Eq. 3.2 can be expressed as:

$$\Delta\rho = \left( -\Delta A_{ii} + \frac{1}{k} \Delta P_{ii} \right) \quad (3.3)$$

For a given subset of isotopes and energy groups,  $j$ , the contribution to the reactivity change is:

$$\Delta\rho_j = \left( -\Delta A_j + \frac{1}{k} \Delta P_j \right) \quad (3.4)$$

For consistency between PWRs and BWRs, the reactivity change is evaluated as an MDC (instead of a temperature or void coefficient), calculated at beginning-of-equilibrium-cycle. The MDC is calculated for a 20 K change in temperature, corresponding to a 0.052g/cm<sup>3</sup> expansion of the coolant for PWRs, and for a change in VF from 45% to 65% for BWRs, corresponding to a 0.140 g/cm<sup>3</sup> change in coolant density. Leakage effects are not included to simplify the comparison.

### 3.2.2. Fuel Cycle Modeling

The feed to incinerate consists of TRU with either <sup>238</sup>U or <sup>232</sup>Th as the fertile component. The single-tier TRU feed from Chapter 2 is utilized, with the equilibrium cycle composition determined by iterating the neutronic simulations for a sufficient number of recycles with a fixed TRU reload fraction in the feed at an assumed equilibrium cycle burn-up (40 GWd/t in the PWR and RMPWR; 60 GWd/t in the RBWR), with full actinide recycle assuming no losses. The exception was the first cycle (i.e. ‘fresh’ Th-TRU) where the fuel was Th-20 at% TRU, to ensure that the interim cycles were representative, although not completely accurate.

To assess the performance of this fuel cycle in different neutron spectra, three fuel assembly configurations are considered: (1) a ‘reference’ PWR; (2) a reduced-moderation PWR (RMPWR); (3) a reduced-moderation BWR (RBWR). The cooling time between irradiation cycles is 5 years, except for the PWR where it is reduced to 1 year, which is necessary to generate a neutronically feasible equilibrium cycle. A long cooling time greatly increases <sup>241</sup>Pu decay into <sup>241</sup>Am which increases the TRU feed necessary to sustain criticality. Remote fabrication of high density fuel is likely to be difficult. Therefore a fuel density of 85% of theoretical was specified, except for the RMPWR where it is increased to 95% of theoretical, as this is necessary to generate a feasible

equilibrium cycle. This means that the performances of the reactors relative to each other are not directly comparable, but the effect of Th relative to U for different spectra can be observed. Equilibrium isotope vectors are given in Table 3.1.

**Table 3.1.** Equilibrium isotope vectors at loading (at%).

	PWR		RMPWR 11.5mm pin		RBWR	
	Th	U	Th	U	Th	U
<sup>241</sup> Am	0.96	1.12	0.88	1.58	0.67	1.15
<sup>242m</sup> Am	0.02	0.03	0.02	0.05	0.03	0.05
<sup>243</sup> Am	1.22	1.16	0.61	0.68	0.36	0.40
<sup>244</sup> Cm	1.55	1.60	0.45	0.53	0.20	0.25
<sup>245</sup> Cm	0.45	0.47	0.23	0.25	0.11	0.11
<sup>246</sup> Cm	0.40	0.39	0.19	0.19	0.08	0.08
<sup>247</sup> Cm	0.06	0.06	0.04	0.04	0.02	0.02
<sup>248</sup> Cm	0.03	0.03	0.02	0.02	0.01	0.01
<sup>237</sup> Np	0.64	0.51	0.43	0.32	0.36	0.21
<sup>238</sup> Pu	3.06	3.10	1.74	2.55	0.99	1.14
<sup>239</sup> Pu	3.96	6.97	2.30	7.90	1.66	7.74
<sup>240</sup> Pu	4.77	6.45	2.83	6.88	2.19	6.50
<sup>241</sup> Pu	2.13	2.66	0.88	1.40	0.49	0.86
<sup>243</sup> Pu	4.22	4.12	1.69	2.09	0.92	1.17
<sup>232</sup> Th	71.5		80.6		82.9	
<sup>233</sup> U	2.88		3.80		5.59	
<sup>234</sup> U	1.15	0.17	1.94	0.21	2.14	0.36
<sup>235</sup> U	0.65	0.14	0.83	0.16	0.76	0.17
<sup>236</sup> U	0.32	0.07	0.51	0.09	0.57	0.14
<sup>238</sup> U		70.9		75.1		79.6

The neutron energy spectra are given in Fig. 2.4. The spectra are normalized to one, and then the RMPWR and RBWR fluxes are plotted relative to the PWR fluxes for each energy group in Fig. 3.1 to illustrate the substantial reduction in moderation, between the RMPWR and PWR, and the further reduction for the RBWR.

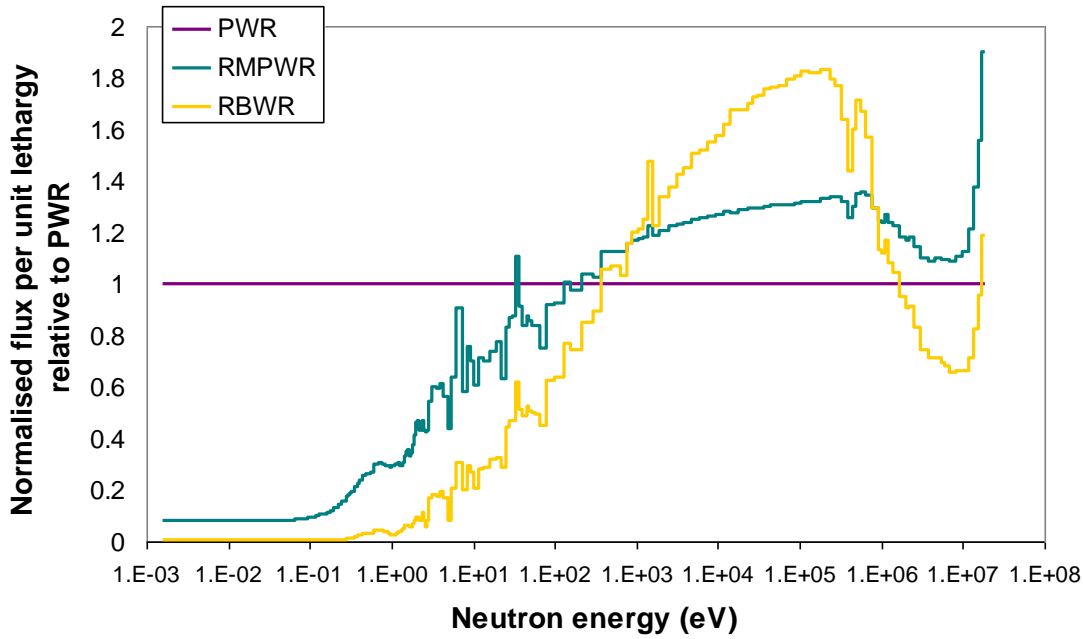


**Fig. 3.1.** Relative neutron flux for RMPWR and RBWR compared to PWR.

### 3.3. Results

#### 3.3.1. Reactor Performance

The performance of the fuel cycle is essentially a trade-off between maximizing the TRU incineration rate and discharge burn-up while respecting the MDC constraint. The TRU incineration rate and discharge burn-up can be increased by increasing the TRU reload fraction in the feed, but this makes the MDC worse. The FVR is also given for completeness. The performance of each fuel type is given in Table 3.2.

**Table 3.2.** Equilibrium cycle performance.

	TRU reload fraction	1-batch burn-up (GWd/t)	MDC ( $\Delta\rho/(g/cm^3)$ )	FVR	Eq. TRU + U3 (at %)
PWR $^{232}\text{Th}$	75%	36	-0.070	+0.067	28.5
PWR $^{238}\text{U}$	65%	22	-0.063	+0.123	29.1
RMPWR $^{232}\text{Th}$	45%	20	-0.024	+0.020	19.4
RMPWR $^{238}\text{U}$	40%	27	+0.087	+0.149	24.9
RBWR $^{232}\text{Th}$	25%	42	-0.037	-0.011	17.1
RBWR $^{238}\text{U}$	15%	36	+0.177	+0.091	20.4

For each reactor, the TRU reload fraction is greater for the Th-fuelled cycle, meaning that the conversion ratio is lower and the TRU incineration rate is higher. The  $^{232}\text{Th}$  population in the reactor is higher than the  $^{238}\text{U}$  population for the same reactor with the U-fuelled cycle (e.g. from

Table 3.1: 71.5%  $^{232}\text{Th}$  in the compared to 70.9%  $^{238}\text{U}$  in the PWR). For a given TRU reload fraction, the U cycle has a higher burn-up due to the smaller thermal capture cross-section and larger fast fission threshold of  $^{238}\text{U}$  compared to  $^{232}\text{Th}$ .<sup>15</sup>

In the more thermal spectrum, a higher TRU reload fraction is necessary to sustain the chain reaction. However, for a given TRU population, the MDC becomes more positive as moderation is reduced. The overall effect is to improve the feasibility of the cycle as moderation is reduced (although this is not obvious from Table 3.2 due to the short cooling time used for the PWR).

In each case, the U-fuelled cycle either has a lower 1-batch burn-up at a less negative MDC than the Th cycle and/or a positive MDC (the RMPWR U cycle has superior burn-up but a substantially positive MDC). The FVR of the U-fuelled cycle is also substantially more positive than for the Th-fuelled cycle in each case.

The TRU incineration rate is roughly (TRU reload fraction x 384 kg/GWthyr), i.e. a TRU reload fraction of 50% gives an incineration rate of 192 kg/GWthyr. The incineration rate reduces with reduced moderation, with a maximum of around 290 kg/GWthyr for the Th-fuelled PWR and a minimum of around 58 kg/GWthyr for the U-fuelled RBWR, which is very low for a burner reactor.

### 3.3.2. Reactivity Decomposition

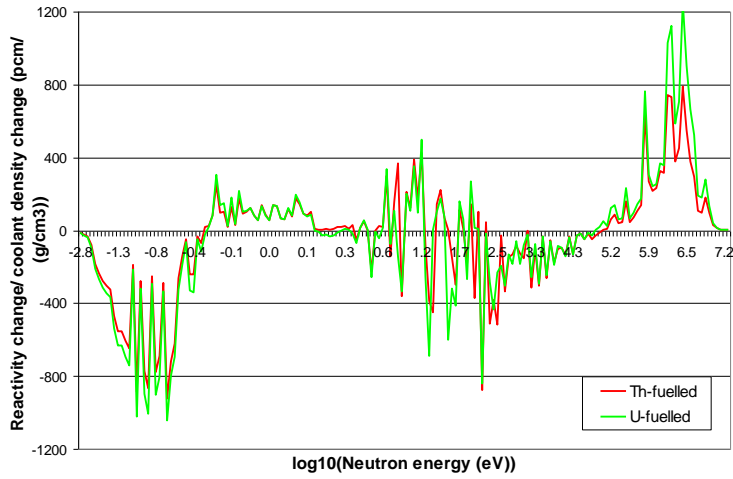
The reactivity decomposition following a change in coolant density has been calculated for every reactor and fuel type using the methodology discussed in Section 3.2. The results as a function of neutron energy are given in Figs. 3.2a-c for the PWR, RMPWR and RBWR respectively. The cumulative reactivity changes are plotted in Fig. 3.3. This is found by integrating Fig. 3.2 from high to low energies and hence shows the total effect over a given energy range. In general, there is a negative reactivity contribution at thermal energies due to decreased thermal fission. Low resonance energies ( $< \sim 5$  eV) feature a positive reactivity contribution due to the decreased resonance capture from the decreasing flux. At higher resonance energies voiding causes a flux increase and therefore resonance capture also increases, with a net decrement in reactivity. At fast energies there is an increase in fast fission with a positive reactivity contribution. There is a noticeably larger increase in fast fission for the U fuel vs Th fuel.

Table 3.3 gives the reactivity decomposition by element. The  $^{232}\text{Th}$  effect is negative and becomes increasingly more negative in the harder spectrum of the RMPWR and RBWR. The  $^{238}\text{U}$  effect is also negative, but smaller in magnitude compared to  $^{232}\text{Th}$  and relatively constant at higher neutron energies where the detrimental effect of fast fission in case of voiding is greater.

---

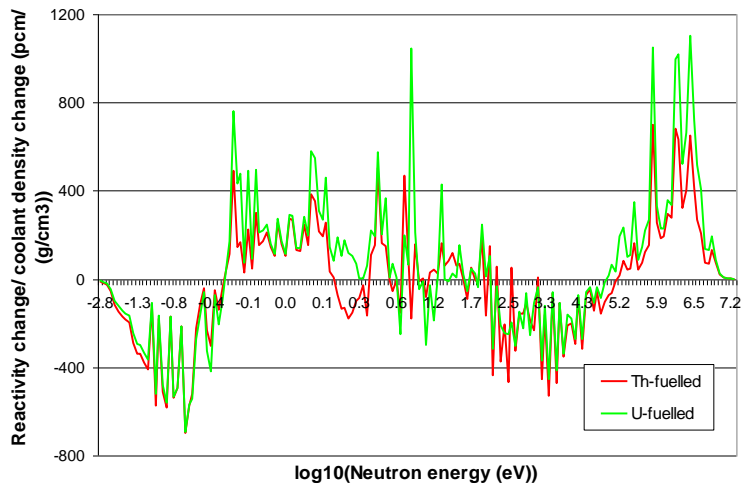
<sup>15</sup> Note that the results for the PWR indicate that with short cooling times, the MDC is negative in both cases. However, the FVR and ZCR are very positive, in particular for the U-fuelled PWR. This is not considered further here.

a



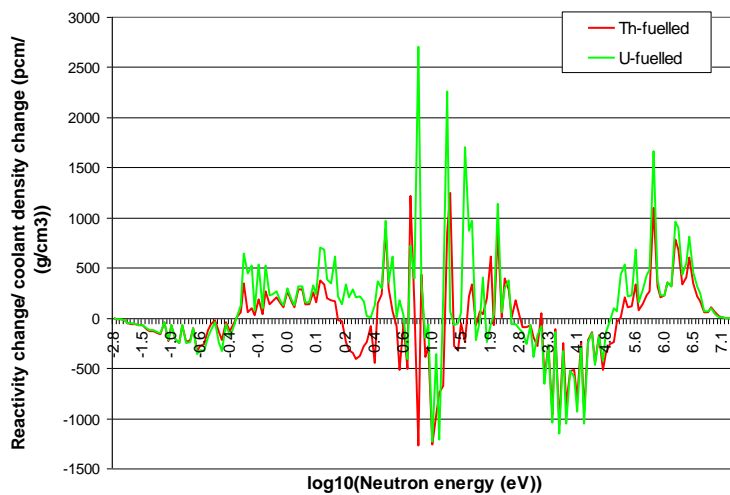
PWR

b



RMPWR

c



RBWR

Fig. 3.2. Reactivity decomposition by neutron energy for (a) PWR, (b) RMPWR, (c) RBWR.

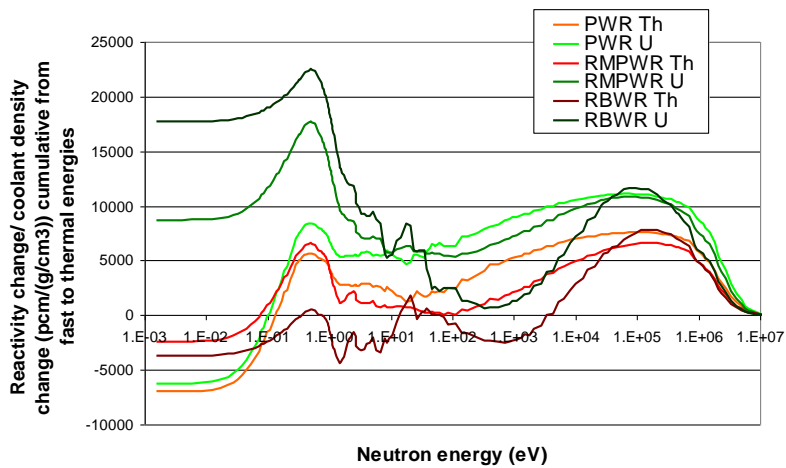


**Fig. 3.3.** Cumulative reactivity decomposition by neutron energy.

**Table 3.3.** Reactivity decomposition by element (pcm/(g/cm<sup>3</sup>)).

		<sup>232</sup> Th/ <sup>238</sup> U	Pu	MA	<sup>233-236</sup> U*
PWR	Th	-8031	725	-2334	1847
	U	-5859	1184	-2175	-164
RMPWR	Th	-11605	5376	1748	2079
	U	-3410	9172	2658	225
RBWR	Th	-19779	10214	4297	3021
	U	-3980	16264	5254	1220

\*For U cycles there is essentially no <sup>233</sup>U.

Pu has a positive effect on MDC due to increased fast fission and reduced resonance capture at higher energies. The effect gets greater with reduced moderation and is also higher for the U fuel where the Pu content is higher.

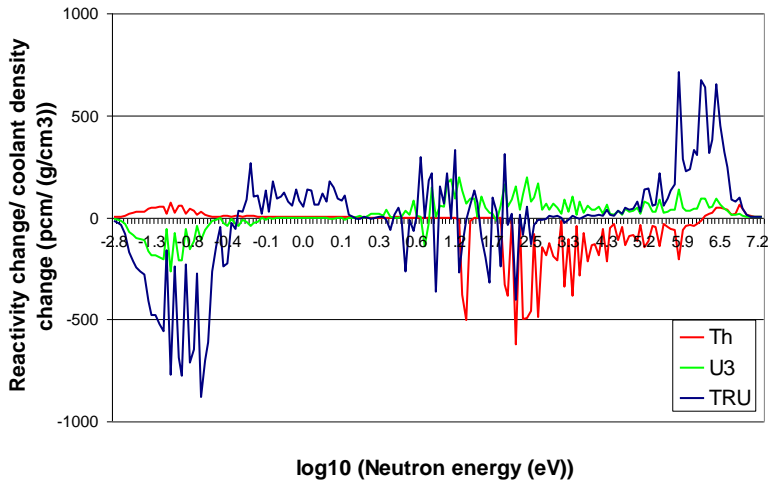
MA (Am, Cm and Np) have a negative effect in the PWR and a positive effect in the harder RMPWR and RBWR spectra. <sup>241</sup>Am, <sup>243</sup>Am and <sup>237</sup>Np behave similarly to <sup>238</sup>U, but have lower fission thresholds. Again, the fast fission effect is worse for U fuel, where their populations are higher.

U3 in Th has a positive effect on MDC, similarly to Pu. However, in contrast to Pu, the effect of U3 is relatively constant with neutron energy. This results in much lower positive reactivity insertion from U3+Pu in RM Th reactors than from Pu in RM U reactors.

The reactivity contributions from <sup>232</sup>Th, <sup>238</sup>U, U3 and TRU are decomposed into 172 groups in Figs. 3.4a-f. <sup>232</sup>Th is not fissile except at very high energies, so contributes negatively to reactivity at energies where flux increases and positively at energies where the flux decreases. U3 is fissile at virtually all energies, so the contribution is of the opposite sign to the <sup>232</sup>Th contribution at virtually

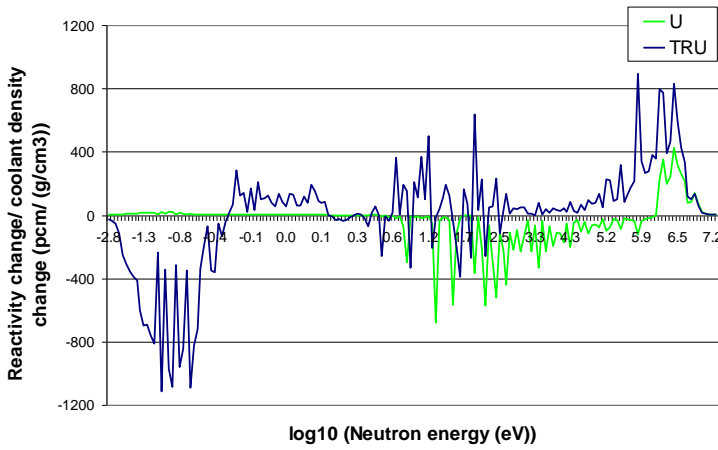
all energies. For Pu, resonance capture is more important at low resonance energies, and the fast fission contribution is greater.

a



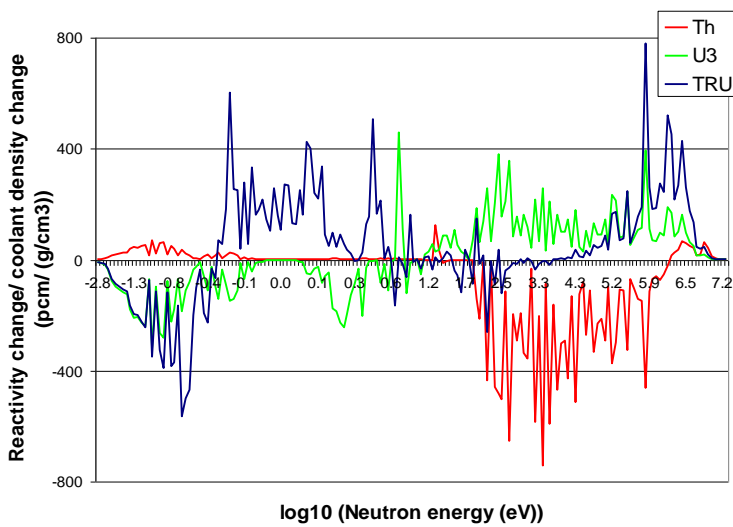
PWR Th

b



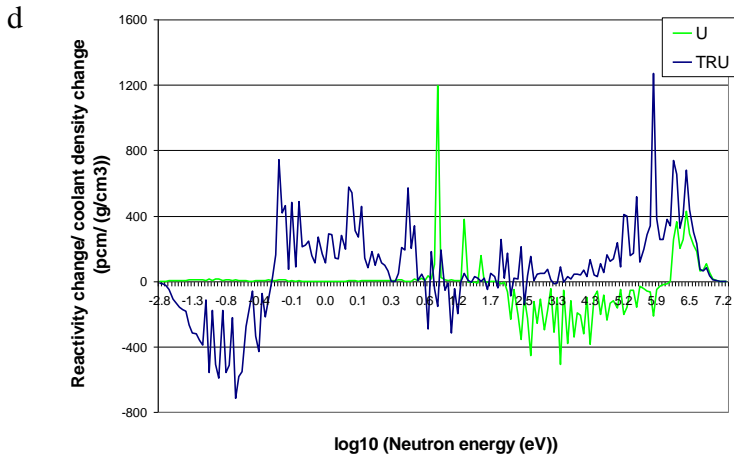
PWR U

c

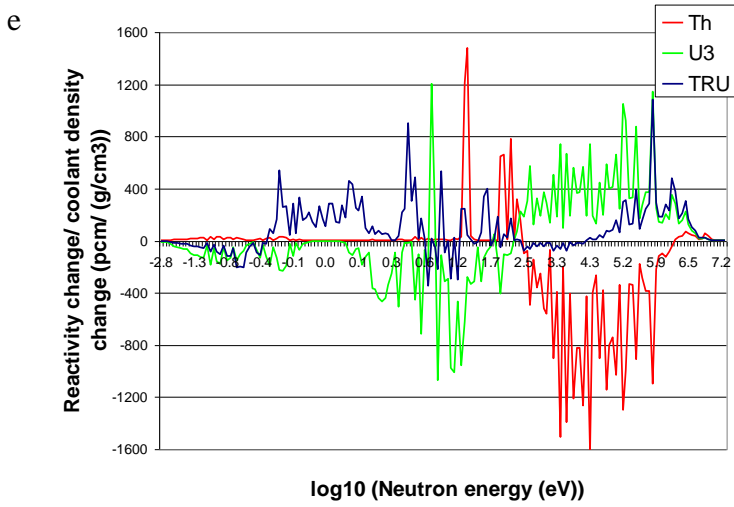


RMPWR Th

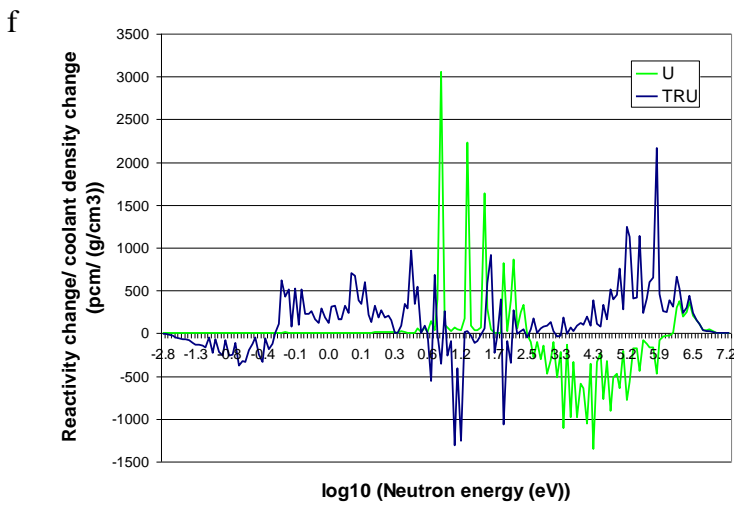
(Figure continues on next page)



RMPWR U



RBWR Th



RBWR U

**Fig. 3.4.** Reactivity decomposition by fuel component and neutron energy for (a) PWR Th, (b) PWR U, (c) RMPWR Th, (d) RMPWR U, (e) RBWR Th, (f) RBWR U.

### 3.4. Discussion

#### 3.4.1. Impact of $^{232}\text{Th}$ vs $^{238}\text{U}$

From Table 3.3, both  $^{238}\text{U}$  and  $^{232}\text{Th}$  have an overall negative reactivity contribution with voiding. From Figs. 3.4a-f, this is due to increased resonance captures from the spectral shift ensuing voiding, which is partially offset by increased fast fission. The  $^{232}\text{Th}$  fast fission threshold is higher (Fig. 3.5) and therefore the detrimental fast fission effect on MDC is lower relative to  $^{238}\text{U}$ .

$^{232}\text{Th}$  also has a higher capture cross-section than  $^{238}\text{U}$ . This has been suggested as a cause of improved MDC for  $^{232}\text{Th}$  relative to  $^{238}\text{U}$ , by increased resonance capture with flux (Xu et al., 2002). However, while the thermal  $^{232}\text{Th}$  cross-section is significantly higher (Fig. 3.5), the resonance and fast absorption cross-sections are similar, hence a higher  $^{232}\text{Th}$  resonance capture cross-section cannot explain the improved MDC. Three-group cross-sections for  $^{238}\text{U}$  and  $^{232}\text{Th}$  condensed using the RBWR spectrum are given in Table 3.4.

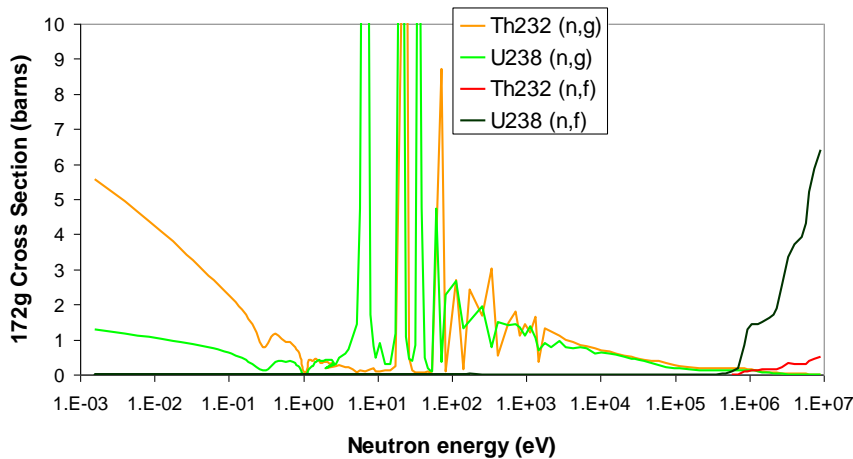


**Fig. 3.5.**  $^{232}\text{Th}$  and  $^{238}\text{U}$  cross-sections in 172 groups (calculated for RBWR).

**Table 3.4.** 3-group absorption cross-sections for  $^{232}\text{Th}$  and  $^{238}\text{U}$  (calculated for RBWR) (barns).

	$^{232}\text{Th}$	$^{238}\text{U}$
Fast (> 9119 eV)	0.22	0.17
Resonance	1.36	1.42
Thermal (< 0.625 eV)	1.59	0.45

The much larger  $^{232}\text{Th}$  negative reactivity effect is therefore due to the smaller fast fission positive reactivity ensuing voiding. The larger negative contribution observed at resonance energies is due to a larger change in flux with voiding than for  $^{238}\text{U}$ , when flux change is normalized to 1000 productions. This larger change in flux comes about as there are fewer additional fast fissions with voiding in Th relative to U, so the flux at high energies needs to increase by more to maintain 1000

productions. This is verified in Fig. 3.6, where the change in flux for the Th and U fuels in Table 3.1 is plotted (normalized to 1000 productions). Also plotted is the change in flux for the Th isotope vector with  $^{232}\text{Th}$  replaced by  $^{238}\text{U}$ , (i.e. the 5<sup>th</sup> column of numbers in Table 3.1 except with 82.9 at%  $^{238}\text{U}$  and 0%  $^{232}\text{Th}$ ) which gives the direct effect of switching the two isotopes.

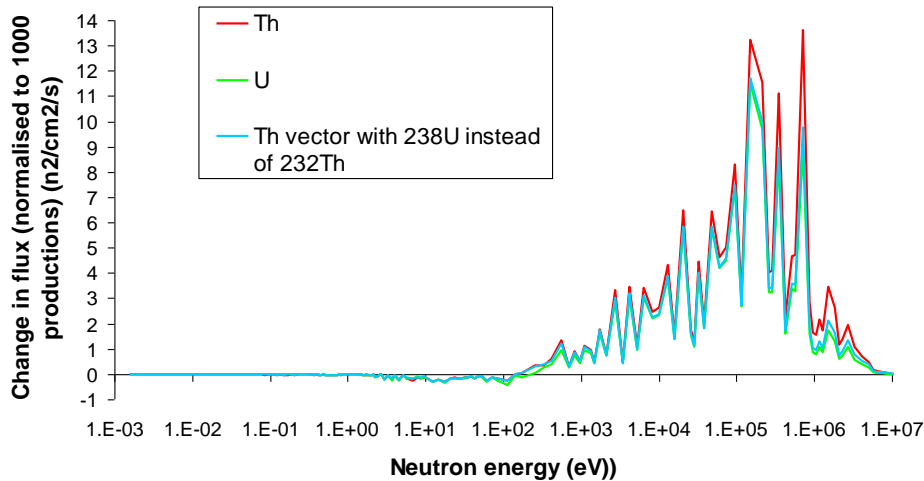


**Fig. 3.6.** Change in flux with coolant density (per 1000 productions in normal and perturbed state) for RBWR.

The higher thermal capture cross-section and lower fast fission cross-section of  $^{232}\text{Th}$  also act to reduce  $k$ , such that a higher TRU reload fraction is needed to sustain criticality. The resulting increased TRU+U3 content acts to make the MDC worse, so to directly compare the effect of  $^{232}\text{Th}$  with  $^{238}\text{U}$ , it is necessary to consider the trade-off between MDC and burn-up. To simplify the comparison, the  $k$ -MDC trade-off for  $^{232}\text{Th}$  and  $^{238}\text{U}$  is plotted in Fig. 3.7, for a mixture of the fertile isotope with TRU. The TRU isotope vector is PWR U from Table 3.1. The performance of the Th-TRU in Fig. 3.7 is not representative of the performance of the closed Th-TRU cycle, but it is illustrative in isolating the ‘direct’ effect of  $^{232}\text{Th}$  from the ‘indirect’ effect of its impact on the equilibrium isotope vector.

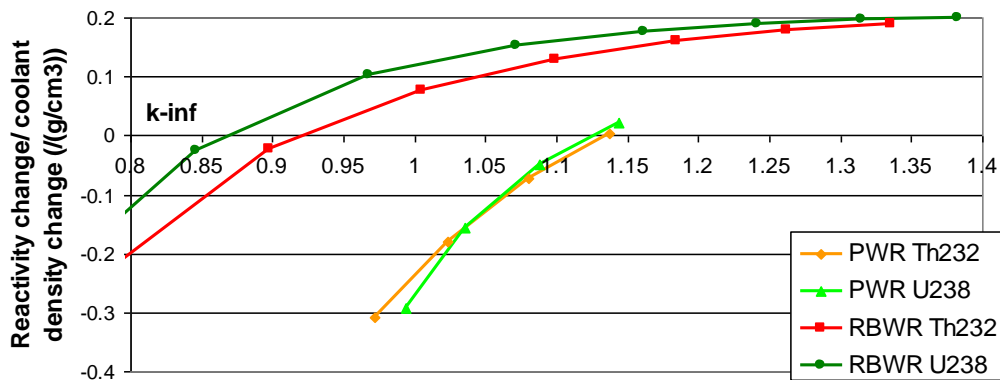


**Fig. 3.7.** Trade-off between  $k$  and MDC for  $^{232}\text{Th}$ -TRU and  $^{238}\text{U}$ -TRU fuels.

In a PWR spectrum, there is no direct benefit to using  $^{232}\text{Th}$ . In an RBWR spectrum, thermal capture is less significant and fast fission is more significant, so there appears to be a slight direct benefit from  $^{232}\text{Th}$ .

### 3.4.2. Impact of U3 vs TRU

From Table 3.3, the combined positive reactivity contribution of U3 and TRU in the Th fuel is lower than the TRU contribution in the U fuel for the RMPWR and RBWR, but higher for the PWR. This behaviour is due to the high resonance  $\eta$  of U3 relative to TRU, especially Pu (Table 3.5, Figs. 3.8a-c, Fig. 3.9).

**Table 3.5.** 3-group  $\eta$  for TRU and U3 (calculated for RBWR).

	$^{232}\text{Th}$ TRU	$^{232}\text{Th}$ U3	$^{232}\text{Th}$ U3+TRU	$^{238}\text{U}$ TRU
Fast (> 9119 eV)	2.47	2.27	2.39	2.53
Resonance	0.78	1.70	1.14	0.95
Thermal (< 0.625 eV)	1.33	2.10	1.47	1.41

Fig. 3.8 shows that for the PWR equilibrium fuel,  $\eta$  of U3-TRU mix in Th fuel is similar to  $\eta$  of TRU in U fuel (Fig. 3.8a). On the other hand,  $\eta$  of U3-TRU in Th fuel is slightly larger than  $\eta$  of TRU in U fuel for the RMPWR (Fig. 3.8b) and significantly larger for the RBWR (Fig. 3.8c).

Fig. 3.9 shows that: U3 has higher thermal and resonance  $\eta$  and lower fast  $\eta$  than Pu; Am and Np are not fissile except above a threshold energy, and for Am at very thermal energies; Cm is fissile.

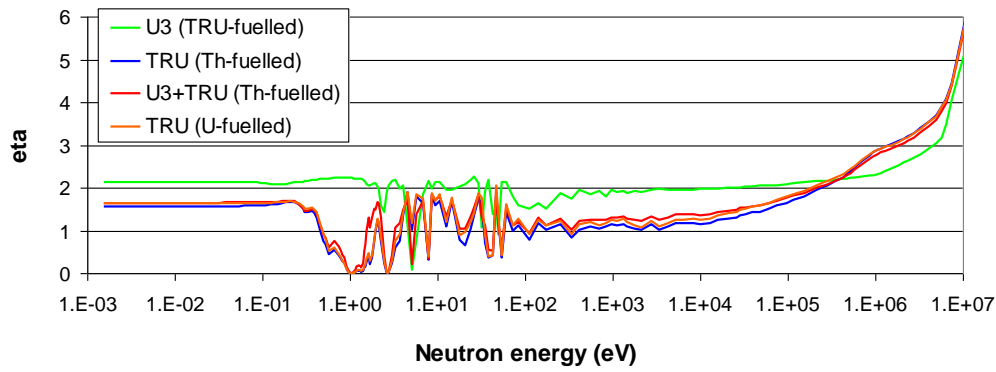
As the coolant voids, there is a decrease in fission at low energies and an increase at high energies. In U3,  $\eta$  is relatively constant with neutron energy, whereas in TRU the resonance  $\eta$  is low but the fast  $\eta$  is high (Table 3.5). This means that, when the coolant voids, there is a greater increase in productions in TRU, and this becomes more significant as the spectrum shifts to fast energies.

In the PWR, coolant voiding leads to a flux increase in the lower resonance energies, which results in a positive reactivity contribution from U3 fission. In the RMPWR and RBWR, the spectrum increases at higher energies in case of voiding and the increased resonance  $\eta$  and lower fast  $\eta$  of U3 compared to TRU become increasingly beneficial. While increased fast fission increases the MDC for both U3 and TRU, the contribution to MDC from the ~1–100 eV spectral range is negative for U3 (reduced fission,  $\eta > 1$ ) but positive for TRU (reduced capture,  $\eta < 1$ ).

The high resonance  $\eta$  of U3 (Fig. 3.9) also leads to high overall  $\eta$ , and thus to an increase in the overall value of  $\eta$  for the U3-TRU mix, relative to TRU in the U-fuelled design (Table 3.6, Figs. 3.8a-c). The TRU in the U fuel has a higher  $\eta$  than the TRU in the Th fuel (Fig. 3.9). This is the

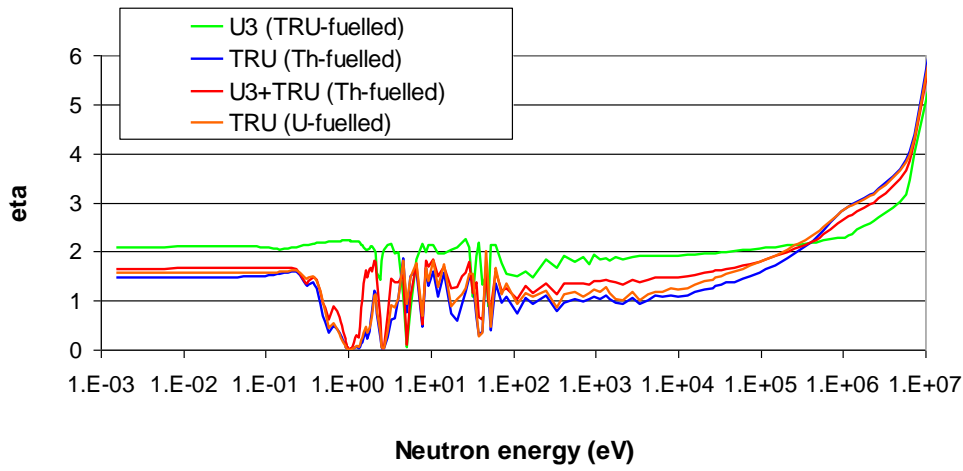
result of the different Pu isotopic composition for the respective TRU vectors (e.g. higher  $^{239}\text{Pu}$  content in U due to the breeding from  $^{238}\text{U}$ ).

a



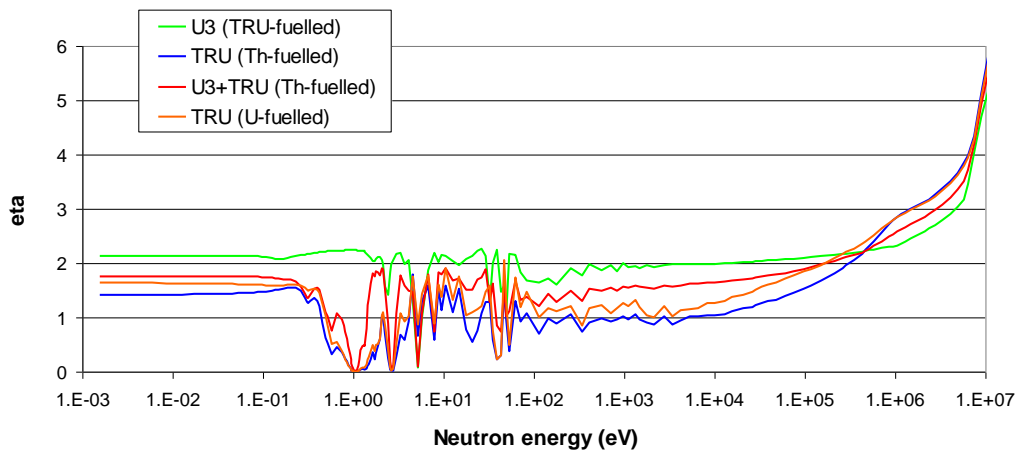
PWR

b



RMPWR

c



RBWR

**Fig. 3.8.**  $\eta$  variation with neutron energy by fuel component for (a) PWR, (b) RMPWR, (c) RBWR.

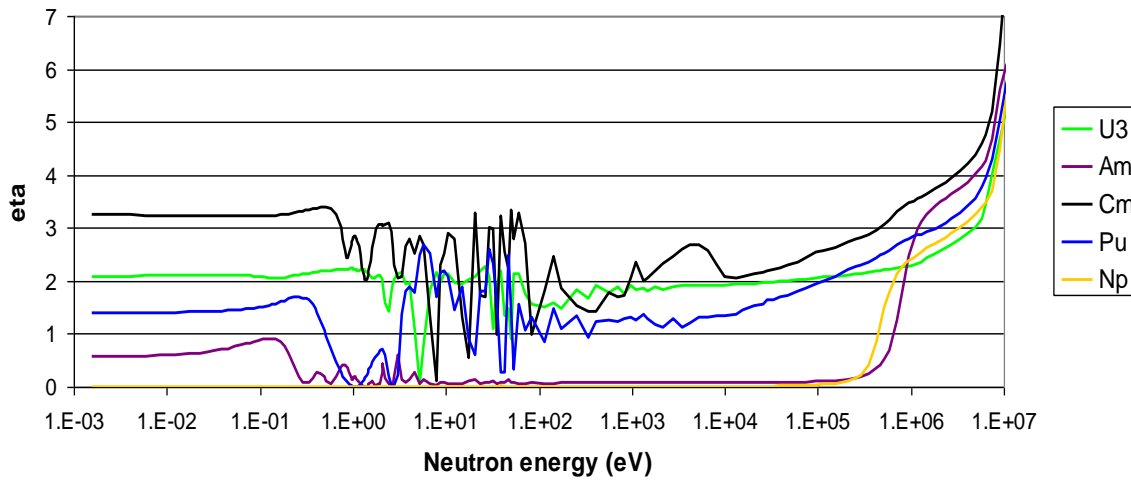


**Fig. 3.9.**  $\eta$  variation by element.

**Table 3.6.**  $\eta$  for TRU, U3 and U3+TRU mix.

	<sup>232</sup> Th TRU	<sup>232</sup> Th U3	<sup>232</sup> Th U3+TRU	<sup>238</sup> U TRU
PWR	1.15	1.81	1.27	1.23
RMPWR	1.10	1.82	1.35	1.27
RBWR	1.16	1.94	1.58	1.28

For a given fertile fuel, a higher  $\eta$  reduces the amount of fissile fuel that is required to sustain criticality. In the Th-fuelled system, this is offset by the higher capture cross-section and reduced fast fission cross-section of <sup>232</sup>Th, which reduce reactivity but benefit the MDC (Fig. 3.7). In addition, the ‘fuel’ (i.e. everything but <sup>232</sup>Th or <sup>238</sup>U) population is lower in the Th-fuelled systems for each reactor type. This confirms that the higher  $\eta$  of U3+TRU in Th than TRU in U allows a reasonable cycle length to be sustained despite the high capture cross-section and low fast fission cross-section of <sup>232</sup>Th.

In the Th-fuelled system, the U3 population increases with reduced moderation due to increased breeding. This increases the beneficial effects of U3 on  $\eta$  (Figs. 3.8a-c) and the MDC.

### 3.5. Heterogeneous Recycle

#### 3.5.1. Assembly Design

The benefits of the TCUP assembly design are now investigated. Homogeneous and TCUP assemblies are compared. For the RMPWR, a pin diameter of 11 mm is used for both the homogeneous and TCUP assemblies, as this is the minimum feasible pin diameter for the TCUP assembly (Chapter 2). The equilibrium isotope vectors are given in Table 3.7. The TCUP

assemblies are given in Fig. 3.10. For the RBWR assembly, the positioning of the Th-U3 pins next to the bypass channel is sensible, as the thermal flux is significantly greater near the bypass channel.

**Table 3.7.** Equilibrium isotope vectors of homogeneous (hom.) and TCUP assemblies (at%).

	RMPWR 11 mm pin		RBWR	
	Hom .	TCU P	Hom.	TCUP
<sup>241</sup> Am	0.95	1.42	0.67	1.24
<sup>242m</sup> Am	0.02	0.04	0.03	0.05
<sup>243</sup> Am	0.69	0.77	0.36	0.54
<sup>244</sup> Cm	0.52	0.51	0.20	0.25
<sup>245</sup> Cm	0.25	0.22	0.11	0.11
<sup>246</sup> Cm	0.22	0.21	0.08	0.12
<sup>247</sup> Cm	0.04	0.05	0.02	0.03
<sup>248</sup> Cm	0.02	0.02	0.01	0.01
<sup>237</sup> Np	0.46	0.58	0.36	0.56
<sup>238</sup> Pu	1.95	2.41	0.99	1.44
<sup>239</sup> Pu	2.47	3.52	1.66	3.17
<sup>240</sup> Pu	3.01	5.43	2.19	5.17
<sup>241</sup> Pu	0.98	1.07	0.49	0.65
<sup>242</sup> Pu	1.95	2.87	0.92	1.95
<sup>232</sup> Th	79.7	74.8	82.9	77.6
<sup>233</sup> U	3.52	2.55	5.59	4.77
<sup>234</sup> U	1.94	2.21	2.14	2.31
<sup>235</sup> U	0.85	0.64	0.76	0.71
<sup>236</sup> U	0.51	0.66	0.57	0.59

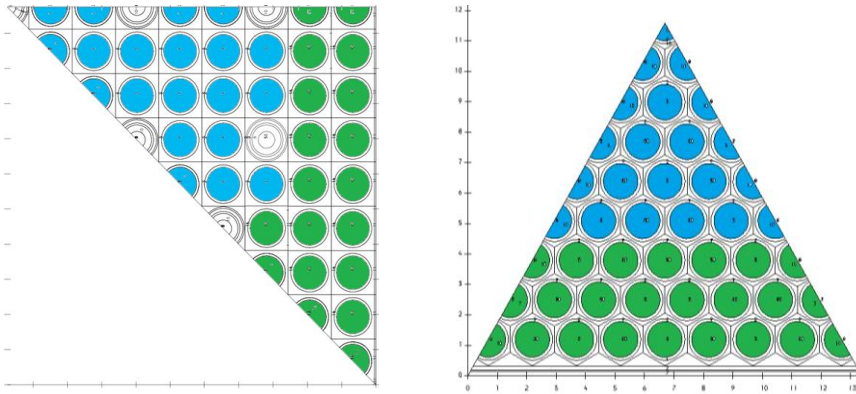


**Fig. 3.10.** TCUP RMPWR (left) and RBWR (right) assembly designs with Th-TRU (blue) and Th-U3 (green) pins.

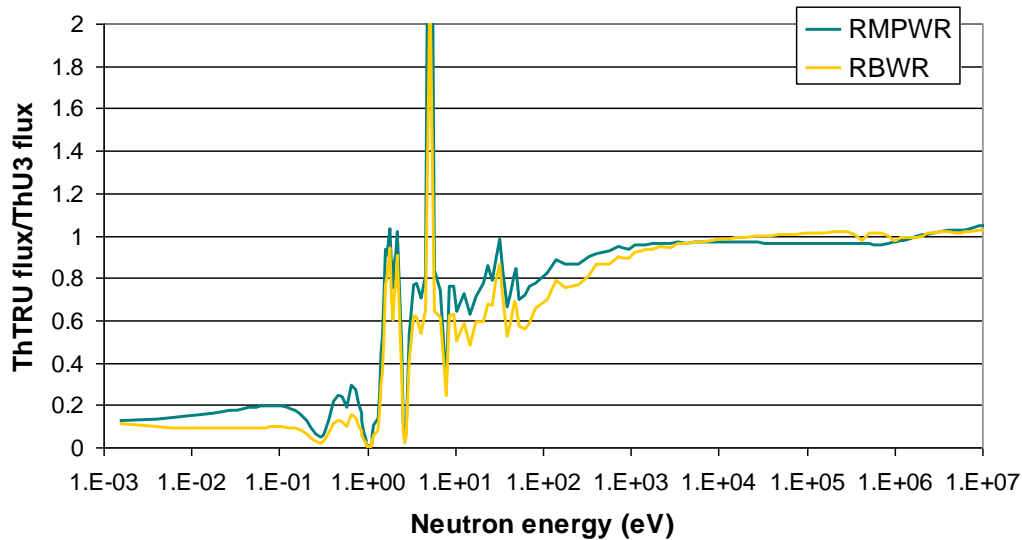
### 3.5.2. Results

Table 3.8 summarizes the performance of the homogeneous and TCUP fuel cycles. Both the discharge burn-up and the MDC are substantially improved by the TCUP fuel configuration. However, the FVR is slightly worse. For the RBWR this is partly a result of the much larger TRU reload fraction. Despite this, the much larger discharge burn-up leads to a design which is advantageous overall.

**Table 3.8.** Performance of homogeneous and TCUP fuel assemblies

	TRU reload fraction	1-batch burn-up (GWd/t)	MDC ( $\Delta\rho / (\text{g/cm}^3)$ )	FVR
RMPWR Hom.	50%	11	-0.036	+0.035
RMPWR TCUP	50%	27	-0.064	+0.039
RBWR Hom.	25%	42	-0.037	-0.011
RBWR TCUP	35%	80	-0.059	-0.003

This is due to the thermal flux in the Th-TRU pins being much lower than in the Th-U3 pins (Fig. 3.11). Concentrating the TRU further increases the resonance absorption effect from TRU isotopes and the large thermal absorption resonances in Pu. Conversely, there is an increased thermal flux in the Th-U3 pins. The thermal diffusion length is of the order of the pin pitch, so while there is some thermal neutron transport between regions, it is relatively limited. When the assembly is fully voided, fast fission effects become more significant, such that the TCUP assembly does not perform as well.



**Fig. 3.11.** Relative flux in Th-TRU compared to Th-U3 pins in TCUP assembly.

Note that the RMPWR fuel assembly design in Fig. 3.10 can also be inverted such that the thermalized Th-U3 pins are near the guide tube positions. This results in a slight improvement by enhancing the spectral variation.

### 3.5.2.1. Effect on $\eta$

The TCUP fuel design results in an improved  $\eta$  for the resultant TRU-U3 vector in the fuel (Table 3.9). This allows criticality to be sustained to higher burn-ups. The  $\eta$  of the TRU increases as a direct result of the harder neutron spectrum, i.e. the fast flux is higher, and  $\eta$  is greater at fast energies. The U3  $\eta$  varies less with neutron energy, and therefore U3  $\eta$  for the homogeneous and TCUP assemblies is similar (Fig. 3.12, Table 3.5).

**Table 3.9.**  $\eta$  and Productions ( $P$ ) for TRU and U3 for homogeneous and TCUP assemblies.

	Hom. $\eta$	TCUP $\eta$	Hom. $P$	TCUP $P$
RMPWR U3	1.79	1.81	430	454
RMPWR TRU	1.08	1.12	552	530
RMPWR U3 + TRU	1.31	1.36	982	984
RBWR U3	1.94	1.93	654	588
RBWR TRU	1.16	1.32	321	390
RBWR U3 + TRU	1.58	1.63	975	978

The equilibrium isotope vector also changes slightly. The TRU is burned in a slightly harder spectrum so a more fissile equilibrium TRU vector could be expected. However, from Fig. 3.12, the homogeneous and TCUP equilibrium TRU vectors have similar  $\eta$  variation with energy.

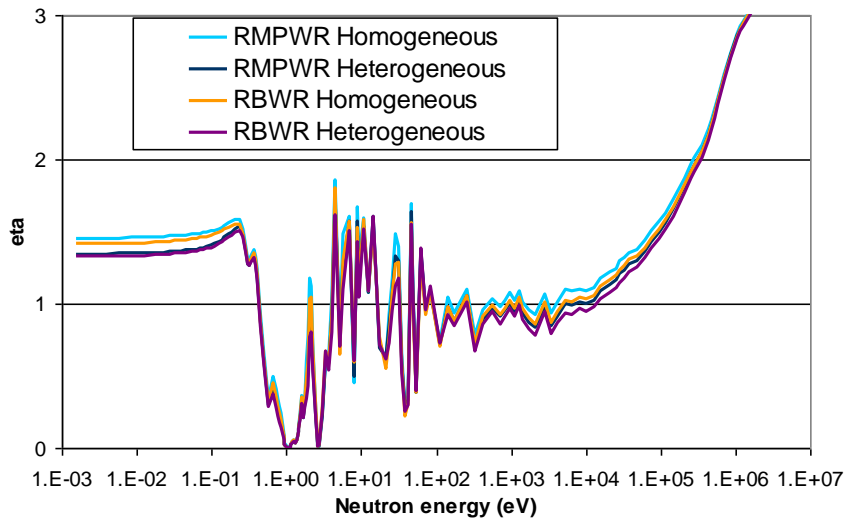


**Fig. 3.12.** TRU  $\eta$  vs neutron energy for homogeneous and TCUP fuel assemblies.

Fig. 3.12 shows that there is little difference in  $\eta$  for homogeneous and TCUP fuel, but overall  $\eta$  for homogeneous fuel is generally slightly higher due to higher equilibrium U3 composition.

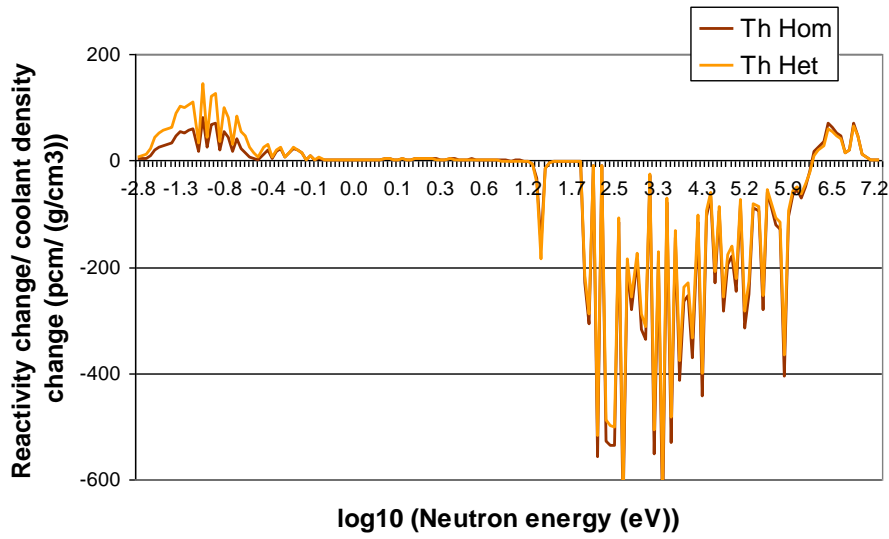
The relatively thermal spectrum in the U3 region, and relatively fast spectrum in the TRU region results in a lower equilibrium U3 population and a higher equilibrium TRU population than the homogeneous recycle case (Table 3.7). However, the higher thermal fission cross-sections can result in a higher overall reaction rate in U3 (for the RMPWR in Table 3.9).

Increasing the number of TRU pins in the assembly tends to increase the TRU reaction rate but improve the TRU  $\eta$  (due to a more fissile isotope vector), leading to a very similar overall performance.

#### 3.5.2.2. Effect on Void Reactivity Feedback

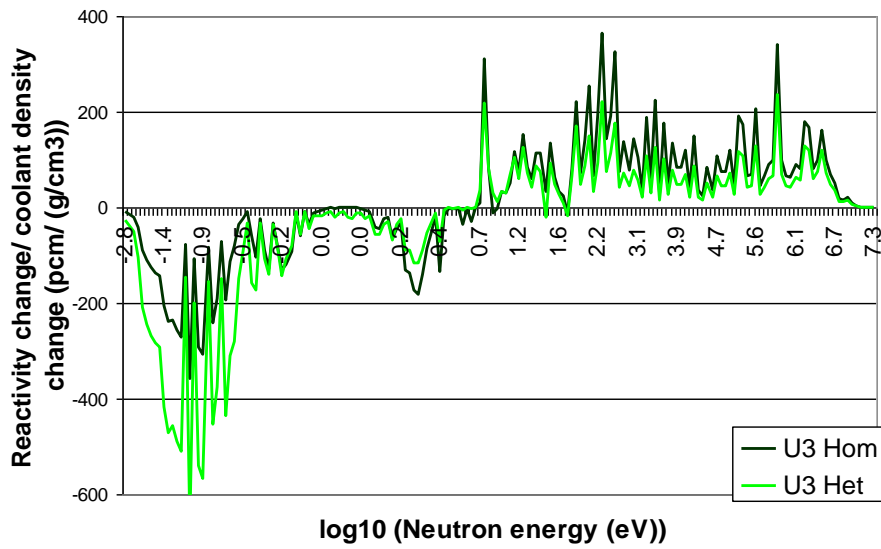
The improvement in MDC from the homogeneous to the TCUP configuration is investigated by decomposing reactivity into Th, U3 and TRU components as before (Figs. 3.13a-c, Table 3.10). This is performed for the RMPWR only as the mechanisms in the RBWR are very similar.

a



<sup>232</sup>Th

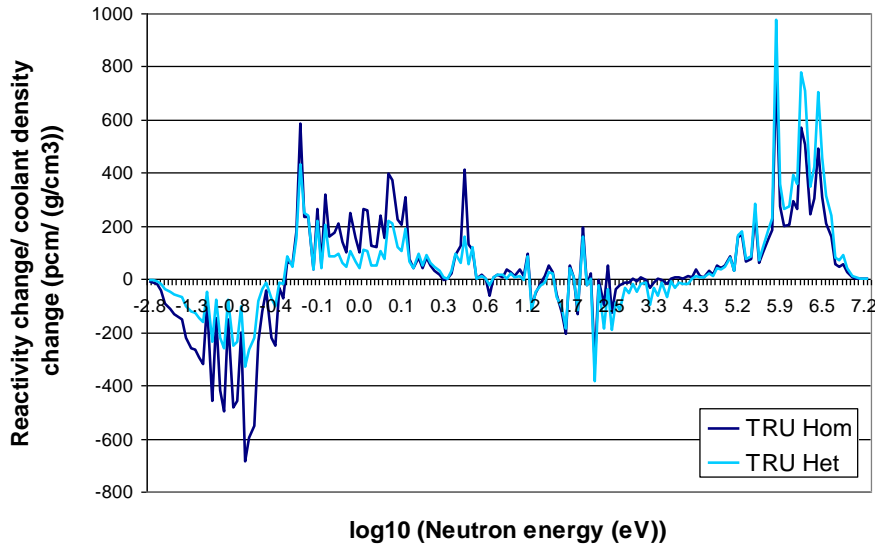
b



U3

(Figure continues on next page)

c



TRU

**Fig. 3.13.** Reactivity decomposition by neutron energy for homogeneous and TCUP RMPWR: (a) Th component, (b) U3 component, (c) TRU component.

**Table 3.10.** 3-group reactivity decomposition for fuel components of homogeneous and TCUP RMPWR.

Group	TRU		U3		Th	
	Hom.	TCUP	Hom.	TCUP	Hom.	TCUP
Fast	6570	8516	3708	2438	-4401	-3993
Resonance	5591	2041	3260	1752	-7834	-7275
Thermal	-6931	-2936	-4750	-9299	1012	1911
Total	5230	7621	2218	-5109	-11223	-9358

The beneficial Th effect is reduced in the TCUP cases as the Th relative content at equilibrium is lower. This is due to slower TRU burning in the faster spectrum of the TCUP pins. Also, the Th content of the Th-U3 pins is greater than the Th content of the Th-TRU pins. This means that on average, the Th experiences a more thermal spectrum in the TCUP assembly compared to the homogeneous assembly.

The detrimental TRU effect is also worsened when moving to TCUP pins, because the thermal flux in the TRU is reduced, and the fast and resonance fluxes are higher.

However, the highly beneficial U3 thermal capture effect is increased, and to a lesser extent the detrimental U3 fast and resonance effects are lower, due to the higher thermal flux in the Th-U3 pins. This is the dominant effect, leading to a net improvement in the MDC. While a fast spectrum

is desirable for TRU burning, thermal neutrons play an important role in keeping the MDC negative, and these effects are increased by the TCUP fuel.

### 3.6. Concluding Remarks

In reduced-moderation or hard-spectrum LWRs, full recycle of TRU is limited by coolant reactivity feedback. Use of  $^{232}\text{Th}$  instead of  $^{238}\text{U}$  as a fertile isotope improves the MDC, and therefore yields superior performance. This is essentially due to the high resonance  $\eta$  of U3, which increases the fissibility of the U3-TRU isotope vector in the Th-fuelled system relative to the U-fuelled system, and also improves the MDC when the spectrum is sufficiently hard (e.g. RMPWR and, even more so, RBWR). While direct substitution of  $^{238}\text{U}$  with  $^{232}\text{Th}$  improves the MDC, it also increases the required fissile loading, such that the benefits of using  $^{232}\text{Th}$  are essentially “indirect”, e.g. by breeding U3. The reduced fast fission threshold of  $^{232}\text{Th}$  compared to  $^{238}\text{U}$  improves the MDC, but also makes the neutron economy worse, as does the higher thermal capture cross-section. The resonance capture cross-sections of  $^{232}\text{Th}$  and  $^{238}\text{U}$  are similar. The performance difference between Th- and U-fuelled systems increases with reduced moderation due to higher U3 breeding, and an increasingly beneficial effect from U3 on the MDC.

Spatial separation of TRU and U3 is possible in the Th-fuelled system, which renders further improvement by hardening the neutron spectrum in the TRU-bearing pins and softening it in the U3-bearing pins. This improves the neutron economy by increasing the TRU  $\eta$ , as well as the MDC performance by enhancing the thermal fission reduction upon voiding in U3.

## **Chapter 4 – Thermal-hydraulic Study of RMPWRs**

In Chapter 2, the minimum pin diameter for RMPWR neutronic feasibility was found to be ~11 mm for the TCUP fuel design and ~11.5 mm for homogeneous fuel. In this chapter, a thermal-hydraulic feasibility assessment is performed for retrofit RMPWR designs with 11–11.5 mm pin diameter. At steady state, the increased pin diameter leads to reduced core flow rate due to the increased pressure drop. This leads to a higher temperature increase across the core, which affects temperature limits and the minimum departure from nucleate boiling ratio (MDNBR). An 11 mm pin diameter appears possible, but 11.5 mm is a stretch case. The most severe transient condition is reflood following a large-break loss-of-coolant accident (LBLOCA). This is difficult to model accurately, and the treatment here is simplified. The increased core pressure drop reduces the reflood speed, which appears likely to lead to the violation of clad limits. A reduced-height core may therefore be required, which would prevent retrofit of an existing PWR core.

This chapter received a major contribution from Dr Paolo Ferroni of Westinghouse Electric Company LLC, who provided extensive guidance on performing the analysis and on a draft version of this chapter.

### **4.1. Introduction**

A simplified thermal-hydraulic study has been performed to investigate the feasibility of the RMPWR concept and to identify the main thermal-hydraulic challenges characterizing this design. The trade-off between burn-up and MTC, and therefore the neutronic performance, tends to improve as the assembly lattice becomes tighter. Therefore interest is focused on the tightest geometry likely to be achievable when accounting for constraints on rod-to-rod spacing and on the design implementation strategy adopted in this study, i.e. use of 17×17 assemblies with the same size as the reference design.

The rod-to-rod spacing is a ‘hard’ constraint imposing a lower limit on the minimum distance between adjacent fuel rods. The numerical value of this constraint depends on how the rods are supported: if grid spacers are used, it is reasonable to require the space needed for the grid strap and dimples to be at least 2 mm which, for a 12.6 mm fuel rod pitch, would limit the maximum fuel rod diameter to ~10.6 mm. However, if tighter lattices are required, wire-wraps can be used instead of spacer grids, since they allow a reduction in the minimum rod-to-rod spacing to ~1.1 mm. The choice of this limit is based on past experience with wire-wraps in fast reactors (rather than on calculations or manufacturing tests). From data found in (IAEA, 2006; NUREG, 1985; Waltar et al., 2012), wire-wrap diameters for experimental fast reactors ranged between 0.7 mm (BOR-60) and

2.1 mm (JOYO), and were usually in the 1.1–1.5 mm range. This corresponds to a maximum pin diameter of 11.5 mm in an unmodified pitch lattice.<sup>16</sup>

If retrofitting an RM core into an existing reactor is pursued, it is preferable to preserve the location of the control guide thimbles. To allow this, the assembly lattice (square) and the fuel rod pitch (12.6 mm) are unchanged with respect to the reference plant. An actual optimization of the RMPWR lattice geometry would require relaxation of this ‘soft’ constraint on the lattice type and fuel rod pitch, and may result in a very different lattice compared to that of typical PWRs. This would likely result in improved reactor performance, but with the disadvantage of not being able to retrofit the core into an existing plant.

## **4.2. Analysis**

### ***4.2.1. Thermal-Hydraulic Constraints***

In this study, reduced moderation is obtained by maintaining the fuel rod pitch at the reference value while increasing the fuel rod diameter. This has several interdependent consequences on the reactor thermal-hydraulics, which require assessment to guarantee that reactor operation is possible, while satisfying safety limits. For example, the transition to the new lattice geometry results in a larger heat transfer area and therefore, if the core power is kept constant, a lower heat flux to the coolant, which has a beneficial effect on MDNBR. However, a tighter lattice also results in a smaller flow area and hydraulic diameter which, mainly because of pressure drop considerations, requires the coolant flow rate to be reduced. Depending on core power and core inlet temperature ( $T_{in}$ ), this reduced flow may result in a higher coolant enthalpy throughout the core, which is detrimental to the MDNBR. Therefore, whether the RMPWR performs better than the reference PWR, from the MDNBR standpoint, depends on how heat flux, coolant velocity and enthalpy compare to those in the reference PWR. It also depends on the direct effect that the tighter lattice has on departure from nucleate boiling (DNB), as discussed in Section 4.2.1.1.

Sections 4.2.1.1 to 4.2.1.5 discuss the thermal-hydraulic constraints that have been considered to allow operability and safety of the proposed RMPWR designs with a reasonable degree of confidence. Table 4.1 summarizes the limit values selected for each constraint.

---

<sup>16</sup> While there is more experience with wire-wraps for triangular lattices, wire-wraps have been used for square lattices in the FERMI reactor. The wire-wraps are welded to the rods to hold the assembly together. Fast reactor fuels generally use stainless steel cladding instead of zircaloy. It is not known if there are any specific issues from using wire-wraps with zircaloy cladding.

**Table 4.1.** Thermal-hydraulic constraints.

Design constraint	Value	Rationale
MDNBR	1.31	MDNBR for the reference core, evaluated with the DDH correlation. See Section 4.2.1.1
RCP performance	Constrained by the RCP characteristic curve	See Section 4.2.1.2
Core outlet temperature $T_{out}$	600 K (feasible case) 603 K (stretch case)	Two values of which the lower is that of the reference plant. See Section 4.2.1.3
Core inlet temperature $T_{in}$	560.3 K	5 K less than the reference case. See Section 4.2.1.4
Assembly lift-off force	N.A.	Calculated, but not used to constrain the design. See Section 4.2.1.5

#### 4.2.1.1. Minimum Departure from Nucleate Boiling Ratio

The design of an RMPWR that can satisfy safety requirements was performed by imposing a minimum allowed DNBR when the reactor is assumed to operate at 112% of its nominal power, 95% of nominal flow and with a  $T_{in}$  2 K higher than the nominal. This minimum value is selected to be equal to the MDNBR of the reference PWR when analyzed in the same conditions, and with the same critical heat flux (CHF) correlation. This approach is not rigorous, but is often used in simplified analyses since it affords reasonable protection against DNB without the need to analyze both nominal conditions and transient-specific power levels. The rationale behind the method is that, when considering DNB, Condition I and II transients are bounded by the operating conditions mentioned above.

The CHF correlation used to evaluate the MDNBR is that developed by Dalle Donne and Hame (1985) which, unlike the most well-known correlations typically used for open lattices, e.g. the W-3 correlation, was developed specifically for tight lattices and demonstrated to be accurate for both open and tight lattices. It must be noted that this correlation was originally formulated for triangular lattices, rather than the square lattices considered here. No systematic study has been found on the effect of the lattice type on the CHF. It is reasonable to assume that the correlation will give good results despite this approximation, but further analysis may be required to support this. To show the non-conservative results that would be obtained if a CHF correlation developed for open lattices was used for tight lattices, results obtained with the W-3 correlation are presented as well (Tong, 1967). The W-3 result is taken directly from a single assembly analysis performed with the COBRA code (see Section 4.2.2), assuming 8 grid spacers in all cases, while a separate calculation, for a single hot channel, was used to evaluate the Dalle Donne-Hame (DDH) MDNBR. An important

parameter in the DDH correlation is the wire-wrap pitch ( $H$ ). The correlation is valid for the range  $13.6 \leq H/D \leq 50$  and values of 14 and 50 are used as ‘bounding’ cases on the design, where  $D$  is the pin diameter.

#### 4.2.1.2. RCP Performance

The flow rate through the reactor cooling system (RCS) is constrained by the performance of the reactor cooling pumps (RCPs) and, specifically, by their head versus flow characteristic curve. In existing PWRs, the RCPs operate at constant speed, which means that the relationship between RCS pressure drop and delivered flow is a fixed curve. Therefore, if one of these plants is retrofitted with an RM core, the flow resistance increase resulting from this change will prevent the RCPs from delivering the same flow as in the original design, and a flow reduction will occur. The new operating point, and therefore the new flow, can be established by finding the intersection of the RCP characteristic curve, which is known, with the RCS curve, which, for the RMPWR, needs to be determined. The pump characteristic curve selected in this study is that of the RCPs of the 4-loop Watts Bar plant, available from (Watts Bar, 2010b) and shown in Fig. 4.1. The RCS curve of the RMPWR can be estimated as a function of the fuel rod diameter is estimated by assuming the following:

- 1) in the highly turbulent regime ( $Re \approx 10^5$ ), the form loss coefficient for spacer grids is assumed to be proportional to (mass flow rate)<sup>-0.2</sup>. This has been inferred from trends found in (Chun and Oh, 1998) referring to grids provided with non-split mixing vanes;
- 2) the form loss coefficient associated with the total pressure drop loss at the entrance (lower core plate and assembly bottom nozzle) and exit (assembly upper nozzle and core upper plate) of the RM core is assumed to be the same as that of the reference core;
- 3) the fraction of RCS flow that it is not effective for removing core heat, i.e. the bypass flow fraction, is the same in the RMPWR and in the reference plant;
- 4) in an unmodified PWR, the core contributes about 30% of the overall RCS pressure drop.

The friction pressure drop for a bare-rod bundle core, i.e. without either grids or wire-wraps, can be expressed as:

$$\begin{aligned}
 \Delta p_{\text{core,bare}} &= f \frac{L}{D_{\text{eq}}} \frac{G^2}{2\rho} = \left( \frac{0.184}{Re^{0.2}} \right) \frac{L}{D_{\text{eq}}} \frac{G^2}{2\rho} = 0.184 \left( \frac{GD_{\text{eq}}}{\mu} \right)^{-0.2} \frac{L}{D_{\text{eq}}} \frac{G^2}{2\rho} = 0.092 \frac{G^{1.8} L \mu^{0.2}}{D_{\text{eq}}^{1.2} \rho} \\
 &= 0.092 \left( \frac{\dot{m}_{\text{core}}}{NA_{\text{flow}}} \right)^{1.8} \frac{L \mu^{0.2}}{\left( 4 \frac{A_{\text{flow}}}{P_{\text{wetted}}} \right)^{1.2} \rho} = 0.092 \left( \frac{\pi}{4} \right)^{1.2} \frac{LD^{1.2} \dot{m}_{\text{core}}^{1.8} \mu^{0.2}}{N^{1.8} A_{\text{flow}}^3 \rho} \quad (4.1)
 \end{aligned}$$

where:  $L$  is the fuel rod length,  $D$  is the fuel rod outer diameter;  $\dot{m}_{\text{core}}$  is the coolant flow rate through the core;  $N$  is the number of subchannels in the core;  $f$  is the McAdams friction factor (Chun and Oh, 1986);  $\rho$  is the coolant density;  $G$  is the coolant mass velocity;  $\mu$  is the dynamic viscosity;  $P_{\text{wetted}}$  is the wetted perimeter; and  $A_{\text{flow}}$  is the subchannel flow area. Using assumption 1 above, the form pressure drop, due to grid spacers as well as losses at the assembly entrance and exit, can be expressed as:

$$\Delta p_{\text{core,form}} = K_{\text{core}} \frac{G^2}{2\rho} = \left( K_{\text{core,nom}} \frac{G^{-0.2}}{G_{\text{nom}}^{-0.2}} \right) \frac{G^2}{2\rho} = K_{\text{core,nom}} \left( \frac{\dot{m}_{\text{core}}}{NA_{\text{flow}}} \right)^{1.8} \left( \frac{\dot{m}_{\text{core,nom}}}{NA_{\text{flow}}} \right)^{0.2} \frac{1}{2\rho} \quad (4.2)$$

where  $K_{\text{core}}$  is the sum of all the core form loss coefficients (core inlet, grids and core outlet), which is flow rate-dependent, while  $K_{\text{core,nom}}$  is the value of  $K_{\text{core}}$  at the nominal flow rate conditions.

Hence, for the reference, grid-spacer-provided core, the friction and form pressure drops can be expressed by combining Eq. 4.1 with Eq. 4.2:

$$\Delta p_{\text{core,ref}} = \Delta p_{\text{core,bare}} + \Delta p_{\text{core,form}} = \frac{\dot{m}_{\text{core}}^{1.8}}{2N^{1.8} A_{\text{flow}}^{1.8} \rho} \left[ 0.184 \left( \frac{\pi}{4} \right)^{1.2} \frac{LD^{1.2} \mu^{0.2}}{A_{\text{flow}}^{1.2}} + \left( \frac{\dot{m}_{\text{core,nom}}}{NA_{\text{flow}}} \right)^{0.2} K_{\text{core,nom}} \right] \quad (4.3)$$

For a RM core provided with wire-wraps, form losses are located at the assembly entrance and exit only, whereas throughout the heated length the pressure drop can be evaluated using a Darcy friction factor specifically formulated for wire-wrap-provided rods using the correlation developed by (Cheng and Todreas, 1986) for the turbulent regime (although this correlation is for hexagonal bundles), i.e.:

$$f = \frac{C_{fT}}{\text{Re}^{0.18}} \quad (4.4)$$

which is valid for  $\text{Re} > \text{Re}_T = 10^{(3.3+0.7P/D)}$ , with the coefficient  $C_{fT}$  given by:

$$C_{fT} = \left\{ 0.8063 - 0.9022 \left( \log_{10} \frac{H}{D} \right) + 0.3526 \left[ \log_{10} \frac{H}{D} \right]^2 \right\} \left( \frac{P}{D} \right)^{9.7} \left( \frac{H}{D} \right)^{1.78-2\frac{P}{D}} \quad (4.5)$$

where  $H$  is the wire pitch, while  $P$  and  $D$  are the rod pitch and outer diameter, respectively.

The pressure drop through the core for the wire-wrap design is therefore equal to:

$$\begin{aligned} \Delta p_{\text{core,RM}} &= f \frac{L}{D_{\text{eq}}} \frac{G^2}{2\rho} + K_{\text{in+out}} \frac{G^2}{2\rho} = \left( \frac{C_{fT}}{\text{Re}^{0.18}} \right) \frac{L}{D_{\text{eq}}} \frac{G^2}{2\rho} + \left( K_{\text{in+out,nom}} \frac{G^{-0.2}}{G_{\text{nom}}^{-0.2}} \right) \frac{G^2}{2\rho} \\ &= C_{fT} \left( \frac{GD_{\text{eq}}}{\mu} \right)^{-0.18} \frac{L}{D_{\text{eq}}} \frac{\dot{m}_{\text{core}}^2}{2\rho N^2 A_{\text{flow}}^2} + K_{\text{in+out,nom}} \left( \frac{\dot{m}_{\text{core}}}{NA_{\text{flow}}} \right)^{1.8} \left( \frac{\dot{m}_{\text{core,nom}}}{NA_{\text{flow}}} \right)^{0.2} \frac{1}{2\rho} \end{aligned}$$

$$\begin{aligned}
&= C_{fr} \left( \frac{4\dot{m}_{core}}{N\mu P_{wetted}} \right)^{-0.18} \frac{LP_{wetted}}{4A_{flow}} \frac{\dot{m}_{core}^2}{2\rho N^2 A_{flow}^2} + K_{in+out,nom} \left( \frac{\dot{m}_{core}}{NA_{flow}} \right)^{1.8} \left( \frac{\dot{m}_{core,nom}}{NA_{flow}} \right)^{0.2} \frac{1}{2\rho} \\
&= C_{fr} \frac{LP_{wetted}^{1.18} \mu^{0.18}}{8 \times 4^{0.18}} \frac{\dot{m}_{core}^{1.82}}{\rho N^{1.82} A_{flow}^3} + K_{in+out,nom} \left( \frac{\dot{m}_{core}}{NA_{flow}} \right)^{1.8} \left( \frac{\dot{m}_{core,nom}}{NA_{flow}} \right)^{0.2} \frac{1}{2\rho} \quad (4.6)
\end{aligned}$$

where  $K_{in+out}$  is a form loss coefficient associated with the total pressure drop loss experienced by the coolant at the core inlet (lower core plate and assembly bottom nozzle) and outlet (assembly upper nozzle and core upper plate).

Eq. 4.6 can be rewritten as:

$$\Delta p_{core, RM} = \frac{\dot{m}_{core}^{1.8}}{2N^{1.8} A_{flow}^{1.8} \rho} \left( C_{fr} \frac{LP_{wetted}^{1.18} \mu^{0.18}}{4 \times 4^{0.18} A_{flow}^{1.2}} \frac{\dot{m}_{core}^{0.02}}{N^{0.02}} + K_{in+out,nom} \left( \frac{\dot{m}_{core,nom}}{NA_{flow}} \right)^{0.2} \right) \quad (4.7)$$

Thus, given an existing PWR retrofitted with a RM core, the core pressure drop ratio can be expressed as:

$$\frac{(\Delta p_{core})_{RM}}{(\Delta p_{core})_{ref}} = \frac{\left( \frac{\dot{m}_{core}}{A_{flow}^{1.8}} \right)_{RM} \left[ C_{fr} \frac{LP_{wetted}^{1.18} \mu^{0.18}}{4 \times 4^{0.18} A_{flow}^{1.2}} \left( \frac{\dot{m}_{core}}{N} \right)^{0.02} + \left( \frac{\dot{m}_{core,nom}}{NA_{flow}} \right)^{0.2} K_{in+out,nom} \right]_{RM}}{\left( \frac{\dot{m}_{core}}{A_{flow}^{1.8}} \right)_{ref} \left[ 0.184 \left( \frac{\pi}{4} \right)^{1.2} \frac{LD^{1.2} \mu^{0.2}}{A_{flow}^{1.2}} + \left( \frac{\dot{m}_{core,nom}}{NA_{flow}} \right)^{0.2} K_{core,nom} \right]_{ref}} \equiv X \quad (4.8)$$

The only ‘unknowns’ in the ratio above are  $(\dot{m}_{core})_{RM}$  and  $(D)_{RM}$  since the reference core parameters are known, the values for  $L$ ,  $\mu$  and fuel rod pitch (the latter needed to evaluate  $A_{flow}$ ) are the same for the two cores, and the loss coefficient representing the pressure drop losses at the entrance and exit of the RM core is assumed to be the same as that of the reference core, following from assumption 2 above.<sup>17</sup>

The overall pressure drop through the RCS,  $\Delta p_{RCS}$ , is the sum of the pressure drop through the core and through the remaining RCS components. The latter, referred to as  $\Delta p_{rest}$ , depends on the coolant flow rate and on the geometry of the RCS components upstream and downstream of the core which, because of the retrofit approach, is the same for the RMPWR and the reference plant. Therefore:

$$(\Delta p_{RCS})_{RM} = (\Delta p_{core})_{RM} + (\Delta p_{rest})_{RM} = X (\Delta p_{core})_{ref} + \left[ \frac{(\dot{m}_{RCS})_{RM}}{(\dot{m}_{RCS})_{ref}} \right]^{1.8} (\Delta p_{rest})_{ref} \quad (4.9)$$

Assuming that the bypass flow is the same as the reference plant (assumption 3), it follows that:

<sup>17</sup> For the reference core, the coefficient  $K_{in+out,nom}$  is calculated as  $K_{core,nom} - 8K_{grid}$ , where the loss coefficient for the eight grids is assumed to be  $\sim 1$  and  $K_{core,nom}$  is obtained from Eq. 4.3, in which  $\Delta p_{core,ref}$  is obtained from  $\Delta p_{RCS,ref}$  (known from (Watts Bar, 2010b)) as  $\Delta p_{RCS,ref}/0.3$ , from assumption 4 above. This gives  $K_{core,nom} = 14.5$  and  $K_{in+out,nom} = 6.5$ .

$$(\Delta p_{RCS})_{RM} = X(\Delta p_{core})_{ref} + \left[ \frac{(\dot{m}_{core})_{RM}}{(\dot{m}_{core})_{ref}} \right]^{1.8} (\Delta p_{rest})_{ref} \quad (4.10)$$

For the reference plant, the pressure drop through the non-core RCS components is proportional to the core pressure drop (assumption 4), i.e.:

$$(\Delta p_{rest})_{ref} = (\Delta p_{RCS})_{ref} - (\Delta p_{core})_{ref} = \frac{(\Delta p_{core})_{ref}}{0.3} - (\Delta p_{core})_{ref} = \frac{0.7}{0.3} (\Delta p_{core})_{ref} \quad (4.11)$$

By introducing Eq. 4.11 into Eq. 4.10, the RCS pressure drop for the RMPWR can be expressed as:

$$(\Delta p_{RCS})_{RM} = \left\{ X + \frac{0.7}{0.3} \left[ \frac{(\dot{m}_{core})_{RM}}{(\dot{m}_{core})_{ref}} \right]^{1.8} \right\} (\Delta p_{core})_{ref} \quad (4.12)$$

Eq. 4.12, with  $X$  calculated using Eq. 4.8, can be used to obtain the RCS pressure drop versus flow curve for an existing PWR retrofitted with a RM core, for a given rod diameter and wire-wrap pitch. Four of these curves, for rod diameters of 11 and 11.5 mm and wire-wrap  $H/D$  values of 14 and 50, are shown in Fig. 4.1 with the RCS curve of the reference plant and the RCP characteristic curve. The intersection between these curves identifies the operating points for each case. The resulting RCS flow rates are summarized in Table 4.2.

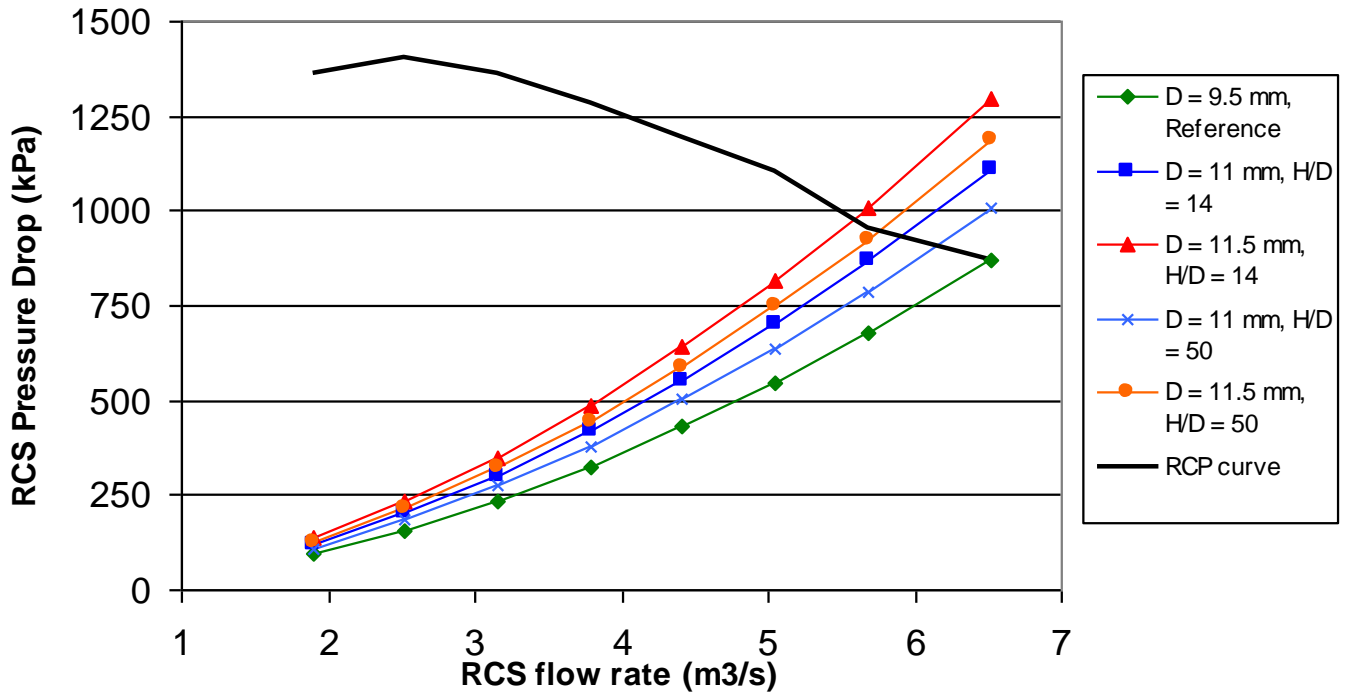


**Fig. 4.1.** 4-loop PWR RCS operating point for different pin diameters. RCP curve based on data from (Watts Bar, 2010b).

**Table 4.2.** RCS flow rates (%) for RM designs relative to reference case.

$H/D$	Pin Diameter (mm)	
	11	11.5
14	91.6	86.5
50	95.7	89.8

It must be emphasized that if the design implementation strategy adopted for this study allowed replacement of the RCPs, then the achievable flow rates would not be constrained to a single value, but would be wider and dependent on the performance of the RCPs available on the market. It must also be noted that a non-retrofit plant would likely have completely different geometry, such as a shorter core, which would make the constraint on flow rate less limiting.

#### 4.2.1.3. Core Exit Temperature

The flow rate reduction imposed by the constraint on RCS pressure drop has implications on the coolant enthalpy at the core exit. Specifically, since  $T_{in}$  cannot be significantly reduced with respect to the reference value (see Section 4.2.1.4), keeping the core power the same as the reference plant results in a higher temperature for the coolant at the exit of the core and, therefore, for the steam generator (SG) tubes. In existing plants, these tubes are made of Inconel 600, which experiences a degradation of mechanical properties above 600 K (Fyfitch, 2003). The SG tube material used in new plants, Inconel 690, has been operated in the range 600–603 K (Cummins et al., 2003; Vanhoenacker, 2009) and can theoretically go higher, but this has not yet been experimentally tested. Therefore, in this analysis, 600 K and 603 K are used as core exit temperature limits for a ‘feasible design’ and a ‘stretch design’, respectively.

#### 4.2.1.4. Core Inlet Temperature

Reducing  $T_{in}$  has a beneficial effect on both DNB (by lowering the coolant enthalpy) and pressure drop (by allowing a reduced flow to remove the same power without increasing  $T_{out}$ ). However, the reduction in  $T_{in}$  must be constrained in order to limit the negative effect on the plant thermodynamic efficiency (due to the lower average temperature of the plant) and, if a retrofit core is specified, to avoid violating the plant limits during overcooling events. This is because the reactor will reach lower temperatures during overcooling accidents, e.g. a steam line break. Components such as the reactor pressure vessel are licensed to operate within pre-established pressure-temperature ranges. If the temperature is lower, then the maximum allowed pressure is also lower. Therefore, reduction of the minimum temperature expected during the vessel operating life would restrict the pressure operation range for the component. As a result, if the reduction in  $T_{in}$  is not constrained, this may require the plant, for example, to operate at a lower nominal pressure or to be provided with more

efficient depressurization systems, both of which are clearly incompatible with a retrofit approach. The maximum allowed reduction in  $T_{in}$  given in Table 4.1, i.e. 5 K, was arbitrarily chosen to limit the deviation from the reference plant operating conditions, while allowing for some flexibility. Some plants have been permitted to operate with a reduced  $T_{in}$  to limit  $T_{out}$ , with temperatures as low as 550 F (560.9 K) being permitted at operating power in some cases (Office of Nuclear Regulation, 1994, 1996).

#### 4.2.1.5. Fuel Assembly Lift-off

Fuel assemblies are subject to a lift-off force due to their interaction with coolant flow. The net force resulting from the balance between this force, buoyancy and gravity is used to design the fuel assembly hold-down springs so that the fuel assemblies are guaranteed to remain in contact with the lower core plate during normal operation, as well as during most of the Condition I and II events. The changes in assembly geometry and core flow investigated in this study cause the lift-off force to change, so that the adequacy of the reference hold-down spring design must be verified for the new conditions. It must be stressed, however, that in contrast to replacing other plant components such as the RCPs, redesigning the hold-down springs would not disallow a retrofit core as it would be possible to modify the springs in an existing core. For this reason, assembly lift-off is not used as a hard constraint for the RMPWR design, and the analysis performed here only assesses whether the implementation of a RM core requires the hold-down springs to be redesigned.

There are three forces acting on the assembly:

1) Drag force ( $F_{drag}$ ): the friction force between the coolant and the fuel assembly. By Newton's third law, this is equal to the force acting on the coolant, which can be calculated from the friction + form pressure drop<sup>18</sup> experienced by the coolant while flowing through the core, as:

$$F_{drag} = \Delta p_{core} P_{FA}^2 \quad (4.13)$$

where  $P_{FA}$  is the assembly pitch.<sup>19</sup>

2) Buoyancy force ( $F_{buoy}$ ): equal to the weight of the water displaced by the assembly.

3) Weight force ( $F_{weight}$ ): the force due to gravity acting on the fuel assembly, which acts against the other two forces. This includes nozzle weight (16 kg, taken from (Yucca Mountain Project, 2007)), and grid spacer weight (0.9 kg, taken from (Watts Bar, 2010a)) and treatment of the fuel, cladding and guide tubes using appropriate volumes and densities.

<sup>18</sup> In the calculation performed in this study, acceleration pressure drop is neglected. This is reasonable since in typical PWR operating conditions the acceleration term is very small.

<sup>19</sup> The area of the assembly envelope is used, in place of the assembly flow area, since  $\Delta p_{core}$  is measured from just below the lower core plate to just above the core upper plate.

The effect of the design changes on the net axial force acting on the assembly can be estimated by calculating the ratio between the net force on the RM assembly and that on the reference assembly, i.e.:

$$F_{\text{ratio}} = \frac{(F_{\text{drag}})_{\text{RM}} + (F_{\text{buoy}})_{\text{RM}} - (F_{\text{weight}})_{\text{RM}}}{(F_{\text{drag}})_{\text{ref}} + (F_{\text{buoy}})_{\text{ref}} - (F_{\text{weight}})_{\text{ref}}} = \frac{X(F_{\text{drag}})_{\text{ref}} + Y(F_{\text{buoy}})_{\text{ref}} - Z(F_{\text{weight}})_{\text{ref}}}{(F_{\text{drag}})_{\text{ref}} + (F_{\text{buoy}})_{\text{ref}} - (F_{\text{weight}})_{\text{ref}}} \quad (4.14)$$

where  $X$  is the core pressure drop ratio defined by Eq. 4.8,  $Y$  is the ratio of the total volumes displaced by the two assemblies (including grid spacer and nozzle volumes, which are approximately constant) and  $Z$  is the ratio of the total weights of the two assemblies, assuming that the grid and nozzle weights are constant.

Therefore, given a RM core with a certain geometry and coolant flow, Eq. 4.14 combined with Eqs. 4.8 and 4.13 can be used to estimate the lift-off force ratio. If this ratio is larger than 1, then the assembly hold-down mechanism for a retrofit core would need to be redesigned.

## 4.2.2 Single-assembly Thermal-Hydraulic Analysis

### 4.2.2.1. Model Characteristics

Single-assembly analyses were performed with the subchannel code COBRA-EN (Basile et al., 1987, revised 1999) to evaluate the thermal-hydraulic performance of the 11 and 11.5 mm rod diameter cases, as well as the 9.5 mm case used as reference. Because the code is not capable of modelling the wire-wrap assumed for the large rod cases, for these designs the pressure drop and the MDNBR were calculated separately, since these parameters are significantly affected by the presence of the wires. Other parameters such as the coolant enthalpy axial profile are instead calculated with COBRA.<sup>20</sup> As the RCPs cannot be replaced in a retrofit core, the coolant flow rate was derived using the RCP performance constraint discussed in Section 4.2.1.2 and given in Fig. 4.1.

Assembly operating conditions, shown in Table 4.3, were selected to be representative of the hot assembly of a RMPWR core and, since no full-core coupled neutronic-thermal-hydraulic analysis has been performed, power peaking factors were assumed. The values used for these parameters are typical design values used for UO<sub>2</sub>-fuelled PWRs, and are therefore assumed to be reasonably conservative for RMPWRs as well. It was also assumed that a RM assembly could be designed with a pin peaking factor as low as that in the UO<sub>2</sub> reference case (1.06) by careful distribution of pins with varying fissile contents.

<sup>20</sup> These basic parameters are easy to calculate by hand. However, as COBRA was also used to calculate parameters such as the MDNBR using the W-3 correlation, values were taken from COBRA where possible for expediency.

**Table 4.3.** Parameters used for thermal-hydraulic analysis.

<i>Fixed parameters</i>	
Assembly lattice type	17×17, square
Assembly length	4.063 m
Assembly heated length	3.66 m
Number of fuel rods per assembly	264
Assembly pitch	0.215 m
Fuel rod pitch	12.6 mm
Control rod guide tube and instrumentation tube OD	12.24 mm
Assembly power and % with respect to nominal	31.4 MWt, 112%
Axial power profile	Chopped cosine, 1.55 peak
Assembly radial power peaking factor	1.587
Hot pin power peaking factor	1.06
Enthalpy rise hot channel factor	1.682 (= 1.587×1.06)
Power fraction in coolant	2.6%
Lower and upper plate and nozzle total loss coefficient ( $K_{in+out,nom}$ )	6.5
<i>Variable parameters</i>	
Fuel rod OD	9.5 (reference), 11 and 11.5 mm
$T_{in}$	Variable (565.3 K is the nominal value for the reference design, increased by 2 K for MDNBR calculation)
Coolant inlet mass flux	Constant with nominal value 3728 kg/m <sup>2</sup> /s, then reduced by 5% for MDNBR calculations (413200 gpm (26073 m <sup>3</sup> /s) flow rate, 9.6% bypass flow = nominal value for the reference design, from (Watts Bar, 2010b))
Wall friction factor	Smooth tube friction factor for grid-supported rods; Eq. 4.4 for wire-wrap designs
Rod support type	Grids (reference); otherwise wire-wrap
Number of grid spacers per assembly	8 (reference assembly design only)
Grid spacer loss coefficient	1.0

#### 4.2.2.2. Results

The performance of 11 mm and 11.5 mm pin diameters relative to the reference case (Case 0) is presented in Table 4.4. Firstly,  $T_{in}$  is held constant and equal to the ‘nominal’ value (Case 1), and then it is dropped by 5 K (Case 2). The RCS flow rate is determined from Table IV. Finally, the mass flow rate is reduced by 10% to examine the sensitivity of the calculations to the pressure drop calculations (Case 3). Wire-wrap  $H/D$  of 14 and 50 were considered. For Cases 1–3, the results in

Table 4.4 are highlighted as follows: bold indicates an acceptable value, bold-italics indicates a value exceeding the ‘feasible case’ limit but still below the ‘stretch case’ limit, whereas italics indicates an unacceptable value.<sup>21</sup>

**Table 4.4.** Results of thermal-hydraulic analysis (*infeasible/ stretch/ feasible*).

Case	Pin OD (mm)	Wire $H/D$	Core flow rate relative to reference (%)	Hot assembly mass flux ( $\text{kg/m}^2/\text{s}$ )	$T_{\text{in}}$ (K)	$T_{\text{out}}$ (K)	MDNBR	
							DDH	W-3*
0	9.5	N/A (grid spacers)	100.0	3728	565.3	598.4	<b>1.31</b>	1.72
1a	11	14	91.6	4612	<b>565.3</b>	<b>601.1</b>	<b>1.33</b>	2.25
1b	11.5	14	86.5	4995	<b>565.3</b>	<b>603.0</b>	<i>1.27</i>	2.17
1c	11	50	95.7	4818	<b>565.3</b>	<b>599.7</b>	<i>1.27</i>	2.52
1d	11.5	50	89.8	5186	<b>565.3</b>	<b>601.8</b>	<i>1.20</i>	2.46
2a	11	14	91.6	4612	<b>560.3</b>	<b>597.0</b>	<b>1.39</b>	2.69
2b	11.5	14	86.5	4995	<b>560.3</b>	<b>599.0</b>	<b>1.32</b>	2.69
2c	11	50	95.7	4818	<b>560.3</b>	<b>595.6</b>	<b>1.33</b>	2.98
2d	11.5	50	89.8	5186	<b>560.3</b>	<b>597.7</b>	<i>1.25</i>	3.01
3a	11	14	82.4	4150	<b>560.3</b>	<b>600.6</b>	<i>1.29</i>	2.01
3b	11.5	14	77.9	4496	<b>560.3</b>	<b>602.8</b>	<i>1.23</i>	1.85

\*Although not used for determining design acceptability, the MDNBR calculated with the W-3 correlation is also shown to highlight the non-conservative results that would be obtained if this correlation was used for tight lattices. This value was calculated without mixing due to wire-wraps for the RM cases.

From Table 4.4 it can be seen that:

- For the 11 mm pin diameter design, the thermal-hydraulic design constraints are met in Case 1a (‘nominal’  $T_{\text{in}}$  and  $H/D=14$ ) and Cases 2a and 2c (reduced  $T_{\text{in}}$  with  $H/D=14$  and 50, respectively). Therefore with this pin size the MDNBR constraint can be satisfied without lowering  $T_{\text{in}}$  (Case 1a). However,  $T_{\text{out}}$  is slightly too high for the ‘feasible’ case, but still within the stretch case limit. This can be readily rectified by dropping  $T_{\text{in}}$  very slightly, as can be inferred from the increase in MDNBR achieved when  $T_{\text{in}}$  is reduced to the lowest acceptable value (Case 2a). As for the transition to the  $H/D=50$  wire design, unless  $T_{\text{in}}$  is reduced (Case

<sup>21</sup> As shown in Table 4.1, while a single limit is used for the MDNBR, for the coolant exit temperature a ‘feasible case’ limit and a ‘stretch case’ limit is used.

2c), the transition to this ‘looser’ wire configuration results in an unacceptable MDNBR (Case 1c). This is because the beneficial effect on MDNBR of the increase in mass flux (4612 to 4818 kg/m<sup>2</sup> s) allowed by the lower pressure drop is offset by the less efficient coolant mixing resulting from the higher  $H/D$ , which yields an overall reduction in MDNBR.

- For the 11.5 mm pin diameter design, the thermal-hydraulic constraints are met in Case 2b only (reduced  $T_{in}$  and  $H/D = 14$ ). Hence, for this rod size design a drop in  $T_{in}$  is required to satisfy the MDNBR constraint.
- If the actual core mass flow is 10% lower than that predicted using the methodology of Section 4.2.1.2, the RM cases are not feasible, even if  $T_{in}$  is dropped by 5 K.

The W-3 correlation gives an inaccurate prediction of the relative performance of (1) the tight-lattice geometries with respect to the reference, open-lattice, geometry, and (2) the  $H/D = 14$  design with respect to the  $H/D = 50$  design. Firstly, the W-3 correlation predicts that all the RM cases (Cases 1a–3b) have much better DNB performance than the reference case (Case 0). This is clearly a consequence of neglecting the inherent differences between large and narrow channel behaviour with respect to DNB, which results in the difference between tight and regular lattices being mainly due to mass flux differences. The W-3 correlation is also incapable of capturing the wire pitch effect on MDNBR. Unlike the DDH correlation, which predicts a higher MDNBR for the  $H/D = 14$  cases compared to the  $H/D = 50$  cases (see, for example, Cases 1a and 1c), the W-3 correlation shows the opposite trend ( $MDNBR_{1a} < MDNBR_{1c}$ ). This is because it does not capture any wire-induced mixing effects, so the difference in DNB performance is due to the difference in mass flux only.

Assembly lift-off results are presented in Table 4.5. As discussed in Section 4.2.1.5, assembly lift-off is not a ‘hard’ constraint and design ‘retrofitability’ should not be based on whether the lift-off forces are higher or lower than the reference design. For the ‘preferred’  $H/D = 14$ , the lift-off force is 1.9 and 2.7 times higher than for the reference assembly, for 11 and 11.5 mm pin diameters respectively. This increase is mainly driven by the higher drag, which, in turn, is due to the higher pressure drop experienced by the coolant while flowing through a tight lattice. It can also be seen that the effect of the higher drag on the net lift-off force is partly reduced by the larger weight of the tight-lattice assemblies, which have larger, and therefore heavier, fuel rods.

**Table 4.5.** Estimated lift-off force per fuel assembly

Pin diameter (mm)	$H/D$	$F_{\text{drag}}$ (kN)	$F_{\text{buoy}}$ (kN)	$F_{\text{weight}}$ (kN)	Net force (kN)
9.5		8.7	0.5	6.2	3.0
11	14	13.4	0.7	8.4	5.8
11.5	14	16.5	0.8	9.1	8.1
11	50	11.1	0.7	8.4	3.5
11.5	50	14.5	0.8	9.1	6.1

Based on the thermal-hydraulic performance summarized in Tables 4.4 and 4.5, the use of a ‘tightly-coiled’ wire-wrap, i.e. with small  $H/D$ , is recommended since it clearly helps to satisfy the DNB safety requirement, especially when  $T_{\text{in}}$  cannot be reduced below the reference value. Adoption of this wire design would also benefit rod performance from a vibration standpoint, since a lower  $H/D$  implies more rod support points per unit of length. The higher pressure drop resulting from the use of a tightly-coiled wire is not considered to be a showstopper, since the reduction in core flow due to the constrained RCP performance is accounted for in the DNB analysis and the higher lift-off forces can be accommodated by eventually redesigning the assembly hold-down mechanism.

Because of the beneficial effect that a reduction in  $T_{\text{in}}$  has on DNB, combining a small  $H/D$  with a slight reduction in  $T_{\text{in}}$  would also yield acceptable performance. Reducing  $T_{\text{in}}$  below the reference value is particularly beneficial for the 11.5 mm rod size design, which satisfies DNB constraint only if  $T_{\text{in}}$  is reduced.

#### **4.2.3. RMPWR Post-LOCA Reflood**

The effect of tightening the fuel rod lattice on the reflood phase of a large-break loss-of-coolant accident (LBLOCA) needs to be investigated to assess whether safety criteria on peak clad temperature (PCT) and clad oxidation are satisfied. Previous studies on the reflooding of tight lattices, e.g. Courtaud et al. (1988), Veteau et al. (1994) and Dreier et al. (1988) provided experimental evidence that, as expected, tight lattices are more difficult to reflood than open lattices. In particular, from (Courtaud et al., 1988), the quench time and PCT will both be worse for a tight lattice design due to the increased pressure drop across the core and lower coolant inventory.

In this study, the reflood of the RM designs has not been investigated either experimentally or computationally. Only some simplified analytical considerations are presented, with the purpose of estimating the difference in coolant upflow velocity between tight and open lattices under the assumptions of the same gravity head and single-phase coolant, i.e. no vaporization. The first

assumption is appropriate as, in a post-LOCA scenario, reflooding is driven by the gravity head of the liquid downcomer, which has to overcome the pressure drop through the core. A tight lattice will have a lower reflood velocity as it has a higher friction pressure drop than an open lattice, and the downcomer gravity head is independent of the lattice. Experimental data (e.g. in the studies mentioned above) compared open and tight lattices reflooding capabilities by imposing the same reflooding velocity at the bundle inlet. However, for gravity-driven reflood, the inlet velocity depends on a momentum balance between the downcomer gravity head and the core pressure drop. The importance of an experimental comparison between tight and open lattices in conditions representative of a gravity-driven reflooding was recognized in (Erbacher and Wiehr, 1988) but no data of this type have been found in the literature. The second assumption, i.e. no vaporization, is not representative of post-LOCA scenarios. However, it simplifies the calculation and allows an upper bound for the tight-to-open lattice reflooding velocity ratio to be obtained. In reality, for the same linear power profile, steam generation will occur earlier in the reflood of the tight lattice due to the lower coolant flow rate, which increases the pressure drop and thus reduces the tight-to-open lattice reflooding velocity ratio below that obtained by neglecting vaporization. This was experimentally verified in (Erbacher and Wiehr, 1988).

The analysis is performed for both the simplified case in which the effect of rod-supporting devices, i.e. grid spacers and wire-wraps, is neglected (bare rods, see Section 4.2.3.1) and for the more realistic case in which it is accounted for (Section 4.2.3.2). Also, for completeness both laminar and turbulent regimes are considered. The operating conditions are arbitrarily assumed to be 0.2 MPa and 100 °C.

#### 4.2.3.1. Reflooding Velocity Comparison for Bare-rod Bundles

From (Rehme, 1987), the laminar friction factor for interior subchannels of square-lattice bundles can be calculated as:

$$f = \frac{40.70}{\text{Re}} \left( \frac{P}{D} - 1 \right)^{0.435} \quad (4.15)$$

where  $P$  is the fuel rod pitch and  $D$  is the rod outer diameter. Therefore, the friction pressure drop is:

$$\Delta p_{\text{fric}} = f \frac{L}{D_{\text{eq}}} \frac{\rho v^2}{2} = \frac{40.70 \mu}{\rho v D_{\text{eq}}} \left( \frac{P}{D} - 1 \right)^{0.435} \frac{L}{D_{\text{eq}}} \frac{\rho v^2}{2} \quad (4.16)$$

where  $v$  is the reflood velocity,  $D_{\text{eq}}$  is the equivalent diameter. Therefore, for the simplified case of bare rods, the pressure drop due to friction is:

$$\Delta p_{\text{fric}} \propto \left( \frac{P}{D} - 1 \right)^{0.435} \frac{v}{D_{eq}^2} \quad (4.17)$$

in the laminar regime, and:

$$\Delta p_{\text{fric}} \propto \frac{v^{1.8}}{D_{eq}^{1.2}} \quad (4.18)$$

in the turbulent regime (as shown in Eq. 4.1).

Therefore, for the same downcomer gravity head, the relation between the inlet velocity of a tight and an open lattice can be estimated by equating the friction pressure drop for the two bare-rod lattices, giving:

$$\frac{v_{\text{tight}}}{v_{\text{open}}} \sim \left[ \frac{\left( \frac{P}{D} - 1 \right)_{\text{open}}}{\left( \frac{P}{D} - 1 \right)_{\text{tight}}} \right]^{0.435} \left[ \frac{\left( D_{\text{eq}} \right)_{\text{tight}}}{\left( D_{\text{eq}} \right)_{\text{open}}} \right]^2 = \left[ \frac{\left( \frac{P}{D} - 1 \right)_{\text{open}}}{\left( \frac{P}{D} - 1 \right)_{\text{tight}}} \right]^{0.435} \left[ \frac{\left( \frac{D_{\text{tight}}}{D_{\text{open}}} \right) \left( \frac{P}{D} \right)_{\text{tight}}^2 - \frac{\pi}{4}}{\left( \frac{P}{D} \right)_{\text{open}}^2 - \frac{\pi}{4}} \right]^2 \quad (4.19)$$

in the laminar regime, and:

$$\frac{v_{\text{tight}}}{v_{\text{open}}} \sim \left[ \frac{\left( D_{\text{eq}} \right)_{\text{tight}}}{\left( D_{\text{eq}} \right)_{\text{open}}} \right]^{\frac{1.2}{1.8}} = \left[ \frac{\left( \frac{D_{\text{tight}}}{D_{\text{open}}} \right) \left( \frac{P}{D} \right)_{\text{tight}}^2 - \frac{\pi}{4}}{\left( \frac{P}{D} \right)_{\text{open}}^2 - \frac{\pi}{4}} \right]^{0.667} \quad (4.20)$$

in the turbulent regime.

Using Eqs. 4.19 and 4.20, it can be seen that:

- for the 11.5 mm pin diameter case:  $\frac{v_{\text{tight}}}{v_{\text{open}}} = \begin{cases} 0.45 & \text{in the laminar regime} \\ 0.64 & \text{in the turbulent regime} \end{cases}$
- for the 11 mm pin diameter case:  $\frac{v_{\text{tight}}}{v_{\text{open}}} = \begin{cases} 0.56 & \text{in the laminar regime} \\ 0.73 & \text{in the turbulent regime} \end{cases}$

#### 4.2.3.2. Reflooding Velocity Comparison for Grid/Wire-supported Rod Bundles

For grid-supported rod bundles, the friction pressure drop in the laminar regime can be expressed as:

$$\Delta p_{\text{ref}} = \left[ \frac{40.70\mu}{\rho v D_{\text{eq}}} \left( \frac{P}{D} - 1 \right)^{0.435} \frac{L}{D_{\text{eq}}} + K_{\text{core}} \right] \frac{\rho v^2}{2} = \left[ \frac{C_1}{v} + K_{\text{core}} \right] \frac{\rho v^2}{2} \quad (4.21)$$

For wire-supported rods, the friction factor in the laminar regime can be expressed as (Cheng and Todreas, 1986):

$$f = \frac{C_{fL}}{\text{Re}} \text{ where } C_{fL} = \left\{ -974.6 + 1612 \frac{P}{D} - 598.5 \left( \frac{P}{D} \right)^2 \right\} \left( \frac{H}{D} \right)^{0.06 - 0.085(P/D)} \quad (4.22)$$

Therefore, the following relation can be obtained for the pressure drop for the RM design:

$$\Delta p_{\text{RM}} = \left[ \frac{C_{fL}}{\text{Re}} \frac{L}{D_{\text{eq}}} + K_{\text{in+out}} \right] \frac{\rho v^2}{2} = \left[ \frac{C_{fL}\mu}{\rho v D_{\text{eq}}} \frac{L}{D_{\text{eq}}} + K_{\text{in+out}} \right] \frac{\rho v^2}{2} = \left[ \frac{C_2}{v} + K_{\text{in+out}} \right] \frac{\rho v^2}{2} \quad (4.23)$$

Equating the pressure drops for the two assembly designs, i.e. Eqs. 4.21 and, 4.23, gives:

$$\left[ C_1 v + K_{\text{core}} v^2 \right]_{\text{pen}} = \left[ C_2 v + K_{\text{in+out}} v^2 \right]_{\text{ight}} \quad (4.24)$$

where  $K_{\text{in+out,nom}} = 6.5$  and  $K_{\text{core,nom}} = 14.5$  (from Table 3.3).  $C_1$  is about 0.3 and  $C_2$  ranges between 2.2 and 3 depending on the tight lattice considered. It must be noted that Eq. 4.24 is only valid for Reynolds numbers below  $\text{Re}_L = 10^{(0.78+1.7P/D)}$ , which represents the validity range for Eq. 4.22 (Cheng and Todreas, 1986). This value is approximately 500 for both tight lattice geometries considered in this study, which corresponds to a coolant velocity  $v_{\text{tight}}$  of  $\sim 2$  cm/s for the operating conditions previously described. Using a typical laminar regime boundary of  $\text{Re} = 2100$  for the reference bundle, the maximum  $v_{\text{open}}$  for which Eq. 4.21 is valid is  $\sim 5$  cm/s.

When the flow is turbulent, rearranging Eq. 4.8 with the pressure drop ratio across the core set equal to unity gives:

$$\frac{\left[ 0.184 \left( \frac{\pi}{4} \right)^{1.2} \frac{LD^{1.2}\mu^{0.2}}{A_{\text{flow}}^{1.2}} + \left( \frac{\dot{m}_{\text{core,nom}}}{NA_{\text{flow}}} \right)^{0.2} K_{\text{core,nom}} \right]_{\text{open}}}{\left[ C_{fT} \frac{LP_{\text{wetted}}^{1.18}\mu^{0.18}}{4 \times 4^{0.18} A_{\text{flow}}^{1.2}} \left( \frac{\dot{m}_{\text{core}}}{N} \right)^{0.02} + \left( \frac{\dot{m}_{\text{core,nom}}}{NA_{\text{flow,nom}}} \right)^{0.2} K_{\text{in+out,nom}} \right]_{\text{tight}}} = \left( \frac{v_{\text{tight}}}{v_{\text{open}}} \right)^{1.8} \quad (4.25)$$

Using the same values for the water properties and loss coefficients as those adopted for the laminar regime case, Eq. 4.25 can be rewritten as:

$$\frac{\left[ 0.109 \frac{D_{\text{open}}^{1.2}}{A_{\text{flow,open}}^{1.2}} + 74.3v_{\text{open}}^{0.2} \right]}{\left[ C_{fT} \frac{L\pi^{1.18} \mu^{0.18} D_{\text{tight}}^{1.18} v_{\text{tight}}^{0.02} \rho^{0.02}}{4^{1.18} A_{\text{flow,tight}}^{1.18}} + 44.6v_{\text{tight}}^{0.2} \right]} = \left( \frac{v_{\text{tight}}}{v_{\text{open}}} \right)^{1.8} \quad (4.26)$$

By entering the geometric parameters of the reference open lattice, Eq. 4.26 becomes:

$$\frac{\left[ 30.1 + 74.3v_{\text{open}}^{0.2} \right]}{\left[ 0.800 C_{fT} \frac{D_{\text{tight}}^{1.18} v_{\text{tight}}^{0.02}}{A_{\text{flow,tight}}^{1.18}} + 44.6v_{\text{tight}}^{0.2} \right]} = \left( \frac{v_{\text{tight}}}{v_{\text{open}}} \right)^{1.8} \quad (4.27)$$

Eq. 4.27 simplifies to:

$$30.1v_{\text{open}}^{1.8} + 74.3v_{\text{open}}^2 = C v_{\text{tight}}^{1.82} + 44.6v_{\text{tight}}^2 \quad (4.28)$$

where the coefficient  $C = 0.800 C_{fT} \left( D_{\text{tight}} / A_{\text{flow,tight}} \right)^{1.18}$ , is equal to ~80 and ~51 for the 11 mm rod OD case (for  $H/D = 14$  and  $50$ , respectively) and equal to ~85 and ~62 for the 11.5 mm rod OD case (for  $H/D = 14$  and  $50$ , respectively). Eq. 4.28 can readily be solved by the Newton-Raphson method for given  $v_{\text{open}}$ . Also, by taking the exponents 1.8, 1.82 and 2 to be 1.9, which gives indicative results for reflood velocities around ~1 m/s, this simplifies to:

$$\frac{v_{\text{tight}}}{v_{\text{open}}} \approx \left( \frac{104.4}{44.6 + C} \right)^{1/1.9} \quad (4.29)$$

i.e.  $v_{\text{tight}}/v_{\text{open}}$  is approximately constant, and

$$\text{- for the 11.5 mm pin diameter case: } \frac{v_{\text{tight}}}{v_{\text{open}}} = \begin{cases} 0.89 & \text{for } H/D = 14 \\ 0.99 & \text{for } H/D = 50 \end{cases}$$

$$\text{- for the 11 mm pin diameter case: } \frac{v_{\text{tight}}}{v_{\text{open}}} = \begin{cases} 0.91 & \text{for } H/D = 14 \\ 1.05 & \text{for } H/D = 50 \end{cases}$$

It must be stressed that Eq. 4.28 is only applicable to the turbulent regime which, for tight lattices, was identified by (Cheng and Todreas, 1986) as  $Re > Re_T = 10^{(3.3+0.7P/D)}$  (see Eq. 4.22). This value is approximately 12000 for both tight lattice geometries considered in this study, which corresponds to a coolant velocity  $v_{\text{tight}}$  of ~50 cm/s. Using a turbulent regime boundary of  $Re > 10000$  for the

reference bundle, the minimum  $v_{\text{open}}$  for which the numerator of Eq. 4.25, and therefore Eq. 4.28, is valid is  $\sim 25$  cm/s.

From Eqs. 4.24 and 4.28 it can be seen that  $v_{\text{tight}}/v_{\text{open}}$  is dependent on the reflood velocity when accounting for the rod supports (unlike for the bare rod case in Section 4.2.3.1). This is shown in Fig. 4.2 (laminar regime) and Fig. 4.3 (turbulent regime). In both figures, it can be seen that:

- the maximum and minimum ratios correspond to the 11 mm rod OD with  $H/D=50$  and the 11.5 mm rod OD with  $H/D=14$ , respectively. This is expected since these RM geometries are those that provide the minimum and maximum resistance to flow, respectively.
- the velocity ratio increases as  $v_{\text{open}}$  increases. This is because, as the velocity increases, the increased friction drag in the RM case becomes less significant relative to the form drag of the grid spacers. This is particularly true in the laminar case, where at very low velocities the friction drag dominates (constant terms in Eq. 4.24). In the turbulent case, the reflood velocities are similar as the form drag is much larger, including  $K_{\text{in+out}}$  which is the same for both open and tight lattices.
- For the laminar case, accounting for the velocity validity range for Eq. 4.24, velocity ratios are between about 0.1 and 0.5. For a hypothetical reflooding velocity of 2 cm/s, the ratio is  $\sim 0.2$ – $0.3$  depending on the tight lattice geometry considered. In comparison, the calculation assuming bare rods (Section 4.2.3.1) provided velocity ratios of 0.45 and 0.56 for the 11.5 and 11 mm rod OD cases, respectively. The wire-wraps cause a pressure drop due to friction, which is larger at low reflood velocities than a grid spacer form loss, which makes the situation worse.
- In the turbulent case, the higher velocity makes the grid spacer loss coefficient of the reference case much larger than the wire-wrap friction. This offsets the higher rod friction of the RM lattice, leading to similar reflood velocities. In comparison, the calculation assuming bare rods (Section 4.2.3.1) provided velocity ratios in turbulent regime of 0.64 and 0.73 for the 11.5 and 11 mm rod OD cases, respectively, which, in contrast to the laminar case, is lower than when accounting for form losses and wire-wraps.

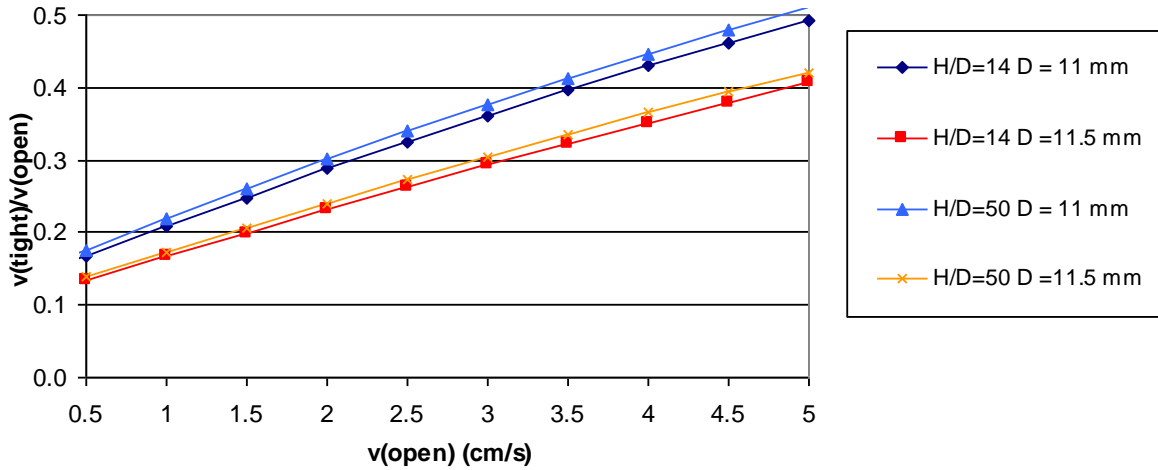


**Fig. 4.2.** Estimated coolant velocity ratio for different tight lattice geometries, in the laminar regime (constant gravity head, no vaporization).

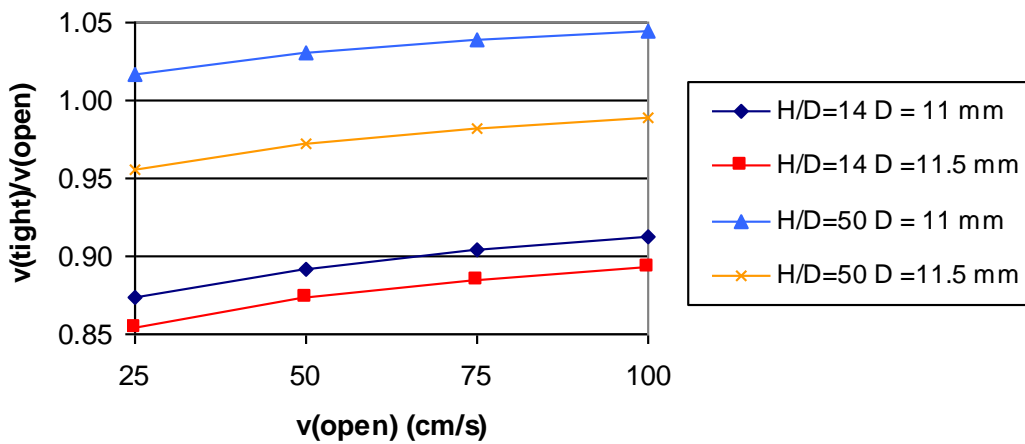


**Fig. 4.3.** Estimated coolant velocity ratio for different tight lattice geometries, in the turbulent regime (constant gravity head, no vaporization).

It must be emphasized that, because of the simplifying assumptions made (mainly the no-vaporization assumption), Figs. 4.2 and 4.3 are not intended to show the actual tight-to-open lattice reflooding velocity ratio but an upflow velocity ratio under the assumptions of gravity-driven flooding and no vaporization. As discussed at the beginning of Section 4.2.3.2, these ratios are expected to represent the upper bound of the actual reflooding velocity ratio.

#### 4.2.3.3. Impact of Slower Reflooding on PCT and Cladding Oxidation

As discussed, experimental results on the reflooding characteristics of tight versus open lattices under gravity-driven conditions have not been found in the open literature, and only data collected imposing the same reflooding velocity for both lattice types are available. Courtaud et al. (1988), Veteau et al. (1994) and Dreier et al. (1988) performed experimental analyses of reflood for tight

lattices compared with open lattices. In all cases, experiments were performed by fixing the inlet velocity. Experimental results for quenching times are available for reductions in hydraulic diameter from the reference (11.8 mm) to values ranging from 4 to 7.9 mm. This compares to 7.4 and 6.1 mm for 11 and 11.5 mm pin diameters respectively. The quenching time generally increased by a factor of 1.5–3 which corresponds to a tight-to-open reflooding velocity ratio of 0.3–0.7. This is shown in Table 4.6.

**Table 4.6.** Comparison between quenching time and PCT of an open and a tight lattice for different initial wall temperature ( $T_{wi}$ ) and linear power ( $q'_{ave}$ ) (inlet flooding velocity  $\sim 3.7$  cm/s,  $T_{flood,in} = 73.5$  °C,  $p = 0.3$  MPa, axial peaking = 1.6) from (Veteau et al., 1994).

	Triangular lattice (tight) ( $D_{rod} = 9.5$ mm, $P_{rod} = 12.23$ mm, $D_{hyd} = 7.86$ mm)		Square lattice (open) ( $D_{rod} = 9.5$ mm, $P_{rod} = 12.6$ mm, $D_{hyd} = 11.8$ mm)		Tight vs open lattice comparison	
	Quenching time (s)	PCT (°C)	Quenching time (s)	PCT (°C)	Quenching time ratio	PCT difference (°C)
Case 1 ( $T_{wi} = 600$ °C, $q'_{ave} = 1$ kW/m)	550	930	350	810	1.6	120
Case 2 ( $T_{wi} = 600$ °C, $q'_{ave} = 0.87$ kW/m)	525	875	280	710	1.9	165
Case 3 ( $T_{wi} = 385$ °C, $q'_{ave} = 0.68$ kW/m)	330	650	120	530	2.8	120

Since the higher PCT resulting from the delay in quenching may violate the cladding temperature limit in LOCA scenarios, a detailed LOCA analysis is required which accounts for the effect of the tight lattice on the reflooding characteristics. Courtaud et al. (1988) and Veteau et al. (1994) reported increases in the PCT of up to 190 K relative to the reference case, although Dreier et al. (1988) measured a much lower ( $\sim 20$  K) increase in PCT. According to NRC (2013) regulations the limit on PCT is 1478 K. Frepoli et al. (2004) modeled a LBLOCA in an *API000*, and found a 95<sup>th</sup> percentile PCT of 1290 K (with at least 95% confidence). The increase in PCT for the tight lattice may violate this limit, necessitating a core de-rating or a reduction in the core height (i.e. a non-retrofit core).

A longer quenching time and a higher PCT also result in more significant cladding oxidation, which could exceed the 17% oxide thickness limit imposed by the NRC (2013). The oxidation progression can be predicted using the reaction constant  $K_R$  found by means of the Baker-Just correlation (Baker and Just, 1962). The time variation of the oxide thickness (m) can be expressed as:

$$\delta_t = \sqrt{\delta_{t-\Delta t}^2 + \Delta t \frac{K_R}{\rho_c^2}} = \sqrt{\delta_{t-\Delta t}^2 + \Delta t \frac{3330 \exp(-22896/T)}{\rho_c^2}} \quad (4.30)$$

where  $T$  is the cladding temperature in K, and  $\rho_c$  is the non-oxidized cladding density in  $\text{kg/m}^3$ . A higher quenching time and PCT can therefore significantly increase cladding oxidation.

Eq. 4.30 allows a very rough estimate of the relative increase in oxidation resulting from a longer quenching time and/or a higher cladding temperature. Fig. 4.4 shows the percentage of cladding thickness converted to oxide as a function of time and cladding temperature, for the reference lattice, obtained using Eq. 4.30 and assuming constant temperature with time. It can be seen that, with respect to an assumed temperature of 1100 K, an increase in temperature that can be reasonably expected for a tight-lattice design, i.e. 200 K, would result in an oxidation percentage:

- 4–5 times higher if the quenching time is assumed to be the same for the two lattices;
- more than 5 times higher if, in addition to the higher temperature, a longer quenching time is also assumed.

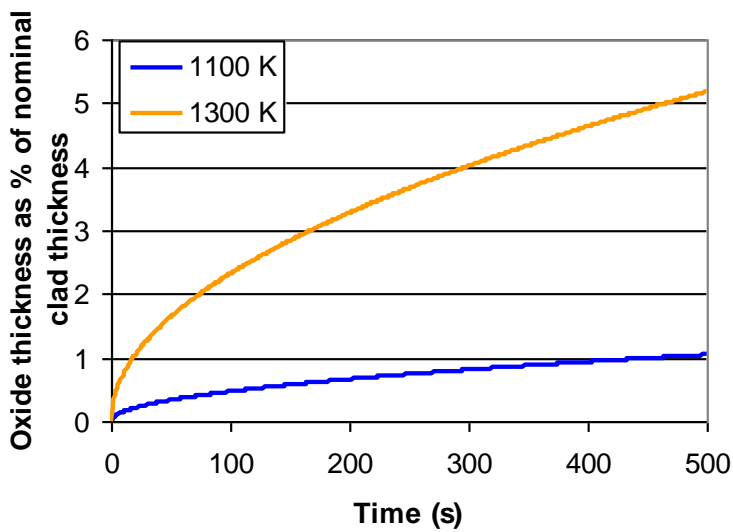


**Fig. 4.4.** Effect of quench time and cladding temperature on clad oxidation.

Clearly, this increase would not be acceptable if the margin from the 17% limit of the reference case was not large. Frepoli et al. (2004) reported that with Westinghouse’s 1996 best estimate methodology, the maximum local clad oxidation was < 12.9% with 95% confidence (compared to a maximum of 17%), and the maximum core-wide clad oxidation was 0.73% (compared to a maximum of 1%). Although improved best estimate methodology will likely reduce these values, it still seems likely that a 200 K increase in clad temperature would result in unacceptable clad oxidation.

### 4.3. Concluding Remarks

For the 11 mm pin diameter design, the MDNBR and  $T_{\text{out}}$  constraints can be satisfied. This may require dropping  $T_{\text{in}}$  slightly, but this is thought to be acceptable. For the 11.5 mm pin diameter design, a 5 K drop in  $T_{\text{in}}$  and a ‘tight’ wire-wrap ( $H/D=14$ ) are required to satisfy the thermal-hydraulic constraints.

However, experimental evidence and analytical calculations seem to indicate that a retrofit RMPWR core will have reduced margin, or even no margin, from LOCA licensing limits if compared to the reference core design. This needs to be confirmed through computational analysis and, ultimately, experimental tests. If proven to be the case, retrofitting a typical PWR core with a RM core would be feasible only after either de-rating the plant or switching to a cladding material with better LOCA performance than Zr-based alloys. Another option would be to design a shorter but wider core, so that the total core power could be preserved with lower linear power and a shorter quenching time. This is preferable for optimizing the overall reactor performance, but incompatible with the retrofit approach investigated in this study. A LBLOCA computational analysis needs to be performed to reach a more definitive conclusion. This requires a code which can adequately simulate the performance of tight pitch lattices. Existing codes may not be able to simulate this design, so a modified code may be required (e.g. (Wu et al., 2012)).

## **Chapter 5 – RMPWR Full-core Analysis**

In Chapter 2, single assembly analyses were used to derive equilibrium fuel designs and isotope vectors for the RMPWR. The fuel pin diameter of a standard 17×17 Westinghouse assembly was increased from 9.5 mm to 11–11.5 mm in order to permit full TRU recycle with adequate discharge burn-up (~40 GWd/t) with a negative MTC. To achieve this, spatial separation of Th-TRU and Th-U3 was necessary. In this chapter, the analysis is extended to multi-tier fuel concepts, and use of in-core fuel management techniques to improve neutronic feasibility is considered. Using different batch management strategies for Th-TRU and Th-U3 is found to be neutronically advantageous, such that the FVR and ZCR can be significantly reduced. An in-depth analysis of the developed in-core fuel management concepts is then presented, including treatment of use of mechanical shim to control excess reactivity with acceptable core power peaking. Core designs with ~40 GWd/t discharge burn-up and negative FVR are identified, although the ZCR is substantially positive.

~2000 pcm of excess reactivity must be controlled with mechanical shim, which increases the power peaking. The maximum fuel enthalpy deposition in a rod-ejection accident (REA) analysis is higher than in conventional PWRs, in part due to the very low effective delayed neutron fraction ( $\beta_{\text{eff}}$ ). It appears likely that licensing limits can still be satisfied.

The initial PANTHER models used in this section, and optimal loading patterns produced using the genetic algorithm in PANTHER, were produced by N. Zara Zainuddin.

### **5.1. In-core Fuel Management**

While it is possible to maintain a negative MTC around the zero void point utilizing TCUP fuel (see Chapter 2), it is also desirable to ensure the core has negative reactivity when fully voided in order to ensure acceptable response to LOCAs. At low coolant density, the reactivity can increase rapidly with reduced coolant density. Two voiding conditions are considered: zero coolant density and coolant density for a core filled with saturated steam at the operating pressure (95.5 kg/m<sup>3</sup>). These are termed the zero coolant reactivity (ZCR) and fully voided reactivity (FVR) respectively.<sup>22</sup> When the core is depressurized, the steam density is essentially zero.

The FVR is relevant because in many design basis accidents the maximum core void fraction (VF) is ~90% (AREVA/EDF, 2012). Hence, if the FVR is negative, this provides protection against all but the most severe LOCAs. Consideration of the ZCR and FVR in conjunction allows the minimum allowable water density in the core to be interpolated. While it is obviously very desirable to have a negative ZCR, it is found that this is almost certainly unachievable for the RMPWR. It

---

<sup>22</sup> i.e. 100% void fraction. This term is selected for consistency with the RBWR analyses, and published papers this thesis is based on. Depending on the relevant core condition, FVR could reasonably be used to mean reactivity at zero coolant density or 100% void fraction.

must be stressed that this is an undesirable condition that may make it difficult to license the core, but it is not necessarily unacceptable.

Based on the analysis of Chapter 4, an 11 mm pin diameter is preferred. The effect of different fuel management strategies on the ZCR and FVR is investigated here.

An alternative to the heterogeneous TCUP assembly concept is whole assembly heterogeneity, here referred to as Whole Assembly TRU U3 (WATU). WATU's principal advantage is the potential to manage the Th-TRU and Th-U3 on different fuel management schemes. It also simplifies the assembly design and quality assurance process in assembly fabrication.

The increased size of the heterogeneous regions in WATU vs TCUP may or may not prove advantageous. The objective of TCUP or WATU is to limit thermal neutron flux in the Th-TRU fuel. By concentrating the TRU, high resonance capture and fast fission in the Th-TRU fuel limits local neutron thermalization and yields the transmutation advantages of a hard spectrum. Increasing the size of the Th-TRU regions reduces thermal neutron transport from the Th-U3 region. The thermal neutron diffusion length is similar to the pin pitch, which implies that TCUP is sufficiently heterogeneous, but there might still be a slight advantage from increasing the size of the heterogeneous regions. For WATU, a checkerboard array of the fuel assembly types appears sensible, and this renders the scheme amenable to placing the Th-U3 assemblies in the rodded positions. As burnable absorbers are not thought appropriate for this design (see Chapter 2), the guide tubes in the Th-TRU assemblies are replaced with additional fuel pins. This has the obvious drawback of constraining the fuel management scheme but hardens the neutron spectrum in the Th-TRU pins. The supercell model for this fuel design is shown in Fig. 5.1. This corresponds to an infinite checkerboard of assemblies. It must be noted that the guide tubes are an important part of the fuel assembly structure, so replacing the guide tubes in this manner will require structural changes to the fuel assembly, or it may be necessary to retain at least some of the guide tubes.

At the relative inventory and composition of U3 and TRU typical of multi-recycled fuel, the Th-U3 regions are supercritical and the Th-TRU regions are subcritical. This leads to neutron transport between regions. At equilibrium, sufficient U3 is bred in the Th-TRU pins to compensate for burning of the Th-U3 pins. If the Th-U3 regions are larger, then there is less neutron transport between regions. To sustain reactivity in the Th-TRU regions, and therefore TRU burning and U3 breeding, it follows that the equilibrium TRU content of the Th-TRU regions must increase with region size.

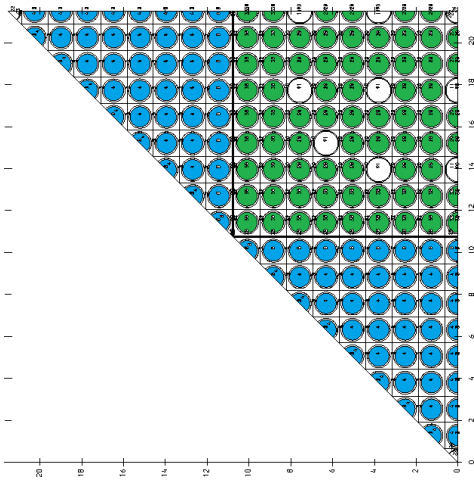


**Fig. 5.1.** Supercell model for WATU fuel design with Th-TRU (blue) and Th-U3 (green) assemblies.

WATU allows management of the different fuel assembly types on different batch strategies. For this fuel type, there is motivation for leaving the Th-TRU pins in the reactor for longer than the Th-U3 pins. The neutron multiplication factor of the Th-TRU fuel is essentially constant over a high burn-up range due to the conversion of fertile isotopes over the cycle. In contrast, Th-U3 initially has a very high neutron multiplication factor, but this reduces very rapidly as the  $^{233}\text{U}$  depletes in the relatively thermal spectrum. This is shown in Fig. 5.2, which is derived for a TCUP assembly with 20.8 at% TRU in the Th-TRU pins and 6.9 at% U3 in the Th-U3 pins (the TCUP-MT-2 case in the subsequent analysis).  $k_{\infty}$  in Fig. 5.2 refers to the neutron multiplication in the oxide fuel, i.e. it does not include clad, grid spacer or coolant absorptions.

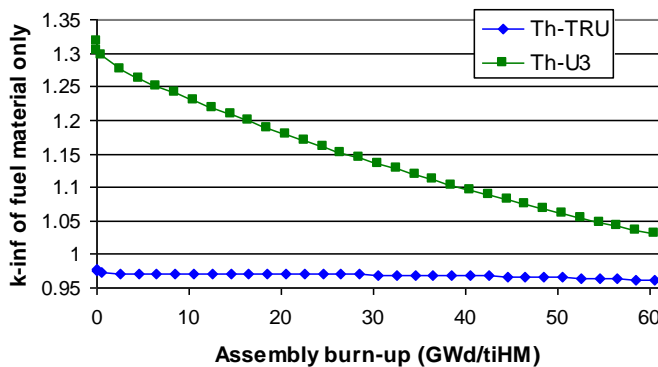


**Fig. 5.2.** Neutron economy in Th-TRU and Th-U3 over the cycle.

In addition, maximizing the burn-up of the Th-TRU improves the ratio of  $^{241}\text{Pu}$  fissions to decays, which improves the neutron economy and reduces the FVR and ZCR.

This Th-TRU multi-pass methodology is also applicable to the TCUP assembly. The Th-U3 ‘driver’ can be replaced with fresh Th-U3 (held in reserve) after one pass (i.e. after 3 cycles) through the core, and the Th-TRU can remain for an additional pass. Separable assembly designs have been considered for U-Th open cycle seed-blanket concepts (Todosow et al., 2004), and no practical

manufacturing obstacles are anticipated. Westinghouse successfully fabricated a demonstration assembly for Lightbridge’s VVERT design (Todosow and Galperin, 2009). Holding Th-U3 pins in reserve in this manner is not anticipated to increase proliferation concerns as any realistic multi-recycle scheme leads to significant out-of-reactor fissile inventories and potentially management of fuel supply of multiple reactors on different outage schedules.

The disadvantage of increasing the number of Th-TRU passes is a decrease in net  $^{233}\text{U}$  breeding and reduced opportunities to load TRU into the core. In this chapter, 2 Th-TRU passes per Th-U3 passes are considered. This allows sensible batch management of the TCUP case. For the WATU case, a pass ratio intermediate between 1:1 and 2:1 may be feasible or preferable. However, it will be demonstrated that a 2:1 pass ratio gives a 1-year equilibrium cycle length. While this is thought reasonable, cycle lengths lower than 1 year are likely to be economically penalizing. The number of Th-TRU pins can easily be varied in TCUP. In WATU, the analogue is to vary the relative number of assemblies, but a 1:1 ratio is used here for simplicity and consistency between the supercell transport calculation and the full-core calculation (see below).

The excess reactivity is partially controlled over the cycle by mixing  $\text{Gd}_2\text{O}_3$  with some or all of the Th-U3 pins. The harder spectrum in the Th-TRU pins would prevent the  $\text{Gd}_2\text{O}_3$  burnable poison (BP) from depleting sufficiently rapidly if placed there. The remaining excess reactivity is controlled using control rods, as will be discussed.

### 5.1.1. Assembly and Supercell Analysis

The ‘reference’ TCUP single-tier case (TCUP-ST-1) has heterogeneous fuel, but the entire assembly is discharged at the same time. This is compared to TCUP and WATU cases with 2 Th-TRU passes per Th-U3 pass (designated TCUP-ST-2 and WATU-ST-2). In addition, multi-tier cases for TCUP are considered, i.e. TCUP-MT-1 and TCUP-MT-2. These cases are summarized in Table 5.1.

**Table 5.1.** Assembly configurations.

Case	Th-TRU pins	Th-U3 pins	$\text{Gd}_2\text{O}_3$ in Th-U3 pins
TCUP-ST-1	132	132	0.2 wt%
TCUP-MT-1	108	156	0.2 wt%
TCUP-ST-2	144	120	0.1 wt%
TCUP-MT-2	108	156	0.1 wt%
WATU-ST-2	288 (unrodded assembly)	264 (rodded assembly)	0.2 wt% in central 144 pins

For TCUP-ST-1 and TCUP-MT-1, the equilibrium cycle burn-up was estimated as 40 GWd/t when converging the equilibrium isotope vector. For the other cases, a burn-up of 30.5 GWd/t per Th-

TRU pass is specified for the isotopic convergence, single assembly analysis and full-core analysis. This corresponds to 347 days of full power operation (i.e. a ~1 year cycle with downtime).

For the 2 Th-TRU pass cases, a proportion of the U3 was held back at the start of the first pass. The fuel was burned to 30.5 GWd/t, and then the fission products were removed from the Th-U3 pins. The retained U3 was then loaded, and the Th fraction set to give the correct fuel proportion. The small quantity of TRU produced during the first pass in the Th-U3 pins was stored for subsequent recycle in the Th-TRU pins. At the end of the second pass, all the fission products were removed and, after 5 years decay, the reactor was refuelled with a mix of  $^{232}\text{Th}$  and the reload isotope vector in Table 2.1, while holding a proportion of the total U3 inventory in reserve. The overall waste reload fraction (fraction of feed which is not  $^{232}\text{Th}$ ) is calculated based on the average waste reload fraction over both passes through the core. In practice, the residual U3 in the Th-U3 pins is obviously not instantly reprocessed at the end of Pass 1 and instead the Pass 2 U3 comes from an earlier pass after cooling and reprocessing. However, the equilibrium fuel cycle methodology is exactly equivalent in this respect. The methodology is shown diagrammatically in Fig. 5.3.

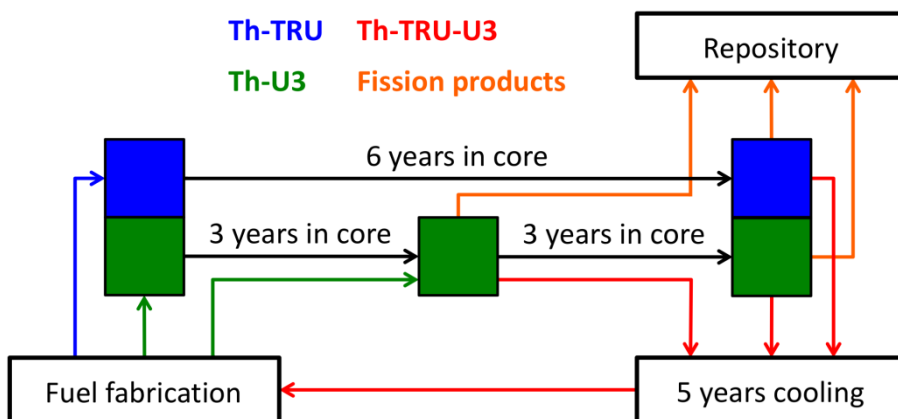


**Fig. 5.3.** Multi-pass fuel loading scheme.

Only a single depletion history was performed, as is typical for PWR calculations. However, it must be noted that the reactivity is somewhat sensitive to the power history of the fuel assembly, due to  $^{241}\text{Pu}$  decay into  $^{241}\text{Am}$ , and  $^{233}\text{Pa}$  decay into  $^{233}\text{U}$  (these effects act somewhat in opposition). The equilibrium isotope vector is somewhat sensitive to the average assembly power, such that it is possible that the power history over the equilibrium cycle is also significant. It is worth considering this effect in future calculations.

The number of Th-TRU and Th-U3 pins in each configuration is selected to give approximately equal powers in both fuel types while satisfying mass balance constraints. The exception is WATU, where the assembly ratio is fixed at 1:1 to simplify the analysis, but this is a fairly appropriate ratio.

The pin powers are not calculated as a delicate balance of fissile proportions is needed across the assembly. This is discussed in Section 5.1.4.

### **5.1.2. Results**

The equilibrium isotope vectors and fuel cycle performance are given in Table 5.2. The vectors are given at the start of Pass 1, so in addition to the U3 in the start-of-cycle (SOC) compositions, there is some U3 held in reserve. The overall waste reload fraction and the incineration rate are calculated for the resultant of both passes. The results of TCUP-ST-1 are repeated for reference. For the ST cases, the multi-batch average burn-up is taken from the full-core analysis of the following section. For the MT cases, a full-core analysis was not performed, so the linear reactivity model is used to estimate the burn-up (Driscoll et al., 1991).

The variation in  $k_{\infty}$  from the lattice (TCUP) and super cell (WATU) calculations up to 30 GWd/t is plotted in Fig. 5.4. Only the first of the two Th-TRU pass schemes is plotted as the reactivity for the two passes is almost identical. It is clear that the Gd<sub>2</sub>O<sub>3</sub> BP for WATU-ST-2 burns out too fast, so the BP design requires optimization.

The MTC is initially positive or nearly zero but becomes negative as the BP burns out (Fig. 5.5). As a uniform coolant density perturbation was assumed, the calculated MTC is not physical and it requires a full-core analysis to evaluate it properly. It will be shown in Section 5.2 that the core MTC is negative at all times due to the presence of multiple batches.

The FVR and ZCR are highly leakage dependent and a full-core analysis is required to accurately evaluate them. However, the FVR and ZCR without leakage are strongly indicative of the relative performance of the cases (Figs. 5.6 and 5.7). Again, the high value at low burn-up is due to the BP.

**Table 5.2.** Results of single assembly/ supercell analysis.

SOC at%	TCUP-ST-1	TCUP-MT-1	TCUP-ST-2	TCUP-MT-2	WATU-ST-2	TPUC-ST-2**
<sup>241</sup> Am	1.42	1.99	1.14	1.91	1.31	1.29
<sup>242m</sup> Am	0.04	0.05	0.03	0.05	0.04	0.03
<sup>243</sup> Am	0.77	1.14	0.71	1.24	0.73	0.74
<sup>243</sup> Cm	0.00	0.01	0.00	0.01	0.00	0.00
<sup>244</sup> Cm	0.51	0.70	0.56	0.83	0.52	0.54
<sup>245</sup> Cm	0.22	0.27	0.23	0.30	0.22	0.22
<sup>246</sup> Cm	0.21	0.15	0.20	0.26	0.19	0.20
<sup>247</sup> Cm	0.05	0.03	0.04	0.06	0.05	0.04
<sup>248</sup> Cm	0.02	0.01	0.02	0.03	0.02	0.02
<sup>237</sup> Np	0.58	0.85	0.56	0.99	0.59	0.59
<sup>238</sup> Pu	2.41	3.04	2.13	3.18	2.17	2.24
<sup>239</sup> Pu	3.52	1.83	3.35	1.86	3.59	3.65
<sup>240</sup> Pu	5.43	5.80	4.45	5.99	5.25	5.12
<sup>241</sup> Pu	1.07	1.09	1.13	1.19	1.07	1.14
<sup>242</sup> Pu	2.87	3.84	2.54	4.35	2.66	2.68
<sup>232</sup> Th	74.81	72.32	77.85	71.27	77.56	77.32
<sup>233</sup> U	2.55	3.15	2.36	2.80	1.95	2.03
<sup>234</sup> U	2.21	2.52	1.71	2.34	1.31	1.54
<sup>235</sup> U	0.64	0.71	0.52	0.66	0.37	0.46
<sup>236</sup> U	0.66	0.50	0.48	0.69	0.40	0.46
<b>U3 retained at SOC Pass 1 for top up in Pass 2 (% of total inventory)</b>	<b>0</b>	<b>0</b>	<b>22</b>	<b>16</b>	<b>20</b>	<b>22</b>
<b>SOC pass 1 waste reload fraction (at %)</b>	<b>50</b>	<b>60</b>	<b>65</b>	<b>75</b>	<b>60</b>	<b>65</b>
<b>Overall waste reload fraction averaged over both passes (at %)</b>	<b>50</b>	<b>60</b>	<b>51</b>	<b>54</b>	<b>45</b>	<b>50</b>
SOC TRU in fuel (%)	19.13	20.80	17.09	22.24	18.41	18.51
SOC U3 in fuel (%)	6.06	6.89	5.06	6.49	4.03	4.49
Fissile fraction* of TRU and U3 (i.e. excl. <sup>232</sup> Th) (%)	30.91	24.50	33.18	22.66	31.13	31.67
Fissile fraction* of fuel (%)	7.79	6.78	7.35	6.51	6.98	7.28
Fissile fraction* of TRU (%)	24.01	14.06	26.18	13.72	25.32	25.86
Fissile fraction* of U3 (%)	52.69	56.02	56.79	53.31	57.66	55.59
<b>3-batch average discharge burn-up (GWd/t)</b>	<b>40.1</b>	<b>39.9</b>	<b>41.6</b>	<b>38.1</b>	<b>41.0</b>	<b>41.2</b>
Multi-batch Th-TRU average discharge burn-up (GWd/t)	45.2	41.3	62.3	65.3	57.8	60.8
Multi-batch Th-U3 average discharge burn-up (GWd/t)	39.2	38.9	29.1	28.6	31.8	30.1
TRU fraction in Th-TRU pins (%)	38.3	50.8	31.3	54.4	35.3	34.9
U3 fraction in Th-U3 pins (%)	12.1	7.1	11.1	11.0	8.4	8.9

\* <sup>233</sup>U, <sup>235</sup>U, <sup>239</sup>Pu, <sup>241</sup>Pu are considered fissile

\*\* TPUC-ST-2 is introduced in Section 5.2.4 but included in Table 5.2 for ease of comparison

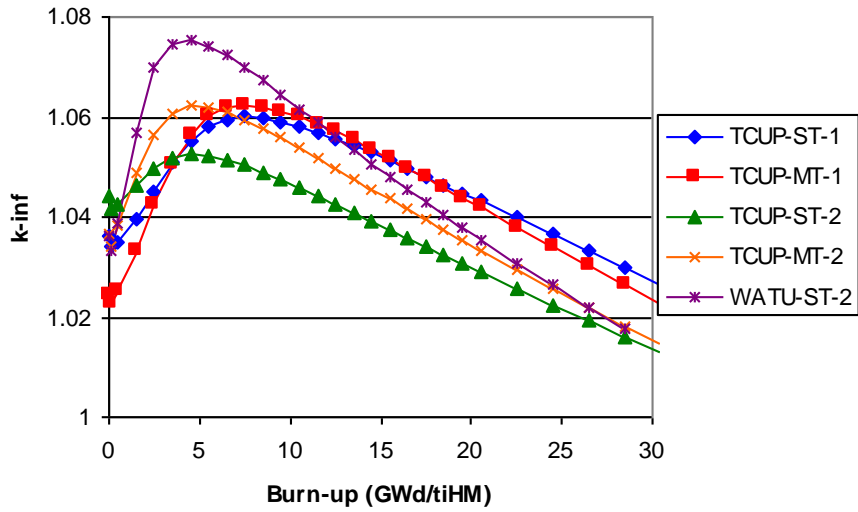


Fig. 5.4. Reactivity variation over cycle.

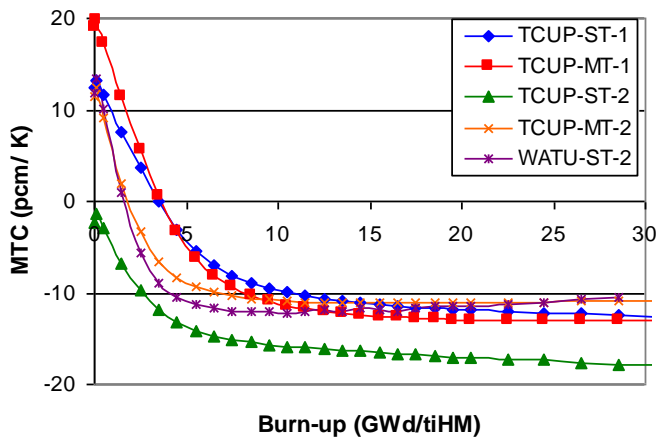


Fig. 5.5. Single assembly MTC variation over cycle.

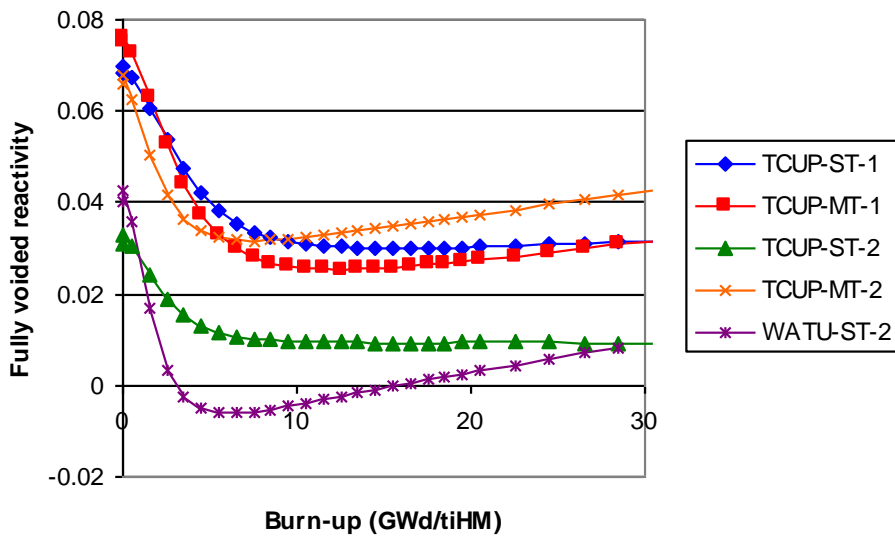
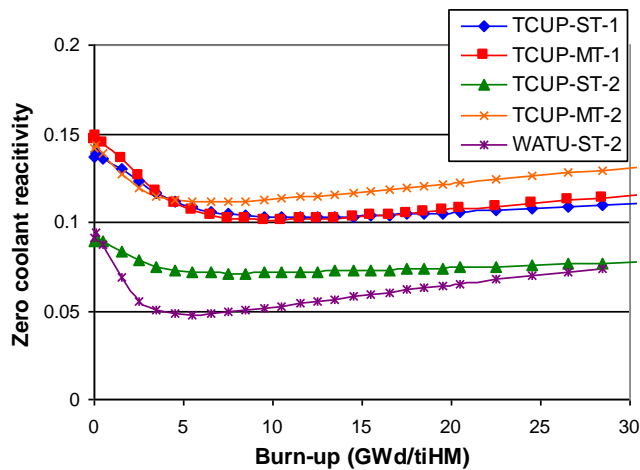


Fig. 5.6. Single assembly FVR without leakage.



**Fig. 5.7.** Single assembly ZCR without leakage.

### 5.1.3. Analysis

The FVR and ZCR are strongly correlated and positive in almost all cases. The FVR appears sufficiently low that it may be possible to achieve a negative FVR when accounting for leakage. However, the ZCR is very positive, and it is unlikely to be negative even with leakage.

The performances of TCUP and WATU designs appear very similar. Therefore, it appears that TCUP is sufficiently heterogeneous to fully exploit the advantages of fuel heterogeneity, but if there is a maximum sensible region size, it is at least as large as a whole assembly.

The MT cases have a slightly reduced burn-up relative to the ST cases. For the 1-pass cases, this is a result of the trade-off between reduced fissile proportion of the feed and the presence of  $^{233}\text{U}$  in the feed, which allows the MT cases to feature higher reload proportions (and overall TRU destruction rates) at very similar MTC, FVR and ZCR values as the ST cases (Figs. 5.5–5.7). This difference is reflected in the 2-pass TCUP cases.

TCUP-ST-1 and TCUP-MT-1 have very similar FVR and ZCR. Therefore, while there is a slight burn-up penalty in the MT case, either could be favoured depending on the overall fuel cycle strategy.

Although the cycle length for the 2-pass cases is lower (Fig. 5.4), the additional Th-TRU pass results in similar average burn-up (Table 5.2). In addition, the ST cases have much reduced FVR and ZCR (Figs. 5.6 and 5.7). There is therefore a strong and clear advantage to using this refueling scheme. However, TCUP-MT-2 has a positive MTC and high FVR and ZCR. Therefore, in the ‘multi-tier’ implementation the 1-pass approach is appropriate, and the best ‘multi-tier’ case is worse than the best ‘single-tier’ case.

TCUP-ST-2 has a ~10% lower TRU inventory than TCUP-ST-1, and in particular it is worth noting the ~25% reduction in  $^{241}\text{Am}$  population. This helps to reduce the FVR. Crucially, the fissile

proportion of both TRU and U3 is higher, which allows the average burn-up to be improved despite this lower TRU inventory. This indicates more efficient TRU burning, in particular as a result of decreasing  $^{241}\text{Pu}$  decays.

Comparing the TCUP-MT cases, the TRU isotope vector does not improve with 2 Th-TRU passes. In this case, a greater proportion of the feed is MA, so the advantage of reduced  $^{241}\text{Pu}$  decays is lower.

The fissile proportion of U3 also changes. For TCUP-ST, the 2-pass case has a U3 vector with better fissile properties than the 1-pass case. For TCUP-MT, this effect is reversed.

To investigate how this comes about, the U3 mass balance is investigated. Table 5.3 gives the SOC and end-of-cycle (EOC) U3. For 2-pass cases, the inputs and outputs from both Th-U3 passes are considered together in the mass balance.  $^{233}\text{Pa}$  and  $^{238}\text{Pu}$  decay to respectively  $^{233}\text{U}$  and  $^{234}\text{U}$  is included.

**Table 5.3.** U3 mass balance for TCUP cases (total U3 normalized to 100).

	Th-TRU passes	SOC U3		EOC U3 in Th-U3		EOC U3 in Th-TRU		U3 from feed
		ST	MT	ST	MT	ST	MT	MT
Total U3	1	100	100	85	83	15	10	7
	2	100	100	81	80	19	11	8
Fissile % ( $^{233}\text{U}$ , $^{235}\text{U}$ )	1	53	56	49	52	76	67	91
	2	57	53	51	48	81	66	91

The U3 fissile fraction in the Th-U3 pins reduces over the cycle as  $^{233}\text{U}$  is burned. This is replenished from  $^{233}\text{U}$  bred in the Th-TRU pins, and, in the MT cases, from highly fissile U3 in the feed. In the ST case with 2 Th-TRU passes, there is a large increase in  $^{233}\text{U}$  breeding in the Th-TRU pins. This is not observed for the MT case.

This difference comes about due to the decrease in TRU fraction in the Th-TRU pins from TCUP-ST-1 to TCUP-ST-2 (resulting in more Th in the pin and less resonance captures in the TRU), compared to the increase in the already high TRU fraction from TCUP-MT-1 to TCUP-MT-2 (Table 5.2).

#### 5.2.3.1. Effect of Changing Relative Number of Th-TRU and Th-U3 Pins

Varying the number of Th-TRU pins in the assembly affects the power distribution between regions, the neutron spectrum and the relative discharge burn-ups of Th-TRU and Th-U3. However, there is little overall effect on the performance.

For a given fuel composition, reducing the number of Th-TRU pins, while keeping the same total core inventory of TRU and U3, increases the reaction rate in the U3, which increases  $k_{\infty}$  and makes the MTC more negative. However, a higher proportion of the U3 is burned, and after multiple cycles the new equilibrium composition has a lower U3 inventory, a higher Th-TRU inventory, and comparable performance to the original case.

The TRU and U3 isotope vectors can be improved (i.e. increased fissile proportion) by increasing the number of Th-TRU pins, but this does not improve the overall performance for a given waste reload fraction. The larger volume of TRU in the core increases the MA incineration rate and  $^{233}\text{U}$  breeding rate. In addition, the reduced number of Th-U3 pins reduces the U3 burn rate. However, the improvement in the isotope vector is offset by the increased reaction rate in the Th-TRU as it is dispersed over a larger number of pins. This acts to make the MTC more positive and reduce  $k_{\infty}$ .

Therefore, the most important consideration in choosing the number of Th-TRU pins is to limit pin power peaking as much as possible.

WATU-ST-2 has slightly lower average discharge burn-up (due to fewer Th-TRU 2-pass pins and the same cycle length) and FVR than TCUP-ST-2, so the exact trade-off is potentially very similar between the two cases. Both appear feasible implementations. The WATU scheme has a slightly higher TRU population and a lower fissile fraction in the TRU, but has a higher power share from the Th-U3 region. As discussed, this is mostly a consequence of the ratio between the two pin types.

This effect is further increased as the Th-TRU assembly is subcritical and the Th-TRU region size for WATU is larger than for TCUP. This reduces the neutron transport from Th-U3 to Th-TRU, which increases the tendency for the U3 to burn out relatively rapidly. This reduces the equilibrium U3 proportion but keeps the power share between regions approximately constant.

#### ***5.1.4. TPUC and WATU Lattice Design***

The TCUP fuel assembly design is now inverted to place the Th-TRU pins at the periphery and the Th-U3 pins at the centre (TPUC). This places the more thermal spectrum Th-U3 pins next to the guide tubes. This slightly increases the spectral variation across the assembly, resulting in a minor improvement in performance. However, the main advantage is an increase in the SDM of around – 300 pcm, by increasing the thermal neutron flux in the guide tubes. The main disadvantage is making the design less suitable for placing MA ‘target’ pins in the guide tube positions – this is discussed in Chapter 7. The TPUC assembly is shown in Fig. 5.8. A new equilibrium isotope vector is derived for this design – shown in Table 5.2.

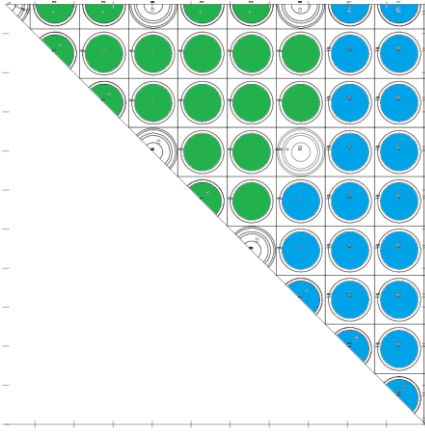


**Fig. 5.8.** TPUC fuel design with 144 Th-TRU pins (blue) and 120 Th-U3 pins (green) per assembly.

As discussed in Chapter 2, power swings between regions over the core life make it difficult to limit pin-level power peaking. The TPUC design utilizes four fissile loading zones for both the Th-TRU and Th-U3 pins, summarized in Fig. 5.9. The assembly design and power peaking up to 20.5 GWd/t are shown in Fig. 5.9. This covers the first 2 cycles of operation within the core. Twice-burned assemblies are assumed not to be the ‘hot’ assembly, such that when the assembly is burned beyond ~20.5 GWd/t higher pin-level power peaking is allowable. The power peaking is limited to 1.09 over the cycle, which is slightly higher than UO<sub>2</sub> assemblies (~1.06) but may still be acceptable in conjunction with low power-peaking core design. The use of enrichment zoning increases the complexity of fuel fabrication: here 8 different pin types will need to be accurately loaded into the assembly with remote fuel fabrication.

Use of mechanical shim can lead to local assembly hot spots when the rods are withdrawn, as the adjacent fuel pins experience depressed flux and are therefore under-burned. However, rod shadowing was found not to adversely affect pin-level power peaking, leading to ~1% increases or decreases in pin-level power peaking.

The WATU supercell enrichment zoning (also utilizing four compositions for both Th-U3 and Th-TRU) is shown in Fig. 5.10, with the power peaking over the cycle also given. In this case, the power peaking is normalized relative to the assembly, rather than the supercell, i.e. Th-U3 pin power is normalized relative to average Th-U3 pin power and Th-TRU pin power is normalized relative to average Th-TRU pin power. Assembly-level power variations will be considered at core level in this case. The Th-TRU pin-level power peaking can be limited to ~1.07. In addition, the assembly contains 288 pins, compared to the usual 264, reducing the power in the average pin. This is discussed further in Section 5.2. The Th-U3 design is further complicated by the use of Gd in only some of the pins. This leads to large power swings across this assembly, and a maximum power peaking of 1.12.

Th-TRU		Th-U3		
Pins/ assembly	TRU loading (at%)	Pins/ assembly	U3 loading (wt%)	Gd <sub>2</sub> O <sub>3</sub> (wt%)
48	41.0	24	10.8	0.1
44	36.7	32	9.8	0.1
36	28.7	56	8.0	0.1
12	22.6	12	7.3	0.1

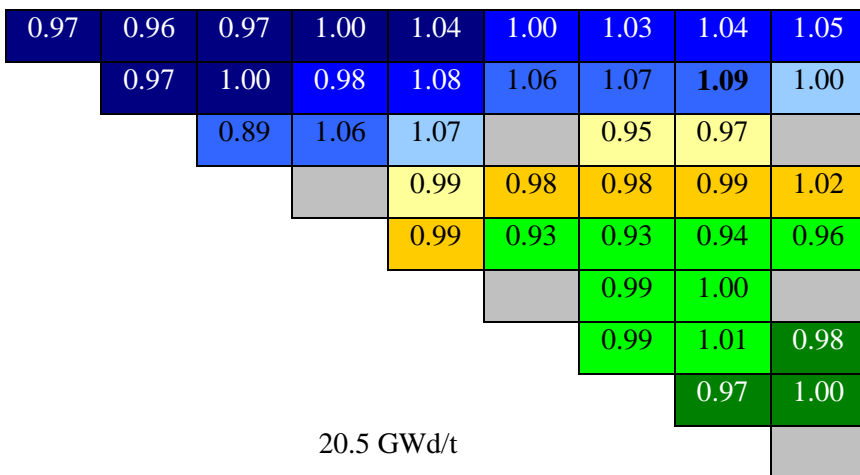
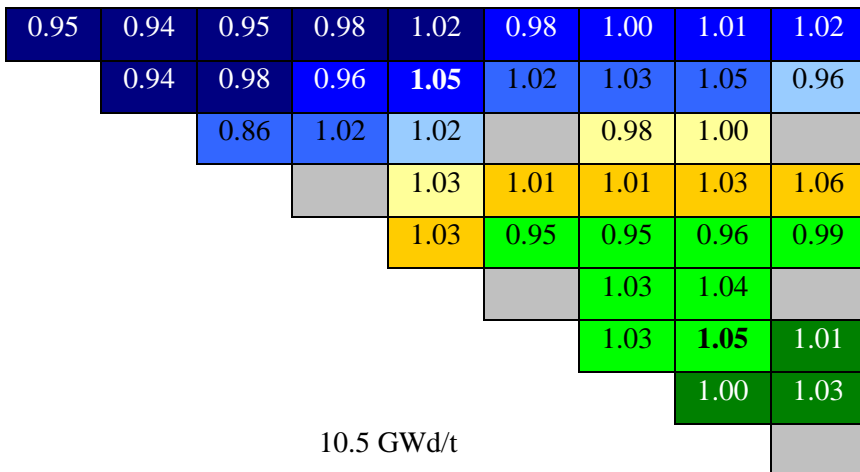
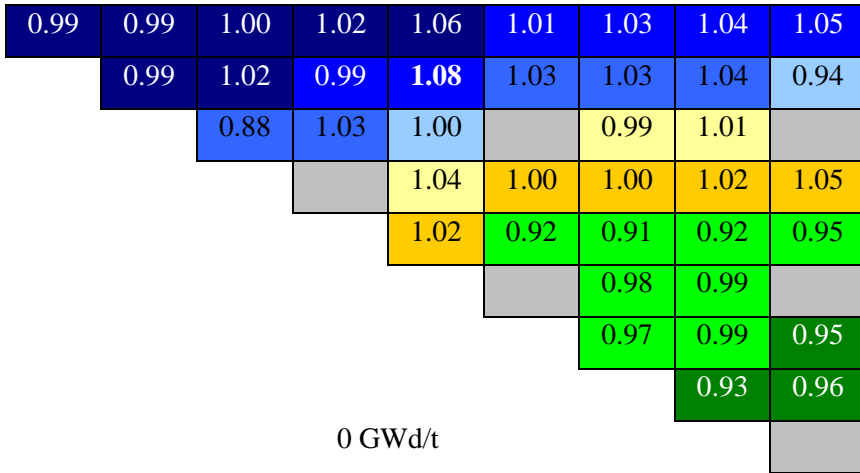
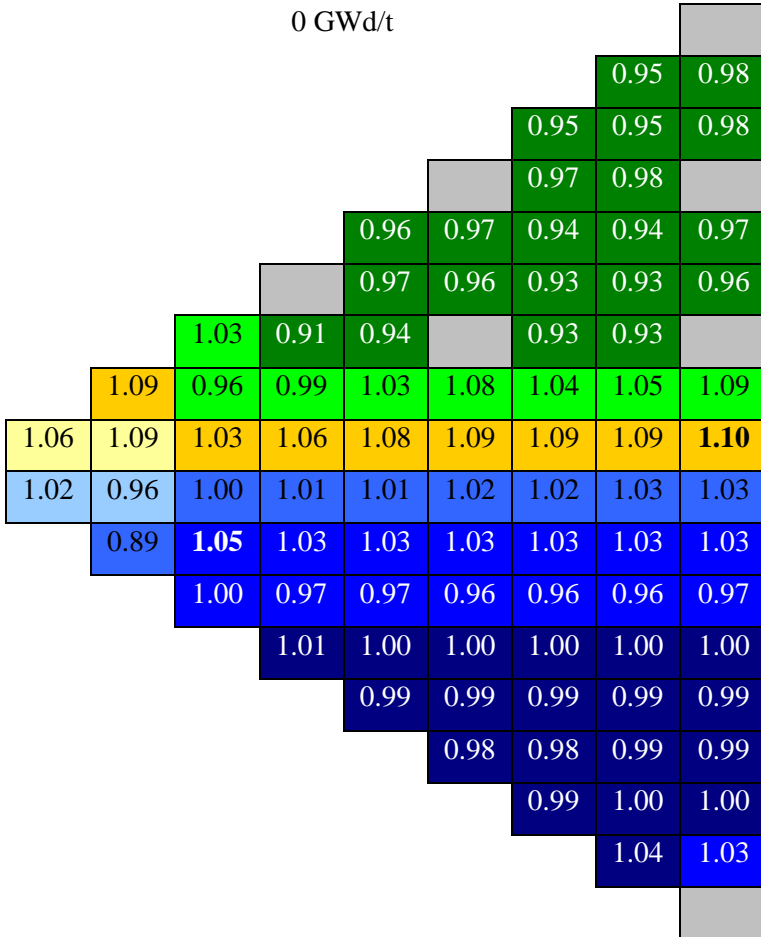


Fig. 5.9. Th-TRU and Th-U3 fissile loadings; assembly design and pin power peaking for TPUC.

Th-TRU		Th-U3		
Pins/ assembly	TRU loading (at%)	Pins/ assembly	U3 loading (wt%)	Gd <sub>2</sub> O <sub>3</sub> (wt%)
116	39.5	140	12.2	0.2
104	36.2	56	11.0	0
56	27.0	56	8.8	0
12	25.0	12	7.1	0



(Figure continues on next page)

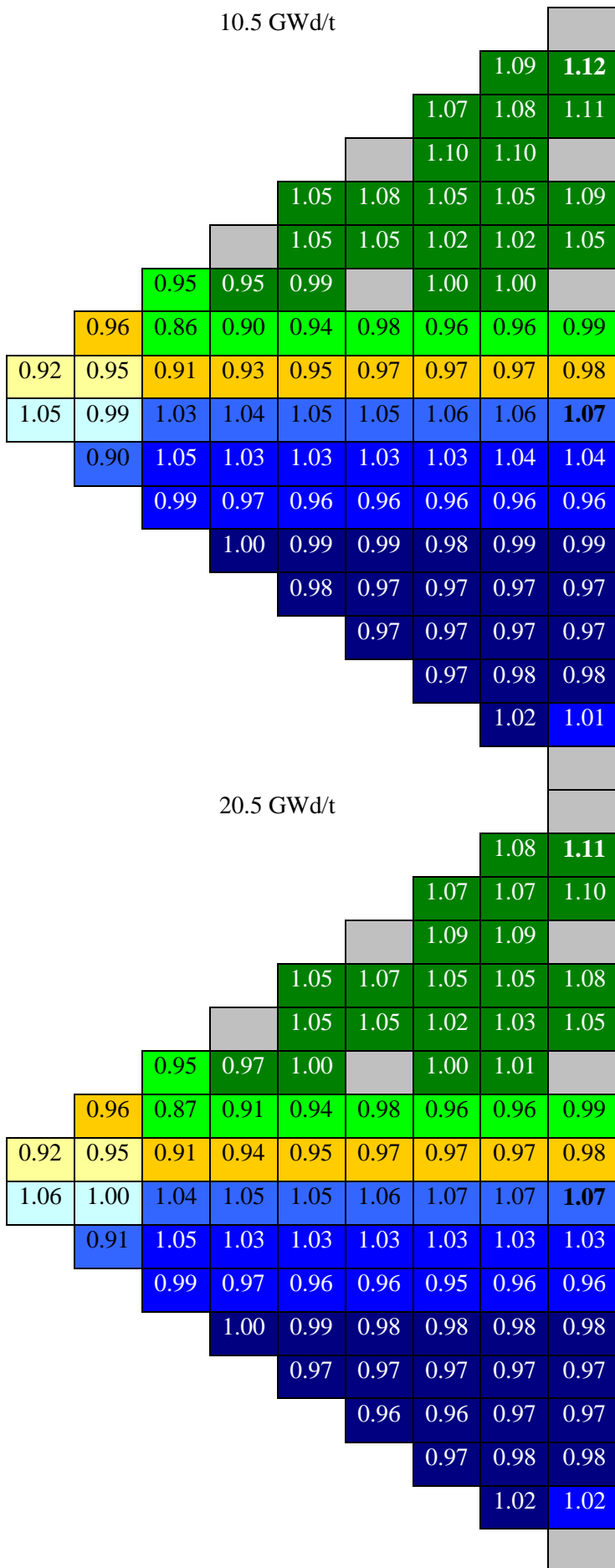
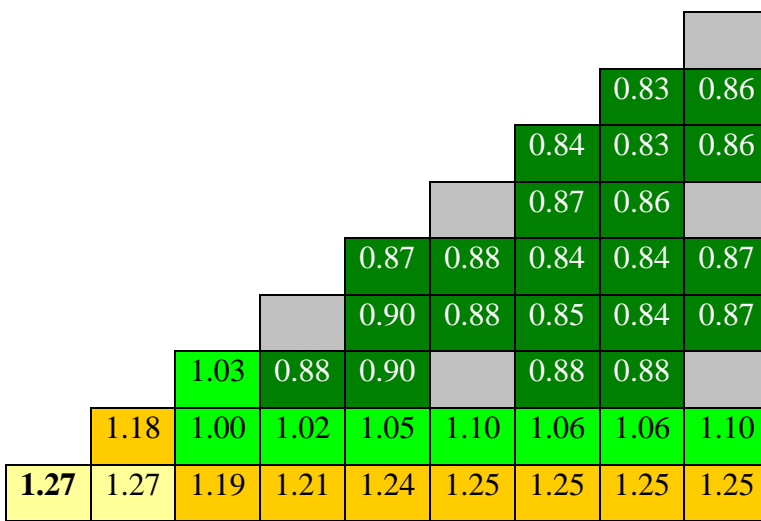


Fig. 5.10. Th-TRU and Th-U3 fissile loadings; assembly design and pin power peaking for WATU.

The above lattice design assumes a perfect checkerboard of Th-TRU and Th-U3 assemblies in the core. However, symmetry conditions necessitate a slight deviation from this pattern, leading to neighbouring assemblies of the same type in some areas of the core. The accurate calculation of local pin-level power peaking requires pin power reconstruction with a core analysis, and the use of several supercell calculations to derive varying discontinuity factors for different core positions, but the effects of identical neighbouring assemblies can be readily approximated by assuming an infinite lattice of one assembly type. An infinite lattice of Th-U3 assemblies with the fissile zoning defined in Fig. 5.10 would have an SOC power peaking of 1.27 (Fig. 5.11). The power peaking reduces to 1.11 (comparable to the supercell design) by the end of the first cycle – when the Gd at the centre of the assembly has burned out.



**Fig. 5.11.** Pin-level power peaking for infinite lattice of Th-U3 assemblies with fissile loadings defined as in Fig. 5.10.

The power peaking in Fig. 5.11 is obviously unacceptable. Changing the fissile zoning for specific assemblies is possible, but leads to problems when shuffling the fuel at EOC. As the problem appears limited to the first pass of fuel, while the Gd burns out, it appears more sensible to change the Gd loading design for the fresh assembly, i.e. utilize different Gd loadings for assemblies in different positions in the core. After the first pass, the Gd has burned out. A rigorous analysis of all fuel loading histories, e.g. where the Th-U3 assembly is initially next to a Th-TRU assembly, then shuffled to be next to a Th-U3 assembly, is needed to confirm this.

## 5.2. Core Analysis

A detailed full-core analysis of the 2-pass TPUC and WATU fuel designs is now performed using PANTHER. A full-core model based on a 193 assembly 4-loop Westinghouse PWR (Watt's Bar, 2009) was used to evaluate the main indicators of the core performance. The analysis was performed using PANTHER (Hutt et al., 1991; Morrison, 2003). 2-group cross-sections for PANTHER were generated by condensing the multi-group cross-sections from the WIMS flux

solution with the same equilibrium isotope vector used in the assembly analysis. This is valid as the discharge burn-up is very similar to the estimated burn-up used in the isotopic convergence in all cases. Given the hard neutron spectrum and heterogeneous fuel, use of a larger number of energy groups may be preferable.

The fuel conductivity for Th-TRU is estimated using the model for Th-Pu in (Cozzo et al., 2011), with the TRU proportion taken as the Pu proportion. This significant assumption is made due to limited data availability. The conductivity for Th-U3 is taken from (Yang et al., 2004). PANTHER's simple thermal feedback model represents only a single pincell type per node, so the average thermal conductivity was derived to represent the net effect of the two separate pin types. This approach is sufficient to treat neutronic-thermal-hydraulic feedback effects to a reasonable degree of accuracy, as the Doppler coefficients (DCs) of the two fuel types are very similar ( $\sim -3.5$  pcm/K for a single-assembly analysis with 100 K perturbation in fuel temperature). For WATU, different conductivities were implemented in different assemblies.

Achieving a high rod worth is difficult in a hard neutron spectrum. The control rods adopted contained solid pellets of  $B_4C$  with 95%  $^{10}B$  enriched boron and a radius of 0.433 cm. Even so, it is difficult to achieve an adequate SDM, partly due to the use of a portion of the rods to provide mechanical shim. Highly enriched  $B_4C$  rods are also under consideration for RBWRs (Downar et al., 2012). As with MOX cores, use of additional rod bank positions (which requires additional modification for retrofit cores due to need to place additional rod-cluster-control-assemblies (RCCAs) with additional holes penetrating the pressure vessel – this is not thought to be a major problem) can be used to reduce the enrichment of  $^{10}B$  required, or to increase the overall control rod worth.

The  $^{10}B$  in the control rods exposed at the high core neutron flux will deplete. This will require dedicated management of the control rods, including shuffling or replacement when the worth has decreased to unacceptable levels or the rod mechanical performance has degraded. The control rods lose  $\sim 5\%$  of their worth when burned to 20 GWd/t. For cycle-average control using 12% of the available worth (typical), this roughly equates to a 5% loss of rod worth over 16 years of operation. The rods will need to be shuffled and replaced regularly and the reduction in worth needs to be taken into account.

The SDM was calculated for a reactor trip from hot full power (HFP) to hot zero power (HZP), with no change in Xe population,<sup>23</sup> with the highest worth rod remaining out of the core. A 10% reduction is made for modeling uncertainties, and a 10% reduction is also made to account for

---

<sup>23</sup> The Xe level increases following trip, but typically no credit is taken for this. Removal of the Xe entirely would make the SDM worse by 600 pcm in this case.

control rod depletion (i.e., an overall reduction of 20%). In each case, the rods in position F10 and symmetry positions are the highest worth rods, and one of these is considered stuck. The Doppler defect is increased by 20% to account for uncertainty. The value of the Doppler defect is ~2000 pcm, leading to a reduction in SDM of ~400 pcm.

Data was taken from the supercell model of Fig. 5.1 for the WATU fuel. The reflective boundary conditions through the assembly midpoints in the supercell model are a good approximation to the conditions in the core and 2-group cross-sections are derived using an appropriate spectrum. Each assembly contained 4 radial nodes in this case.

In PANTHER, it is possible to employ assembly discontinuity factors such that the PANTHER fluxes are forced to match the lattice solution, resulting in an exact match in  $k_{\infty}$  for an identical problem (Knight et al., 2013). It is possible to generate approximate discontinuity factors in PANTHER ‘on the fly’ using an ‘embedded method’ described in (Knight et al., 2013). While practical, this method is currently difficult and time-consuming to set up, so the discontinuity factors were not implemented for the WATU model. It is also possible to derive the discontinuity factors using a supercell calculation in WIMS, and pass the calculated assembly average and assembly edge fluxes to PANTHER – again this is difficult and time-consuming to set up and is not performed here. This results in errors of ~0.5% in the fast neutron flux, and ~8% in the thermal neutron flux in PANTHER relative to the WIMS solution, which can lead to errors of ~5% in interface pin powers. This is deemed acceptable for the purposes of this feasibility analysis but any future analysis should use discontinuity factors.

The TPUC core accounts for flux variation across the assembly by normalising to the cell edge flux rather than the cell average flux. This is the usual procedure employed in PANTHER, and is acceptable because, as is usual, the reflective boundary condition at the assembly edge is an accurate approximation to core conditions. WIMS contains a specific calculation route to account for reflector effects, by setting fast and thermal cross sections to accurately reproduce the neutron currents at the core/assembly interface.

Pin power reconstruction is not employed for the full-core model, due to the unsuitability of the method (no discontinuity factors) for deriving them. A complex fuel design is needed to achieve adequate pin power peaking (discussed in Section 5.1.4), and evaluation of an accurate maximum pin power peaking also needs to consider control rod history effects on pin-level power peaking due to the use of mechanical shim. These in-depth calculations are beyond the scope of this feasibility study, and a simpler approach is adopted with pin-level and assembly-level power peaking considered separately, and multiplied together to estimate total power peaking.

The MTC in PANTHER is calculated by perturbing the flow rate. Additional uncertainty in the MTC, FVR and ZCR will be introduced in PANTHER, as the averaging of the mesh-by-mesh MTCs in the core may introduce inaccuracies and for the FVR and ZCR the treatment of leakage becomes extremely important. Convergence of the FVR and ZCR in PANTHER is problematic. This is thought to be a result of the almost zero thermal neutron flux. Calculation of the FVR and ZCR in PANTHER using 2-group diffusion theory is of questionable validity, in particular because of the importance of accurate treatment of the reflector. While the reflector model was derived for fully voided conditions using the calculation methodology described above, this methodology may not be accurate under fully voided conditions. Hence the FVR and ZCR calculated here can only be regarded as an estimate.

Given the hard neutron spectrum and heterogeneous fuel, use of 2 energy groups may not be sufficient, and use of more groups should be considered in future. Furthermore, additional uncertainty in the MTC, FVR and ZCR will be introduced in PANTHER, as the averaging of the mesh-by-mesh MTCs in the core may introduce inaccuracies, and for the FVR and ZCR the treatment of leakage becomes extremely important.

### ***5.2.1. Core Design and Mechanical Shim***

Some LWRs, such as AP1000s (Onoue et al., 2003), utilize mechanical shim for load following and to reduce the number of changes in boron concentration. However, rod insertion typically results in a depressed local power distribution, with a subsequent power spike when the rods are extracted due to the rod shadowing the fuel. This tends to increase the core form factors (Franceschini and Petrovic, 2009). Partial axial insertion of the rods skews the power towards the bottom of the core, which increases power peaks and triggers Xe transients (Franceschini and Petrovic, 2008). This is mitigated by the low reactivity swing to be controlled by rods of less than 2000 pcm, due to: the high content of MA and even-numbered isotopes of Pu in the fuel; the hard neutron spectrum; and the use of burnable absorbers. The hard neutron spectrum also acts to reduce power variations across the core by increasing the mean neutron path. The RMPWR core considered in this chapter does not use soluble boron.

Dedicated lighter worth (“gray”) banks are often used for reactivity control to minimize the above effects, but this increases the number required, and reduces the SDM. Extensive reactivity control with control rods is also taxing for the fuel, especially during transients, and proper investigation of the fuel rod performance under these conditions must be undertaken.

Achieving adequate core power peaking requires derivation of a suitable loading pattern (LP). Here, this is combined with use of mechanical shim, which also necessitates finding a suitable control rod program (CRP). PANTHER contains optimization algorithms that can be used to derive suitable

LPs, but the process is complicated by the need for a complementary CRP. For the TPUC core, an approximate LP (shown in Fig. 5.12) is used to repeatedly shuffle and deplete the core, to generate fuel with a characteristic range of burn-ups for an equilibrium cycle. The fuel loading is then optimized for the final ‘equilibrium’ cycle using the genetic algorithm in PANTHER (Parks, 1996) (Fig. 5.13). This does not represent true equilibrium, but, in reality, a true equilibrium cycle is almost never reached, and cycle-by-cycle LP design is pursued in any case. This process is therefore highly appropriate for determining the feasibility of finding a suitable LP plus CRP which results in acceptable core form factors.

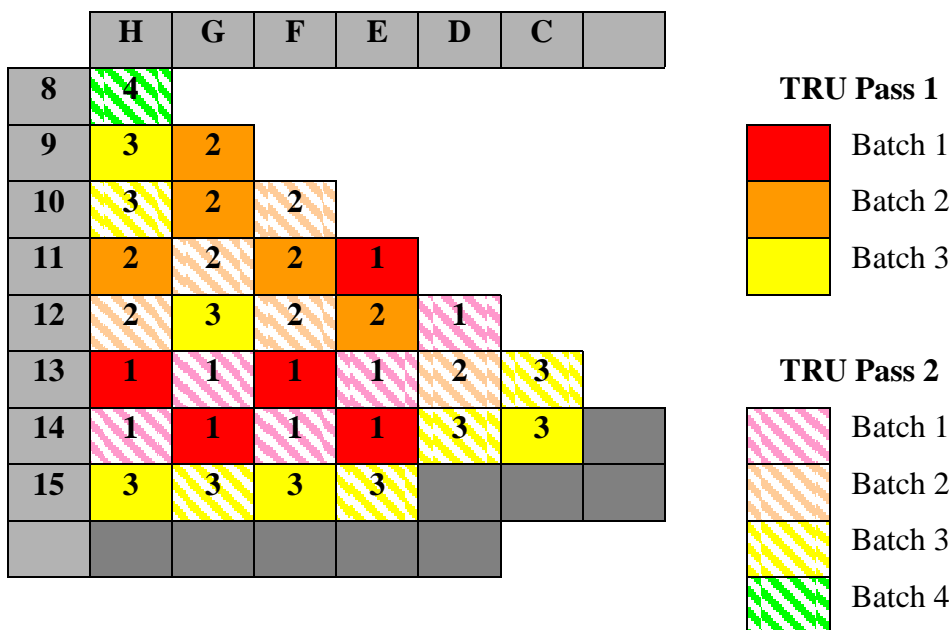


Fig. 5.12. LP used to bring the TPUC core to equilibrium.

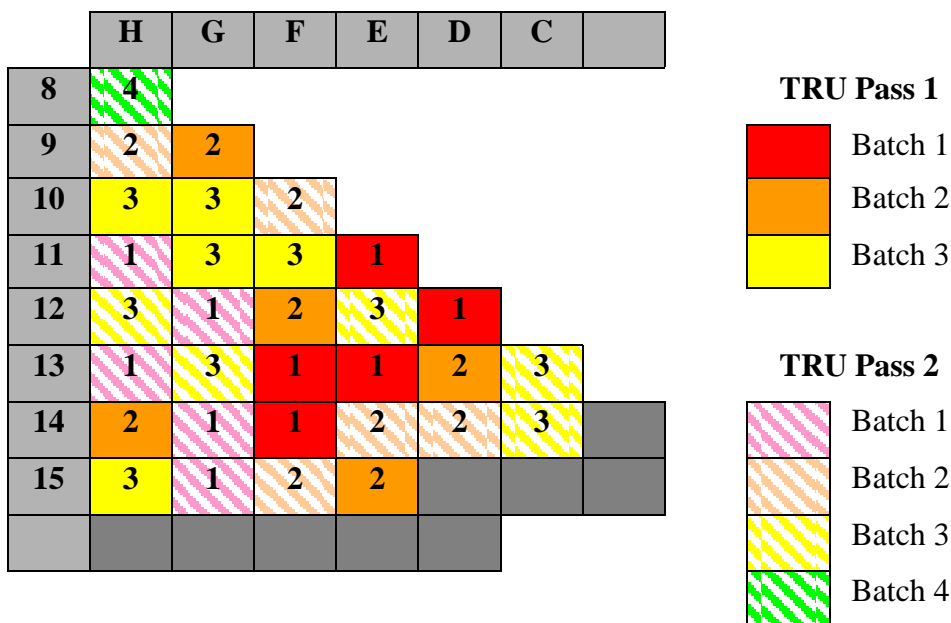
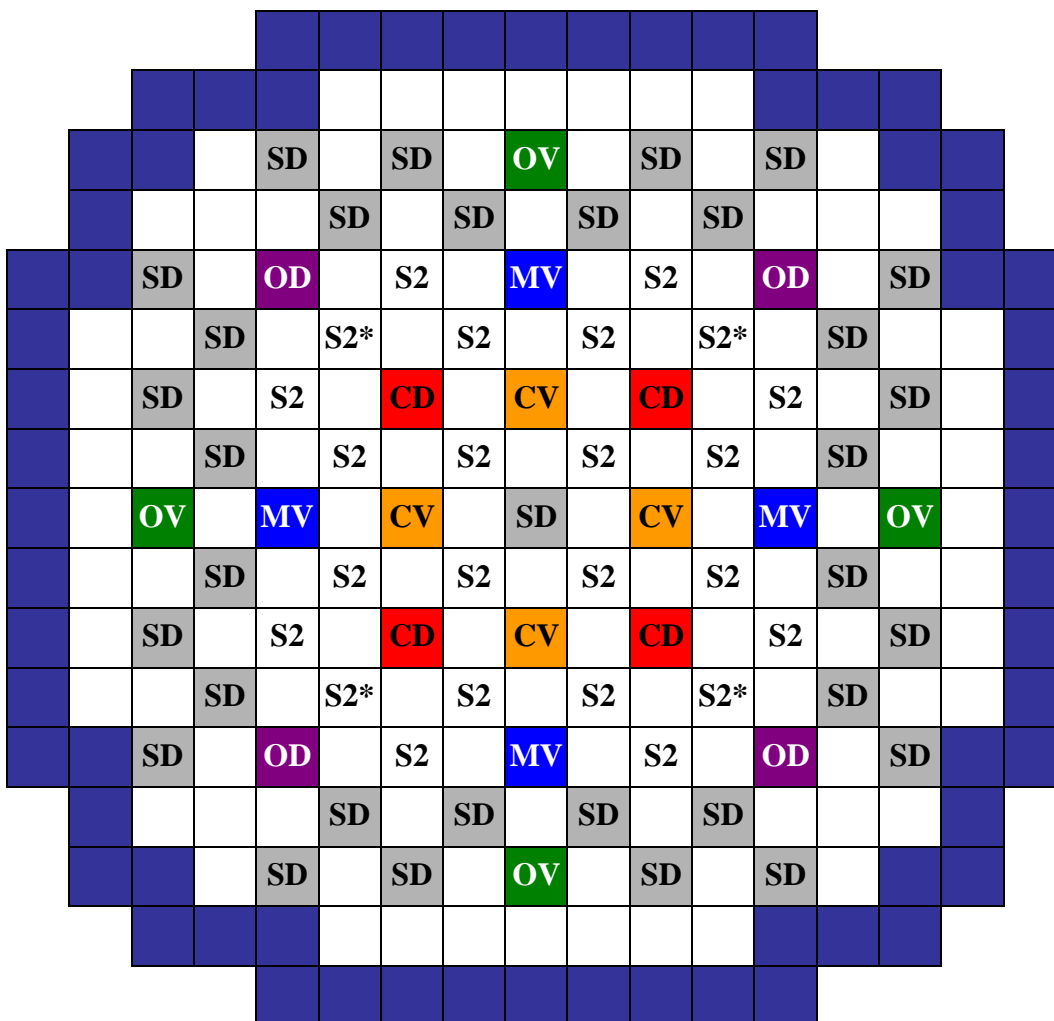
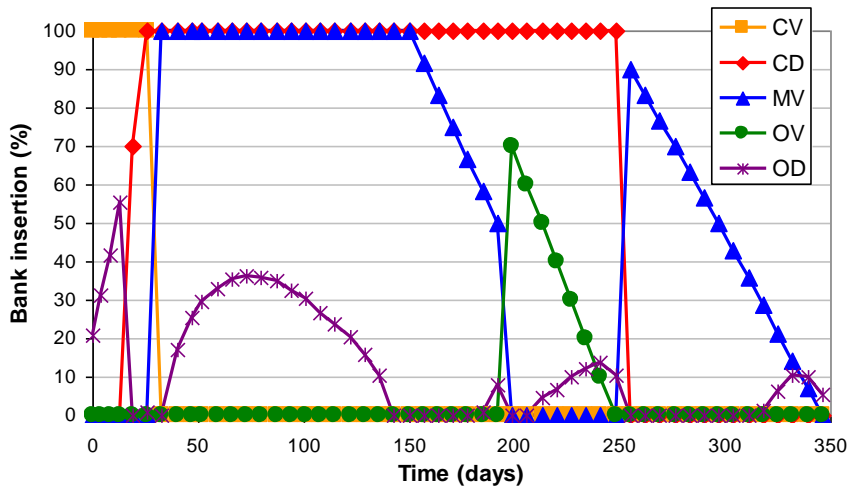


Fig. 5.13. LP used for the TPUC equilibrium cycle.

Rod banks are defined as in Fig. 5.14, and a basic CRP is defined both for the initial cycles and the final equilibrium cycle (i.e. this CRP is fixed during the genetic algorithm search). The full CRP for the final cycle is then derived by hand, and is shown in Fig. 5.15. The basic CRP utilizes banks CV and CD only, with insertions as in Fig. 5.14, with the additional banks utilized only in the final cycle. A criticality search throughout the cycle is defined using bank OD, such that  $k_{eff}$  is maintained at 1.0015 for most of the cycle. The maximum dip in criticality of 70 pcm occurs in the middle of the cycle where bank OD is fully withdrawn; this would, in practice, be compensated for by adjustment of bank MV, but this is cumbersome to perform in PANTHER. The cycle length is 346 days, corresponding to a cycle length of ~1 year and the discharge burn-up matching that used in deriving the equilibrium fuel composition.



**Fig. 5.14.** Rod bank definition for the TPUC and WATU cores. ‘S2’ denotes an independent set of shutdown rods which is not present in Westinghouse 4-loop PWRs but is added in Section 5.2.4 for LBLOCA mitigation. \* Not present in WATU core as incompatible with LP.



**Fig. 5.15.** CRP used for the TPUC equilibrium cycle.

The WATU LP is more difficult to define, as a checkerboard loading scheme for the Th-TRU and Th-U3 assemblies is desired. It was therefore defined by hand, and was identical for the initial cycles and the equilibrium cycle (Fig. 5.16). A CRP was only defined for the equilibrium cycle and is shown in Fig. 5.17. The checkerboard condition is violated in positions E12, D12, D13 and C13 due to symmetry constraints, but is satisfied elsewhere. There are 96 Th-TRU assemblies and 97 Th-U3 assemblies, which is close to the 1:1 ratio used in the supercell analysis (which did not consider the 4<sup>th</sup> batch assembly at the reactor centre). Therefore, the supercell analysis described in Section 5.1 is deemed valid for deriving equilibrium fuel compositions and 2-group cross-sections. All rod bank positions contain a Th-U3 assembly with guide tubes. The core performance is almost identical with a Th-TRU assembly at the core centre, but a Th-U3 assembly is needed to utilize the central shutdown RCCA.

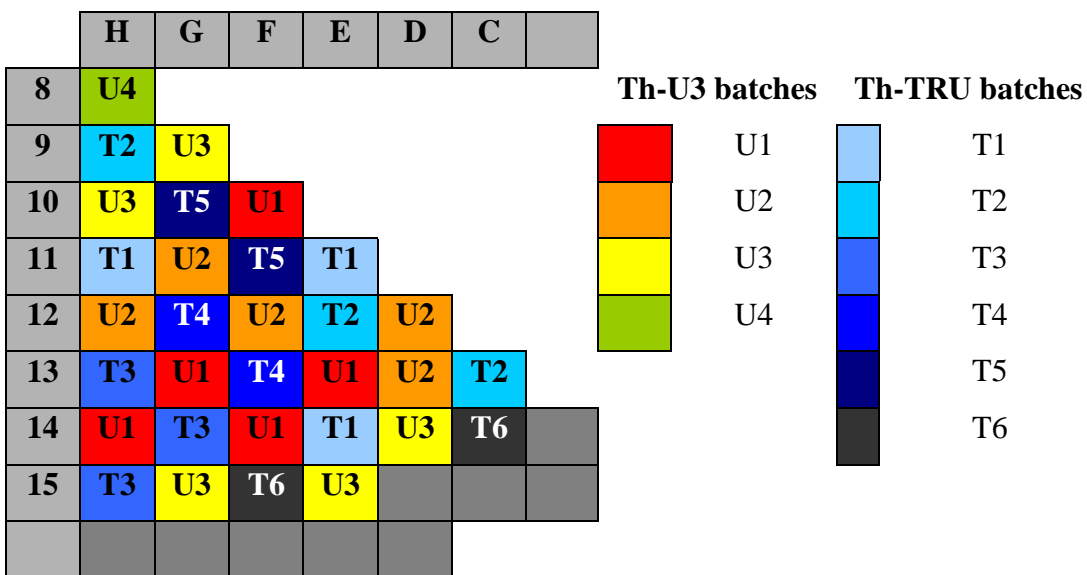


**Fig. 5.16.** LP used to bring the WATU core to equilibrium, and for the WATU equilibrium cycle.

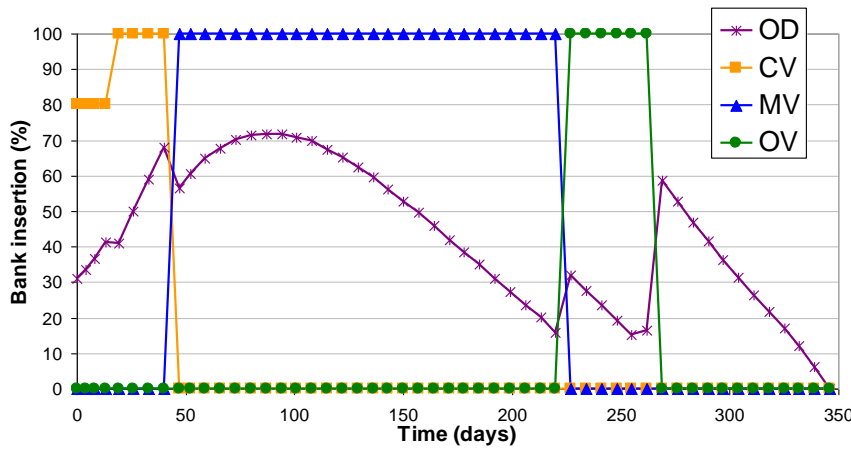


**Fig. 5.17.** CRP for the WATU equilibrium cycle.

The cycle length is 346 days, and  $k_{\text{eff}}$  is maintained at 1.0000 by a criticality search on bank OD, except for the final ~5 days, where the reactor becomes slightly subcritical. EOC  $k_{\text{eff}}$  is 23 pcm subcritical. A slight increase in TRU loading is therefore necessary to maintain criticality over the cycle.

### 5.2.2. Reactivity Coefficients

The reactivity coefficients for both designs are given in Table 5.4. There is substantial margin of subcriticality for the MTC and FVR. This gives reasonable confidence that the FVR is negative despite uncertainties in the calculation. However, the ZCR is substantially positive, to such an extent that it appears unlikely that the design can be modified to make it negative. Increasing the pin diameter will allow the TRU reload fraction to be reduced and hence the ZCR to be made less positive, but this may violate thermal-hydraulic limits (see Chapter 4).

**Table 5.4.** Core reactivity coefficients.

		MTC (pcm/K)	DC (pcm/K)	FVR	ZCR
TPUC	SOC (rods out)	-12.1	-3.6	-0.020	0.040
	SOC	-10.1	-3.8	-0.025	0.039
	SOC (all rods in)	-68.0	-2.7	-0.066	-0.018
	EOC	-19.6	-3.8	-0.035	0.030
WATU	SOC (rods out)	-8.8	-3.8	-0.013	0.040
	SOC	-9.5	-3.8	-0.021	0.031
	SOC (all rods in)	-58.4	-2.7	-0.126	-0.008
	EOC	-17.4	-3.9	-0.026	0.035

In general, insertion of control rods improves the MTC, FVR and ZCR, so calculation of reactivity coefficients with rods out leads to a conservative evaluation. The DC is comparable to or slightly

more negative than that of UO<sub>2</sub>-fuelled reactors (AREVA/EDF, 2011; Westinghouse Electric Company LLC, 2010a) due to the use of Th and the high resonance flux in the reactor. The neutronic response to a LBLOCA is discussed in Section 5.2.4.

### 5.2.2. Core Form Factors

The maximum radial form factor (RFF) calculated for normalized hot channel rise in enthalpy for the TPUC design is 1.41 (Fig. 5.18). The axial form factor (AFF) is calculated as the maximum power in an XY plane of the reactor divided by the average power of an XY plane of the reactor. An AFF based on the maximum ratio of peak to average power in an individual channel would be misleading as this ratio is very high in channels with partially inserted rods, due to very low power at the top of the rod. The AFF is 1.42 and the maximum total power peaking is 1.97. The AFF is slightly higher than without the use of rod shim, but still less than the chopped cosinusoidal distribution typically used in MDNBR calculations. Multiplying the maximum RFF by the pin power peaking of 1.09 gives an estimate of the maximum pin-level normalized hot channel rise in enthalpy (FΔH) of 1.54. Applying an uncertainty factor of 1.05 and an engineering tolerance factor of 1.03 (as in (Westinghouse Electric Company LLC, 2010a)) gives a total power peaking of 2.32.

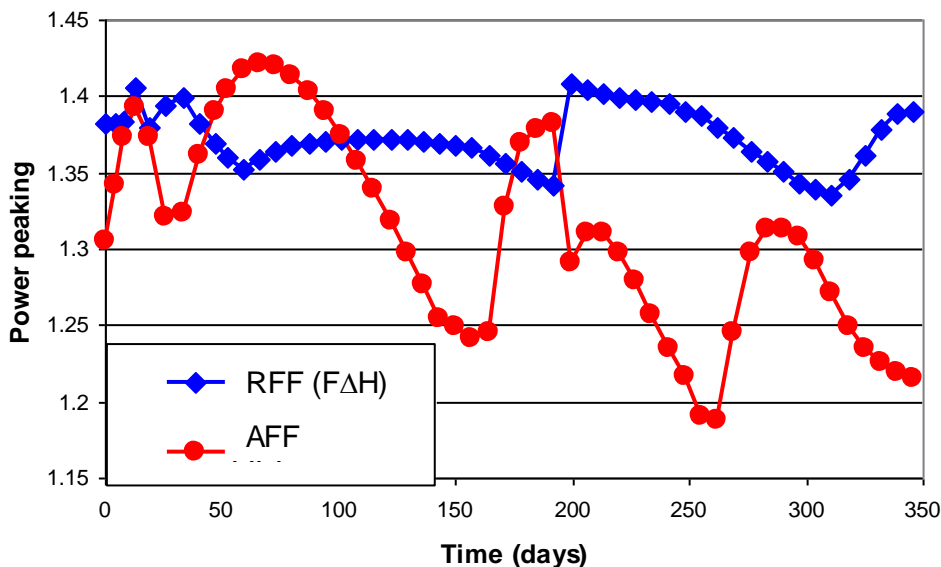


**Fig. 5.18.** RFF and AFF for the TPUC equilibrium cycle.

For comparison, (Watts Bar, 2009) allows a total heat flux hot channel factor of 2.40 and a maximum FΔH of 1.55, so the TPUC design just satisfies these criteria. The AP1000 allows somewhat higher values of 2.60 for total heat flux hot channel factor and 1.65 for maximum FΔH (Westinghouse Electric Company LLC, 2010a).

The core power distribution over life is given in Fig. 5.19. The rod bank switching leads to large changes in the flux profile over the reactor life, with large flux depressions around the inserted

banks. However, the bank switching prevents high power peaking due to rod shadowing effects at EOC.

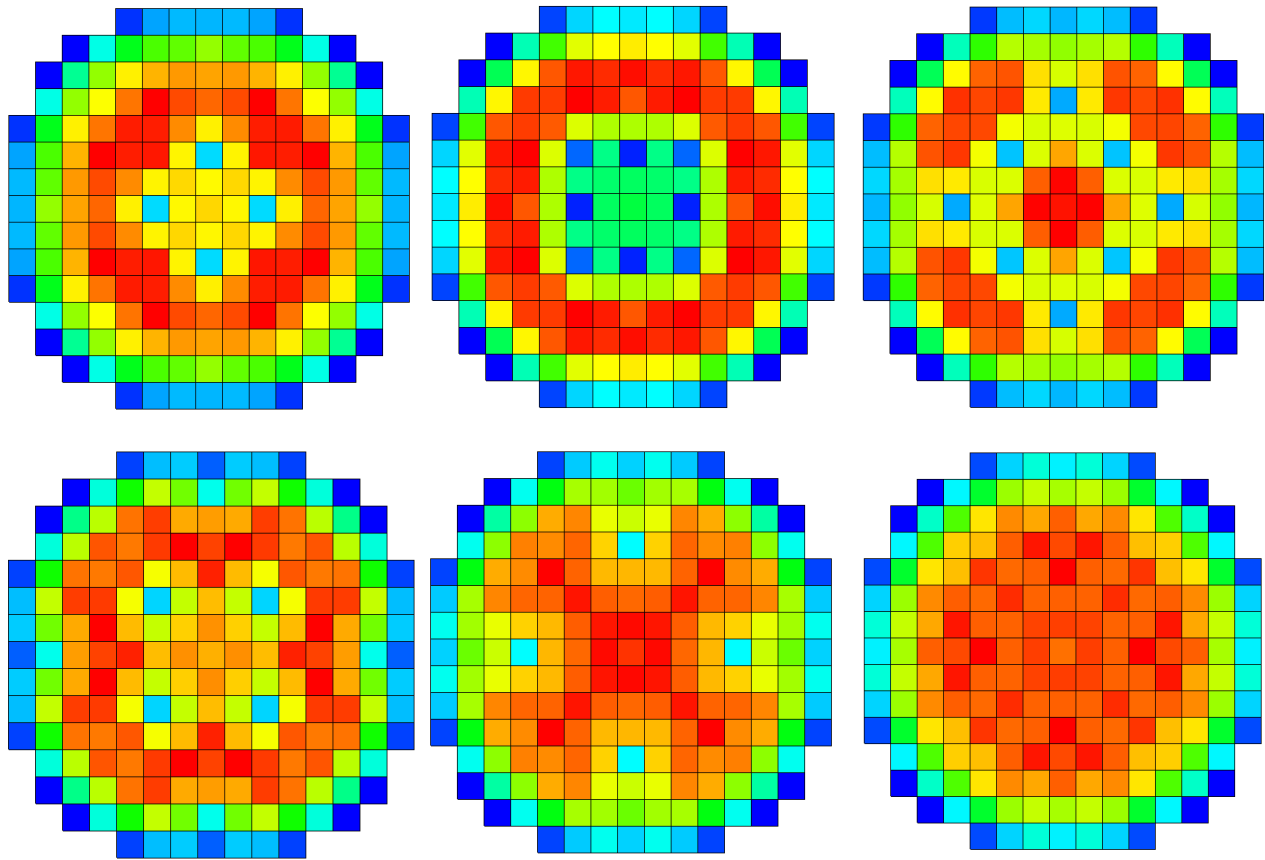


**Fig. 5.19.** Core power distribution for the TPUC equilibrium cycle at (left to right) 0, 26, 33 (top row), 199, 255 and 346 days (bottom row). Spectral colour scale represents channel power: red = hot, blue = cold, normalized to extreme values (highest power shown in Fig. 5.18, lowest power  $\sim 0.3$ – $0.35$ ).

The RFF and AFF for the WATU design are given in Fig. 5.20. The maximum RFF is 1.47 (occurring at SOC) but in the Th-U3 the RFF is at most 1.41. A higher RFF is allowable in the Th-TRU assemblies due to the larger number of pins. The AFF is at most 1.55, which is less than that used for chopped cosine MDNBR calculations but higher than desirable. This is due to partial insertion of a high worth rod bank. Allowing for pin power peaking, the maximum F $\Delta$ H in the Th-U3 is estimated as 1.58, which exceeds the allowable value of 1.55 for Watt's Bar but is within the AP1000 design value. Due to the restricted core design, it appears advisable to seek improved lattice designs with power peaking of at most 1.10 (compared to 1.12) as this will allow the Watt's Bar design limit to be satisfied. The maximum F $\Delta$ H in Th-TRU is  $\sim 1.44$  (including pin power peaking but adjusting for the larger number of pins in the assembly, i.e. normalizing power for a 264-pin assembly) which is substantially lower than the design value.

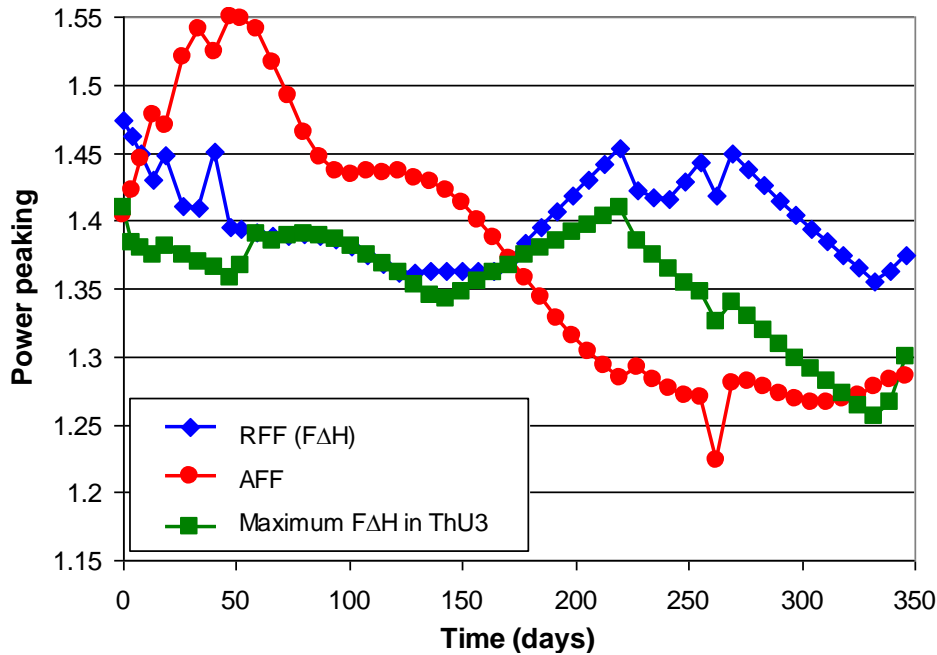


**Fig. 5.20.** RFF and AFF for the TPUC equilibrium cycle.

The total power peaking in the Th-U3 is approximately 2.59 (allowing for uncertainties and engineering tolerances), which exceeds the Watt’s Bar design value but is just within the AP1000 criterion of 2.60. Significant reduction of the AFF over the early part of the cycle is advisable to achieve an acceptable value, which requires use of a lower worth rod bank for partial insertion to bring the reactor to criticality, although this is difficult to achieve with the selected LP without increasing the RFF. The total power peaking in the Th-TRU is 2.42, which is slightly greater than the Watt’s Bar design value. Computational optimization seems advisable. The WATU rod banks are higher worth than the TPUC rod banks. However, as both satisfy the SDM criterion (Section 5.2.3), it may be acceptable to reduce the worth of some of the WATU rod banks, which may improve the AFF.

The RFF over life for the WATU design is given in Fig. 5.21. At EOC, there is a suppressed power distribution in the centre of the core, due to the placement of low reactivity twice-burned Th-U3 assemblies close to the core centre and limited use of inner rod banks (CD and CV) over the cycle.

The axial offset of the power peak from the centre of the core is given in Fig. 5.22. This is generally larger for the WATU design than the TPUC design, consistent with the AFF. As expected, the offset position becomes positive towards EOC as the rod banks are withdrawn, due to rod shadowing effects.

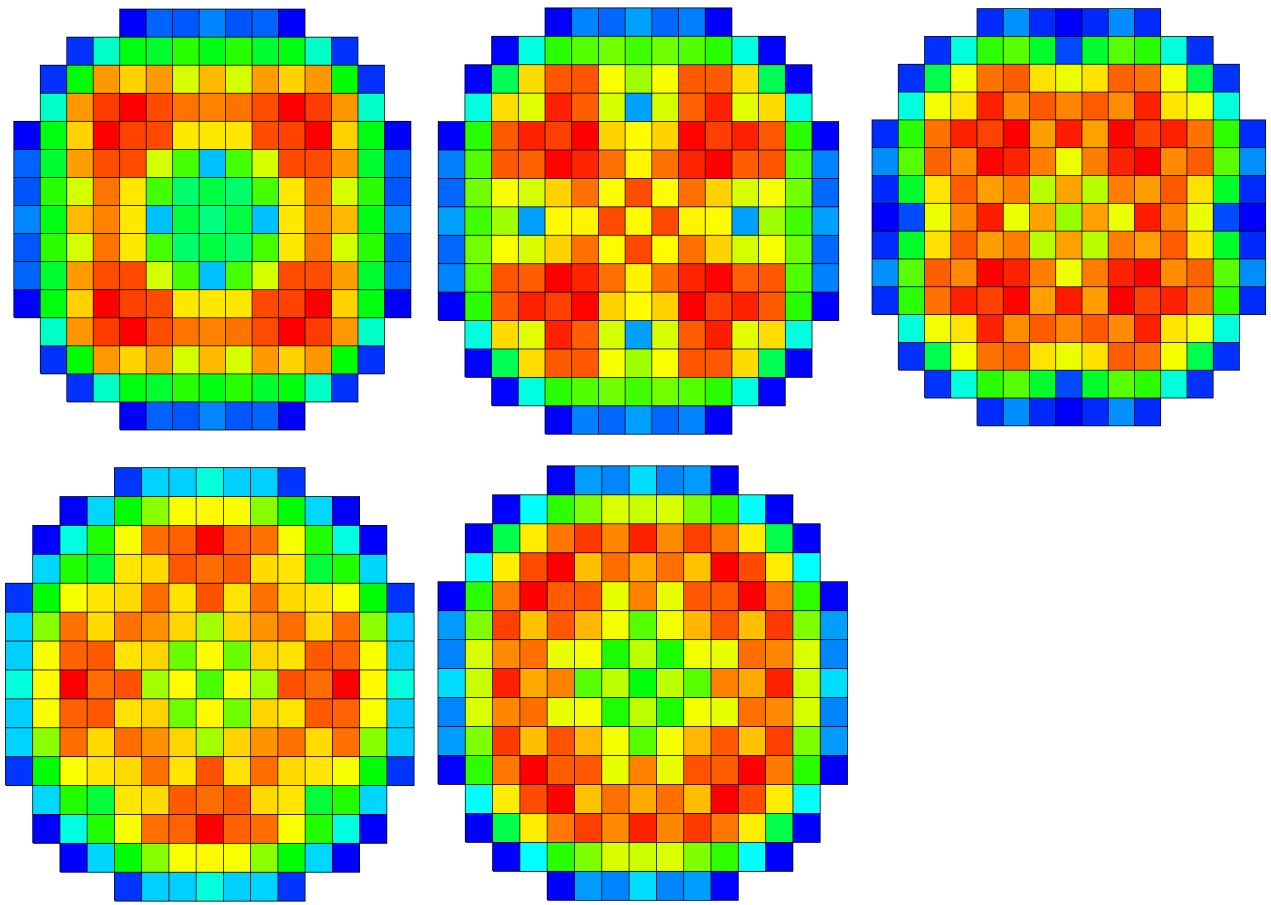


**Fig. 5.21.** Core power distribution for the WATU equilibrium cycle at (left to right) 0, 47, 227 (top row), 269 and 346 days (bottom row). Spectral colour scale represents channel power: red = hot, blue = cold, normalized to extreme values (highest power shown in Fig. 5.20, lowest power  $\sim 0.3$ – $0.35$ ).

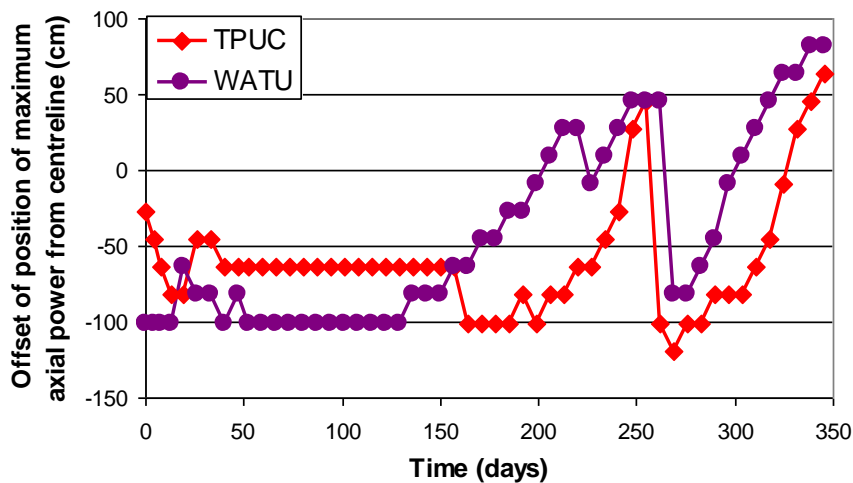


**Fig. 5.22.** Axial offset of position of maximum axial power for the TPUC and WATU equilibrium cycles.

### 5.2.3. Shutdown Margin

For both the TPUC and WATU designs, the highest worth rod throughout life is F10 and its symmetry positions, i.e. the rods of bank CD. In the TPUC design, rod bank CD is inserted for most of life, including at the time of minimum SDM, but no credit is given for this when assuming a stuck rod during a trip, as subcriticality must also be ensured if the highest worth rod is accidentally removed from a shut-down reactor. The variation in the SDM over the equilibrium cycle for both designs is given in Fig. 5.23.

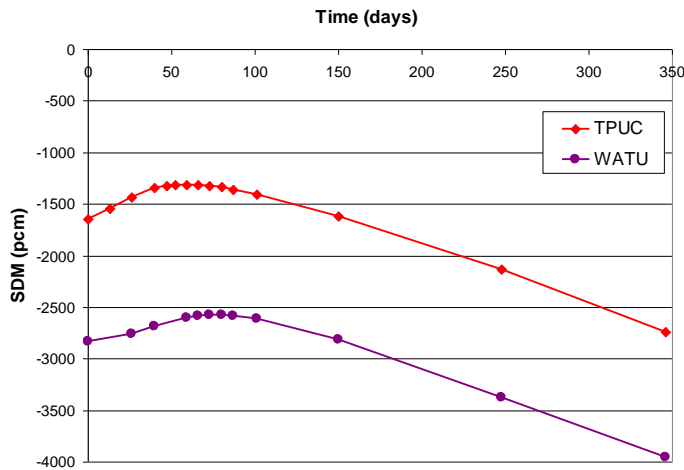


**Fig. 5.23.** SDM over the equilibrium cycle for the TPUC and WATU designs.

The SDM is always better than the minimum allowable  $-1300$  pcm (Watt's Bar, 2009). The minimum SDM for the TPUC and WATU designs is  $-1311$  pcm and  $-2576$  pcm respectively, so the SDM requirement for the TPUC design is only just met. The highest worth rod is  $\sim 1330$ – $1400$  pcm for TPUC and  $\sim 1600$ – $2500$  pcm for WATU.

The WATU design gives a much higher SDM than the TPUC design, partly due to a higher thermal neutron flux in the guide tube positions (Fig. 5.24). This is especially pronounced without Gd in the Th-U3 pins (i.e. when the Gd has burned out). Most rod captures are for neutron energies of around 1000 eV, so the increase in rod worth for the WATU design may be partly explained by reduced thermal neutron availability for  $^{233}\text{U}$  fissions. The SDM for the WATU design is comparable to conventional PWRs (Fridman and Kliem, 2011) and is high enough that the enrichment of  $^{10}\text{B}$  in B in the control rods can be reduced somewhat.

As the WATU control rod worth is  $\sim 35\%$  higher than the TPUC total control rod worth, and the TPUC design meets the SDM criteria, this implies that the  $^{10}\text{B}$  enrichment in the WATU rods can be reduced from 95% to roughly 70% (a higher reduction might be possible due to saturation effects). This will reduce control rod cost. A slight further reduction is possible in both cases, as the

SDM is slightly greater than the minimum. Alternatively, highly enriched rods can be replaced less often.

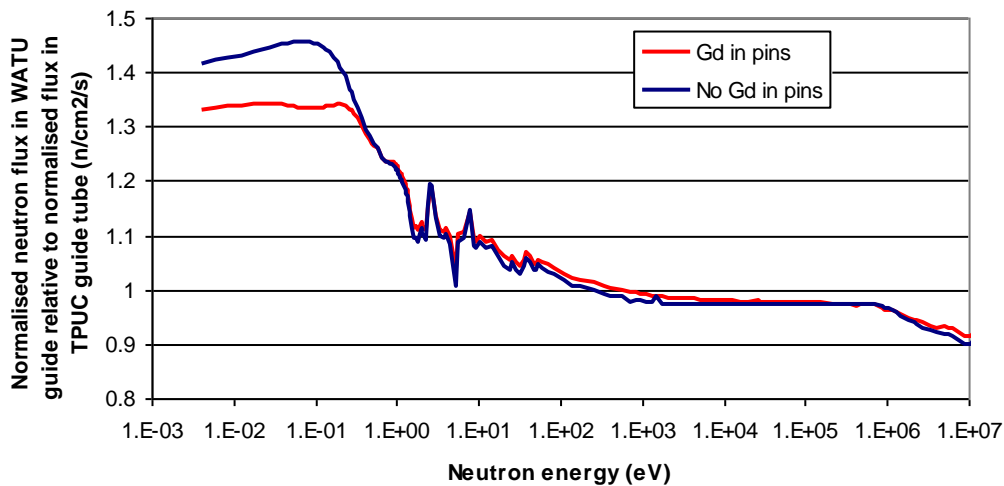


**Fig. 5.24.** Ratio of the flux in control rod guide tubes in WATU core relative to TPUC core.

It may be possible to increase the shutdown worth and reduce rod shadowing effects by utilising control rods which are longer than the fuel assemblies. This would allow different sections of the bank to be utilised for mechanical shim and for shutdown. As a result, it may be possible to employ a lower worth section for shim (towards the bottom of the bank) and a higher worth section for shutdown (towards the top of the bank, which is only inserted during shutdown). Use of longer control rods may not be compatible with the pressure vessel, and the feasibility of this needs to be established.

### 5.2.3. Neutronic Response to LOCA

During an LBLOCA, the primary circuit depressurizes over a period of ~50 s and the coolant drains out of the reactor core in a period of around 20 s. The core is then reflooded by the emergency core cooling system such that the collapsed liquid level rises substantially above zero after around 50 s (AREVA/EDF, 2012; Westinghouse Electric Company LLC, 2010b).

For the design basis accidents considered in (AREVA/EDF, 2012), the mid-core VF is limited to at most ~90% for 9 of the 10 considered break sizes, the exception being a surge line break. The top of core is uncovered for smaller breaks. The negative FVR protects against these LOCAs – hence it is considered advantageous to design for a negative FVR even when a negative ZCR is not possible. Even in a surge line break, the VF in the lower core is still substantially less than 1 at all times. A more detailed thermal-hydraulic analysis is necessary to take into account the increased pin size, in conjunction with coupled neutronics to accurately determine whether a criticality accident is possible in this case.

In the postulated design basis accident, reactor trip is assumed so the reactor shuts down rapidly. In any case, for LEU-fuelled cores the FVR and ZCR are substantially negative such that a trip is not necessary to shut down the core. For the RMPWR LBLOCA design basis accident, the reactor is shut down provided the reactor trips and the control rod worth is sufficient to shut down the reactor under fully voided conditions. For beyond design basis accidents, where the reactor does not trip, the RMPWR may experience a criticality accident during a LBLOCA if the water level in the core drops to a sufficiently low level following depressurization. This could lead to reactor containment being breached.

While it should still be possible to license a plant with a positive ZCR, this is likely to concern a regulator. If it is possible to achieve a negative ZCR with a modified design, then it may be difficult to justify a positive ZCR. If not, then the likelihood of beyond-design-basis accidents, where the positive VC of the RMPWR becomes a concern, must be assessed, together with a severe accident analysis. This may lead to the requirement of additional safety measures, and a demonstration that the risks are as low as reasonably practical.<sup>24</sup>

In the UK, the licensing regime allows for a positive VC provided it is controllable and does not lead to unacceptable consequences – hence a limit needs to be placed on the maximum allowable ZCR if the condition is plausible in a LBLOCA. It is also required that “unintended criticality cannot occur unless at least two unlikely, independent concurrent changes” in conditions occur. In an LWR, this can correspond to a LBLOCA without trip, i.e. failure of both the coolant and trip systems. Common-mode failures can be problematic, notably due to earthquakes (where lateral movement of the core relative to the reactor roof could jam any control rod actuator).<sup>25</sup> Two independent means of shutting down the reactor are also required (UK Office of Nuclear Regulation, 2008).

In the extremely unlikely case of a LBLOCA combined with ejection of all the control rods, the core will undergo a severe accident even if the VC at 100% VF is kept negative by using rods. Any reactor which relies on mechanical shim (e.g., any BWR) will experience a more severe accident if a LBLOCA is combined with simultaneous full rod withdrawal from the core. A LBLOCA without trip is presumably a more likely event (in particular, common-mode failures must be rigorously investigated) but a full understanding of the licensing requirement is necessary to properly assess the design.

Here, the requirement for two independent means of shutting down the reactor is interpreted as necessitating a redundant set of shutdown rods with separate actuators, such that either set can shut

---

<sup>24</sup> Private communication with Dr Peter Dolan, August 2013; Prof. Mike Weightman, October 2013.

<sup>25</sup> Private communication with Dr Tony Judd, October 2013.

down the reactor in a LBLOCA. This is similar to the use of two independent sets of shutdown rods in SFRs, although in these the void reactivity is often limited to  $\sim 6\%$  ( $<2000$  pcm) (Tobita, 2013), about half the value of the ZCR for the RMPWR (up to  $\sim 4000$  pcm or  $\sim 12\%$ ). Some designs of sodium-cooled fast reactor have a higher sodium void reactivity, especially burner designs (Hoffman et al., 2006).

An alternative is to use a completely separate shutdown system, e.g. a shutdown assembly at the centre of the core – although this would require a substantially modified reactor design. Use of separate redundant shutdown systems is also used in CANDUs, which have a positive ZCR of  $\sim 500$ - $1500$  pcm (much lower than that considered here). This takes the form of a set of shutdown rods and gadolinium salt injection into the calandria (CANDU, 2012). In CANDUs, the shutdown rods have the advantage of operating in a relatively low pressure core, although in a LBLOCA core depressurization has also occurred which may help ensure the reliability of any redundant shutdown system, including a set of redundant shutdown rods as described in this section.

The additional shutdown rods are shown in Fig. 5.14 labeled ‘S2’. It must be noted that higher prediction of FVR (and ZCR) values in JEF-2.2 than ENDF/B7 and the discrepancy relative to a multi-group Monte Carlo calculation could lead to an overestimate of as much as  $\sim 2000$  pcm in the FVR and ZCR values. This would not make the ZCR negative, but would make it substantially less positive.

The SDM with zero coolant density for the usual and added set of rods is given in Table 5.5 (note the total reactivity in Table 5.5 includes the ZCR and the control rod worth). A 10% uncertainty factor in the rod worth is assumed in both cases. 10% rod depletion is considered for the usual rods, but, as the added rods are not used for shim, no depletion is assumed for these. The highest worth rod is assumed to be stuck for both rod banks. There is no Doppler defect as the rods are not required to achieve HZP, there is essentially no heat transfer when the core has zero coolant density and the DC is in any case very low with zero coolant density ( $\sim -0.2$  pcm/K). The very small DC also prevents Doppler effects from terminating overpower transients before containment is breached in a criticality accident, for this high a ZCR. The SDM is calculated for 52 and 73 days into the cycle for TPUC and WATU respectively as these are the points of lowest SDM under operating conditions. Results are strongly indicative that a satisfactory SDM can be maintained throughout the cycle and that a reactor trip will still shut down the reactor at zero coolant density.

**Table 5.5.** SDM with zero coolant density (pcm).

	Usual rods	Added emergency shutdown rods
TPUC	-4313	-2261
WATU	-7242	-2650

### 5.3. Rod Ejection Accident Analysis

The most severe reactivity accident in a typical PWR is typically a REA. The RMPWR operates with effective delayed neutron fraction<sup>26</sup> ( $\beta_{\text{eff}}$ ) of  $\sim 0.00318$ , significantly lower than that of a typical PWR (Diamond et al., 2002), so the enthalpy deposition in the fuel can be expected to be much higher than with conventional fuel. The enthalpy deposition from a prompt supercritical rod ejection can be predicted by the zero-dimensional adiabatic Nordheim-Fuchs model to be proportional to (reactivity insertion  $- \beta_{\text{eff}}$ ) (Hetric, 1993). For the WATU fuel, this can be as high as  $\sim 2200$  pcm. Fortunately, the enthalpy deposition is typically much less than the maximum permissible, such that a substantial increase in this value is allowable.

The Nordheim-Fuchs model generally gives the correct relationship, but not the constant of proportionality determined by the power peaking (Diamond et al., 2002). PANTHER is used here with rod ejection at the point of maximum rod worth. No reactor trip was modelled. Results were checked by comparing with a point kinetics model, with the RFF in the ejected assembly taken from PANTHER. The point kinetics code PTS-ADS (Ahmad et al., 2012) was used, and gave good agreement with PANTHER for maximum fuel temperature rise.

Using MOX fuel typically results in a lower  $\beta_{\text{eff}}$ . For MOX cores, this is somewhat mitigated by the lower control rod worth due to the hard neutron spectrum (Fridman and Kliem, 2011). However, in this case the rod worth is similar to or greater than that for typical PWRs due to the use of enriched  $B_4C$  rods. Higher rod worth is required to achieve the same SDM due to the use of mechanical shim. Increasing the number of control rods would reduce the required individual rod worth.

The enthalpy deposition must be limited due to pellet cladding mechanical interaction and fuel melting criteria. The limit depends on burn-up due to effects of hydrogen pick-up and oxide wall

---

<sup>26</sup> The effective delayed neutron fraction ( $\beta_{\text{eff}}$ ) was calculated using the Monte Carlo code SERPENT (Leppänen, 2007) (for a 2D lattice calculation) due to limitations with WIMS when calculating the kinetic parameters of Th-U3 fuels. For this fuel, there were problems when calculating an accurate value of  $\beta_{\text{eff}}$  with JEF-2.2 in SERPENT. Therefore the ENDF/B7 data library was used instead. Use of different data libraries for different parameters in this manner is not ideal, but the JEFF-3.1 and ENDF/B7 data libraries were found to give virtually identical values of  $\beta_{\text{eff}}$  giving confidence that this is acceptable.

thickness in the clad. In the UK EPR, the enthalpy deposition limit (cal/g) on clad failure<sup>27</sup> up to 69 GWd/t is (AREVA/EDF, 2012):

$$\text{Min}\left(162.26; 141.4 - 29 \tanh\left(\frac{BU - 49}{8.5}\right)\right) \quad (5.1)$$

for linear heat rate = 0 W/cm, and

$$\text{Min}\left(123.68; 108.66 - 35.6 \tanh\left(\frac{BU - 54.6}{11.1}\right)\right) \quad (5.2)$$

for linear heat rate = 200–300 W/cm, where  $BU$  is the burn-up in GWd/t.

Applying these formulae at HFP and HZP for the Th-TRU fuel in the TPUC assembly, with a maximum average discharge burn-up of 61 GWd/t, gives enthalpy deposition limits of 115.7 and 90.1 cal/g respectively. In the WATU case, the hot assembly contains only Th-U3, with a maximum discharge burn-up of ~32 GWd/t, giving enthalpy deposition limits of 162.3 and 123.7 cal/g respectively. However, the neighbouring assembly to the ejected rod can have a power up to ~90% as high as in the ejected assembly, such that the 61 GWd/t limits are adopted throughout. These limits may not be appropriate to the different fuel type considered here, but are indicative of an acceptable fuel enthalpy deposition rate.

The reactor was assumed to be held at HZP with all the control rods in. This renders the reactor slightly subcritical but provides a reasonable approximation to the power peaking and rod worth of the worst REA conditions. As rods are withdrawn to bring the reactor to criticality, it is assumed the highest worth rods are withdrawn first, such that the conditions for the postulated REA do not get worse for other HZP states. A  $\beta_{\text{eff}}$  value of 318 pcm was used in this analysis, but it is possible that it could be even lower at some point in the cycle, and  $\beta_{\text{eff}}$  is often reduced in REA analysis to account for uncertainties – this is not performed here.

REA simulations are typically performed for a 100 ms ejection time and a HZP level of  $10^{-4}\%$  of full power (Diamond et al., 2002). This results in complete ejection of the rod before the fuel temperature spike acts to insert negative reactivity. However, the RMPWR has a much reduced neutron lifetime of ~3  $\mu\text{s}$  compared to ~30  $\mu\text{s}$  in a conventional PWR. This means that Doppler feedback can act to limit the maximum reactivity insertion before the rod is fully ejected, depending on the speed of the ejection and the zero power level. Therefore, simulations are performed for 10 ms and 100 ms ejection times and  $10^{-6}$  and  $10^{-9}$  power levels.

---

<sup>27</sup> Non-SI units of cal/g are used throughout this section in accordance with standard practice.

The reactivity insertion and maximum fuel temperature rise for 100 ms ejections for the TPUC case are given in Fig. 5.28. The rod worth is 1422 pcm, but the maximum reactivity increase is much less. The reactivity oscillations are a consequence of the temperature rise occurring before the rod has fully ejected. This behaviour has also been predicted using PTS-ADS and is further discussed in Section 5.3.1.

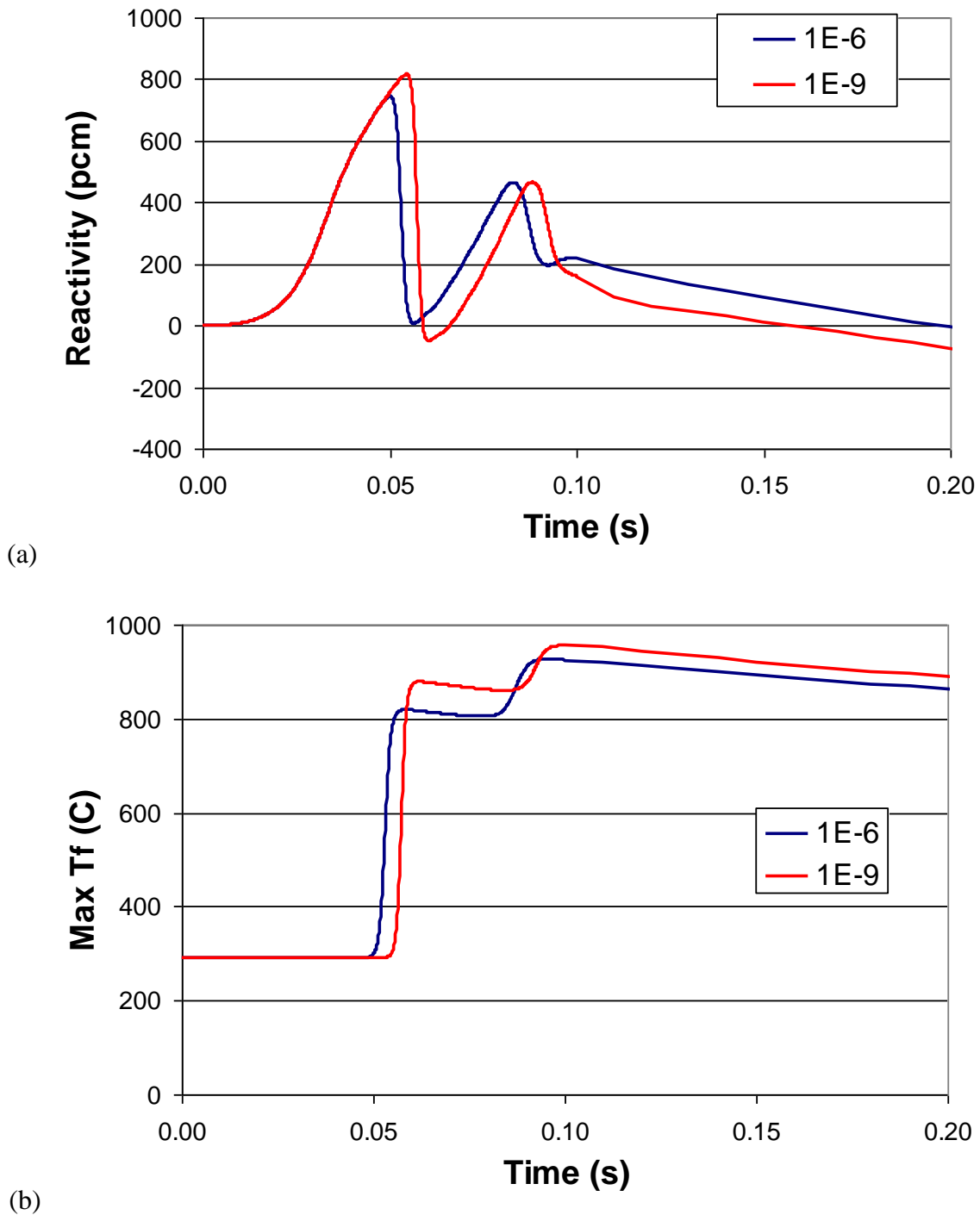
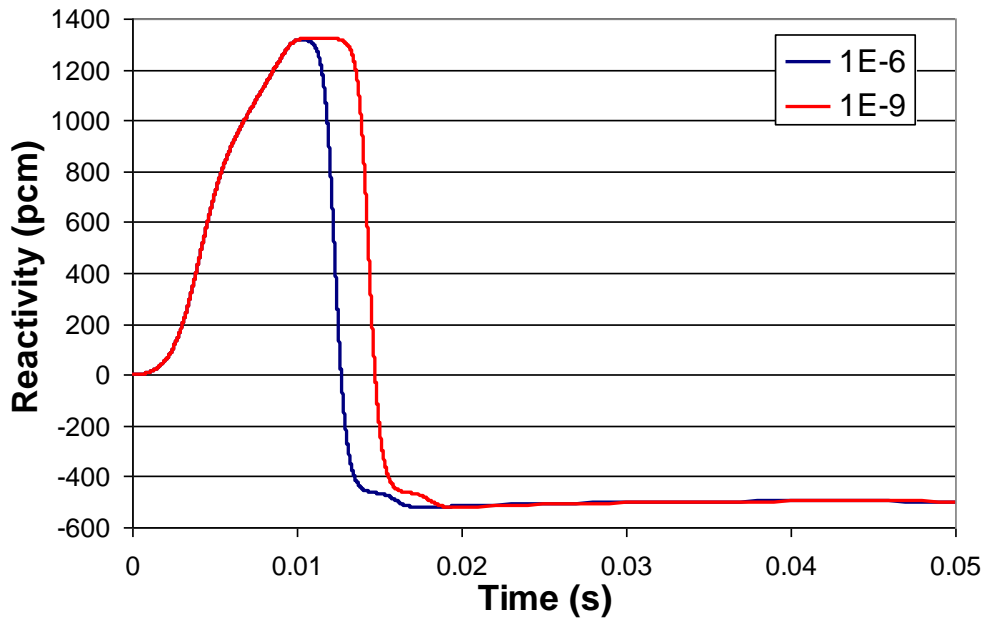
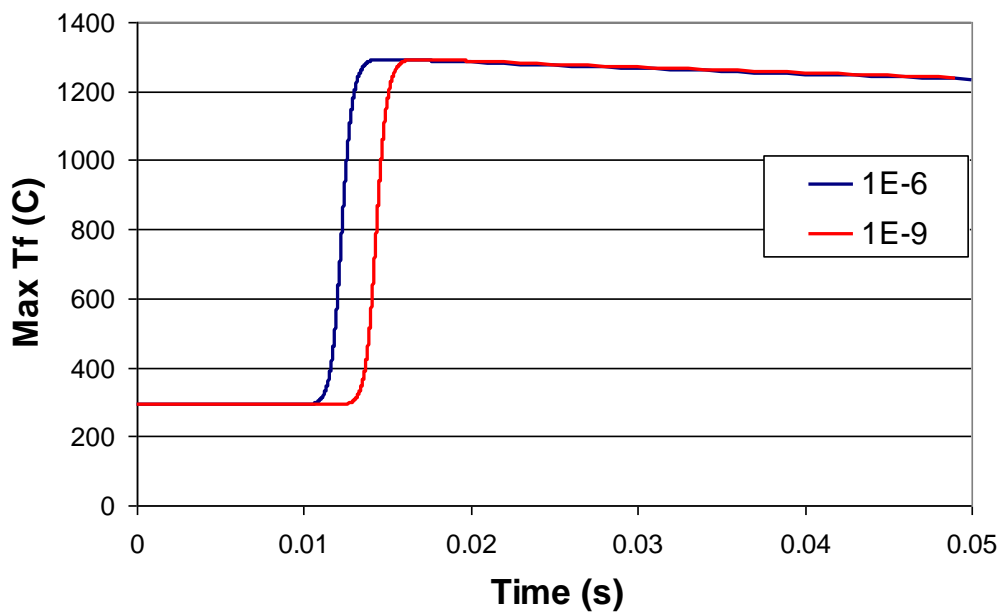


**Fig. 5.28.** (a) Reactivity and (b) Maximum fuel temperature for TPUC 100 ms rod ejection at  $10^{-6}$  and  $10^{-9}$  power levels.

If the rod ejection time is reduced to 10 ms, the rod fully ejects for both zero power levels, leading to a higher reactivity insertion and fuel temperature increase (Fig. 5.29).



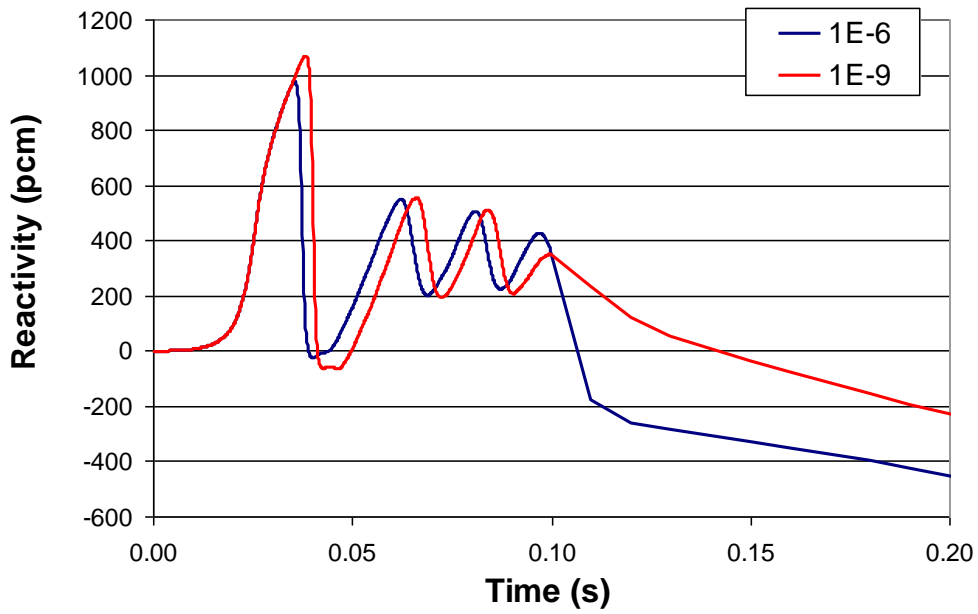
(a)



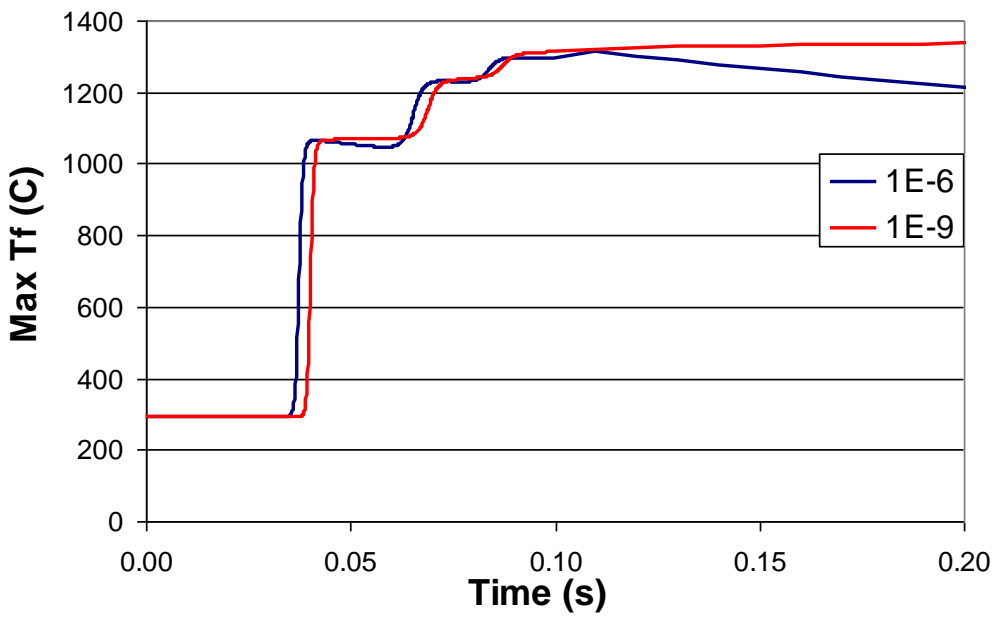
(b)

**Fig. 5.29.** (a) Reactivity and (b) Maximum fuel temperature for TPUC 10 ms rod ejection at  $10^{-6}$  and  $10^{-9}$  power levels.

For the WATU fuel, the rod worth is 2480 pcm, but again for a 100 ms ejection time the maximum reactivity is limited by the fuel temperature rise (Fig. 5.30). The maximum fuel temperature rise is  $\sim 400$  K higher than for the TPUC case. For a 10 ms ejection time, the rod almost fully ejects, leading to an even larger maximum fuel temperature rise (Fig. 5.31).

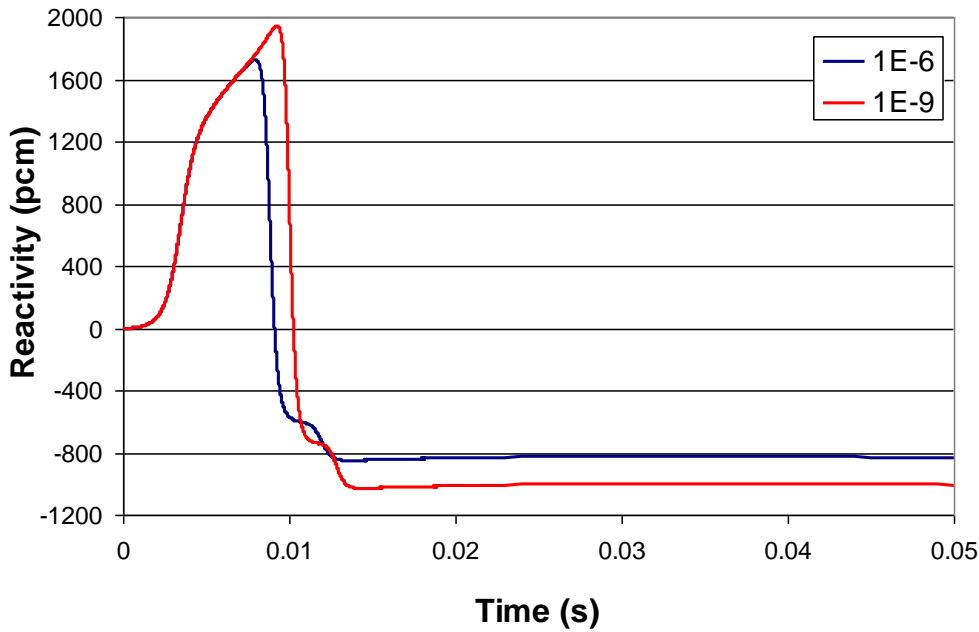


(a)

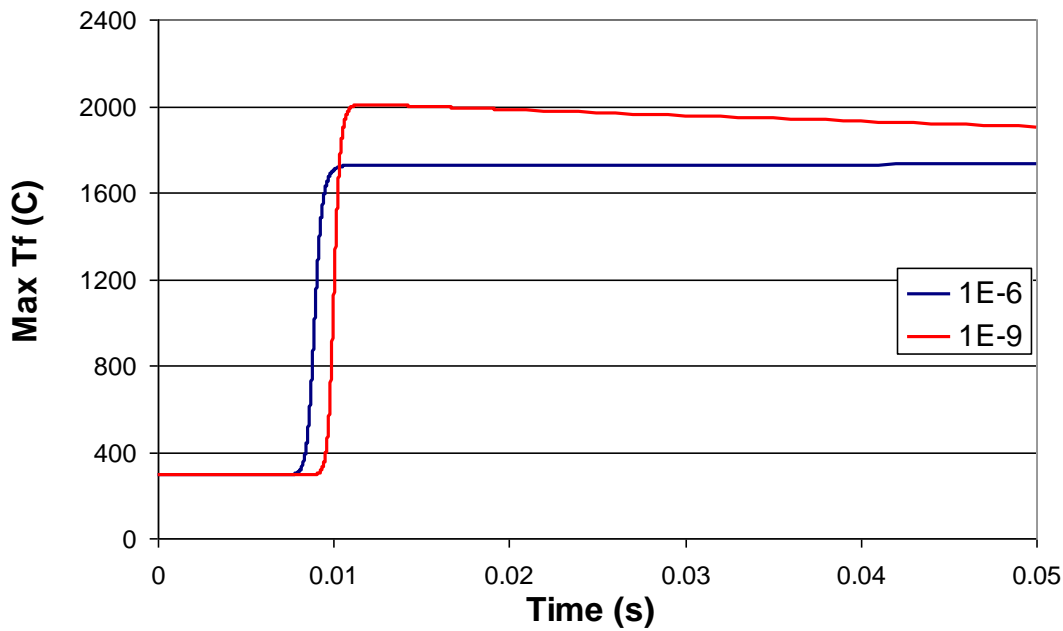


(b)

**Fig. 5.30.** (a) Reactivity and (b) Maximum fuel temperature for WATU 100 ms rod ejection at  $10^{-6}$  and  $10^{-9}$  power levels.



(a)



(b)

**Fig. 5.31.** (a) Reactivity and (b) Maximum fuel temperature for WATU 10 ms rod ejection at  $10^{-6}$  and  $10^{-9}$  power levels.

The maximum enthalpy rises, peak reactivity insertions and power pulse width (defined as the time during which the power is  $>50\%$  of the maximum; noting that the reactivity oscillates in some cases leading to secondary power pulses as shown in Fig. 5.32 are given in Table 5.8). These only include assembly-level effects, so the hot pin may have a  $\sim 10\%$  higher enthalpy rise. For the WATU case, the maximum enthalpy rise may exceed the limit for a 10 ms ejection. When allowing for uncertainties, or potentially a lower maximum enthalpy rise, this may necessitate a reduced control

rod worth, or being able to demonstrate that the rod ejection will not be this rapid. The enthalpy deposition is not particularly sensitive to the zero power level.

**Table 5.8.** REA analysis results

Ejection time (ms)	Zero power level	Maximum fuel enthalpy rise (cal/g)		Power pulse width (ms)		Peak reactivity (pcm)	
		TPUC	WATU	TPUC	WATU	TPUC	WATU
100	$10^{-6}$	42.7	69.5	2.6	1.8	746	973
100	$10^{-9}$	44.7	70.4	2.3	1.6	816	1068
10	$10^{-6}$	69.6	111.6	1.2	0.8	1317	1726
10	$10^{-9}$	69.6	123.5	1.2	0.7	1322	1940
Approx. HZP enthalpy deposition limit:		115.7					

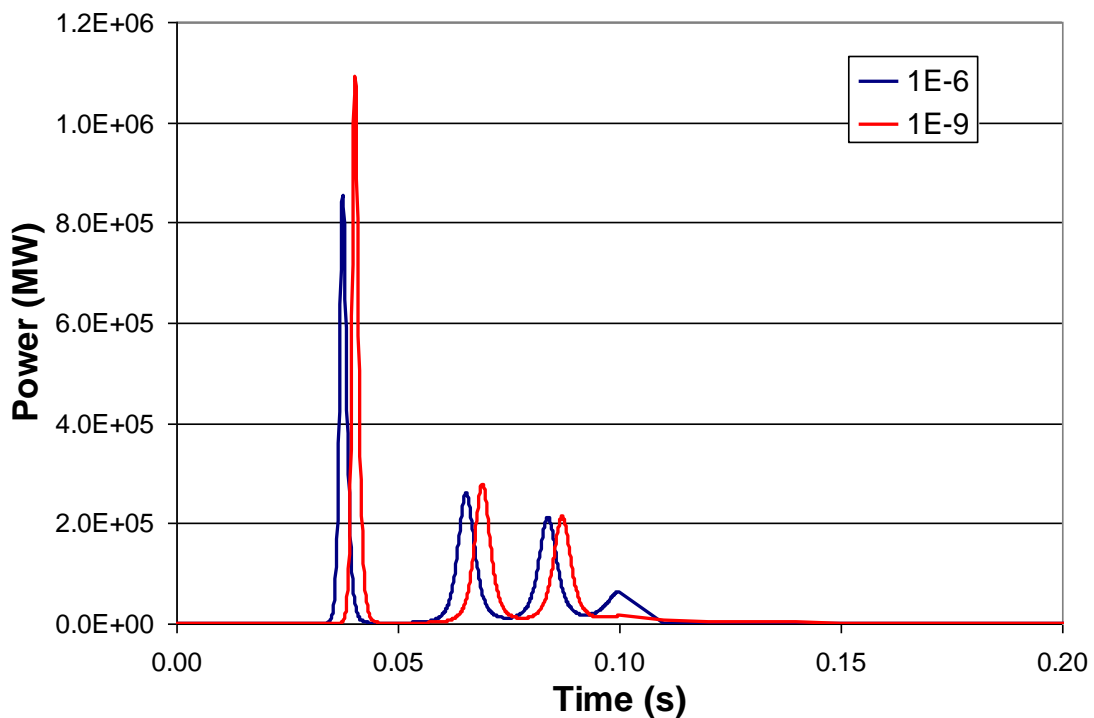


**Fig. 5.32.** Power for 100 ms REA at  $10^{-6}$  and  $10^{-9}$  power levels with WATU fuel. Reactivity and power both oscillate leading to secondary power pulses

The rod ejection speed is determined by power level, reactor height, system pressure and the RCCA material. However, as it can be difficult to justify the assumptions used for ejection time and zero power level, it is thought that conservative values should be used. HFP was also considered, both

for switch-on and due to the use of mechanical shim. However, the enthalpy deposition in this case was much lower due to rapid fuel and coolant feedback.

The effect of the neutron lifetime on limiting the fuel temperature increase can be effectively demonstrated by artificially reducing the neutron velocity by an order of magnitude – resulting in a similar neutron lifetime to a conventional PWR. This is obviously non-physical. In the test case shown in Fig. 5.33 the reactivity insertion when the rod is fully ejected is  $\sim 700$  pcm. A 10 ms ejection, or 100 ms ejection with artificially increased neutron lifetime, result in a fully ejected rod before temperature feedback effects compensate. This leads to a maximum fuel temperature rise of  $\sim 500$  K in both cases. With a 100 ms ejection time with the correct neutron lifetime, the reactivity increase is limited to  $\sim 500$  pcm, leading to a proportionally lower fuel temperature rise.

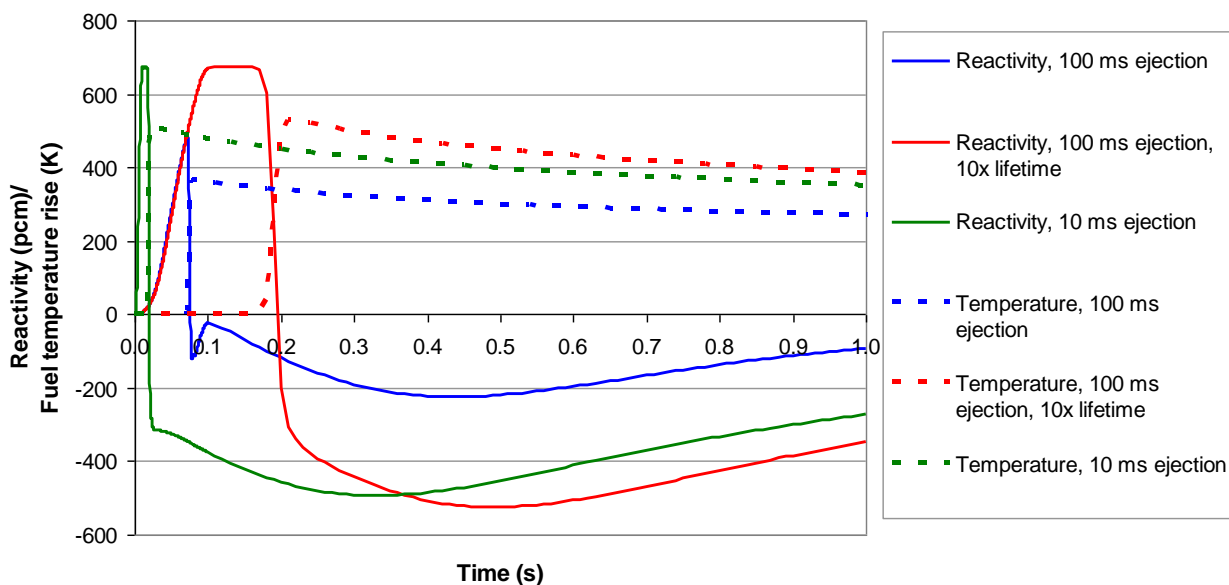


**Fig. 5.33.** Reactivity and fuel temperature rise variation for REA test cases of 10 ms ejection, 100 ms ejection and 100 ms ejection with artificially increased neutron lifetime.

### 5.3.1. Cause of Reactivity Oscillations

The power pulse shown in Fig. 5.32 occurs at  $\sim 0.04$ s compared to  $\sim 0.3$ s for an REA in a conventional PWR (Diamond et al., 2002). This is due to the shorter neutron lifetime. The fuel enthalpy deposition is effectively the integral of the power spike, and hence they occur simultaneously, resulting in the enthalpy deposition also taking place more rapidly than usual. This is demonstrated using a point kinetics model with zero delayed neutron fraction, i.e.:

$$\frac{dP}{dt} = \frac{\rho P}{\Lambda} \quad (5.1)$$

Where  $\Lambda$  is the prompt neutron lifetime and  $\rho$  is the reactivity.

Assuming reactivity insertion at a linear rate of 1000 pcm per 100 ms, with all heat deposited in the fuel:

$$\rho = 0.1t + \alpha T \quad (5.2)$$

Where  $T$  is the difference in fuel temperature from the steady-state fuel temperature and  $\alpha$  is the DC.

By assuming a constant heat removal rate in the fuel equal to the steady state power:

$$\frac{dT}{dt} = k(P - P_0) \quad (5.3)$$

Where  $k$  is the constant of proportionality between power and change in fuel temperature (i.e. inverse of the product of mass and specific heat capacity) and  $P_0$  is the initial power.

By expressing power in units such that  $k = 1$ , it follows that  $P_0 = 1$ , Eq. 5.3 can be simplified to:

$$\frac{dT}{dt} = P - 1 \quad (5.4)$$

Eq. 5.1, 5.2 and 5.4 reduce to:

$$\Lambda \frac{dP}{dt} = (0.1 - \alpha)Pt + \alpha P \int P dt \quad (5.5)$$

From numerical solution, constant amplitude reactivity oscillations are observed, which are at higher frequency for shorter prompt neutron lifetime, with corresponding power pulses and fuel temperature increases (Fig 5.34).

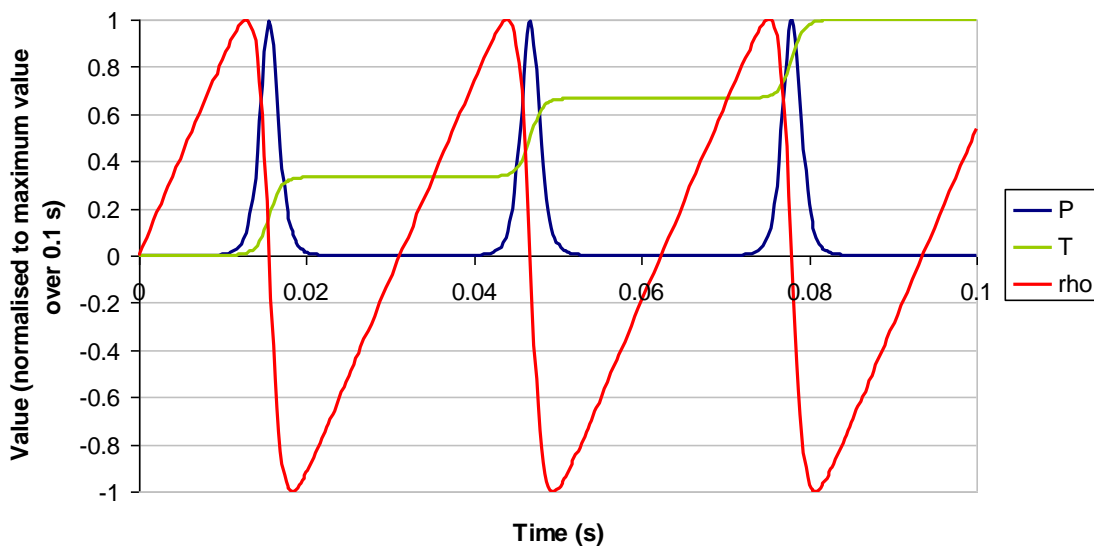


**Fig. 5.34.** Reactivity oscillation behaviour for model with short ( $1 \mu\text{s}$ ) neutron lifetime.

## 5.4. Concluding Remarks

It has been established that a heterogeneous fuel configuration is neutronically advantageous, specifically by spatial separation of U3 and TRU. This fuel layout provides the option for innovative fuel management where Th-U3 and Th-TRU regions are run on different batch management schemes. Specifically, it can be advantageous for the Th-TRU to reside twice as long in the core as the Th-U3. This can be implemented using a heterogeneous assembly design (TCUP or TPUC) or whole assembly heterogeneity (WATU). For a standard 4-loop 193 assembly core with a 17×17 assembly, 12.6 mm pin pitch and pin diameter increased from 9.5 mm to 11 mm, this scheme allows discharge burn-up to be maintained, while simultaneously ensuring that the FVR is negative, which improves the response to LOCAs. However, the ZCR is substantially positive, which could lead to positive reactivity in some LOCA scenarios, for example a surge line break, if the reactor does not trip. To protect against this beyond-design-basis accident, a second redundant set of shutdown rods is added to the reactor, so that either the usual or secondary rods can trip the reactor when there is zero coolant in the core. Even so, this condition is likely to be concerning from a regulatory standpoint. The additional control rods introduce some additional complication if retro-fitting an existing core, due to the need to place additional RCCAs which penetrate the pressure vessel.

A cycle length of 1 year is possible with an average fuel discharge burn-up in of ~40 GWd/t. This scheme is only beneficial for a ‘single-tier’ fuel cycle with the TRU feed coming directly from existing UO<sub>2</sub>-fuelled PWRs. The ‘multi-tier’ fuel cycle, consisting of an intermediate Th-Pu pass in a conventional PWR, which gives similar or favourable performance in the RMPWR for simpler loading schemes, is not amenable to this loading scheme. The ‘single tier’ scheme therefore appears preferable.

Refueling schemes which do not utilize variable batch management strategies have a lower peak discharge burn-up, but require an increased pin diameter (~11.5 mm) for the FVR to be negative. This is detrimental to thermal-hydraulic feasibility (see Chapter 4), and reduces the achievable TRU incineration rate.

The ability of the TPUC and WATU fuel designs to satisfy power peaking, SDM and REA accident conditions has been investigated. Despite use of mechanical shim, designs with relatively low RFF values of ~1.41 have been identified for both designs (for WATU it is slightly higher in the Th-TRU assemblies, but the larger number of pins mean that this is allowable). However, the relatively high pin-level power peaking makes it difficult to satisfy likely RFF constraints, meaning that a large number of fissile zones is necessary to limit assembly-level power peaking. For the WATU design, this is further complicated by slight deviation from a checkerboard assembly design. The

TPUC design satisfies power peaking limits, but the WATU design has a high AFF leading to an unacceptable total hot channel factor. This requires use of a lower reactivity worth partially inserted rod bank in the CRP.

The TPUC design can just satisfy the SDM requirement and likely limits on enthalpy deposition in the fuel following a REA. The actual enthalpy deposition is sensitive to the rod ejection speed, although a conservative value can be used for this. The WATU design allows a higher SDM to be achieved, but the increased rod worth leads to a worse REA response. This is readily mitigated by reducing the  $^{10}\text{B}$  enrichment in the control rods, such that the SDM requirement is still satisfied but the REA performance is improved. This may also improve the AFF by reducing the worth of the partially inserted control bank. Overall, the TPUC design appears preferable for ease of designing a core with acceptable power peaking, meaning that safety criteria can be more readily satisfied, but the WATU design allows a reduction in  $^{10}\text{B}$  enrichment in the control rods.

The low  $\beta_{\text{eff}}$  and low neutron lifetime associated with these fuels may also adversely affect the response to other transients and accidents, in particular accidents involving reactivity insertion due to inadvertent rod withdrawal etc. In any case, the core control system will require ‘re-tuning’. Detailed analysis of LOCAs, and analysis of other transients are the next steps to be pursued in analysing this design.

## **Chapter 6 – RBWR Full-core Analysis**

In Chapter 2, a single-assembly analysis was performed of a 217 pin RBWR assembly based on the JAEA design from (IAEA, 2004). A homogeneous fuel composition was found to give acceptable neutronic performance. A coupled neutronic-thermal-hydraulic model is required to accurately analyse a RBWR core, due to strong feedback between neutronics and thermal-hydraulics. This is performed in this chapter. Axial leakage is often an important mechanism in ensuring a negative VC, and this is sensitive to treatment of the axial reflectors and blankets. The analysis is extended to treat heterogeneous TCUP assemblies and a multi-tier fuel cycle implementation.

The RBWR is capable of achieving a high average discharge burn-up with a negative VC. The VC and DC values are sensitive to how they are calculated, so there is some uncertainty as to their exact magnitude. A higher discharge burn-up is possible with a tall core, but a higher waste reload fraction is possible in a shorter, higher leakage core. In particular, a waste reload fraction of 35% appears possible when utilizing a TCUP assembly, with good performance achievable with single- or multi-tier fuel cycles. Due to the use of axially homogeneous fuel, it is possible to achieve a sufficient maximum critical power ratio (MCPR) with a higher power density than the JAEA RMWR design (with the same fuel assembly configuration). The MCPR is particularly good for tall cores, and it may be possible to use a core of the same area and rating as an ABWR, rather than requiring a larger core area. However, radial power peaking within the assembly may be higher if TCUP fuel is used.

While axially homogeneous fuel is preferable to limit fuel fabrication costs, it is worth evaluating if a substantial performance improvement is possible with axially heterogeneous fuel. A preliminary assessment is made of different axially heterogeneous fuel types using Monte Carlo 3D pincell calculations. The axially heterogeneous designs do not outperform the TCUP design. The axially homogeneous TCUP design is therefore preferred.

The neutronic-thermal-hydraulic models used in this chapter are heavily based on models developed at the University of Michigan, and the author would like to acknowledge the help of Andrew Hall, and the rest of Prof. Thomas J. Downar's group at the University of Michigan.

### **6.1. Full-core Analysis of RBWR with Homogeneous Fuel**

The Th-fuelled RBWR was modelled by coupling the nodal code PARCS (Kozlowski et al., 2004) with the thermal-hydraulic code RELAP5 (Fletcher and Schultz, 1995). The PARCS model was based on a RBWR model developed at the University of Michigan, rated at 3926 MWth with 720 assemblies with one-third rotational symmetry (Downar et al., 2012). The LP consists of 4 complete batches and one partial batch (Fig. 6.1). The RELAP5 model was also based on the University of

Michigan model, with 121 parallel pipe components, each modelling the flow through 1 or 2 assemblies (Fig. 6.2). As described in (Downar et al., 2012), PARCS and RELAP5 are coupled using a Generic Interface. PARCS, RELAP5 and the Generic Interface are separate processes that communicate using message passing protocols in the Parallel Virtual Machine. As discussed in Chapter 2, 125 cm and 200 cm cores were modelled to investigate the relative merits of high and low leakage. The core power is the same in both cases, and the 200 cm core contains more fuel and so has a lower fuel rating.

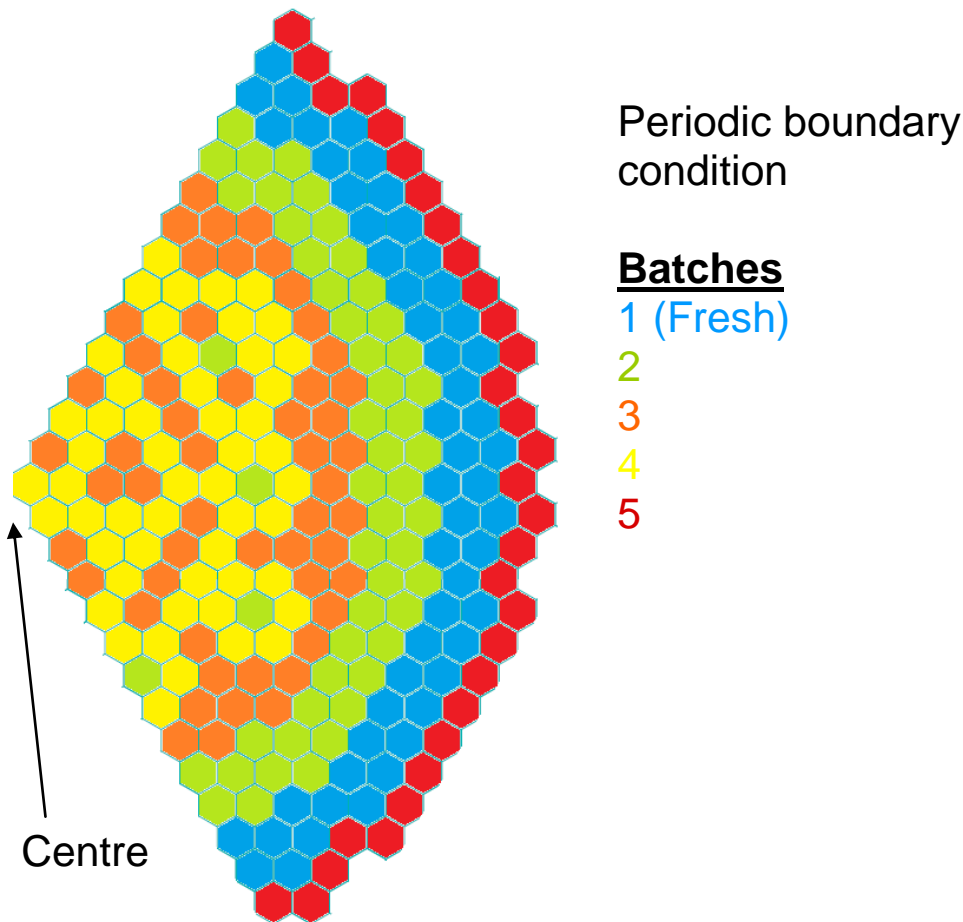


**Fig. 6.1.** RBWR core fuel LP in one-third rotational symmetry.

Many RBWR designs proposed are highly heterogeneous in the axial direction, necessitating 3D neutronic models with accurate coolant density distributions, which are themselves dependent on the power and therefore flux solutions. However, for the axially homogeneous fuel proposed in the Th-based RBWR design investigated, 2D lattice calculations are appropriate for lattice data generation for the core simulator. Therefore 12-group cross-sections were generated using WIMS and converted to the PMAXS format required in PARCS (Xu and Downar, 2006).

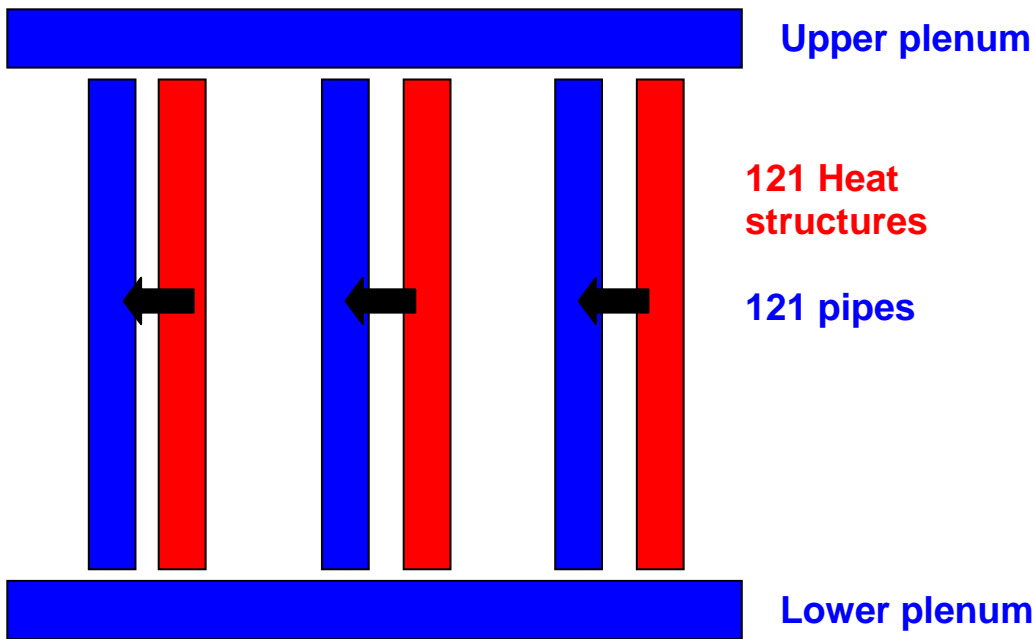


**Fig. 6.2.** RELAP5 model.

The shim rods contain 95% enriched  $^{10}\text{B}_4\text{C}$  in 20 vertical solid pellets of 0.471 cm diameter in each blade. Lower and upper water reflector regions of 7 cm and 30 cm respectively were modelled in PARCS. It is possible to borate either or both reflectors to increase neutron leakage (Downar et al., 2012), but this was not considered here. There are 43 shim rods in the core, distributed approximately evenly within the central region (batches 3 and 4) of the core.

RELAP5 was first run in stand-alone mode to generate an initial guess at the thermal-hydraulic solution, which was used in the coupled analysis. The equilibrium cycle was determined by depleting over a cycle, shuffling and refuelling until the equilibrium cycle had converged. The equilibrium cycle is influenced by the CRP, but determination of an appropriate CRP is beyond the scope of an initial analysis, so the depletion was performed with rods out. This will change how the core depletes, but should not greatly affect the equilibrium cycle burn-up.

The VC and DC of the equilibrium cycle were evaluated at SOC and EOC by alternately perturbing the core power and flow rate and solving Eq. 6.1 (Downar et al., 2012). Due to the coupled code system, perturbing the power and flow rate affects both the void and temperature distributions so a linear system is required in order to solve for the reactivity coefficients. The perturbed conditions were 110% overpower and 90% flow rate. A 75% flow rate condition was also considered in some cases.

$$\begin{bmatrix} \Delta Void_1 & \Delta Temp_1 \\ \Delta Void_2 & \Delta Temp_2 \end{bmatrix} \begin{bmatrix} VC \\ DC \end{bmatrix} = \begin{bmatrix} \rho_1 \\ \rho_2 \end{bmatrix} \quad (6.1)$$

A few depletion cycles are necessary for RELAP5 to converge on the correct flow distribution, so the RELAP5 restart file used for the 90% flow calculation was produced by depleting the reactor for a few cycles at 90% flow rate, to give RELAP5 a better starting guess from which to converge on the 90% flow rate thermal-hydraulic solution. Evaluating with the perturbed conditions at a single state-point generally did not significantly change the flow conditions from their converged values.

It is problematic to accurately converge RELAP5 for the perturbation cases. This makes the VC and DC sensitive to how they are evaluated and therefore leads to uncertainty in the calculated values. More consistent values for the DC and VC were achieved by performing the 110% power calculation with the same flow solution as the 100% power case – i.e. without depleting the reactor with the reduced flow case (Table 6.1). In the test case shown in Table 6.1, three perturbations were performed: overpower, flow reduction, and overpower without updating the flow solution. Combining the reactivity results from any two of these perturbations enables the DC and VC to be found using Eq. 6.1. The selected combination of perturbations gives a VC in agreement with one of the other cases and a DC in agreement with the third case.

**Table 6.1.** Calculation of VC and DC for RBWR.

Perturbations	SOC DC (pcm/K)	SOC VC (pcm/% Void)	EOC DC (pcm/K)	EOC VC (pcm/% Void)
<b>Fuel temperature only from 110% overpower; 75% flow</b>	<b>-4.6 pcm</b>	<b>-30.7</b>	<b>-4.3</b>	<b>-12.0</b>
110% overpower; 75% flow	-5.9 pcm	-30.7	-5.2	-12.0
110% overpower; fuel temperature only from 110% overpower	-4.2 pcm	-57.1	-4.3	-26.8

There was some variation in the VC calculation. The VC is sensitive to the radial power distribution, which requires good convergence of RELAP5 to accurately calculate. This is often difficult to achieve. The calculation methodology therefore needs improving, or a large margin needs to be placed on the design to account for uncertainty. In particular, an improved thermal-hydraulic solution (perhaps using a steady-state solution rather than a time-marching approach) would be preferable to reduce uncertainty.

The branch and history cases were again based on the University of Michigan’s models. 6 histories (3 coolant densities with rods in and out) were modelled, and 22 branches were evaluated per burn-up step, including the reference case. This encompassed 5 coolant densities, 3 fuel temperatures and the control rods.

Two short burn-up steps of 60 MWd/t and 440 MWd/t were used to model Xe and Sm build-up, followed by ten 2500 MWd/t steps and subsequently 5000 MWd/t steps. In comparison, 2000

MWd/t steps were used in the assembly analysis. Larger steps were used for the full-core analysis to limit the number of state-points required and therefore the computational cost.

A TRU reload fraction of 26% was selected for the 200 cm high core based on the analysis. The leakage fraction from the fuel region was calculated at ~4.5%, ~1% and 3.5% radially and axially, respectively. To find the achievable discharge burn-up, the cycle length in the full-core analysis was increased until the EOC  $k_{\text{eff}}$  was less than 1. The equilibrium cycle burn-up was ~94 GWd/t, so it is apparent that a large burn-up is neutronically achievable in the RBWR core design considered (Table 6.2). The cycle length is very long resulting in an assembly core residence time of 18.5 years (for the 5-batch assemblies), which may exceed cladding limits. The VC was negative but there was a large uncertainty in its value depending on how it was calculated, so it may be appropriate to introduce a substantial ‘uncertainty margin’ on the maximum allowable VC, and/ or improve the calculation methodology.

**Table 6.2.** 200 cm RBWR core performance.

Discharge burn-up (GWd/t)	EOC $k_{\text{eff}}$	SOC DC (pcm/K)	SOC VC (pcm/% Void)	EOC DC (pcm/K)	EOC VC (pcm/% Void)	Cycle length (years)
~47	1.032	-2.6	-50.4	-4.3	-30.8	1.9
75.5	1.010	-4.6	-30.7	-4.3	-12.0	3.2
90.5	1.009	-3.4	-19.7	-4.8	-10.6	3.5
94.3	1.005	-3.5	-10.3	-3.9	-9.8	3.7
94.3 (different RELAP restart file)		-3.8	-18.0 (-39.4 with all shim rods in)	-4.4	-8.2	3.7
104.9	< 1					4.1

As the burn-up was increased, the radial power profile (Fig. 6.3) flattened, with a peak towards the core peripheral assemblies appearing at high burn-ups. This is a consequence of the RBWR LP, where fuel is moved inwards over the first four batches (Fig. 6.1), with an incomplete fifth batch at the core periphery. The axial power distribution was approximately cosinusoidal as the fuel of the Th-fuelled RBWR is axially homogeneous. There is a slight axial positive skew at the all-rods-out condition due to the slightly negative VC and a significant reflector effect (Fig. 6.4).

The VC shown in Table 6.2 deteriorates at higher burn-up, which may impose a lower TRU reload fraction to comply with the VC requirement. This is consistent with the results of the assembly calculations in Chapter 2. In particular, the assembly-level VC in the high VF history increases

rapidly over the cycle. Better quantification of the uncertainties in the VC calculation is required and could be performed in future work.

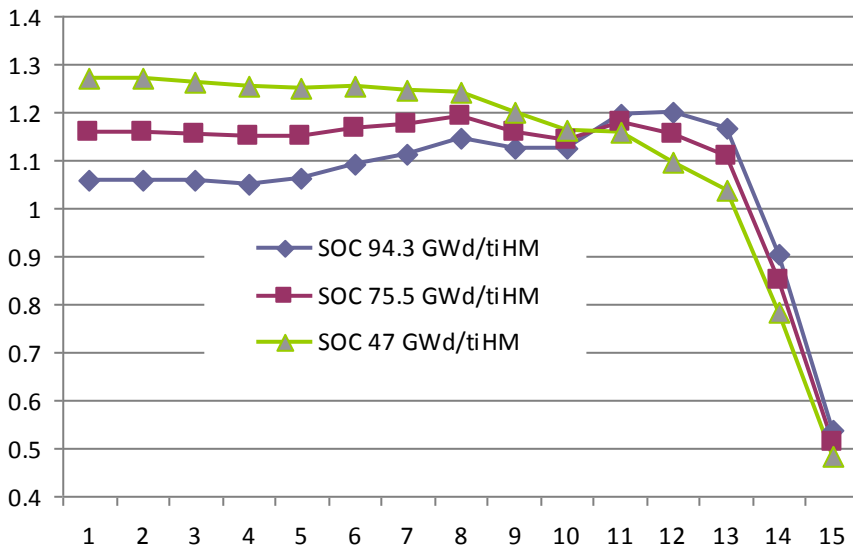


**Fig. 6.3.** Radial power distribution in the 200 cm RBWR core for different discharge burn-ups.

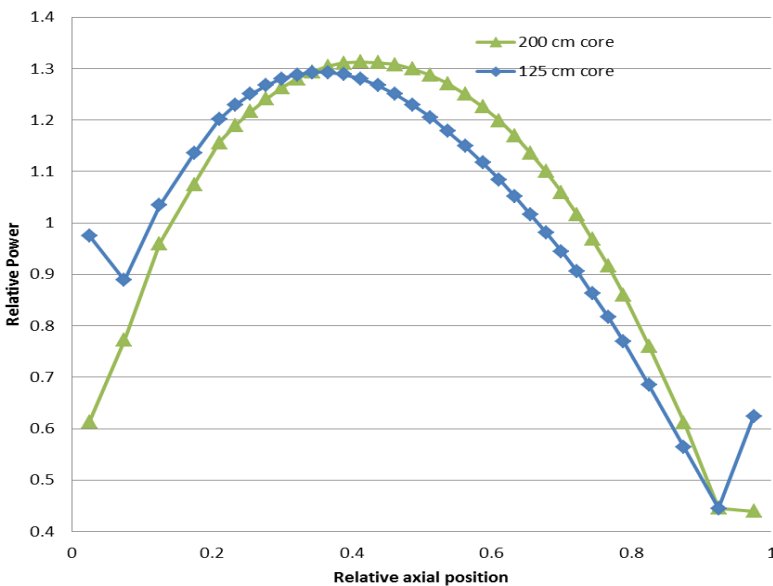


**Fig. 6.4.** Axial power distributions in 125 cm and 200 cm RBWR cores over active fuel length.

The spectrum is too hard to use BPs so mechanical shim is necessary to control the reactor. The shim rod configuration is the same as used by Downar et al. (2012). With all the shim rods in,  $k_{\text{eff}}$  was reduced from 1.021 to 0.997. The shim rods therefore just provide sufficient worth to control the reactor over the cycle, although this may result in unacceptable form factors due to the need for nearly full shim rod insertion at SOC. The CRP used in (Downar et al., 2012) has partial insertion of all the shim rods at SOC, so the number of shim rods being operated simultaneously is the same. The cold shutdown margin (CSDM) may be worse than the U-Pu RBWR due to the more negative

VC. This is investigated in Section 6.5. It may be necessary to increase the number of control rods in the reactor, which can be accomplished by placing rods on all sides of the assembly. This increases moderation slightly, but, as the achievable burn-up is high, this should not greatly affect performance. Similarly to the RMPWR, insertion of the rods improves the VC, but this cannot be credited as a VC mitigating action at EOC since all the rods are extracted.

The decay and refuelling of the EOC discharge isotope vector was modelled, and refuelling was simulated with the appropriate TRU reload fraction. The ‘next’ cycle isotope composition was in very good agreement with the isotope composition in the previous cycle. This indicates that converging the equilibrium isotope vector using a 2D lattice calculation at the core-average VF was a good approximation.

A 30% TRU reload fraction was used with the 125 cm core. The leakage was ~7.4%. The equilibrium cycle burn-up dropped to ~60 GWd/t. The VC was slightly positive at EOC and therefore the design is not feasible with this TRU reload fraction (Table 6.3).

**Table 6.3.** 125 cm RBWR core performance.

Discharge burn-up (GWd/t)	EOC $k_{\text{eff}}$	SOC DC (pcm/K)	SOC VC (pcm/% Void)	EOC DC (pcm/K)	EOC VC (pcm/% Void)	Cycle length (years)
59.5	1.003	-3.5	-18.7	-3.9	+0.1	1.5

The lower burn-up results in a nearly flat radial power profile across the core (Fig. 6.5).

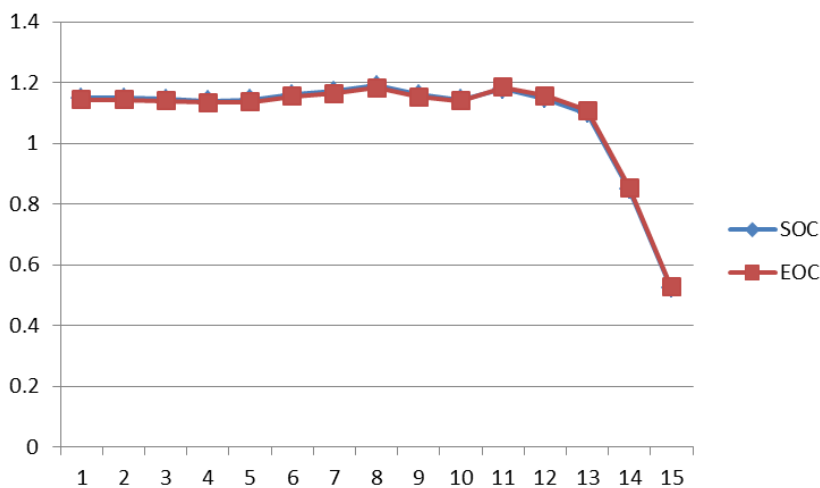


**Fig. 6.5.** Radial power distribution in the 125 cm RBWR core.<sup>28</sup>

The short core has a more bottom-skewed power distribution with rods out compared to the tall core (Fig. 6.4).

<sup>28</sup> Note that in this case, the almost identical power distribution at SOC and EOC is coincidental.

The 125 cm core has lower discharge burn-up than the 200 cm core. The effect of increased leakage outweighs the higher TRU reload fraction. The reactivity swing is low as the fissile inventory ratio is quite close to unity and, as with the RMPWR, due to the significant content of TRU isotopes with even mass-number, which effectively behave as fertile neutron absorbers. This means that the burn-up is sensitive to core leakage. However, while leakage improves the VC, the axial reflector acts to limit this advantage, so the VC of the short core is more positive than predicted by the lattice calculation.

The short core burn-up is consistent with that expected from a 53% VF 2D calculation with 7.4% leakage. From Fig. 2.10, the one-batch burn-up is ~38 GWd/t.

For the 200 cm core with 26% TRU reload fraction, 4.5% leakage, the one-batch burn-up is about 46 GWd/t, so a 4–5-batch burn-up of ~75 GWd/t is expected. The burn-up calculated in the full-core analysis is significantly higher than this. This could be due to the relative influences of the high and low VF regions of the core. The highly voided region has nearly constant  $k_{\infty}$  over the cycle, while the lower voided region burns out relatively fast. The variation in spectrum over the core affects the evolution in power distribution and  $k_{\text{eff}}$  over the cycle, improving the neutron economy such that the cycle is longer than expected. These effects seem to be more significant for the tall, high discharge burn-up core than the short, lower discharge burn-up core. This requires further analysis.

In the high leakage core, the relatively high reactivity top region of the core experiences higher leakage, so might be expected to contribute less to the overall reactivity. This is consistent with the bottom-skewed power distribution of the short core. In the relatively low leakage core, the higher reactivity of the highly voided region may have a more significant beneficial influence on the overall neutron balance.

In conclusion, a tall core appears more appropriate for the homogeneous RBWR design, although the high full-core burn-up requires further scrutiny.

The MCPR of this design was evaluated using Liu's correlation for RBWRs (Liu et al., 2007), assuming careful enrichment balancing limits the local peaking factor in the assembly to 1.05 (as in current RBWR designs). Based on the results in Fig. 6.5, a radial power peaking factor of ~1.2 is used, which is similar to existing RBWR designs. The core mass flow of the reference design is 7222 kg/s, which corresponds to an average mass flux of 842 kg/m<sup>2</sup>/s. It may be possible and desirable to reduce this for the tall RBWR to reduce the pressure drop, but in general the pressure drop is low for the RBWR core as it is short (Ishikawa and Okubo, 2009). Using the calculated axial power distributions, the MCPR for the short and tall cores is 1.48 and 1.76 respectively. These large

thermal-hydraulic margins are expected from the homogeneous core configuration, and compare favourably with the U-Pu RBWR MCPR and are higher than the minimum acceptable 1.32 (Liu et al., 2008). It is worth noting that the core considered here has 720 assemblies (as with the Hitachi RBWR), compared to 900 for the JAEA RMWR in (Liu et al., 2008). However, the JAEA assembly design is utilized. Therefore the core power per unit area is higher than in the JAEA design. The core area of the 720 assembly design considered here is ~50% larger than the ABWR.

If the number of fuel assemblies in the 200 cm core is reduced to 480, then the core area is approximately the same as the ABWR. If the average mass flux is at least  $998 \text{ kg/m}^2/\text{s}$ , corresponding to a core mass flow of 5613 kg/s, then the MCPR is at least 1.32 for the assembly design considered.<sup>29</sup> The core-average VF is slightly increased due to the lower core mass flow (hence allowing an acceptably hard spectrum to be maintained), and although the core pressure drop is expected to be higher than for a shorter core, as discussed, the relatively low pressure drop of RBWRs means this is unlikely to be a problem. Therefore, for a ‘tall’ core, the MCPR can be satisfied without requiring an increase in core area relative to an unmodified ABWR. This also reduces the core residence time by 1/3. Retrofit of an existing ABWR still appears unlikely as the assembly design, and in particular the control rod positions, are very different to an existing ABWR.

If necessary, the core height can potentially be increased above 200 cm in order to satisfy the MCPR constraint. Gorman et al. (2014) considered a Th-RBWR breeder design with a 380 cm core height.

## **6.2. Radially Heterogeneous Fuel in RBWRs**

The TCUP fuel assembly is also an effective design for RBWRs. It is sensible to place the Th-TRU pins at the centre of the assembly, with the Th-U3 pins at the periphery near the bypass channels. Placing Th-TRU and Th-U3 in different assemblies is also possible, but results in Th-TRU pins next to the bypass channel, which thermalizes them and reduces the control rod worth, so this design is not pursued. Utilizing variable residence time for the Th-TRU and Th-U3 pins is not appropriate because the burn-up is clad limited, so it makes sense to achieve as uniform a burn-up as possible. The design is shown in Fig. 6.6. The proportion of Th-U3 pins is larger than for the RMPWR TCUP assembly due to the lower TRU and higher U3 populations in the RBWR.

---

<sup>29</sup> This conclusion is consistent with the work of Shaposhnik et al. (2013; 2014), which considered a RBWR breeder core of the same area as an ABWR. With a 200 cm seed region height, a core de-rating was necessary if a core exit VF above 90% was required (leading to a much higher core exit quality than that considered here). However, it was possible to ensure that the core did not need to be de-rated if the flow rate was increased above the reference value.

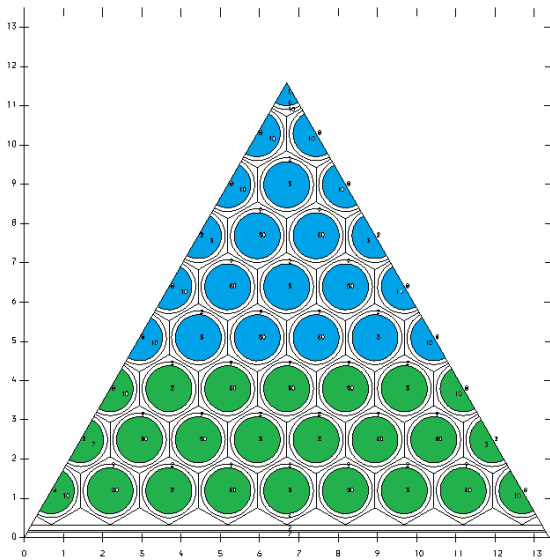


**Fig. 6.6.** RBWR TCUP assembly with 91 Th-TRU pins (blue) and 126 Th-U3 pins (green) per assembly.

This design improves the neutron economy and the MTC, such that a single-assembly analysis indicates that a TRU reload fraction of more than 35% is possible, compared to 26% for the 200 cm homogeneous fuel core. With 35% TRU reload fraction, the VC at 53% VF is negative without leakage (Fig. 6.7). The equilibrium fuel isotope vector is presented and discussed in Chapter 7.

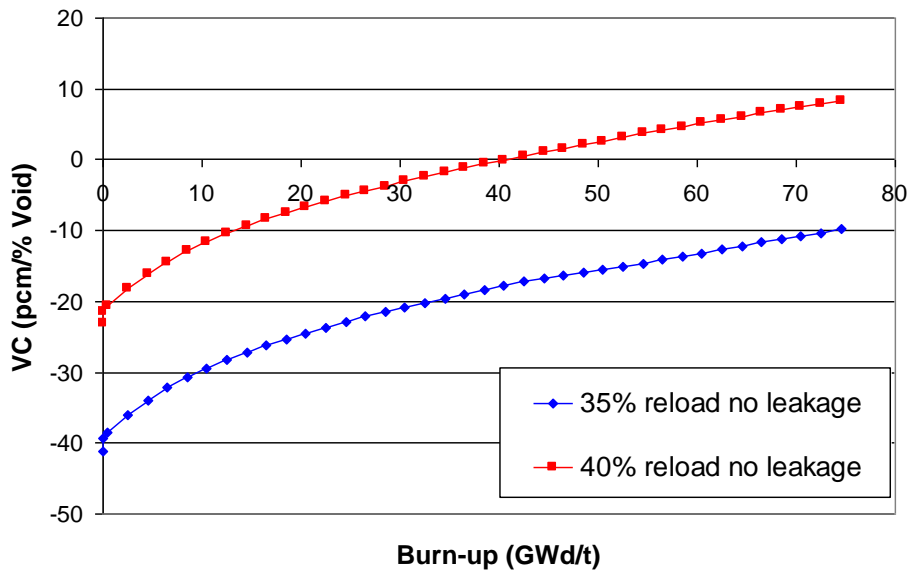


**Fig. 6.7.** Void coefficient for single assembly average VF model of RBWR TCUP assembly.

However, at higher VFs, the VC gets worse as the thermal flux is reduced, such that fast fission effects dominate. For the TCUP assembly, this worsening is greater than for a homogeneous assembly, as the beneficial flux differences between Th-TRU and Th-U3 regions become less. This makes the full-core VC worse than would be expected from a 2D average VF analysis. Still, a significant improvement appears possible over homogeneous fuel.

This effect is shown in Fig. 6.8, where the VC from 95% to 100% voiding is shown for the 26% TRU reload homogeneous fuel and for the 35% TRU reload TCUP fuel. At average VF, the 35% TRU reload TCUP fuel has a significantly lower VF than the homogeneous fuel (Fig. 2.10, Fig. 6.7), but the reverse is true at 95% VF.

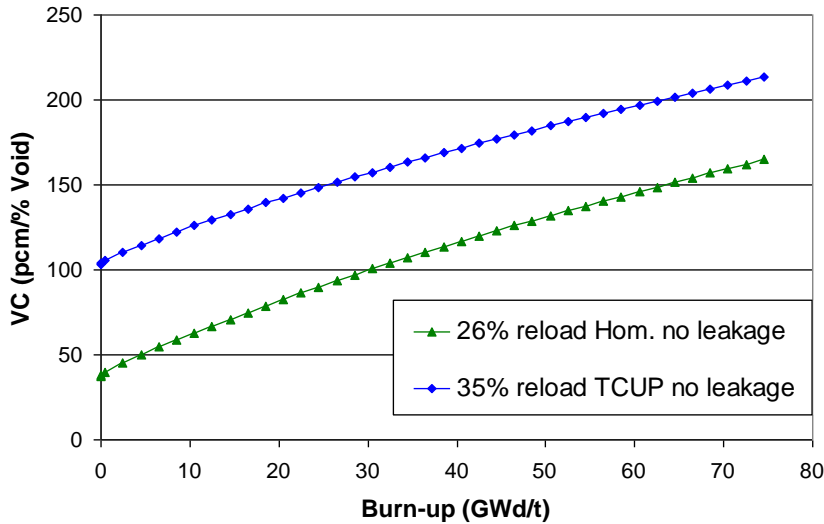


**Fig. 6.8.** VC for 95% to 100% voiding for homogeneous (Hom.) and TCUP assemblies at typical TRU reload fractions.

The TCUP assembly with 35% TRU reload fraction allows a critical cycle to be maintained for a very high cycle length. This is shown in Fig. 6.9 – at a single assembly burn-up of 75 GWd/t,  $k_{\infty}$  is  $\sim 1.05$ , c.f. leakage of  $\sim 4.5\%$  for a 200 cm core. From the linear reactivity model, an average discharge burn-up of  $>120$  GWd/t appears possible.

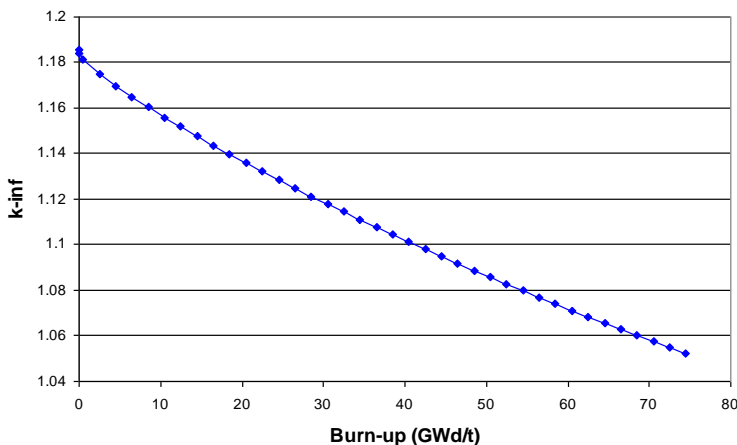


**Fig. 6.9.** Variation of  $k_{\infty}$  with burn-up for TCUP assembly with 35% TRU reload fraction.

A full-core analysis with PARCS-RELAP5 indicates that core criticality can indeed be maintained up to  $\sim 154$  GWd/t. The VC is negative for a discharge burn-up of up to  $\sim 118$  GWd/t (Table 6.4), with the VC becoming positive at higher average discharge burn-ups. For average discharge burn-

ups less than 154 GWd/t, there is excess reactivity at EOC. The obvious means to reduce this is to reduce the core height, hence increasing the neutron leakage. This also makes the VC more negative, hence, for the 118 GWd/t case, the margin by which the VC is negative will be increased. However, reducing the core height makes the MCPR worse, which probably results in a larger core area being required. An alternative is to slightly increase the moderation in the fuel assembly.

**Table 6.4.** Core performance with TCUP fuel assembly with 35% TRU reload fraction, 200 cm core height.

Core-average discharge burn-up (GWd/t)	118	154
Cycle length (yr)	4.6	6.1
Reactivity swing (pcm)	3171	3621
SOC VC (pcm/% Void)	-4.5	21.7
EOC VC (pcm/% Void)	-1.9	99.9
SOC DC (pcm/K)	-4.5	-3.9
EOC DC (pcm/K)	-3.0	-5.4

Again, it must also be emphasized that this high discharge burn-up is not achievable with current cladding technology and will also exceed fuel performance limits. The core residence time is also a concern. This can be limited by increasing the power density – either by reducing the core height or the number of assemblies. Limiting the discharge burn-up to 80 GWd/t and reducing the number of assemblies to 480 would reduce the cycle length to ~2 years.

The high burn-up of these cycles results in larger reactivity swing over the cycle, which in turn results in unacceptably high power peaking in the fresh fuel assemblies. Modifying the LP may improve this. The axial and radial power peaking are also shown in Fig. 6.10. The negatively skewed power distribution of the 154 GWd/t case is due to the strongly positive VC. These factors also resulted in difficulties in converging on the equilibrium cycle with PARCS-RELAP5.

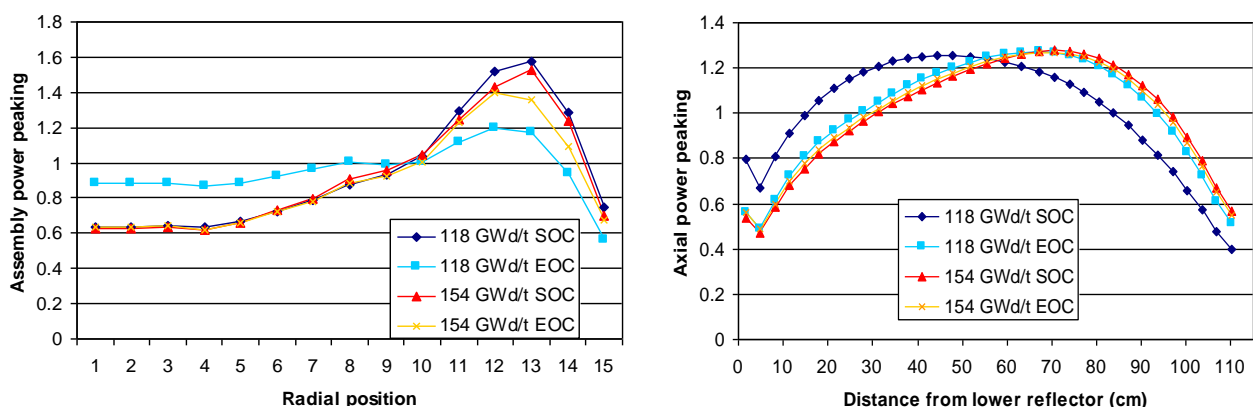


**Fig. 6.10.** Radial (left) and axial (right) power peaking with TCUP fuel, 200 cm core height.

### 6.3. Implementation of a Multi-tier Fuel Cycle in RBWRs

With a suitably optimized fuel LP, the neutronic performance of the 200 cm TCUP RBWR appears likely to be excellent. However, the high burn-up is not achievable with current clad technology. To reduce the burn-up without overly compromising the fuel cycle performance, a multi-tier fuel cycle is implemented. Here, a ‘short’ core height of 115 cm with 720 assemblies is considered. The waste reload fraction (TRU + U3 in the multi-tier feed) is kept constant at 35%. The TCUP assembly for this fuel has 85 Th-TRU pins and 126 Th-U3 pins.

Th-Pu discharge burn-ups of 50 GWd/t and 84 GWd/t are considered for the first tier, leading to different fuel isotope vectors and different performances. The performance is summarized in Table 6.5. The cycle length in both cases is reduced to an attractive value; the reactivity swing and the core-average discharge burn-up are also reduced, although the latter still pushes the limits achievable with Zircaloy cladding technology (noting that the peak discharge burn-up may be higher as a result of the non-integer batch strategy).

**Table 6.5.** Core performance with multi-tier TCUP fuel, 115 cm core height.

	Case 1	Case 2
Th-Pu discharge burn-up in PWR (first tier) (GWd/t)	50	84
Cycle length (yr)	1.86	1.57
Reactivity swing (pcm)	2241	1785
Average discharge burn-up (GWd/t)	82.4	69.6
Waste incineration rate (kg/GWthyr)	135	135

The assembly power peaking is reduced to around 1.24, similar to the Hitachi design (Downar et al., 2012), and the axial power peaking is around 1.2 (Fig. 6.11).

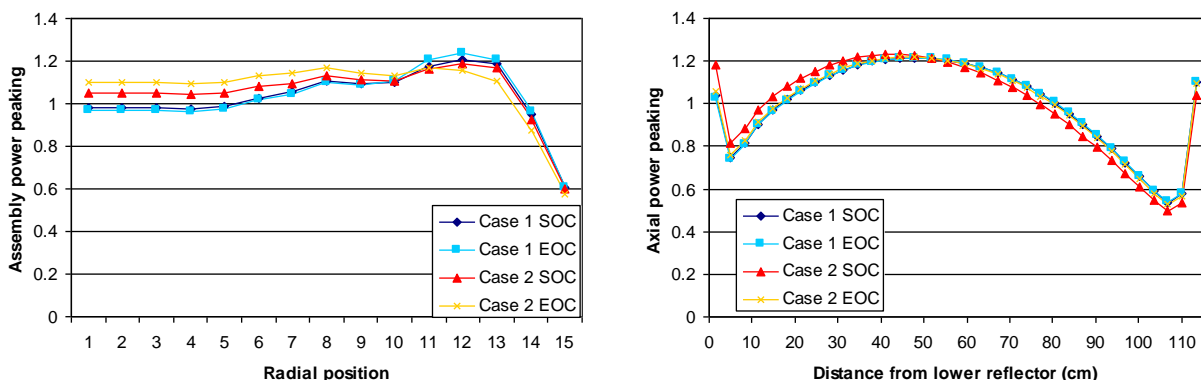


**Fig. 6.11.** Radial (left) and axial (right) power peaking with multi-tier TCUP fuel, 115 cm core height.

With assembly power peaking of 1.2 and pin-level power peaking of 1.05 (as in current RBWR designs), the MCPR is 1.43. However, power swings between Th-U3 and Th-TRU are likely to

increase the radial form factor of the assembly and thereby reduce the MCPR. Therefore, it will be difficult or impossible to achieve such a low value for power peaking with radial heterogeneity. Careful fissile proportion selection is likely to be necessary across the assembly. An MCPR of 1.32, the minimum acceptable with active core cooling (Liu et al., 2008), can be achieved for a maximum assembly-level power peaking of 1.14. Further analysis is required to determine if this is feasible, but it appears a reasonable design goal. Designing for a 480 assembly core would require an increased core height (which would make the VC worse), and, as discussed, the core flow rate would also need to be increased.

An unexpectedly low magnitude value was found for the DC in some cases. This appears concerning, but it is not thought to be physical as single-assembly analysis verifies that the DC is substantially negative across a range of VFs for this fuel type. It is possible that the core reactivity is sensitive to the convergence of RELAP5 such that consistent values for the VC and DC cannot be obtained. The value of the VC was found to vary significantly depending on initial conditions for the convergence of RELAP5 but in all cases was substantially negative. The DC is also sensitive to the overpower condition used in the perturbation calculations.

The VC and DC are given in Table 6.6. The isothermal FVR is also given: this is calculated for a core filled with steam with a fuel at a uniform temperature equal to the average temperature of the fuel at power conditions. This is just negative over the cycle.

For Case 1, lattice calculations for the SOC fuel composition with VFs of 0%, 45% and 80% give DCs of -3.3, -3.3 and -2.7 pcm/K respectively.

**Table 6.6.** VC and DC for multi-tier TCUP fuel, 115 cm core height.

	Case 1		Case 2	
	SOC	EOC	SOC	EOC
<b>VC (pcm/% Void)</b>	-93.5	-17.8	-131.1**	-73.6
<b>DC (pcm/K)</b>	-3.1	-1.4*	-4.0**	-3.6
<b>Isothermal FVR</b>	-0.0111	-0.0013	-0.0106	-0.0008

\* -2.7 pcm/K with 104.5% overpower condition

\*\* Values of (-98.7 pcm/% Void, -1.7 pcm/K) and (-91.2 pcm/% Void, -4.7 pcm/K) calculated with slightly different RELAP5 initial conditions used for converging solution for perturbation calculations

### 6.3.1. Sensitivity to TRU Feed

A 2D equilibrium VF analysis indicates that  $k_{\infty}$  with a 20-year TRU cooling time following UO<sub>2</sub> discharge is 1000–2000 pcm lower than for a 10-year cooling time (Fig. 6.12). The RBWR

equilibrium cycle average discharge burn-up is estimated to drop by 9% from 82.4 GWd/t to 75.0 GWd/t based on single-assembly calculations using the linear reactivity model. This affects the fuel cycle performance but not the fuel cycle feasibility. The single-assembly VC is very slightly higher (Fig. 6.12). However, the core-average discharge burn-up will be lower, which will act to reduce the VC, such that overall feasibility will be maintained.

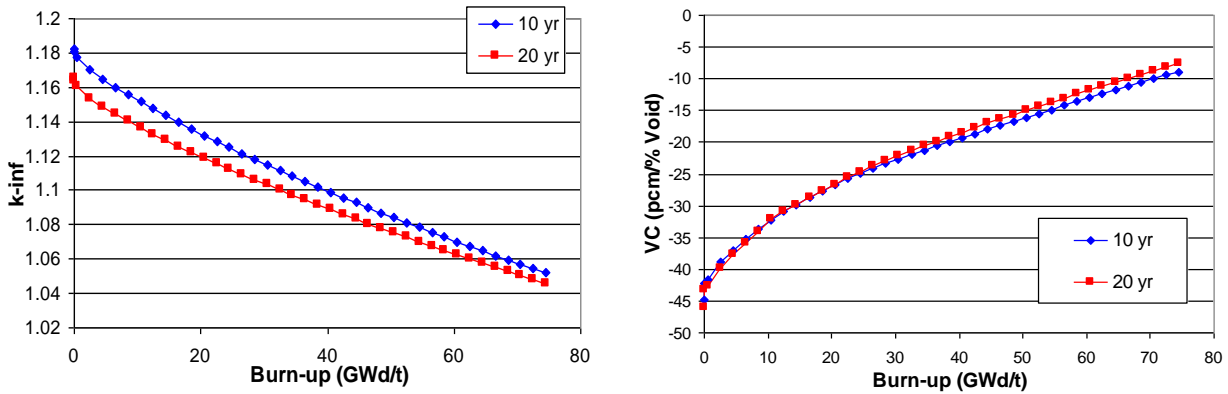


**Fig. 6.12.** Single assembly  $k_{\infty}$  (left) and VC (right) for RBWR with TRU vector generated using different cooling times.

#### 6.4. Variable Pin Diameter Fuel

An alternative method of increasing the incineration rate of the RBWR is to soften the neutron spectrum by increasing the H/HM ratio. The simplest way is to reduce the pin diameter while keeping the lattice pitch constant. This results in a lower discharge burn-up being achievable while satisfying the constraint that the VC must be negative. However, as the performance is most sensitive to achieving a hard neutron spectrum in the Th-TRU, one option is to preferentially harden the neutron spectrum in the Th-TRU using a variable pin diameter. The pin diameter of the Th-U3 pins is reduced to 9.5 mm (Fig. 6.13). This results in approximately double the H/HM ratio relative to the reference assembly design (but still only ~27% that of a conventional PWR). A multi-tier fuel cycle with 50 GWd/t burn-up in the first pass was implemented.

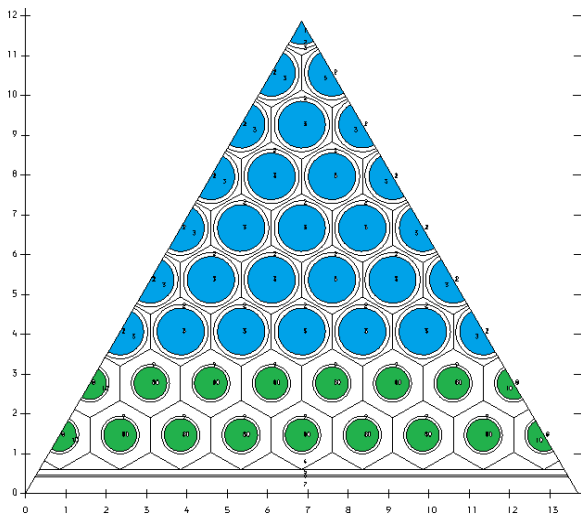


**Fig. 6.13.** Variable pin diameter assembly design with 127 Th-TRU (blue) pins and 90 Th-U3 (green) pins.

By selecting the number of Th-U3 pins appropriately, it is possible to limit the power peaking in the assembly. As the Th-U3 pins are smaller, this leads to a higher burn-up rate in these pins. As the burn-up is clad-limited, it is sensible to utilize a seed-blanket-unit approach and pass the Th-TRU pins through the core twice as many times as the Th-U3 pins to achieve a roughly uniform burn-up. The Th-TRU reactivity is approximately constant with burn-up, as U3 is bred and  $^{241}\text{Am}$  and even isotopes of Pu are burned over the cycle, which compensate for the depletion of fissile Pu and accumulation of fission products. Assemblies with fresh Th-U3 and Th-TRU are shuffled according to the batch strategy in Fig. 6.1. The burned Th-U3 pins are replaced, and a further 4–5 passes are performed, with fresh Th-U3 assemblies being batch 1 (from Fig. 6.1), but having 4 or 5 times burned Th-TRU, and so on. The Th-TRU therefore resides in the core for 8–10 batches. As discussed in Chapter 5, separating the assembly in this manner is expected to be feasible.

Use of variable nozzle sizes and/or grid spacer design for variable loss coefficient within the assembly can compensate for linear heat rating and pin diameter variations across the assembly (Lindley et al., 2013c), although a more detailed thermal-hydraulic analysis is necessary to determine feasibility.

The reactor core was modelled as before. The core flow rate was increased from 7222 kg/s to 8000 kg/s to maintain a similar core-average VF to before. A core height of 120 cm was appropriate for the selected TRU reload fraction and equilibrium cycle burn-up. The performance is summarised in Table 6.7.

**Table 6.7.** Performance of variable fuel pin diameter design.

<b>Waste loading fraction in feed</b>	52.7%
<b>Waste incineration rate</b>	202 kg/GW <sub>th</sub> yr
<b>Assembly-average burn-up/pass</b>	40.0 GWd/t
<b>Average Th-U3 discharge burn-up</b>	75.3 GWd/t
<b>Average Th-TRU discharge burn-up</b>	54.8 GWd/t
<b>Average discharge burn-up</b>	63.1 GWd/t
<b>Cycle length</b>	259 days
<b>Reactivity swing over cycle</b>	1805 pcm

By comparison with the RMPWR analysis (see Chapters 2, 5 & 7), the waste loading fraction, and therefore the waste incineration rate, is significantly larger than could be expected by a uniform reduction in pin diameter. However, the average discharge burn-up is somewhat lower than in Section 6.3, and given the complexity of the design, implementation may not be worthwhile.

The selected core configuration only achieves a cycle length of 9 months. This is likely to be unacceptably low, implying that a taller core with lower power density is necessary to achieve a minimum 12 month cycle. A single-tier fuel cycle is also likely to allow a longer cycle length. The radial and axial power peaking were both ~1.2.

Reliable values for the VC and DC were not found: using Eq. 6.1 a substantially negative VC was calculated but low (and in some cases positive) values for the DC were calculated, with variation depending on how RELAP5 was converged. Lattice calculations with fresh fuel and 0%, 53% and 95% VF give a DC of -2.5, -2.9 and -2.1 pcm/K respectively. The inconsistent values for the DC and VC are a cause for concern and reduce confidence in the analysis. This implies that there are problems with the methodology described in Section 6.1 for solving for the VC and DC based on perturbing the power and the flow, for example due to different values of the VC for different flow perturbations. It is also clear that convergence of RELAP5 is a problem – lack of convergence to an accurate solution to the flow under perturbed conditions leads to inaccurate values for the VC and DC. This is in part due to the time-marching solution in RELAP5, In future it is therefore recommended that statepoint or quasi-static calculations are carried out using a steady state thermal-hydraulic code instead of a time-marching code.

Due to the inaccurate values of VC and DC in this case, the change in reactivity with overpower and reduced-flow is instead presented in Table 6.8 for two different evaluations with different RELAP5 solutions. The different evaluations results in differences of around 3 pcm/% overpower and 3 pcm/% flow rate. The matrix solution method for calculating the VC and DC given in Equation 6.1 can exacerbate these uncertainties and lead to calculation of a positive DC, which is

unphysical. The overpower coefficient is around zero and may indeed be slightly positive, which indicates that the TRU loading may need to be reduced slightly. In general, if the fuel and coolant reactivity coefficients cannot be evaluated accurately, a significant margin for error is required.

**Table 6.8.** Overpower and reduced flow coefficients for variable pin diameter design.

	Evaluation 1		Evaluation 2	
	SOC	EOC	SOC	EOC
<b>Overpower (pcm/% overpower)</b>	-15.5	+1.2	-13.3	-2.0
<b>Flow rate (pcm/ % flow rate)</b>	-19.2	-13.1	-21.8	-10.2

### 6.5. Cold Shutdown Margin

For a Th-RBWR breeder, it can be difficult to achieve an adequate CSDM due to the high VF at operating conditions (Ganda et al., 2011; Shaposhnik et al., 2013; 2014). A Th-RBWR burner (i.e. a Th-fuelled RBWR which is loaded with and incinerates TRU) has substantially less negative VC, which makes it easier to meet this constraint. However, if the CSDM is insufficient, it is possible to increase the size and number of the control rods. This results in a softer neutron spectrum due to larger bypass channels, which will reduce the achievable discharge burn-up.

A hot zero power PARCS calculation was performed for Case 1 in Section 6.3. One control rod was assumed per 3 assemblies, i.e. control blades in all available positions with asymmetric control rods. The cold zero power reactivity was then calculated by finding the reactivity from hot zero power to cold zero power for a single rodded assembly. The results are given in Table 6.9. In future, the effect of  $^{233}\text{Pa}$  decay into  $^{233}\text{U}$  also needs to be taken into account.

**Table 6.9.** CSDM analysis.

Hot zero power reactivity (PARCS), all rods in except central stuck rod	-5450
Single assembly rodded reactivity from hot zero power to cold zero power	1904
$^{135}\text{Xe}$ worth from single assembly calculation	64
Total control rod worth, calculated for single assembly at cold zero power	16519
Reduction in control rod worth for uncertainties and control rod depletion	3303
<b>CDSM (pcm)</b>	<b>-178</b>

The CSDM is substantially negative before allowing for uncertainties and depletion of the  $^{10}\text{B}$  in the control rods. Approximately 10% of the rods are inserted on average throughout the cycle and the rods lose ~5% of their worth when burned to 20 GWd/t which is similar to the cycle burn-up. Therefore if the rods are replaced every ~10 years then a ~5% reduction in rod worth needs to be accounted for. Allowing a 10% reduction for control rod depletion, and ~10% for uncertainties, the rod worth is reduced such that the CSDM is insufficient, relative to a design criterion of -1000 pcm

(Fennern, 2007) and also substantially lower than the value of  $\sim -2000$  pcm in ABWRs (Ito et al., 1998). However, as only a small increase in control rod worth is necessary, making the control rods slightly wider or placing control blades to completely surround assemblies will allow a satisfactory CSDM, or comparable worth to that in conventional ABWRs to be achieved. Alternatively, the control rods can be replaced more frequently.

The reprocessing requirements for full recycle can be evaluated as the product of waste incineration rate and discharge burn-up (see Chapter 7 for a full discussion). This is comparable for designs with uniform pin diameter and reduced pin diameter in the Th-U3 pins. Increasing the size of the bypass channel has a similar effect on the spectrum as reducing the Th-U3 pin diameter. A larger bypass channel allows larger control rods to be used, introducing additional control rod worth. Therefore, it appears that larger control blades will not significantly affect reprocessing requirements. This leads to confidence that the CSDM constraint can be met without adverse consequences.

## **6.6. Preliminary Assessment of Axially Heterogeneous Fuel**

While axially homogeneous fuel is highly desirable to reduce fuel fabrication costs, it is worthwhile to evaluate the performance of axially heterogeneous fuel for comparison purposes. For example, if a superior waste incineration rate can be achieved with axially heterogeneous fuel, this could reduce reprocessing and fuel fabrication throughput and may offset the unit cost increase. Some performance increase is expected from axially heterogeneous fuel as this is employed in U-Pu RBWR burner designs. It is also worth noting that remote fabrication of fuel with external axial blankets is much less difficult than remote fabrication of fuel with internal axial blankets. Axially heterogeneous fuel design requires 3D lattice calculations.

The Monte Carlo code Serpent (Leppänen, 2007) with the ENDF/B7 data library was used to perform axially heterogeneous calculations. A single pincell was modelled to reduce computational requirements. The best estimate model in (Shirvan et al., 2013), based on the model developed by Liao *et al.*, was used to calculate the void distribution, with a representative power distribution in the pincell. 7 cm and 30 cm upper and lower reflectors were modelled. These differences in lattice calculation methodology and thermal-hydraulics mean that a consistent basis of comparison is not possible with the axially homogeneous lattice and core studies. Therefore, homogeneous fuel is also analysed in the same way to provide a consistent reference case.

To speed up the calculations, convergence to equilibrium was performed with a coarse axial structure of 5–7 regions, and statistical error of 25 pcm. 30% and 35% TRU reload fractions were used, 30% being similar to that feasible with homogeneous fuel for a short core, and 35% being the best case with radially heterogeneous fuel. Detailed analysis of equilibrium cycles was performed with 25 axial regions and statistical error of 14 pcm. Due to large changes in the axial power profile

over the cycle, the equilibrium isotope vector is highly burn-up dependent, and the refined nodalization of the equilibrium cycle also affects the results. Therefore, while the isotope vectors were close to equilibrium, the TRU incineration rates differ slightly between cases of the same TRU reload fraction. The incineration rate of the equilibrium cycle is used in the ensuing analysis. The TRU incineration rate is used rather than the TRU+U3 incineration rate as TRU is generally limiting to the FVR and the net U3 incineration is close to zero. Based on the conclusions of Section 6.3, a multi-tier fuel cycle scheme was selected.

A negative FVR was used as the measure of moderator feedback coefficient. This is generally a stronger constraint than a VC based on partial voiding, overpower or reduced flow rate, and it is quicker to calculate accurately with a stochastic code. Accurate determination of the VC generally requires a full-core analysis.

This analysis is not a thorough treatment of all possible axially heterogeneous fuel forms. The objective is to quantify the potential performance advantage from axially heterogeneous fuel designs only. Should axially heterogeneous fuel designs be pursued, full-core analysis with cross-sections produced from 3D lattice calculation is necessary, the methodology for which is under development (Hall et al., 2013; 2014).

#### **6.6.1. Fuel Forms Considered**

The axially heterogeneous fuel designs for burners are shown in Fig. 6.14. The typically considered heterogeneous RBWR design has external and internal blankets of fertile fuel (Fig. 6.14b). These promote breeding, while the internal blanket should also encourage neutron leakage and therefore allow the waste reload fraction to be increased. In the U-Pu RBWR, these may help maintain the balance between feasible cycle length and incineration rate. In the Th-fuelled RBWR, the  $^{232}\text{Th}$  blankets will increase the reactor's  $^{233}\text{U}$  inventory, which does not make the VC much worse, but may still impact waste incineration rate. Improving the reactor's neutron economy may not seem worthwhile given the high achievable burn-ups with homogeneous fuel, but improved neutron economy allows a high leakage design with reasonable cycle lengths, which is advantageous. It is also worth noting that the impact of the reflector in the RBWR is large and difficult to model accurately. Axial blankets may help reduce these uncertainties.

It is also worth considering designs with spatial separation of U3 and TRU. This has been shown to be advantageous at the assembly level. A variant on the radially heterogeneous assembly is axially heterogeneous fuel with similar region size (Fig. 6.14e).

Macro-heterogeneous fuel design is also worth considering here. Fig. 6.14c shows a design with Th-TRU at the top of the core and Th-U3 at the bottom. There are two possible motivations here:

(1) movement of the active core over life between the fast-burning Th-U3 region and the slow-burning Th-TRU region to improve discharge burn-up; (2) placement of the Th-TRU in the highly voided, hard spectrum region at the top of the core.

An alternative design with high axial leakage is shown in Fig. 6.14d. This places the TRU at the top and bottom of the core in thin, highly concentrated zones with a large central Th-U3 zone. The objectives of this design are to harden the neutron spectrum in the TRU-bearing regions and promote axial leakage from TRU in case of voiding. For Case (d) only, borated upper and lower reflectors were used, to increase leakage, as in some U-Pu RBWR designs (Downar et al., 2012).

A core height of 105 cm was selected, as a short core is appropriate for designs which seek to maximize the incineration rate and it was assumed that a good neutron economy and low assembly power peaking would be possible with axially heterogeneous designs.

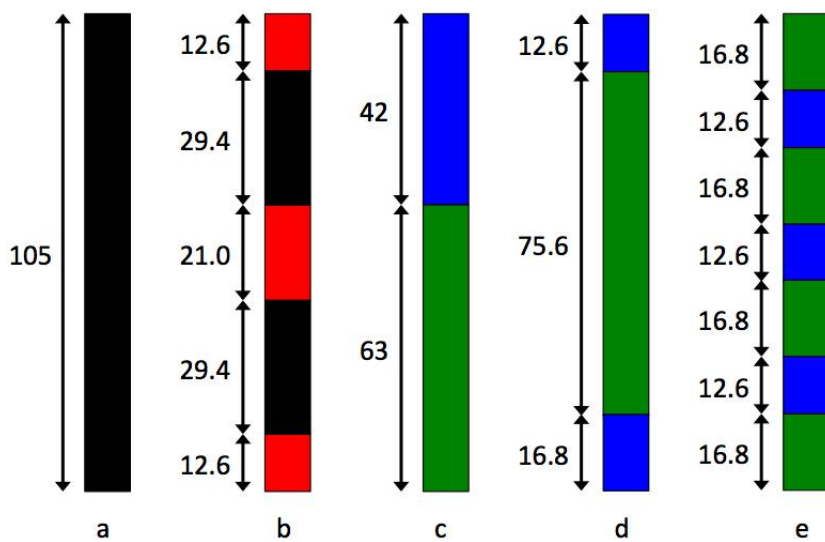


**Fig. 6.14.** Fuel designs considered in Serpent (black = Th-U3-TRU, red = Th, green = Th-U3, blue = Th-TRU): (a) axially homogeneous; (b) internal and external blankets with Th-U3-TRU seed regions; (c) axially macro-heterogeneous with Th-U3 at bottom and Th-TRU at top; (d) Th-TRU at top and bottom with Th-U3 in centre; (e) alternating layers of Th-U3 and Th-TRU.

### 6.6.2. Results and Discussion

The main parameter of interest is the TRU incineration rate (the burn-up is likely limited by clad and fuel constraints), so the actual length of the equilibrium cycle is a secondary concern. The selected core height is low, such that the thermal-hydraulic constraints may be active or violated. This corresponds to a core design which seeks to maximize TRU incineration rate over discharge burn-up.

The near-equilibrium fuel compositions averaged over the whole pin are given in Table 6.10. For the near equilibrium cycle, there is a slight increase of 0–3% in U3 population, except for Design (c) where there is a decrease of 0–3%.

**Table 6.10.** Near-equilibrium fuel compositions used for equilibrium cycle analysis.

	Design (a)		Design (b)		Design (c)		Design (d)		Design (e)	
	30%	35%	30%	35%	30%	35%	30%	35%	30%	35%
<sup>241</sup> Am	0.97	1.18	0.79	1.00	1.70	1.76	2.60	2.85	1.23	1.46
<sup>242m</sup> Am	0.04	0.04	0.03	0.04	0.07	0.07	0.09	0.10	0.06	0.07
<sup>243</sup> Am	0.67	0.81	0.58	0.71	1.00	1.08	1.28	1.44	0.77	0.88
<sup>243</sup> Cm	0.00	0.00	0.00	0.00	0.00	0.00	0.00	0.00	0.00	0.00
<sup>244</sup> Cm	0.37	0.45	0.37	0.45	0.37	0.45	0.34	0.41	0.39	0.42
<sup>245</sup> Cm	0.15	0.17	0.13	0.16	0.11	0.13	0.11	0.12	0.13	0.14
<sup>246</sup> Cm	0.08	0.10	0.07	0.08	0.06	0.07	0.06	0.06	0.09	0.08
<sup>247</sup> Cm	0.01	0.02	0.01	0.01	0.01	0.01	0.01	0.01	0.02	0.01
<sup>248</sup> Cm	0.01	0.01	0.01	0.01	0.01	0.01	0.01	0.01	0.01	0.01
<sup>237</sup> Np	0.52	0.62	0.46	0.56	0.99	0.97	1.65	1.68	0.64	0.75
<sup>238</sup> Pu	1.26	1.45	0.96	1.11	1.80	1.84	2.52	2.70	1.51	1.70
<sup>239</sup> Pu	0.91	1.16	0.87	1.12	1.48	1.63	2.10	2.38	1.19	1.40
<sup>240</sup> Pu	2.81	3.49	2.55	3.24	5.74	5.98	8.09	8.90	4.51	5.23
<sup>241</sup> Pu	0.59	0.74	0.57	0.74	0.62	0.76	0.66	0.82	0.60	0.68
<sup>242</sup> Pu	1.70	2.08	1.49	1.84	2.84	3.02	3.87	4.28	2.33	2.63
<sup>232</sup> Th	78.01	75.51	81.17	78.88	73.40	71.82	66.47	63.85	76.27	74.01
<sup>233</sup> U	6.90	7.03	5.86	5.97	5.18	5.58	5.09	5.20	5.62	5.63
<sup>234</sup> U	3.37	3.46	2.74	2.76	3.09	3.24	3.38	3.47	3.14	3.32
<sup>235</sup> U	0.85	0.87	0.66	0.66	0.71	0.74	0.79	0.80	0.72	0.75
<sup>236</sup> U	0.78	0.81	0.66	0.66	0.81	0.84	0.88	0.91	0.78	0.84

The cycles are analysed using the non-linear reactivity model, assuming 4 batches. The EOC  $k_{\text{eff}}$  generally needs to be at least 1.01 for a feasible cycle (to account for ~1% radial leakage), but the same cycle length is assumed in each case for a consistent comparison. Table 6.11 gives the performance of each design. First, a discharge burn-up is assumed. Then the non-linear reactivity model is applied to calculate the EOC  $k_{\text{eff}}$  (including axial leakage but not radial leakage) and FVR for the two different TRU incineration rates. As the FVR becomes more positive with TRU

incineration rate, the maximum TRU incineration rate is that at which the FVR is zero. This is estimated by interpolating the results at the two different TRU incineration rates.

**Table 6.11.** Performance of axially heterogeneous fuel designs.

Discharge burn-up	Max TRU incineration rate (kg/Gwthyr)		EOC $k_{\text{eff}}$ at this incineration rate	
	60 GWd/t	80 GWd/t	60 GWd/t	80 GWd/t
<b>Design (a)</b>	117	111	1.017	0.998
<b>Design (b)</b>	119	117	1.051	1.038
<b>Design (c)</b>	115	109	1.061	0.998
<b>Design (d)</b>	126	120	0.998	0.977
<b>Design (e)</b>	143	133	1.020	1.004

For a discharge burn-up of 60 GWd/t, Design (a) has an incineration rate of 117 kg/GWthyr, which is almost identical to the result in Section 6.1 obtained by a full-core WIMS/PARCS-RELAP5 analysis. The radial leakage is generally slightly less than 1.7%, so Serpent predicts a slightly longer cycle length, and the core height is shorter (so we would expect a slightly higher incineration rate and lower  $k_{\text{eff}}$ ), but the results are broadly in agreement.

Similarly, Design (e) has a maximum incineration rate of ~133 kg/GWthyr for a discharge burn-up of 80 GWd/t which is almost identical to the TCUP fuel assembly design in Section 6.3. In this case, the EOC  $k_{\text{eff}}$  is slightly too low, when accounting for radial leakage, although the core is shorter than in Section 6.3. While the geometry, and therefore inter-region collision probabilities are different for the axial and TCUP heterogeneous designs, both involve spatial separation of TRU and U3 on the scale of a few thermal neutron diffusion lengths, so it is unsurprising that their behaviours are similar. Therefore, as expected, there is no advantage to implementing Design (e), as the TCUP design provides simpler fuel manufacturing.

A conventional seed/blanket structure without spatial separation of U3 and TRU (Design (b)) yields a similar maximum TRU incineration rate to the homogeneous core but with a much superior neutron economy. Neutronically, this leads to the option of an even shorter core and further increased leakage, but the high power peaking of Design (b) means this is unlikely to be feasible (see Section 6.6.3). The high axial power peaking and possibility of decoupling between seed regions (Kawashima et al., 1992) are also disadvantageous. The high power peaking also leads to high variation in discharge burn-up along the fuel rod, which could reduce the achievable discharge burn-up from fuel and cladding performance perspective. Further improvement may be possible by combining seed/blanket and TRU/U3 design features, but this is not investigated here. In Design

(b), the FVR is worse at SOC, as the central blanket is quite transparent to neutrons, so there is only a small leakage effect into the central blanket. As U3 breeds in the internal blanket, a larger proportion of the power comes from the Th-U3 region, which acts to make the FVR negative. The FVR is minimized at around ~35 GWd/t, before increasing again. As such, the maximum TRU incineration rate is relatively insensitive to discharge burn-up. The maximum discharge burn-up for EOC  $k_{\text{eff}}$  of 1% is ~120 GWd/t, so this design is attractive if a high discharge burn-up is pursued.

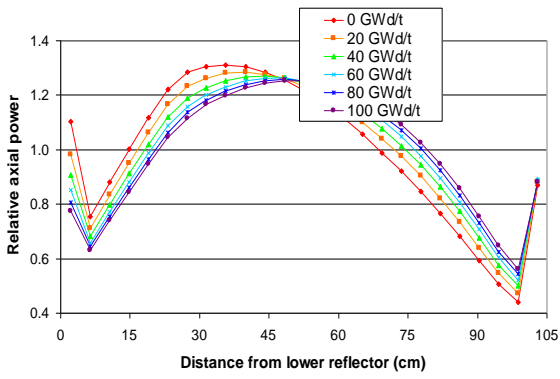
Placement of TRU at the top of the core (Design (c)) allows it to be burned in a harder neutron spectrum, leading to a superior neutron economy. There is a large axial power shift over the cycle from the Th-U3 to the Th-TRU, such that the FVR, which is dominated by the Th-TRU, rises rapidly over the cycle as the Th-U3 burns out. This leads to a net balance of U3 only being achieved for a discharge burn-up of >90 GWd/t for the isotope vector analysed. This leads to a very good neutron economy for the 60 GWd/t burn-up case as the U3 burns out: indicating that a ‘true’ equilibrium cycle has not been found. There is a much higher TRU incineration rate for the same TRU loading at higher burn-ups, so at 80 GWd/t the allowable TRU loading is substantially less than at 60 GWd/t, leading to much lower  $k_{\text{eff}}$ , but the TRU incineration rate is not much lower. The TRU incineration rate is not improved over the homogeneous core, and indications are (from the 80 GWd/t case with a lower net U3 burn) that the neutron economy is not superior to homogeneous fuel.

Concentrating the TRU in thin axial regions and borating the lower reflector (Design (d)) allows a slight increase in TRU incineration rate, although the high leakage design leads to an inferior neutron economy. Hence the core height would need to be increased, leading to a decrease in the maximum TRU incineration rate. The bimodal power distribution can also make the design sensitive to high power peaking in one of the thin Th-TRU regions.

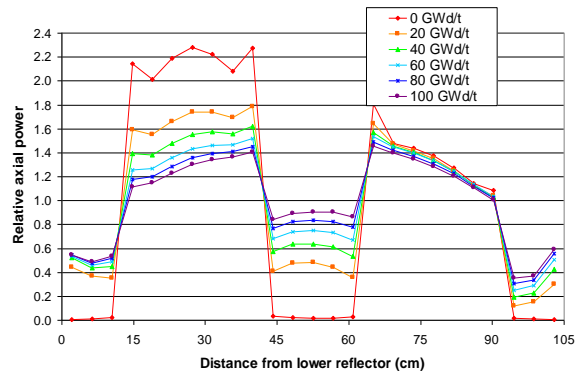
In summary, Design (e) is the best performing design for achieving a high TRU incineration rate. However, this design is roughly equivalent to the axially homogeneous TCUP assembly design, hence the axially homogeneous design is preferred.

### 6.6.3. Thermal-hydraulics

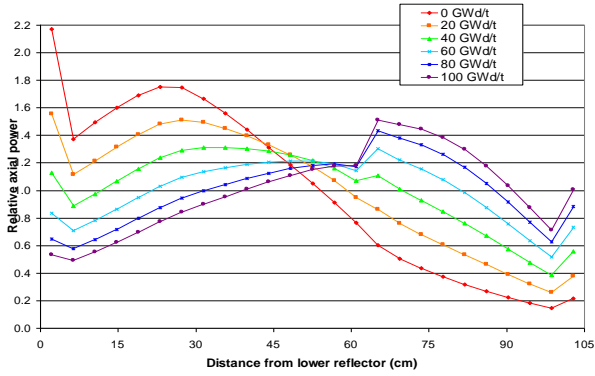
The axial power profiles and void distributions for the five cases are shown in Figs. 6.15 and 6.16. The void distributions were kept constant over the cycle as it was deemed superfluous to model axial void distribution shifting effects without a full-core, multi-batch analysis. The void distributions were calculated using fuel compositions at ~40 GWd/t from the convergence to equilibrium calculations, using an iterative procedure, and were the same for both TRU reload fractions. The plateau at ~30% void fraction (VF) is a direct result of the modified Liao correlation.



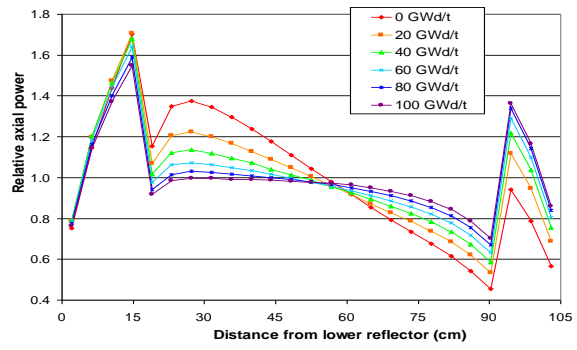
Design (a)



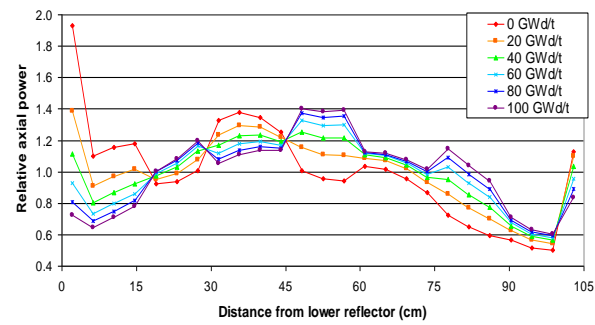
Design (b)



Design (c)



Design (d)



Design (e)

**Fig. 6.15.** Axial power distribution for different fuel designs (30% waste reload fraction).

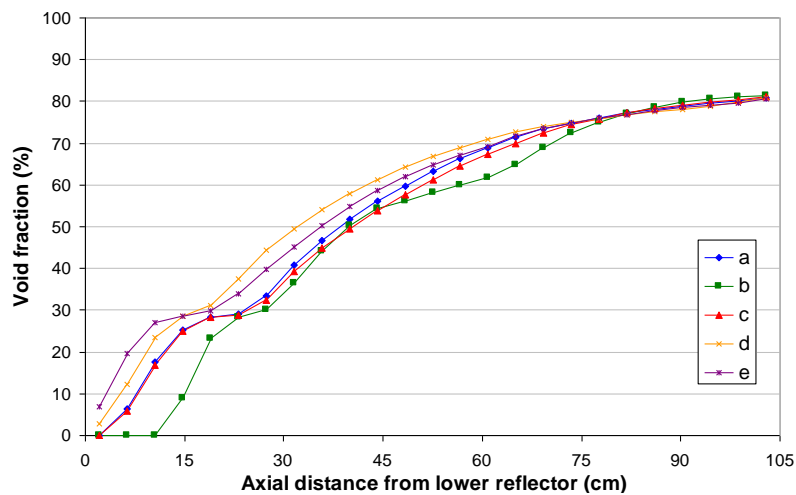


**Fig. 6.16.** Axial VF distributions for axially heterogeneous designs.

A pin power of 25 kW/pin was used, with a coolant mass flux of 850 kg/m<sup>2</sup>/s. The average VF is 55–58% for Designs (a), (c) and (e), which is comparable to the 57% average VF from the core analysis in the preceding PARCS-RELAP analysis (which used the drift-flux model in RELAP to calculate VF). Design (b) has an average VF of 51% as boiling is delayed by the lower blanket, and Design (d) has an average VF of 61% due to the high power in the lower Th-TRU region. The MCPR (calculated for a single channel assuming radial power peaking of 1.2 and assembly power peaking of 1.05) exceeds the minimum value of 1.32, except for Designs (b) and (c) (Table 6.12). In Design (b), the power in the seed assemblies is nearly zero at SOC, leading to very high power peaking. However, the MCPR rises rapidly due to breeding in the internal blanket. In Design (c), the positively skewed power distribution at SOC leads to a low MCPR. In both cases, multi-batch effects will act to increase the MCPR.

**Table 6.12.** MCPR for axially heterogeneous designs.

<b>Design</b>	<b>a</b>	<b>b</b>	<b>c</b>	<b>d</b>	<b>e</b>
<b>0 GWd/t</b>	1.35	0.99	1.19	1.36	1.38
<b>50 GWd/t</b>	1.36	1.29	1.37	1.36	1.37
<b>100 GWd/t</b>	1.36	1.32	1.34	1.33	1.36

The MCPR can be increased by increasing the core height. Increasing the core height by 10 cm improves the MCPR by ~0.09 for Design (b). However, a taller core reduces neutron leakage, which makes the FVR worse. For Design (c), it was found that raising the core height to 125 cm increased the FVR by 0.02. The TRU loading and therefore the TRU incineration rate must be reduced to compensate. A reduction in TRU incineration rate of ~10 kg/GWthyr was found to reduce the FVR by ~0.01. A 10 kg/GWthyr drop in incineration rate would almost eliminate the advantage of Design (b) relative to Design (a).

Increasing the coolant mass flux is preferable. This thermalizes the spectrum slightly, and increases the pumping power, although the pumping power is compensated for by the short core height. Increasing the mass flux by 100 kg/m<sup>2</sup>/s increases the MCPR by ~0.07 for Design (b).

## 6.7. Concluding Remarks

Th-fuelled RBWRs can achieve high discharge burn-ups with a negative VC and FVR. This gives them some flexibility to incinerate TRU with different isotope vectors, allowing for longer cooling times and the implementation of multi-tier fuel cycles. The VC and DC values are sensitive to how they are calculated, so there is some uncertainty as to their exact magnitude. Spatial separation of Th-TRU and Th-U3 into regions of the order of a few thermal neutron diffusion lengths greatly improves neutronic performance. This can be accomplished radially or axially, but radial separation

results in significantly easier fuel fabrication. A waste reload fraction of 35% appears possible when utilizing a TCUP assembly.

Axial seed-blanket heterogeneity improves neutron economy at the expense of high power peaking. Separation of Th-TRU and Th-U3 into larger regions is not effective, due to increased power density in the Th-TRU region with voiding and with burn-up, leading to a more positive VC. High leakage fuel designs (with highly fissile Th-TRU regions at the edge of the core) do not appear desirable as the power in these regions increases as the core voids, increasing the VC. Leakage is an insufficient mechanism to counter this effect, due to substantial reflector effects from water and the core structure.

Due to the use of axially homogeneous fuel (without internal blankets), it is possible to achieve a sufficient MCPR with a higher average power density than the JAEA RMWR design (with the same fuel assembly configuration). The MCPR is particularly good for tall cores. However, power peaking within the assembly may be higher if TCUP fuel is used. This can be mitigated by increasing the coolant mass flow rate, or increasing the core height. While a higher TRU incineration rate can generally be achieved with a shorter core, the capability to reduce the core area to that of an unmodified ABWR by utilizing a taller core with improved MCPR leads to a trade-off. With a discharge burn-up of  $\sim 80$  GWd/t, the cycle length is  $\sim 2$  years for  $\sim 200$  cm cores with 480 assemblies, or  $\sim 115$  cm cores with 720 assemblies.

## **Chapter 7 – Fuel Cycle Performance**

In Chapters 2, 5 and 6, the feasibility of a range of reactor and fuel configurations has been examined, and the methodology has been developed to investigate a range of designs. In this chapter, a comparative analysis is performed, focussing on the relative performance of the different designs. Comparison is made with alternative LWR candidate designs utilizing U and inert matrix fuel and with Th-fuelled SFRs.

Th-based transmutation is a much less developed technology than U-based transmutation. While further developments are required in either case for full recycle of TRUs, notably for MA reprocessing and fuel fabrication, additional technology developments are required for the Th fuel cycle. Reprocessing of Th fuel is not currently an industrial-scale process, and the Th-TRU fuel cycle introduces a greater range of isotopes that need to be recovered compared to U-TRU and Th-U<sub>3</sub> cycles in isolation. Remote fuel fabrication is required in any case due to SN emission from Cm isotopes (and Cf for thermal recycle schemes), but the presence of U<sub>3</sub> further complicates this due to the high-energy gamma emitters present in its decay chain. Use of Th-Pu pins (i.e. which do not contain MAs or U<sub>3</sub>) allow reduced remote fuel fabrication requirements, but impact neutronic performance. Comparisons of Th- and U-based transmutation strategies from a point of view of fuel fabrication and reprocessing requirements were made by Franceschini et al. (2013; 2014), utilizing some results from this chapter.

The harder neutron spectrum of a RBWR leads to superior fuel cycle performance to a RMPWR. Homogeneous, micro-heterogeneous and macro-heterogeneous fuel configurations all have their merits. A multi-tier fuel cycle is technically reasonable and is better suited to the RBWR than to the RMPWR. This strategy would reduce the number of reactors operating in reduced-moderation mode, and delay and reduce the amount of fuel to be made remotely.

An economic analysis suggests that Th-RBWRs are the lowest cost TRU incineration option, with inert-matrix schemes in LWRs of comparable cost. The economics analysis was performed in collaboration with Dr Carlo Fiorina (who also performed SFR calculations), Dr Fausto Franceschini and Prof. Edward J. Lahoda, with results also reported in (Franceschini et al., 2014).

### **7.1. Description of Fuel Cycle Cases**

Twelve fuel cycle cases are considered. Cases are designated P1–6 (RMPWR) and B1–6 (RBWR).

From Chapters 2 and 5, the RMPWR MTC, FVR and ZCR are evaluated with BP loadings appropriate to limit the reactivity swing over the cycle to around 2000 pcm. The remaining excess reactivity is assumed to be controlled using control rods, as soluble boron would make the MTC, FVR and ZCR worse. The control rods improve the MTC, FVR and ZCR, but in calculating these

quantities no credit is given for the effect of control rods. Therefore, the MTC and FVR are calculated in a conservative and consistent manner.

The methodology, and in many cases the results, of the full-core analyses for the RMPWR and RBWR are given in Chapters 5 and 6 respectively. The discharge burn-up is taken from full-core models except where otherwise indicated. In all cases, the equilibrium isotope vector is determined using single assembly neutronic simulations. For the RMPWR, the linear reactivity model (Driscoll et al., 1991) gives a very good approximation to the average discharge burn-up. This has been confirmed using PANTHER (Morrison, 2003). In addition, the FVR and ZCR are highly leakage-dependent and these are calculated using a full-core model.

The reactivity swing in the RBWR is generally around 2000 pcm, which is similar to the shim rod worth. For high burn-up cases, it can increase to ~3500 pcm. However, current designs of RBWR (Downar et al., 2012; Fukaya et al., 2009a) only have space for shim rods in some of the bypass channels. By enlarging these bypass channels (which softens the spectrum slightly, but not enough to significantly impact design performance), additional shim rods can be placed. It is therefore possible to achieve sufficient worth to control the core. Similarly, placement of additional shutdown rods, if necessary, should allow a sufficient SDM to be achieved.

The MTC, VC and FVR are calculated from full-core analyses where appropriate. In some cases, a core analysis is unnecessary because the assembly neutronic properties change only slightly from other cases. The core analyses establish the trend between assembly and core reactivity coefficients, such that feasibility can be inferred with sufficient reliability for cases where only an assembly analysis is performed. The RBWR is expected to have a negative ZCR (and if the ZCR is positive and the FVR is negative, it would only take a very minor reduction in TRU feed or core height to render it negative), while it is positive for the RMPWR. This is a major advantage for the RBWR over the RMPWR as it makes it easier to justify the safety performance of the reactor in beyond-design-basis accidents.

The additional constraints of finding a suitable CRP to limit power peaking, SDM and accident response could introduce performance differences between the RMPWR and RBWR once accounted for. For instance, if the RMPWR violates thermal-hydraulic constraints, a redesign of the core to meet these constraints may render it non-retrofittable, e.g. a shorter core may be required, which would reduce the attractiveness of this implementation.

The achievable discharge burn-up and core residence time will be limited by cladding and fuel performance. These constraints are not applied to the neutronic analysis, as it is instructive to determine the neutronic limitations on the design, e.g. the viability of the design may be dependent on future advances in cladding technology. However, designs are selected with a view to mitigate or

satisfy likely limits on material performance.

WIMS models the isotopes which are relevant to the reactor physics. These include isotopes of Cm up to  $^{248}\text{Cm}$ ,  $^{232}\text{Th}$  and  $^{233}\text{Pa}$ , but not other isotopes of Th, Pa or  $^{232}\text{U}$ . There is therefore no implicit assumption of the treatment of Pa in the WIMS analysis. For selected cases (see Section 7.5), WIMS 9 was interfaced with the inventory code FISPIN (Answers, 2007) to evaluate full inventories, activities and decay heat for a larger set of nuclides, assuming all actinides are recycled in the fuel.

### **7.1.1. RMPWR Cases**

#### *7.1.1.1. Homogeneous Recycle*

**P1:** RMPWR with 11.5 mm 95% TD fuel, homogeneous assembly design. An 11.5 mm pin diameter is approximately the minimum required for acceptable neutronic performance (negative MTC and adequate cycle length) in an RMPWR with homogeneous Th oxide fuel. The MTC for this case is approximately zero without considering the impact of reactivity control and the core has slightly positive reactivity when fully voided. See Chapter 2 for further details.

#### *7.1.1.2. Heterogeneous Recycle Schemes*

**P2:** RMPWR with 11 mm, 95% TD fuel, heterogeneous TCUP assembly design with 132 Th-U3 pins. A negative MTC is achievable throughout the cycle, but the core has positive FVR. To achieve negative FVR with this assembly design, the pin diameter needs to be increased to 11.5 mm and the TRU reload fraction needs to be reduced, making the fuel cycle performance worse<sup>30</sup> and potentially violating the thermal-hydraulic constraints (Chapter 4).

**P3:** Multi-tier implementation of P2 (see Chapter 5). The cycle incineration rate and burn-up are evaluated as a weighted average of the Th-Pu stage and the RMPWR, based on the relative proportions incinerated at each stage, with the U3 in the feed to the RMPWR counted as a liability to be incinerated.

The feed to the equilibrium cycle has lower fissile quality than the single-tier cases, and therefore a higher TRU reload fraction than in the geometrically identical single-tier counterpart is required, leading to a higher overall incineration rate. (Note that the reload proportion is counted here as the total incineration liability, i.e. everything except  $^{232}\text{Th}$ .) However, the presence of in-bred U3 offsets the negative effects of the deterioration in the Pu fissile quality and the increased MA (Np/Am/Cm) content of the multi-tier vs single-tier case, leading to a comparable MTC and discharge burn-up to P2. However, the FVR is still positive. The MTC and FVR are calculated

---

<sup>30</sup> This has been confirmed by core analysis (Lindley et al., 2014b).

using a single assembly in lieu of a full-core calculation as their values are similar to the single-tier case, and accordingly are expected to be similar to the single-tier case full-core values.

**P4:** As P2, but the fuel density of Th-U3 pins is reduced to 85% TD. In addition, MAs are placed in separate pins, modelled as low density MAO<sub>2</sub>. In practice, an inert matrix (e.g. ZrO<sub>2</sub>) may be used (e.g. Hyland et al., 2011). In the unrodded assemblies, these low density pins can replace the guide tube positions, as standard burnable absorber inserts are not foreseen in the RMPWR (they are ineffective as the spectrum is too hard). As the pins are low power, the radius is increased to almost the lattice pitch. These extra rod positions should allow the thermal-hydraulic conditions to be satisfied with some of the conventional fuel rods also displaced. This is necessary to satisfy mass flow considerations while minimizing the required MA density. The density of MAs assumed in this study for the target pins is ~3.4 gHM/cm<sup>3</sup>. This is required to satisfy the mass balance constraints of this fuel assembly. Previous studies have considered a wide range of densities: (Hyland et al., 2011) with Am/Cm/lanthanide mixture occupying 5–60% of the total pin volume. The pins are ~65 wt% Am, 21 wt% Cm and 14 wt% Np. The power of the MA target pins is ~70% that of normal rods.

The lattice calculation model assumed rod cluster control assemblies (RCCAs) positioned in a checkerboard configuration. The MA-bearing pins should be distributed within the Th-Pu pins so as to favour a more even power distribution in the assembly by lowering the thermal flux impinging on the MA-bearing pins. However, if the design of the assembly containing MAs is not compatible with the MA absorber inserts being removed and redistributed between cycles, the fuel management scheme is constrained. This is a problem as the 1<sup>st</sup> and 2<sup>nd</sup> batches are often deployed in a checkerboard to minimize power peaks, so if one type of assembly is only compatible with alternate positions in the core, it cannot be shuffled from the usual batch 1 positions to the adjacent batch 2 positions due to the incompatibility of MA inserts with the presence of control rods.

It is desirable that the MA rods can be removed at the end of the cycle to follow their own loading scheme to allow movement of the assembly from the position with a RCCA to the position without a RCCA. However, pin-level shuffling of the MAs is likely to be impractical (movement of individual pins is slow and may result in high risk of breakage), resulting in further constraints on the fuel management scheme. It is also difficult to keep pin-level power peaking low, even with variable pin compositions, due to the spectral variation between pins of different types causing them to burn at different rates. This can be mitigated by allowing the pin-level power peaking to be higher in the twice-burned assemblies, as the hot pin will not be in the twice-burned fuel.

These considerations, combined with the use of control rods for mechanical shim, may make it difficult to achieve a LP with acceptably low form factor. The core design will be challenging and a

full-core analysis is required to identify a feasible configuration and demonstrate concept viability.

As the MA pins should be placed near the Th-Pu pins to maximize spectral hardening, this means the Th-Pu pins should be positioned at the centre of the assembly, i.e. next to the guide tubes where the MA pins will be inserted (Fig. 7.1). However, this does result in a harder neutron spectrum in the control rods, reducing their worth, as they are next to the hard spectrum Th-Pu pins rather than the soft spectrum Th-U3 pins. Similarly, in the assembly without MAs, the Th-Pu pins are thermalized by the vacant guide tube positions.

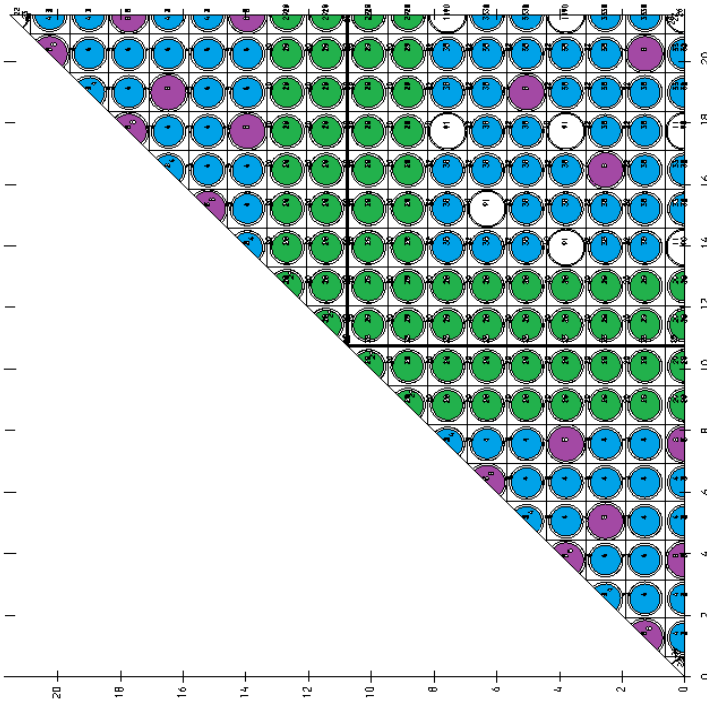


**Fig. 7.1.** P4 TCUP model with Th-U3 pins (green), Th-TRU pins (blue) and MA pins (purple) centred on where 4 assemblies meet. In this case there were 132 Th-TRU pins and 120 Th-U3 pins per assembly, with 12 MA pins in rodded assemblies and 36 MA pins in unrodded assemblies.

While it is possible to achieve a negative MTC throughout the equilibrium cycle, there is a penalty compared to P2. This is primarily attributable to the reduction in density of the Th-U3 pins and the flux dip in MA pins. An increase in actinide waste reload proportion is necessary to maintain a cycle length of  $\sim 40$  GWd/t, which increases the incineration rate at equilibrium but makes the MTC less negative. A full-core analysis was not performed for this configuration, and is necessary to determine if an acceptable core configuration can be achieved with an 11 mm pin diameter, or if a larger pin is required. However, the effect of the design on the discharge burn-up, incineration rate, MTC, FVR and ZCR, i.e. the parameters of interest for this study, can be reliably inferred from the assembly analysis – as the MTC and FVR are more positive in the assembly calculation compared to P2, they can also be expected to be larger than P2 in the full-core calculation.

### 7.1.1.3. Variable Batch Management Schemes

The variable batch management schemes from Chapter 5 are considered, where the Th-TRU resides twice as long in the core as the Th-U3, such that the Th-U3 is refuelled twice as often. This allows sensible batch management of the TCUP case.

**P5** is the single-tier implementation of this variable batch management strategy with 95% TD fuel, 11 mm pin diameter and 144 Th-TRU pins per assembly; **P6** is the multi-tier implementation with 95% TD fuel, 11 mm pin diameter and 108 Th-TRU pins per assembly. P5 has negative FVR and P6 has positive FVR. However, the ZCR remains positive in both cases.

As for P3, the MTC and FVR of P6 are calculated using a single-assembly calculation only. The FVR is more positive for P6 than for P5 (and also for the multi-tier single-pass strategy, P3), therefore the core FVR will also be positive.

As negative FVR is highly desirable, and the fuel cycle performance of the 11 mm RMPWR cases (P2–6) is generally similar, the multi-pass scheme (P5) seems appropriate for the single-tier fuel cycle, and the single-tier fuel cycle is preferable to the multi-tier fuel cycle for the RMPWR.

The fuel cycle performance of the WATU concept is similar to the TCUP concept, although with improved SDM, so this scheme is not discussed further here.

## 7.1.2. RBWR Cases

### 7.1.2.1. Homogeneous Recycle

**B1:** RBWR with 85% TD homogeneous fuel. This has a relatively low incineration rate but excellent burn-up potential. However, MAs cannot be added until a first Th-Pu pass is completed and U3 is bred in to ensure a negative VC and negative reactivity when the core is fully voided. 200 cm (tall) core height is specified to improve the discharge burn-up versus incineration rate trade-off (Chapter 6).

**B2:** Multi-tier implementation of B1. This multi-tier approach again allows more rapid implementation than straight full TRU recycle, which is particularly relevant to a strategy in which the transmutation starts in current PWRs while a RBWR is licensed and the reprocessing and fabrication technologies for TRU fuel are developed. A similar reload proportion to B1 is appropriate to give the same VC, corresponding to a lower Pu enrichment. The cycle incineration rate and burn-up are evaluated as a weighted average of the Th-Pu stage and the RBWR, based on the relative proportions incinerated at each stage, with the U3 in the feed to the RBWR counted as a liability to be incinerated.

There is a substantial burn-up penalty compared to B1, but a discharge burn-up of ~78 GWd/t

should be possible. In addition, the incineration rate in the first stage is very high so the overall incineration performance is good.

Indeed, this trade-off appears highly favourable as the burn-up in the RBWR is likely to be constrained by materials considerations. Therefore trading burn-up in the equilibrium cycle for incineration rate in the first stage is not unreasonable. With the added bonus of postponing RBWR deployment, this result is encouraging.

#### 7.1.2.2. *Heterogeneous Recycle Schemes*

**B3:** As B1 but with a heterogeneous TCUP assembly with 91 85% TD Th-TRU pins and 126 85% TD Th-U3 pins per assembly. This approach is neutronicly extremely effective, improving the VC and therefore allowing substantially increased reload enrichment and discharge burn-ups competitive with a FR, with the caveat that a suitable cladding material for the high discharge burn-up and long residence time of the RBWR fuel must be developed. Core analysis in Chapter 6 indicates that a burn-up of ~118 GWd/t is neutronicly feasible. Reducing the core height, radius or discharge burn-up is therefore advisable to make the VC more negative.

In order to reduce the burn-up of B3 to an achievable level without overly compromising the fuel cycle performance, it is necessary to increase the incineration rate. To achieve this, a multi-tier fuel cycle was implemented. Stage 1 discharge burn-ups of 50 GWd/t (**B4**) and 84 GWd/t (**B5**) were considered. A higher burn-up in the first tier reduces the burn-up of the second tier, and therefore results in a slight decrease in the fuel cycle average discharge burn-up (despite the high burn-up of the first tier). However, a greater proportion of the waste is burned in the low conversion ratio PWR and therefore the overall incineration rate is higher in the B5 scenario.

**B6:** Spatial separation of TRU and U3 is less critical to viability of the RBWR than the RMPWR, but still advantageous to performance. Positioning the MAs in the Th-Pu pins is neutronicly preferable, but segregating MA from Pu in the U3 pins reduces remote fuel fabrication requirements. Therefore a micro-heterogeneous ‘checkerboard’ of 78 95% TD Th-Pu pins and 139 85% TD Th-U3-MA pins is considered (Fig. 7.2). Assembly calculations indicate a slightly reduced reload proportion is appropriate and a slightly higher burn-up is achievable relative to B1. An average VF assembly calculation is not sufficient to accurately calculate the full-core burn-up, so the same discharge burn-up as B1 was assumed, as the assembly variation in  $k_{\infty}$  with discharge burn-up was very similar.

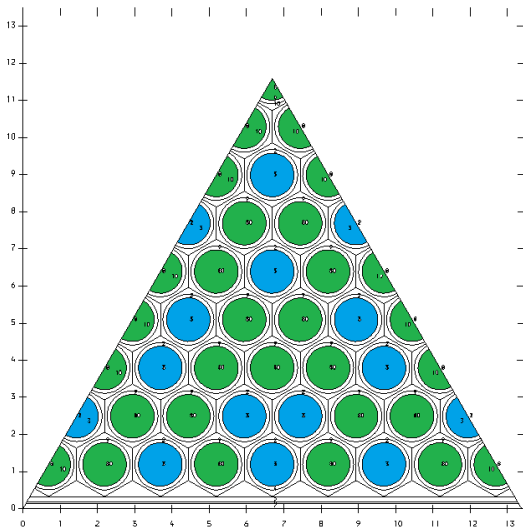


**Fig. 7.2.** Micro-heterogeneous B6 RBWR fuel design with 78 Th-Pu pins (blue) and MAs in the  $^{139}\text{Th}$ -U3 pins (green).

### 7.1.3. Summary of Fuel Cycle Cases

The RMPWR cases stretch the limits of neutronic, thermal-hydraulic or fuel fabrication feasibility. However, the RMPWR conversion ratio is intrinsically lower than that for the RBWR, which is desirable from the incineration performance standpoint.

In contrast, the RBWR cases have more favourable neutronic, thermal-hydraulic and fabrication feasibilities. However, an RBWR has a radically different core configuration to current BWRs which may increase the burden on technology development and licensing. In addition, the achievable incineration rate is low without heterogeneous fuel. This makes the multi-tier options of considerable interest as they delay the time before a RBWR is required. In particular, cores with TCUP fuel assemblies are found to have good fuel cycle performance without relying on currently unachievable (from a materials standpoint) burn-ups. Moreover, the overall fuel cycle performance is relatively insensitive to the burn-up of the first stage, leading to flexibility in the fuel cycle implementation.

These cases were selected to cover a range of combinations of reactor, fuel design and fuel cycle options and therefore allow the key trade-offs and performance measures to be identified. The range essentially covers: homogeneous recycle; heterogeneous fuel for improved neutronic performance (TCUP); heterogeneous fuel for reduced remote fuel fabrication requirements (also discussed in (Franceschini et al., 2013)); two passes of Th-TRU through the reactor; and multi-tier fuel cycles for RMPWRs and RBWRs. Table 7.1 summarises the objectives and scope of each case.

**Table 7.1.** Summary of considered fuel designs.

	Single-tier	Multi-tier	Multi-tier high burn-up
Homogeneous	P1, B1*	B2	B5*
Heterogeneous	P2*, B3*	P3, B4*	
Heterogeneous with Th-Pu pins	P4, B6		
2 Th-TRU pass	P5*	P6	

\* full-core analysis performed

The homogeneous RMPWR scheme has poor performance so is only considered for the single-tier fuel cycle. The heterogeneous schemes with Th-Pu pins are only considered for the single-tier case for simplicity. The multi-pass schemes are not appropriate for the RBWR as they increase the ratio of maximum to average discharge burn-up, and the RBWR performance is to an extent limited by the maximum achievable discharge burn-up. The multi-tier scheme is considered appropriate only for the RBWR due to performance limitations of the multi-tier scheme in the RMPWR. The RBWR multi-tier schemes are considered for the heterogeneous TCUP fuel configuration as this has superior performance to the homogeneous fuel.

The full-core performances of B2 and B6 have been inferred from the performance of B1, which has the same core height and neutronicallly similar fuel design. This may result in slight errors in the discharge burn-up, but it will not affect the relative performance of the cases.

## 7.2. Fuel Cycle Performance

The equilibrium isotope vectors for all the cases are given in Tables 7.2 and 7.3. In both cases  $^{246}\text{Cm}$  and above isotopes are not fully converged to equilibrium due to the impractically long time required for convergence. However, the impact on reactor physics is negligible. The RMPWR generally has significantly higher content of TRU and lower U3 and  $^{232}\text{Th}$  contents. The higher conversion ratio of the RBWR leads to lower equilibrium Pu and higher equilibrium U3. The Am and Cm populations are dominated by the amount in the external feed, and are therefore lower in the RBWR, mostly as a result of the lower TRU fraction in the feed, although the increased fissibility of TRU isotopes does contribute slightly. Note that many of these vectors are repeated from previous chapters, but are included again here for ease of reference.

Table 7.4 summarizes the fuel cycle performance of each case. Compared to multi-tier FR approaches, e.g. (Franceschini et al., 2013), the reactor support ratio is less of a concern from a standpoint of cost minimization. Once the sunk costs of licensing have been met, an RMPWR or RBWR is expected to have similar cost to conventional LWRs, except for the fuel cycle costs.

**Table 7.2.** Equilibrium isotope vectors of RMPWR cases (at%).

	P1	P2	P3	P4	P5	P6
<sup>241</sup> Am	0.882	1.423	1.992	2.102	1.145	1.907
<sup>242m</sup> Am	0.023	0.038	0.053	0.058	0.027	0.049
<sup>243</sup> Am	0.613	0.770	1.137	1.043	0.711	1.238
<sup>243</sup> Cm	0.005	0.005	0.007	0.006	0.004	0.007
<sup>244</sup> Cm	0.453	0.515	0.701	0.627	0.558	0.832
<sup>245</sup> Cm	0.232	0.218	0.267	0.201	0.230	0.305
<sup>246</sup> Cm	0.195	0.207	0.152	0.131	0.198	0.258
<sup>247</sup> Cm	0.036	0.048	0.028	0.026	0.041	0.060
<sup>248</sup> Cm	0.018	0.023	0.008	0.014	0.019	0.025
<sup>237</sup> Np	0.427	0.583	0.846	0.699	0.558	0.991
<sup>238</sup> Pu	1.743	2.409	3.039	2.471	2.133	3.179
<sup>239</sup> Pu	2.297	3.520	1.834	3.587	3.349	1.859
<sup>240</sup> Pu	2.831	5.427	5.802	5.867	4.445	5.986
<sup>241</sup> Pu	0.883	1.073	1.090	1.170	1.126	1.192
<sup>242</sup> Pu	1.688	2.871	3.841	3.100	2.545	4.354
<sup>232</sup> Th	80.592	74.803	72.315	73.284	77.848	71.273
<sup>233</sup> U	3.804	2.555	3.151	2.571	2.358	2.796
<sup>234</sup> U	1.935	2.211	2.523	1.968	1.711	2.336
<sup>235</sup> U	0.831	0.641	0.706	0.570	0.517	0.662
<sup>236</sup> U	0.511	0.658	0.505	0.503	0.476	0.693
U3	<b>7.080</b>	<b>6.065</b>	<b>6.886</b>	<b>5.612</b>	<b>5.062</b>	<b>6.486</b>
Pu	<b>9.442</b>	<b>15.300</b>	<b>15.607</b>	<b>16.196</b>	<b>13.598</b>	<b>16.569</b>
Am	<b>1.518</b>	<b>2.232</b>	<b>3.182</b>	<b>3.203</b>	<b>1.882</b>	<b>3.193</b>
Cm	<b>0.939</b>	<b>1.016</b>	<b>1.163</b>	<b>1.005</b>	<b>1.051</b>	<b>1.486</b>

**Table 7.3.** Equilibrium isotope vectors of RBWR cases (at%).

	B1	B2	B3	B4	B5	B6
<sup>241</sup> Am	0.701	0.776	1.225	1.316	1.356	0.656
<sup>242m</sup> Am	0.027	0.028	0.052	0.053	0.057	0.024
<sup>243</sup> Am	0.365	0.506	0.533	0.787	0.805	0.332
<sup>243</sup> Cm	0.002	0.003	0.003	0.005	0.005	0.002
<sup>244</sup> Cm	0.203	0.287	0.248	0.483	0.485	0.184
<sup>245</sup> Cm	0.113	0.152	0.105	0.181	0.188	0.101
<sup>246</sup> Cm	0.084	0.114	0.118	0.123	0.134	0.080
<sup>247</sup> Cm	0.019	0.026	0.032	0.028	0.031	0.017
<sup>248</sup> Cm	0.008	0.010	0.013	0.010	0.011	0.008
<sup>237</sup> Np	0.366	0.462	0.549	0.664	0.681	0.354
<sup>238</sup> Pu	1.113	1.154	1.424	1.677	1.751	0.982
<sup>239</sup> Pu	1.797	0.739	3.127	1.326	1.177	1.660
<sup>240</sup> Pu	2.312	1.880	5.106	4.442	4.452	2.373
<sup>241</sup> Pu	0.513	0.476	0.642	0.774	0.691	0.466
<sup>242</sup> Pu	0.966	1.177	1.928	2.492	2.538	1.042
<sup>232</sup> Th	82.580	82.182	76.616	76.068	76.044	82.457
<sup>233</sup> U	5.588	6.107	4.709	5.577	5.427	5.603
<sup>234</sup> U	1.983	2.446	2.287	2.549	2.675	2.298
<sup>235</sup> U	0.722	0.837	0.699	0.771	0.804	0.740
<sup>236</sup> U	0.538	0.637	0.586	0.672	0.686	0.619
U3	<b>8.830</b>	<b>10.027</b>	<b>8.280</b>	<b>9.569</b>	<b>9.591</b>	<b>9.259</b>
Pu	<b>6.702</b>	<b>5.426</b>	<b>12.227</b>	<b>10.711</b>	<b>10.609</b>	<b>6.523</b>
Am	<b>1.093</b>	<b>1.311</b>	<b>1.810</b>	<b>2.156</b>	<b>2.218</b>	<b>1.012</b>
Cm	<b>0.429</b>	<b>0.591</b>	<b>0.518</b>	<b>0.831</b>	<b>0.855</b>	<b>0.393</b>

**Table 7.4.** Fuel cycle performance of each case.

Case	Stage 2 waste reload fraction in feed* (at%)	Fuel pins types	Incineration ( <i>I</i> ) (kg/GWthyr) Stage 1, Stage 2, Overall	Burn-up ( <i>BU</i> ) (GWd/t) Stage 1, Stage 2, Overall	kg burned/t reprocessed ( <i>X</i> )	kg burned/t fabricated remotely ( $X_{remote}$ )	FVR, ZCR	Specific power (MW/t)	Support ratio** Stage 1, Stage 2
P1	45%	Th-U3-TRU	172.9	34.9	16.5	16.5	Positive	26.0	0.52
P2	50%	Th-TRU Th-U3	191.9	42.7	22.4	22.4	Positive	28.8	0.47
P3	60%	Th-TRU Th-U3	184.1, 236.9, 222.3	50.0, 39.9, 41.8	25.5	33.2	Positive	28.8	0.11, 0.29
P4	55%	Th-Pu MA Th-U3	217.6	40.5	24.1	50.9	Positive	28.0	0.41
P5	51%	Th-TRU Th-U3	195.3	41.6	22.2	22.2	FVR < 0 ZCR > 0	28.8	0.46
P6	54%	Th-TRU Th-U3	184.1, 214.9, 207.0	50.0, 38.1, 40.3	22.8	28.9	Positive	28.8	0.11, 0.32
B1	26%	Th-U3-TRU	101.3	94.3	26.2	26.2	Negative	15.1	0.89
B2	26%	Th-U3-TRU	184.1, 101.2, 112.8	50.0, 78.2, 69.2	21.4	28.8	Negative	15.1	0.11, 0.69
B3	35%	Th-TRU Th-U3	135.7	117.7	43.7	43.7	Negative	15.1	0.66
B4	35%	Th-TRU Th-U3	184.1, 135.4, 144.1	50.0, 82.4, 71.8	28.3	41.1	Negative	26.2	0.11, 0.51
B5	35%	Th-TRU Th-U3	215.9, 135.4, 151.5	84.0, 69.6, 73.2	30.4	36.3	Negative	26.2	0.12, 0.48
B6	24%	Th-Pu Th-U3-MA	93.5	94.3	24.0	37.5	Negative	15.1	0.96

\* Feed to Stage 2. E.g. if feed to Stage 2 is 60 at% <sup>232</sup>Th and 40 at% U3+TRU then waste reload fraction is 40%

\*\* GWthyr in Stage 1 and Stage 2 per GWthyr in LEU-fuelled LWR. 90 kg/GWthyr TRU production in LEU-fuelled LWR

A Th-fuelled RBWR uses the same plant as an ABWR, but the 720 assembly design considered here has a core area of 33.5 m<sup>2</sup>, which is around 50% larger than an ABWR (GE Nuclear Energy, 1997). This will increase construction costs. The capability to manufacture such large pressure

vessels does not currently exist. While this is technically feasible, the related infrastructure must be developed. Alternatively, the RBWR plant size and rating can be reduced, such that the core is the size as an ABWR and the plant is smaller. However, this results in a poor economy of scale (a disadvantage of small reactors) while still requiring a large forged pressure vessel. De-rating an ABWR plant by 33% is unlikely to be economically attractive. However, if a ‘tall’ 200 cm core is utilized and the flow rate is increased above the reference value, then the number of assemblies can be reduced to 480, which results in a similar core area to the ABWR. This will reduce the maximum achievable incineration rate (Chapter 6) but a larger pressure vessel would not be required.

Minimizing the fuel cycle costs, which essentially corresponds to limiting the rate of reprocessing and the number of pins which must be fabricated remotely, is a key objective: kg burned/t reprocessed is therefore considered as primary figure-of-merit. The reprocessing requirements vary from the remote fuel fabrication requirements for the various designs, so the optimal design will depend upon the relative costs of remote fabrication and reprocessing.

The incineration rate is the rate at which TRU from a complementary fleet of UO<sub>2</sub>-fuelled LWRs is burned. In equilibrium, the rate at which TRU is incinerated in the Th-TRU-fuelled reactors equals the rate at which TRU is produced in the UO<sub>2</sub>-fuelled reactors. The support ratio is defined as the ratio of TRU-burning reactors to conventional UO<sub>2</sub>-fuelled LWRs at which the total fuel cycle TRU production rate is zero. Hence the support ratio of TRU-burning reactors to conventional LWRs reduces as the incineration rate of the TRU-burning reactors increases. A reactor fleet with the power capacity in the proportions shown in the last column of Table 7.4 will produce zero net TRU.

For multi-tier schemes, the average discharge burn-up and incineration rate are calculated as follows:

Let  $p$  = the proportion of TRU burned in Stage 1 and  $q$  = the proportion of thermal power capacity which is in Stage 1 reactors.

The thermal power capacity in each stage is proportional to the proportion of TRU burned in each stage, such that:

$$q = \frac{p / I_1}{p / I_1 + (1 - p) / I_2} = \frac{pI_2}{(1 - p)I_1 + pI_2} \quad (7.1)$$

where  $I_1$  and  $I_2$  are the incineration rate in Stages 1 and 2 respectively in kg/GWthyr.

The overall incineration rate is the total incineration per GWthyr, i.e.:

$$I_{\text{overall}} = qI_1 + (1 - q)I_2 \quad (7.2)$$

The average discharge burn-up is the ratio of total energy to total loaded mass. Let  $BU_1$  and  $BU_2$  be the discharge burn-ups of Stages 1 and 2 respectively. The fuel mass requirement for Stage 1 is  $1/BU_1$  in t/GWd of energy production in Stage 1, and similarly for Stage 2.

Therefore the mass of fuel throughput per GWd is:

$$m = q / BU_1 + (1 - q) / BU_2 \quad (7.3)$$

The average burn-up is the reciprocal of this:

$$BU_{\text{overall}} = \frac{BU_1 BU_2}{(1 - q) BU_1 + q BU_2} \quad (7.4)$$

and the proportion of fuel fabrication which is in Stage 1 reactors is:

$$r = \frac{q / BU_1}{q / BU_1 + (1 - q) / BU_2} = \frac{q BU_2}{(1 - q) BU_1 + q BU_2} \quad (7.5)$$

Finally, the remote fuel fabrication requirement is:

$$X_{\text{remote}} = X / (1 - r) / u \quad (7.6)$$

where  $X$  is the kg burned/t reprocessed, our primary figure-of-merit and  $u$  is the proportion of the fuel for Stage 2 which is fabricated remotely (this is 1 except where there are Th-Pu MOX pins in Stage 2).

Implementation in an RMPWR is a delicate compromise between neutronic, thermal-hydraulic and fuel fabrication constraints. It may not be possible to satisfy all these constraints in a retrofit core design, and in any case the ZCR is likely to be positive. Implementation in a new LWR design gives flexibility to optimize the performance. As discussed in Chapter 5, a single-tier fuel cycle with TCUP fuel assembly and multi-pass fuel management strategy appears appropriate.

Dedicated MA target pins and/or reduced density Th-U3 pins could improve fabrication feasibility (P4), but further analysis is necessary to determine if this is possible within the neutronic constraints, and if fabrication advantages are sufficient to compensate for any burn-up penalty. The large Pu inventory of the RMPWR leads to a more than 50% reduction in the remote fuel fabrication requirements if Th-Pu pins are implemented (P4), so there is a strong incentive to do this if possible.

A homogeneous fuel single-tier RBWR (B1) requires almost as much RBWR thermal power generation as conventional LWR power generation to achieve zero net TRU production. This is also the case for B6. The RBWR fleet capacity required can be reduced to around half the conventional LWR capacity by implementing heterogeneous fuel and a multi-tier fuel cycle (B4 and B5). This is

comparable to the RMPWR single-tier case with negative FVR (P5). The minimum support ratio of RM reactors is achieved with a multi-tier cycle with a RMPWR (P3 and P6) but these cases have positive FVR.

The RBWR has the neutronic potential to reach very high burn-ups. In particular, the performance of B3 (TCUP) far exceeds the performance of the other cases due to the neutronic capability of achieving a very high average discharge burn-up. However, a suitable cladding must be developed, e.g. SiC (Hallstadius et al., 2012), or it may be possible to utilize stainless steel cladding in the hard spectrum of a RBWR as considered by Nakano et al. (2007). Hydrogen uptake of Zircaloy cladding has been found to be worse in the hard spectrum of the RBWR (Mieloszyk and Kazimi, 2014), which worsens the performance in accident scenarios. This degradation in performance occurs at relatively low burn-ups, such that a new cladding material is likely to be necessary. While the spectrum of the RMPWR is substantially softer and the burn-up is much lower than that of the RBWR, this may also be a concern for the RMPWR, so this requires further investigation.

A lower burn-up RBWR is less competitive relative to a RMPWR due to its lower incineration rate – leading to increased reprocessing costs. It is possible to increase the RBWR incineration rate by increasing the TRU reload fraction and decreasing the core height (to keep the VC negative by increasing leakage), although decreasing the core height generally results in a larger core area being required and the achievable kg burned/t reprocessed from a neutronic perspective is worse relative to a low-leakage RBWR. Use of multi-tier fuel cycle helps increase the incineration rate and therefore achieve a better overall fuel cycle performance. Increasing the burn-up of the Th-Pu fuel in the PWR (i.e. Stage 1) results in similar fuel cycle performance (B5), increasing the flexibility with which this fuel cycle scheme can be implemented.

A core could be specified with an H/HM ratio between the RBWR and the 11.5 mm pin diameter RMPWR, by designing a RBWR with a less tight lattice or a RMPWR with a tighter lattice. A tighter lattice RMPWR would require a new design, probably with a lower core height and more control rods, to satisfy SDM and thermal-hydraulic constraints.

The B6 assembly scheme can be used, potentially in conjunction with a multi-tier recycle strategy (B2), to decrease the number of pins that must be fabricated remotely. This is clearly advantageous compared to homogeneous recycling, but reduces the discharge burn-up and incineration rate relative to the TCUP scheme. Inferring from the similarity of B1 and B6, a multi-tier approach to the B6 assembly design probably has similar performance to B2. Less than 40% of the pins are Th-Pu, and the decrease in pins requiring remote fabrication per assembly is offset by the reduced incineration rate. Alternatively, a scheme with MA target pins could partially reap the advantages of the TCUP scheme while also limiting the number of pins that must be fabricated remotely.

### **7.3. Comparison with Other Incineration Schemes**

In this section, the fuel cycle performance of the Th-fuelled RMPWR and RBWR is compared to other TRU incineration schemes. This discussion is limited to LWR and SFR incineration schemes. The various schemes are described in Sections 7.3.1 to 7.3.5 and fuel cycle performance is compared in Section 7.3.6.

#### **7.3.1. U-TRU-fuelled RBWR**

In this thesis,  $^{232}\text{Th}$  is considered as a fertile carrier for TRU incineration as an alternative to  $^{238}\text{U}$ . In RBWRs, incineration with  $^{238}\text{U}$  requires axially heterogeneous fuel (Fukaya et al., 2009a). The VC of burner designs is calculated in Japanese studies as being negative, while a recent US study calculates it as being substantially positive (Downar et al., 2012). It must also be noted that axially homogeneous Th-fuelled RBWRs achieve a much superior performance to axially homogeneous U-fuelled RBWRs (Chapter 3). The performance of the U-fuelled RBWR design is considered here for completeness.

#### **7.3.2. LEU/U-TRU Mixed PWR Core**

Typically,  $^{238}\text{U}$ -based TRU multi-recycle schemes in LWRs consider mixed LEU-TRU cores to achieve around zero net incineration rate. Over-moderated designs are often considered to increase TRU destruction rates and limit the required Pu content in the fuel, e.g. (Puill and Bergeron, 1997). Here, PWR designs based on  $17\times 17$  fuel assemblies are considered. The presence of LEU allows a substantially negative MTC to be maintained. An increased moderation ‘CORAIL’ design from (Kim et al., 2002) is selected here as a basis for comparison. This contains 88 U-TRU pins and 176 LEU pins per assembly.

#### **7.3.3. LEU/TRU Inert Matrix Mixed PWR Core**

An alternative to fertile fuels is inert matrix fuels. This allows TRU destruction rates to be increased due to the lack of breeding from a fertile isotope. Loading of inert matrix fuels in isolation results in a reduced magnitude DC and MTC. Here, the CONFU design is considered, which contains a mix of 48 fertile-free TRU-bearing pins and 216 LEU pins (Case 4 from Table 6.4.I in (Shwageraus, 2003)).

Increased enrichment of LEU from ~4.2% to 5.00% (CONFU) and 5.07% (CORAIL) is necessary to maintain an 18 month cycle length and have net TRU incineration rates of around zero. To analyse these concepts within the same framework as the Th-TRU designs presented earlier, the ‘support ratio’ of TRU to LEU pins is evaluated, with the incineration rate of the TRU pins considered in isolation. The increased LEU reprocessing requirement compared to an equivalent core fuelled entirely with 5% LEU is added to the reprocessing requirement of the TRU-bearing

pins, to achieve a consistent comparison. However, this penalty is not introduced to the remote fabrication requirements.

#### **7.3.4. U-TRU-fuelled SFR**

FRs have a more favourable neutron spectrum for fission of MAs, and for SFRs the use of stainless steel cladding enables fuel with higher discharge burn-up. Hence they can be expected to have a superior fuel cycle performance, although this may be offset by higher reactor costs and arguably reduced technological maturity. SFRs with conversion ratios from 0.0 to 1.0 have been proposed (Hoffman et al., 2006), so the incineration rate is to some extent flexible, although safety parameters generally get worse with higher TRU loading. A 1000 MWth oxide-fuelled SFR design based on the Toshiba-Westinghouse ARR (Dobson, 2008) is considered here. The fuel contains 38.1% TRU loading, from (Franceschini et al., 2013), leading to a TRU incineration rate of 198 kg/GWthyr.

As fuel that does not contain MAs does not have to be fabricated remotely, it is assumed that MAs are loaded into heterogeneous blankets containing 20% MAs (Franceschini et al., 2014). The remaining fuel is U-Pu, which can be fabricated in glove boxes. This greatly reduces remote fabrication requirements. In this case, only 11% of the fuel needs to be fabricated remotely.

#### **7.3.5. Th-TRU-fuelled SFR**

In SFRs, use of Th fuel improves coolant expansion and void reactivity coefficients, which in a burner design can allow the maximum TRU incineration rate to be increased (Fiorina et al., 2013c). An oxide-fuel design is considered with 44.9% TRU loading, from (Franceschini et al., 2013), leading to a TRU incineration rate of 225 kg/GWthyr. As with Case B6, it is possible to use Th-U3-MA and Th-Pu fuel to limit remote fuel fabrication requirements. Due to the relatively high TRU loading in the core, only ~25% of the fuel is Th-U3-MA. In SFRs, the neutron migration length is substantially greater than the pin pitch, such that a micro-heterogeneous pin layout will have virtually the same neutronic performance as homogeneous fuel.

#### **7.3.6. Fuel Cycle Performance**

Incineration performance is summarised in Table 7.5. The support ratio for CORAIL and CONFU is defined as the ratio of TRU-bearing pins to LEU pins. The mass of inert matrix fuel to be reprocessed and fabricated is calculated assuming the fuel has the same density as LEU. This is to prevent crediting lower density pins as being less demanding to reprocess or fabricate, as the volume of material and number of pins are the same. Both the CORAIL and CONFU designs consider 7 years between recycles, which penalises these designs slightly compared to the Th-fuelled cases.

The U-fuelled RBWR burns ~5 kg/t reprocessed less than the best Th-fuelled cases due to its lower discharge burn-up. However, the incineration rate is higher than many of the Th-fuelled RBWR cases (~140 kg/GWthyr).

The CORAIL design has high fuel reprocessing requirements due to the large LEU burn-up penalty. The remote fuel fabrication requirement is also slightly higher than most of the Th-fuelled RMPWR designs, as either the incineration rate in the U-TRU pins is lower than the RMPWR, or the rate at which TRU is produced in the LEU pins (in kg/GWthyr) is higher than in conventional LEU designs. This design has the advantage, of course, of not requiring fabrication and reprocessing of Th-U3 fuels.

**Table 7.5.** <sup>238</sup>U and inert matrix fuel performance in LWRs.

Case	Burn-up (GWd/t)	kg burned/t reprocessed	kg burned/t fabricated remotely	Support ratio (GWth/GWth)
U-fuelled RBWR	65.0	25.2	25.2	0.64
CORAIL	45.0	12.7*	19.0	0.50
CONFU	52.6	31.7*	53.3	0.22
U-fuelled SFR	110.0	59.6	542	0.45
Th-fuelled SFR	118.0	72.7	661	0.41

\* Includes additional reprocessing from lower LEU discharge burn-up

The CONFU design allows a large reduction in remote fuel fabrication requirements due to the concentration of TRU in a small number of pins. This is reflected in the low support ratio. Despite the reduction in LEU burn-up, the reprocessing requirements are also competitive with the best Th-fuelled RBWR designs. This is due to the high incineration rate that is achieved in the TRU-bearing pins. Reprocessing of additional LEU fuels is also likely to be more straightforward than reprocessing multi-recycled fuels. Use of inert matrix pins in conventional PWRs therefore provides an attractive alternative to Th-fuelled RMPWRs or RBWRs, although any advantage depends on limiting the cost of reprocessing and remotely fabricating inert matrix pins.

SFRs have a higher thermal efficiency than LWRs, can achieve a significantly higher discharge burn-up and can also achieve a relatively high incineration rate. Heterogeneous fuel utilization is possible, leading to relatively low remote fuel fabrication requirements. These factors lead to much superior fuel cycle performance and a relatively low support ratio.

#### 7.4. Economics

As discussed above, SFRs have a much superior fuel cycle performance than LWR-based incineration schemes. However, SFRs are generally considered to cost ~25% more per GW<sub>e</sub>yr than LWRs of the same rating (which is assumed here). Delene et al. (1999) and Crette (1998) consider 10–20% but this is thought to be a relatively generous estimate.<sup>31</sup> The least expensive option will depend on the relative reprocessing, fuel fabrication and plant capital costs. As plant capital costs typically dominate, relatively small differences in plant capital cost may offset or negate the much larger differences in reprocessing and fuel fabrication throughput. It must be noted that plant capital costs are difficult to predict (Maloney and Diaconu, 2003).

RBWRs are anticipated to be more expensive than conventional LWRs and RMPWRs if a larger pressure vessel is needed. The 720 assembly core considered in Chapter 6 has an area ~50% greater than an ABWR, which would require a larger pressure vessel. An RBWR which can fit into an ABWR pressure vessel is found to be economically attractive (see also (Lindley et al., 2013g) and (Franceschini et al, 2014)). This leads to the selection of a 480 assembly, 200 cm core, using the fuel configuration from Case B6 to reduce the amount of remote fuel fabrication required as the least cost RBWR design. Use of TCUP fuel is also an option. This reduces the number of RBWRs required but necessitates more remote fuel fabrication. Provided the core can fit into an ABWR pressure vessel and the burn-up is limited by cladding to ~80 GWd/t, the B6 fuel design is slightly cheaper than the TCUP fuel design (e.g. Case B3). Use of stainless steel cladding is worth considering, as in the hard spectrum of the RBWR the reactivity penalty is limited to around 2000 pcm. This would allow improved accident performance and discharge burn-up, provided that sufficient TRU can be safely loaded in the core to compensate for neutron capture in the stainless steel.

The economics analysis assumptions and results are summarized in Table 7.6 and Table 7.7 respectively, although these are subject to a large degree of uncertainty. The RMPWR has higher fuel cycle costs because its low discharge burn-up leads to high reprocessing and remote fuel fabrication requirements. The U-SFR and Th-SFR are both substantially more expensive than the RBWR due to lower assumed SFR capacity factor (85% compared to 95% for LWRs) and the higher capital costs. Single- and multi-tier fuel cycles have similar performance. All options are substantially more expensive than the reference once-through cycle in LWRs.

The higher LEU enrichment required for the CONFU and CORAIL designs increases the LEU fuel cost. The only additional assumption is that reprocessing of CONFU fuel costs the same as

---

<sup>31</sup> Private communication with Prof. Edward J. Lahoda, Jan 2014.

reprocessing of Th fuel as both require hydrofluoric acid for aqueous reprocessing. Th fuel reprocessing is considered to be 50% more expensive than U fuel reprocessing (IAEA, 2012).

CORAIL is relatively expensive due to its high reprocessing throughput but slightly cheaper than the RMPWR primarily due to lower remote fuel fabrication costs from higher discharge burn-up. CONFU is of comparable cost to the RBWR due to the relatively low number of pins that require remote fuel fabrication, although this is slightly balanced out by low discharge burn-up and higher LEU enrichment cost. Hence the lowest cost options utilize LWRs with either inert matrix or Th fuel.

**Table 7.6.** Economic analysis assumptions (see also (Franceschini et al., 2014)).

Reference LWR base capital cost	\$5000/kW for 1150 MWe plant
Reprocessing plant operating cost (includes capital pay off)	\$500/kg
Operating + plant reprocessing cost (includes capital pay off)	\$1380/kg (50% surcharge for thorium)
Remote fuel fabrication cost (includes capital pay off)	\$10000/kg
Glove-box fuel fabrication cost	\$2000/kg
LEU LWR finished UO <sub>2</sub> fuel cost	\$2300/kg (assumes ~\$50/lb U <sub>3</sub> O <sub>8</sub> , \$100/kg-SWU, \$12/kg conversion, \$200/kg fabrication, no financial charges)
Capital + Operations and Maintenance (O&M) (without fuel) cost (assumes 8% discount rate for 60 yr)	\$560M/GWeyr for LWR/RMLWR \$700M/GWeyr for SFR (+25%)
Capacity factor	95% LWR/RMLWR; 85% SFRs
Disposal cost: once-through (assumes ~100 GWeyr fleet for 60 yr)	\$100B; 2 mils/kWhr
Disposal cost: full recycle	50% of once-through cycle
Development costs	SFR: \$10B; RMLWRs: \$2B (Retrofit); Reprocessing \$5B (\$10B for Th); Remote fabrication: \$1B (\$2B for Th); Transmutation fuel: \$1B (\$2B for Th); Th-MOX \$200M

**Table 7.7.** Cost of different transmutation options (\$M/GWeyr).

	Once-through LEU	U-SFR (ST)	Th-SFR (ST)	RMPWR	RBWR (ST)	CORAIL	CONFU	U-SFR (MT)	Th-SFR (MT)	RBWR (MT)
Reprocessing	0	23	24	37	28	33	31	27	28	29
Hands-on fuel fabrication	48	30	31	33	24	39	38	29	33	25
Remote fuel fabrication	0	6	7	82	44	77	37	8	7	45
Glove-box fuel fabrication	0	6	4	0	5	0	0	9	6	5
Fleet capital, O&M	490	558	554	490	488	490	490	541	533	488
Development	0	13	15	9	9	5	7	13	15	9
Geological disposal	17	8	8	8	8	8	8	8	8	8
Total	555	645	644	659	606	651	611	636	630	610
Cost relative to once-through LEU	1.00	1.16	1.16	1.19	1.09	1.17	1.10	1.15	1.13	1.10

### 7.5. Repository Radiotoxicity and Decay Heat

In this section, repository loadings are calculated for the equilibrium fuel cycle. Single-tier fuel cycle cases are compared (P5 and B3 with a burn-up of 82.4 GWd/t). To assess the effect of utilizing a thermal spectrum reactor for TRU incineration, results are compared with the Th-fuelled SFR. Comparison with U-based incineration schemes is beyond the scope of this thesis and is the subject of numerous other studies – see for example (Fiorina, 2013). Radiotoxicity and decay heat calculations for the RMPWR and RBWR were performed using FISPIN with burn-up-dependent 1-group cross-sections for the key actinides provided by WIMS.

The radiotoxicity of actinides in the repository is calculated assuming 0.1% reprocessing losses, which is a typical assumption (OECD, 2006b),<sup>32</sup> using dose conversion factors from (ICRP, 1996), and normalized by GWeyr. A reference level radiotoxicity is adopted (as, for example, in (OECD, 2002)), which corresponds to the radiotoxicity of the natural U required to fuel a typical once-through LWR of the same electrical energy output. Daughter products from the decay of natural U are assumed to be at their equilibrium values. Using a European Pressurized Reactor (EPR) as the

<sup>32</sup> However, typical modern reprocessing cycles operate at around 1% reprocessing losses with losses occurring in: the head end (where the fuel is chopped up); the dissolver; the aqueous or pyrochemical separation of elements; and fabrication.

reference once-through LWR to determine natural U requirements, this results in a time-constant reference radiotoxicity level equal to  $5.9 \times 10^6$  Sv/GWeyr (Fiorina, 2013).

It must be emphasised that the relevance of equilibrium radiotoxicity calculations is questionable. Any real reactor fleet operates over a finite timeframe, resulting in a significant end-of-life inventory at the end of the nuclear programme. This inventory can dominate over radiotoxicity losses, such that actual repository radiotoxicity is much larger than the equilibrium radiotoxicity (Gregg and Hesketh, 2013). It is generally acknowledged that a repository is in any case required (OECD, 2006b). Also, while the heavy metal content in the repository dominates the radiotoxicity, this is by no means the only measure of repository loading or radiological hazard. The decay heat at time of loading and over the first few hundred years affects the repository size. Fission product isotopes (e.g. of I, Cs and Tc) are often the most mobile and hence form a large part of the radiological hazard (Lalieux et al., 2012; Nuclear Decommissioning Authority, 2010). However, the equilibrium radiotoxicity is nevertheless presented here for comparative analysis.

The actinides discharged from the RMPWR have a higher radiotoxicity than the other implementations (Fig. 7.3). This is due to its high reprocessing requirements. The RBWR has comparable radiotoxicity to the SFR. In this case, the higher reprocessing requirements are mitigated by the lower TRU loading in the core.

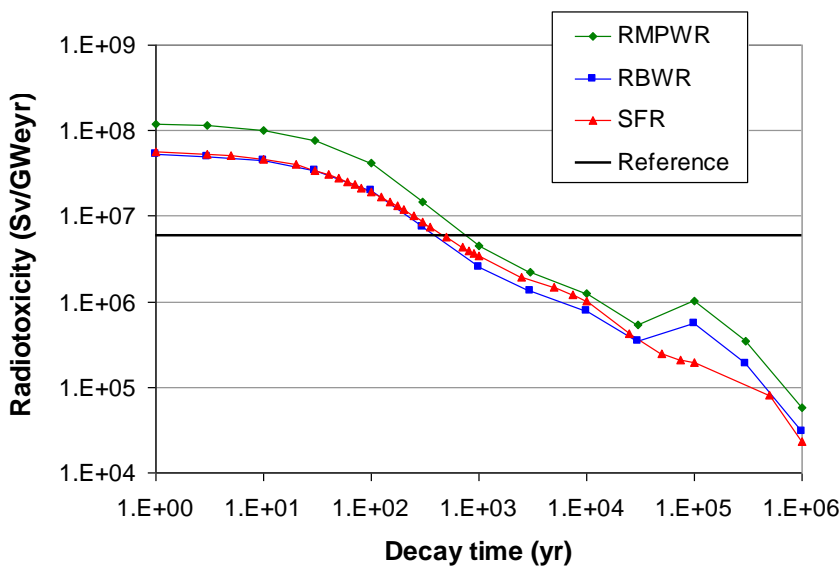


**Fig. 7.3.** Radiotoxicity of actinides discharged from burner reactors.

The RMPWR and RBWR have lower incineration rates than the SFR and this contributes to their lower TRU loadings. It is therefore instructive to normalize the repository loading by the waste incineration rate (Fig. 7.4). The SFR performs best by this measure.

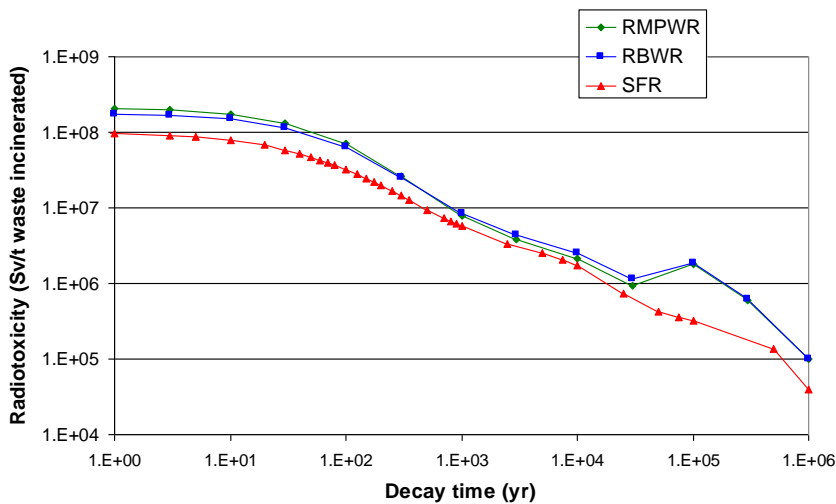


**Fig. 7.4.** Radiotoxicity of actinides discharged from burner reactors normalized by incineration rate.

To account for fuel utilization efficiency and incineration rate, it is best to normalize the radiotoxicity over the whole fuel cycle. An LEU-fuelled reactor produces  $\sim 90$  kg/GWthyr of TRU waste. 1 GWthyr of RMPWR, RBWR or SFR burner capacity therefore balances the TRU produced by 2.2 GWthyr, 1.5 GWthyr and 2.8 GWthyr LEU-fuelled reactor capacity respectively. The radiotoxicity and energy output of these LEU-fuelled reactors are now included.<sup>33</sup> This means summing the radiotoxicity of the losses from the LEU-fuelled reactor and the burner and normalizing by the total energy output from both. Fig. 7.5 gives the radiotoxicity averaged over the LEU and incineration stages of the fuel cycle. By this measure, the performances of the RBWR and SFR are very similar until  $\sim 30\,000$  years.

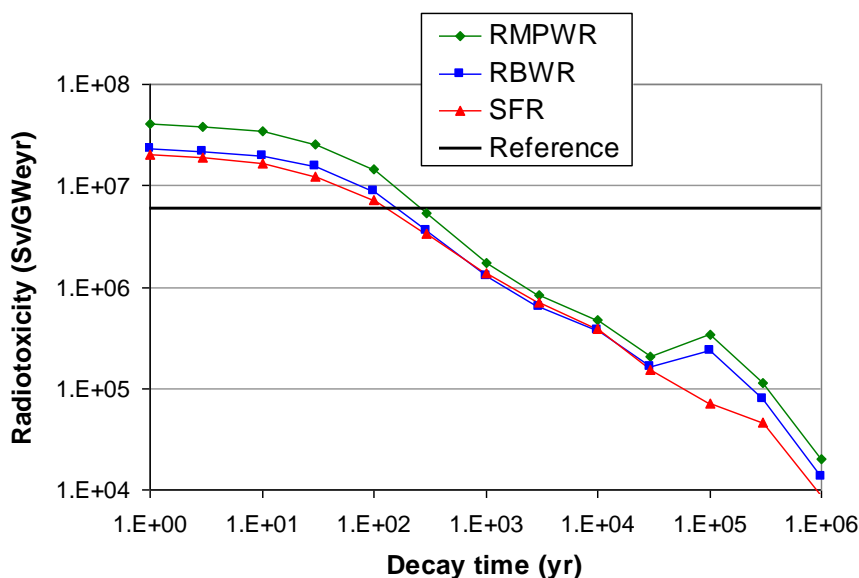


**Fig. 7.5.** Radiotoxicity of actinides discharged from burner reactors averaged over the fuel cycle.

<sup>33</sup> The radiotoxicity in Fig. 7.4 is therefore the average radiotoxicity for a full actinide recycle scenario based on LEU-fuelled LWRs and RMPWR, RBWR or SFR burners. However, this analysis is still valid for comparison between the burner reactors if only a proportion of the reactor fleet operates in this manner. These fuel cycle schemes are further discussed in (Franceschini et al., 2013).

The RBWR has a lower burn-up and higher conversion ratio than the SFR, increasing the RBWR reprocessing requirements. Reprocessed RBWR and SFR fuel has much higher radiotoxicity than LEU fuel. However, the SFR core has a higher TRU loading relative to its incineration rate, which acts to increase radiotoxicity and offsets the thermal efficiency and burn-up advantages of a SFR by this performance measure.

Over the whole fuel cycle, the RBWR and SFR actinide waste decays to the reference level in a little over 100 years. The RMPWR waste takes ~300 years to decay to the reference level, which still appears reasonable, although the limited validity of an equilibrium radiotoxicity analysis must again be stressed. The RMPWR radiotoxicity is in part limited by using different batch strategies for Th-TRU and Th-U3. The Th-TRU remains in the core for twice as long as the Th-U3, limiting the Th-TRU reprocessing requirement, which is responsible for the large majority of the decay heat.

The RMPWR results in much higher decay heat loading than the RBWR and SFR due to higher reprocessing throughput per unit electricity. This is  $\sim 1/3^{\text{rd}}$  lower than if the Th-TRU and Th-U3 fuel had the same discharge burn-up, because (as with radiotoxicity) the Th-TRU is responsible for a large majority of the decay heat. However, the RBWR has a lower decay heat than the SFR (Fig. 7.6). This is a result of the much lower TRU loading in the RBWR.

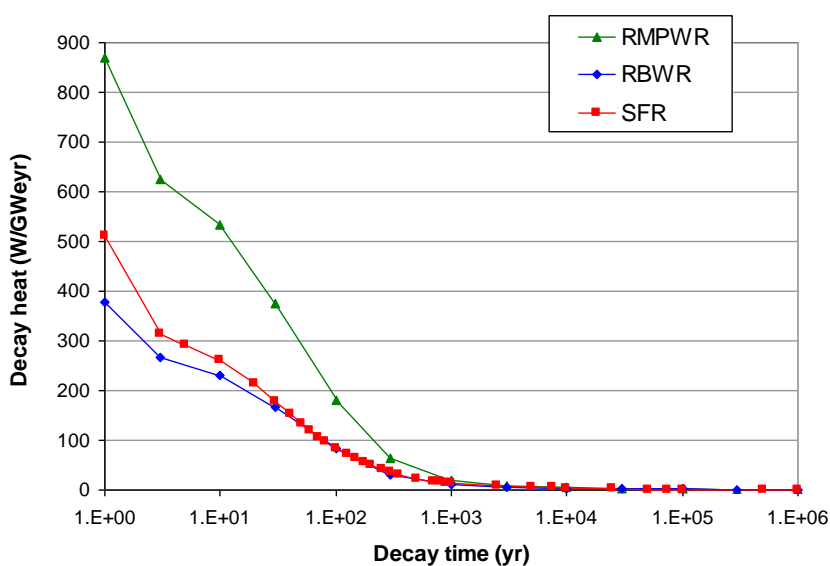


**Fig. 7.6.** Decay heat of actinides loaded in repository for burner reactors.

### 7.6. Decay Heat and Radiation Field Affecting Fuel Fabrication

The closed Th fuel cycle results in major challenges for fabrication and reprocessing technology. The most significant problem for fuel fabrication is the high-energy gamma emitters  $^{208}\text{Tl}$  and  $^{212}\text{Po}$  in the decay chain of  $^{232}\text{U}$ . This necessitates remote fuel fabrication. Similarly, a major obstacle to MA transmutation is the need to fabricate fuel remotely, primarily due to a large SN source and, to a lesser extent, gamma source. Therefore multi-recycle and burn of Pu with Th is economically

disadvantageous compared to using  $^{238}\text{U}$ , unless MA transmutation is also pursued, in which case there is relatively little disadvantage relative to using  $^{238}\text{U}$ , especially if a homogeneous recycle scheme is pursued. As discussed, for heterogeneous configurations, MA incineration in  $^{238}\text{U}$  systems greatly reduces remote fabrication requirements compared to Th. However, for RMPWRs, and RBWRs, use of U may be precluded, or greatly complicated, by MTC and VC constraints.

In this section, decay heat load, SN source and gamma field are all determined for the RMPWR and RBWR. As with the previous section, Cases P5 and B3 are considered. Comparison is again made with the Th-fuelled SFR to assess the difference between thermal and fast spectrum Th-fuelled reactors. Comparison with U-based incineration schemes is again beyond the scope of this thesis and is the subject of numerous other studies (e.g. (Fiorina, 2013)).

The inventories for various RMPWR and RBWR cases were calculated using FISPIN to assess the respective sources. Cross-sections of less significant actinides (e.g. higher than  $^{245}\text{Cm}$ ) were calculated assuming they were evenly distributed across the assembly. This is not accurate for the heterogeneous RMPWR and RBWR assemblies, where essentially all the TRU is in the Th-TRU pins. These isotopes are therefore within a significantly harder neutron spectrum than that assumed in the FISPIN calculation. Notably, this will lead to an overestimate in the SN source, which is acceptable as a conservative first approximation.

### 7.6.1. Decay Heat Load at Fabrication

The decay heat in W/GW<sub>th</sub> is, as in Fig. 7.6, multiplied by 1000 (i.e. without reprocessing losses). To evaluate the difficulty of handling fuel assemblies, it appears more relevant to consider the decay heat per unit mass and per assembly (noting that the RMPWR contains 193 assemblies, the RBWR 720 and the SFR 324, plus 90 blanket assemblies for the breeder, so there are large differences in the number of assemblies that need to be handled between reactors).

During fuel fabrication, the dominant decay heat contributions come from  $^{238}\text{Pu}$  and  $^{244}\text{Cm}$ . There is also a contribution from  $^{241}\text{Am}$ . The MA population in the reactor is dominated by the TRU loading rather than generation in situ – so the decay heat at fabrication is roughly proportional to the incineration rate (Table 7.8). The decay heat of a SFR assembly is substantially lower than the other assemblies due to the smaller mass.

**Table 7.8.** Decay heat load at fabrication.

	W/kg	kW/assembly	W/kg per (kg/GW <sub>th</sub> yr incinerated)
RMPWR	25.7	15.8	0.13
RBWR	19.6	4.1	0.14
SFR	42.7	1.2	0.17

### 7.6.2. Spontaneous Neutron Source

Table 7.9 gives the SN source at discharge. The value is highly dependent on the number of recycles, and takes a long time (> 25 recycles) to reach equilibrium, due to the very slow build-up of <sup>252</sup>Cf. 25 recycles were performed for the RMPWR and RBWR and 40 recycles for the SFR.<sup>34</sup>

**Table 7.9.** SN source at discharge.

	n/s/tiHM	n/s/GWeyr	n/s/fuel rod
RMPWR	$6.3 \times 10^{12}$	$1.1 \times 10^{14}$	$1.5 \times 10^{10}$
RBWR	$1.1 \times 10^{12}$	$1.4 \times 10^{13}$	$1.0 \times 10^9$
SFR	$1.9 \times 10^{11}$	$1.5 \times 10^{12}$	$2.1 \times 10^7$

The RMPWR and RBWR have much higher SN sources than the SFR due to the higher neutron capture cross-sections for TRU isotopes in a thermal neutron spectrum. <sup>252</sup>Cf dominates over a cooling time of up to 10 years, but <sup>250</sup>Cf and even-numbered isotopes of Cm also make a contribution. OECD (2002) reported neutron sources at fabrication of around  $10^{10}$  and  $10^{11}$  n/s/t for a fast breeder reactor and a fast TRU incinerator respectively – the latter being comparable with the Th-SFR figure reported in Table 7.9.

The SN source per tonne is likely to be most relevant for determining the cost of the fuel fabrication facility, as this affects the amount of shielding required. The RBWR SN source per GWeyr is ~5 times higher than the SFR due to the softer spectrum. Similarly, the RMPWR has a ~5 times higher source than the RBWR, again due to the softer spectrum. The shielding costs for the fuel loading area are roughly proportional to the n/s/fuel rod. In this case, the advantage for the SFR is increased by an order of magnitude as the fuel pins have a smaller radius.

For a thick concrete shield, the dose from the gamma source of a Th-fuelled FR can be more than an order of magnitude greater than the dose from the SN source (Wenner et al., 2012), so a significant increase in SN source can be allowed before it becomes the limiting factor. The SN values at fabrication over a realistic number of recycles are substantially larger than for the FR, but still within the range where <sup>232</sup>U is expected to be a comparable contributor to shielding requirements. Conversely, multiple thermal recycle with <sup>238</sup>U fuel also results in a large SN source which must be shielded (for all the pins which contain MAs), so use of <sup>232</sup>Th fuel with the additional gamma source may only result in a limited further increase to the fabrication difficulty. However, it must be

<sup>34</sup> 25 recycles corresponds to 100 effective full power years (EFPYs) for the RMPWR and 180 EFPYs for the RBWR. After 120 EFPYs (i.e. the same as the SFR), the SN source is expected to be ~10% higher and ~20% lower for the RMPWR and RBWR, respectively.

noted that neutron shielding is implemented differently to gamma shielding, such that an optimized shield for both SN and gammas may contain multiple materials of different thicknesses, and as such may be more complicated than shielding for either in isolation.

### 7.6.3. *Gamma Source*

Prompt fabrication after reprocessing reduces the  $^{208}\text{Tl}$  source as the intermediaries in the decay chain, notably  $^{228}\text{Th}$  with a half-life of 1.9 years, take time to re-accumulate via  $^{232}\text{U}$  decays. This is only true if Th is separated from U3, and the Th is left for several years before recycling while the  $^{228}\text{Th}$  component decays. The TRU content also makes a large contribution to the overall gamma source. While Th recycling is advisable to use fuel resources efficiently and limit spent fuel mass, it is appropriate to cool this for a longer period of time until  $^{228}\text{Th}$  and its daughters have decayed (e.g. (Franceschini et al., 2013)). The Th would then be suitable again for use in unshielded (yet glove-box) fresh fuel.

The data available for gamma source at fabrication for the SFR (see (Lindley et al., 2013g)) was calculated by cooling the fuel for 3 years, then reprocessing, removing all isotopes lighter than and including Th, and then analysing the gamma source for over the timeframe after the Th is removed. For consistency, the same scheme was adopted to evaluate the gamma source of the RMPWR and RBWR (despite the cooling time of 5 years generally assumed in this analysis).

The gamma source per unit mass of fuel is shown in Fig. 7.7. As with the SN source, this is indicative of the amount of shielding required in the fuel fabrication facility. The SFR has a much higher gamma source than the RMPWR and RBWR. Immediately after reprocessing, this is due to the higher TRU content of the fuel, notably of  $^{241}\text{Am}$  and  $^{244}\text{Cm}$ .  $^{238}\text{Pu}$  is also a significant gamma source. The faster rise is then due to a higher  $^{232}\text{U}$  population, which is a result of higher flux at very high neutron energies, leading to higher (n, 2n) reaction rates for  $^{232}\text{Th}$  and  $^{233}\text{U}$ , and thus more rapid production of the high-energy photon sources  $^{208}\text{Tl}$  and  $^{212}\text{Bi}$ .

In MeV/GWeyr terms, the RBWR source is still slightly lower than the SFR (despite the lower discharge burn-up and thermal efficiency), although the RMPWR source is substantially higher (Fig. 7.8).

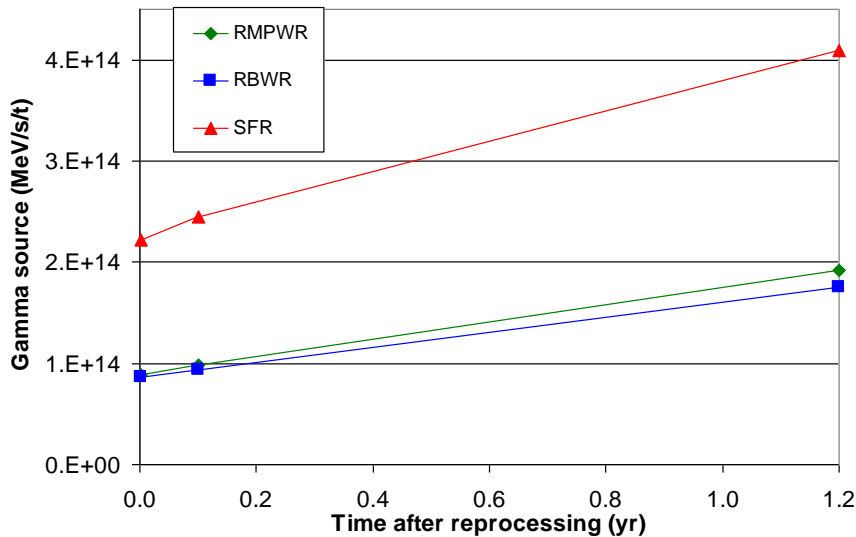


Fig. 7.7. Gamma source per unit fuel mass after Th removal.

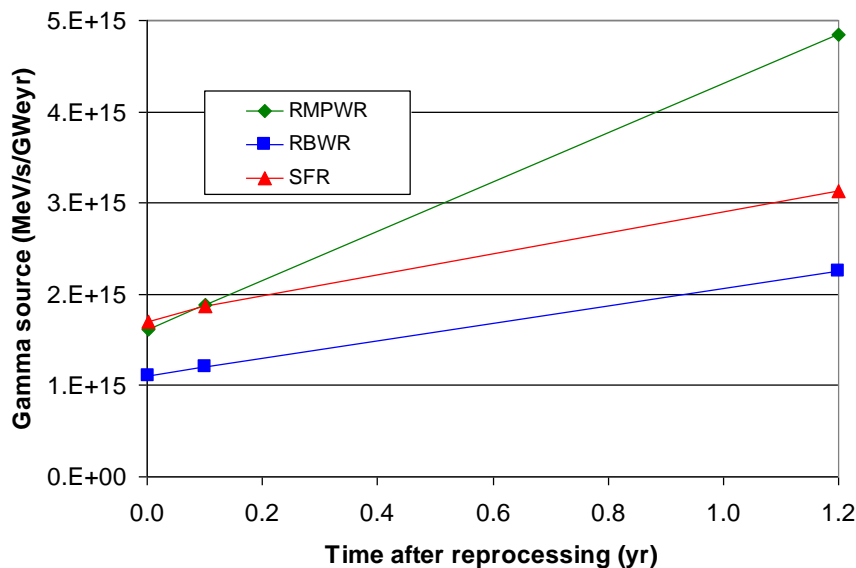


Fig. 7.8. Gamma source per unit energy production after Th removal.

### 7.7. Concluding Remarks

Neutronically,  $^{232}\text{Th}$  is a far superior carrier to  $^{238}\text{U}$  for this fuel cycle to the point of making it possibly the only practical option, at least for RMPWRs. However, the Th fuel cycle is much less technically mature than the U fuel cycle. Industrial reprocessing of Th irradiated fuel needs to be developed and appears more challenging than U-based fuel. Remote handling is required for multiple recycle of  $^{232}\text{Th}$ , which is required in any case for MA recycle, but relative amounts vary and are lower in U assuming heterogeneous recycle is acceptable and pursued.

RMPWRs have the advantage of a potentially relatively rapid first-stage implementation and intrinsically low conversion ratios, especially if the reduction in moderation occurs through a larger pin diameter. However, it is challenging to simultaneously satisfy operational and fuel cycle

constraints. A homogeneous fuel RMPWR requires a large reduction in moderation, which is not achievable in a retrofit plant design, and would require a very different core design. In a retrofit plant, intra-assembly fuel zoning is necessary to achieve an acceptable trade-off, and sufficiently reduced moderation may not be possible without a new plant design. The ZCR is positive, which leads to a need for additional RCCAs, and the RMPWR may have worse performance than the RBWR in beyond-design-basis accidents. The LOCA thermal-hydraulic response may not be satisfactory (Chapter 4), which would similarly disallow a retrofit core and, in addition, potentially require a larger, more expensive pressure vessel.

A RBWR may potentially take longer to implement than a RMPWR as a new plant is required, although much of the design is based on current technology. A RBWR has a lower incineration rate than a RMPWR. The harder neutron spectrum in a RBWR leads to more favourable fuel cycle performance. Homogeneous, micro-heterogeneous and macro-heterogeneous fuel configurations all have their merits.

A two-stage fuel cycle, where the first pass is Th-Pu MOX, is a technically reasonable implementation but is better suited to the RBWR than to the RMPWR. This strategy would reduce the number of reactors operating in RM mode, and delay and reduce the amount of fuel to be made remotely. Use of an unmodified PWR is reasonable, giving additional time for the RBWR to be designed and licensed. The first stage of the fuel cycle can therefore be implemented at relatively low cost as a Pu disposal option, maintaining flexibility for introducing a further policy option of full recycle in the medium term utilizing RBWRs, or potentially RMPWRs. This is a potential advantage of Th-Pu MOX over U-Pu MOX.

An economic analysis suggests that Th-fuelled RBWRs are cheaper than SFR-based recycling options, provided they can utilize the same size pressure vessel as an ABWR. RMPWRs and LEU/U-TRU PWRs (CORAIL) perform worse due to high reprocessing and fuel fabrication requirements. A LEU/TRU inert matrix PWR (CONFU) is of comparable cost to the RBWR, with the relative merits of these schemes likely to depend on the relative costs of Th-U3 and inert matrix fuel fabrication and reprocessing. The much lower reprocessing and fuel fabrication requirements of SFRs are likely offset by a higher plant capital cost and lower availability factor

A RBWR has higher reprocessing and fuel fabrication requirements than a Th-fuelled SFR, but has a comparable radiotoxicity, decay heat and radiation field, while the RMPWR is less competitive in these aspects.

## **Chapter 8 – Conclusions**

With sufficiently reduced moderation, a Th-fuelled LWR can operate on full TRU recycle while burning an external supply of TRU, e.g. recovered from reprocessing used fuel discharged from once-through LWR operation. A Westinghouse 17x17 PWR assembly with 12.6 mm pin pitch can achieve sufficiently low moderation to perform full TRU recycle if the pin diameter is increased from 9.5 mm to 11–11.5 mm. This requires fuel of 95% TD to sufficiently reduce the H/HM ratio. However, a RBWR has a sufficiently fast neutron spectrum to comfortably maintain a high burn-up equilibrium fuel cycle even with homogeneous 85% TD fuel. This is not possible if  $^{238}\text{U}$  is used as a fertile isotope.

In reduced-moderation or hard-spectrum LWRs, full recycle of TRU is limited by coolant reactivity feedback. Use of  $^{232}\text{Th}$  instead of  $^{238}\text{U}$  as a fertile isotope improves the MDC, and therefore yields superior performance. This is essentially due to the high resonance  $\eta$  of U3, which increases the fissibility of the U3-TRU isotope vector in the Th-fuelled system relative to the U-fuelled system, and also improves the MDC when the spectrum is sufficiently hard (e.g. RMPWR and, even more so, RBWR). While direct substitution of  $^{238}\text{U}$  with  $^{232}\text{Th}$  improves the MDC, it also increases the required fissile loading, such that the benefits of using  $^{232}\text{Th}$  are essentially “indirect”, e.g. by breeding U3. The reduced fast fission threshold of  $^{232}\text{Th}$  compared to  $^{238}\text{U}$  improves the MDC, but also makes the neutron economy worse, as does the higher thermal capture cross-section. The resonance capture cross-sections of  $^{232}\text{Th}$  and  $^{238}\text{U}$  are similar. The performance difference between Th- and U-fuelled systems increases with reduced moderation due to higher U3 breeding, and an increasingly beneficial effect from U3 on the MDC.

Spatial separation of TRU and U3 is possible in the Th-fuelled system, which renders further improvement by hardening the neutron spectrum in the TRU-bearing pins and softening it in the U3-bearing pins. This improves the neutron economy by increasing the TRU  $\eta$ , as well as the MDC performance by enhancing the thermal fission reduction upon voiding in U3. In particular, this fuel design is necessary for the 11 mm pin diameter RMPWR design to be neutronicly feasible. It is also possible to manage the Th-TRU and Th-U3 pins on different batch management schemes.

For the RMPWR with 11 mm pin diameter design, the thermal-hydraulic MDNBR and  $T_{\text{out}}$  constraints can be satisfied. This may require dropping  $T_{\text{in}}$  slightly, but this is thought to be acceptable. For the 11.5 mm pin diameter design, a 5 K drop in  $T_{\text{in}}$  and a ‘tight’ wire wrap ( $H/D = 14$ ) are required to satisfy the thermal-hydraulic constraints.

However, experimental evidence and analytical calculations seem to indicate that a retrofit RMPWR core will have reduced margin, or even no margin, from LOCA licensing limits if

compared to the reference core design. This needs to be confirmed through computational analysis and, ultimately, experimental tests. If proven to be the case, retrofitting a typical PWR core with a RM core would be feasible only after either de-rating the plant or switching to a cladding material with better LOCA performance than Zr-based alloys. Another solution, preferable for optimizing the overall reactor performance, but incompatible with the retrofit approach investigated in this study, would be to design a shorter but wider core, so that the total core power could be preserved while lowering the axial hot spot and, eventually, reducing the linear power. This would increase the reactor capital cost.

For a RMPWR with a standard 4-loop 193 assembly core with a 17×17 assembly, 12.6 mm pin pitch and pin diameter increased from 9.5 mm to 11 mm, a core with negative MTC and FVR has been designed. However, the ZCR is substantially positive, which could result in positive reactivity in a LBLOCA without trip. This may make the reactor more difficult to license, and necessitate a second, redundant set of shutdown rods, which may disallow a retrofit core.

A cycle length of 1 year is possible with an average fuel discharge burn-up of ~40 GWd/t. A single-tier fuel cycle is preferred for the RMPWR. An adequate SDM can be achieved with the TPUC or WATU fuel management schemes, but highly enriched B<sub>4</sub>C rods are required. Higher boron enrichment is required with the TPUC scheme. With integral BPs in the fuel, the reactivity swing over the cycle is under 2000 pcm. It appears possible to use mechanical shim while maintaining adequate core power peaking, particularly with the TPUC scheme. This is necessary as use of soluble boron for reactivity control should be avoided entirely due to its ineffectiveness at the RMPWR spectral conditions and its tendency to make the MTC and FVR positive. The fuel enthalpy deposition in a REA is higher than in conventional PWRs, but within typical licensing limits.

The RBWR is capable of achieving a high average discharge burn-up with a negative VC. The VC and DC values are sensitive to how they are calculated, so there is some uncertainty as to their exact magnitudes. A higher discharge burn-up is possible with a taller core although a higher TRU incineration rate is generally possible with a shorter core. A waste reload fraction of 35% appears possible when utilizing a TCUP assembly, with good performance achievable with single- or multi-tier fuel cycles. Due to the use of axially homogeneous fuel, it is possible to achieve a sufficient MCPR with a higher power density than the JAEA RMWR design (with the same fuel assembly configuration). The MCPR is particularly good for tall cores, and it appears possible to maintain the core area and rating of an existing ABWR which is a major economic advantage. However, power peaking within the assembly may be higher if TCUP or micro-heterogeneous Th-U3-MA/Th-Pu fuel is utilized. A 3D pincell analysis indicated little motivation to pursue further investigation of

axially heterogeneous fuel, especially given that this greatly increases the difficulty of remote fuel fabrication.

Neutronically,  $^{232}\text{Th}$  is a far superior carrier to  $^{238}\text{U}$  for this fuel cycle to the point of making it possibly the only practical option, at least for RMPWRs. However, the Th fuel cycle is much less technically mature than the U fuel cycle. Industrial reprocessing of Th irradiated fuel needs to be developed and appears more challenging than U-based fuel. Remote handling is required for multiple recycle of  $^{232}\text{Th}$ , which is required in any case for MA recycle, but relative amounts vary and are lower in U, assuming heterogeneous recycle is acceptable and pursued.

RMPWRs have the advantage of a potentially relatively rapid first-stage implementation and intrinsically low conversion ratios, especially if the reduction in moderation occurs through a larger pin diameter. However, it is challenging to simultaneously satisfy operational and fuel cycle constraints. A homogeneous fuel RMPWR requires a large reduction in moderation, which is not achievable in a retrofit plant design, and would require a very different core design. In a retrofit plant, intra-assembly fuel zoning is necessary to achieve an acceptable trade-off, and sufficiently reduced moderation may not be possible without a new plant design.

An RBWR may potentially take longer to implement than a RMPWR as the design is a more radical departure from existing plants. A new plant may be required, although much of the design is based on current technology. Provided the core area is limited to that of an ABWR, the plant capital cost should be comparable to LWRs and RMPWRs.

The harder neutron spectrum of a RBWR leads to more favourable fuel cycle performance. Micro-heterogeneous and macro-heterogeneous fuel configurations both have their merits. RMPWR and RBWR options have lower reprocessing and fuel fabrication requirements than the CORAIL assembly, but this advantage may be offset by the cost of reprocessing and fabricating Th-U3 fuel. The reprocessing throughput of the RBWR is generally similar to CONFU, but the remote fuel fabrication requirement is somewhat higher. The relative merits of these schemes will depend upon the relative costs of the Th-U3 and inert matrix fuel reprocessing and fabrication.

An RBWR has higher reprocessing and fuel fabrication requirements than a SFR, but has a comparable radiotoxicity, decay heat and radiation field. The RMPWR is less competitive in all aspects. SFRs are likely to have higher plant capital cost, which offsets their fuel cycle performance advantage.

A preliminary economic study suggests that Th-fuelled RBWRs are cheaper than SFR based recycling options. CONFU is of comparable cost to RBWRs. CORAIL and RMPWRs perform worse due to high reprocessing and fuel fabrication requirements.

A two-stage fuel cycle, where the first pass is Th-Pu MOX, is a technically reasonable implementation but is better suited to the RBWR than to the RMPWR. This strategy would reduce the number of reactors operating in RM mode, and delay and reduce the amount of fuel to be made remotely. Use of an unmodified PWR is reasonable, giving additional time for the RBWR to be designed and licensed. The first stage of the fuel cycle can therefore be implemented at relatively low cost as a Pu disposal option, maintaining flexibility for introducing a further policy option of full recycle in the medium term utilizing RBWRs, or potentially RMPWRs. These are some of the potential advantages of Th-Pu MOX over U MOX. Single- and multi-tier options have similar economic performance.

## **8.1. Recommendations for Future Work**

### ***8.1.1. Fuel Cycle Modelling***

The scope of this thesis is limited by the almost universal consideration of a single TRU waste feed vector, notably with fixed cooling times before loading and between recycles. The effect of varying both of these cooling times should be investigated. It is noted from Chapter 3 that a short (1 yr) cooling time may allow full recycle in a conventional PWR at a significantly higher incineration rate (although it may not be possible to design for acceptable FVR/ZCR in this case), and from Chapter 6 that increasing the TRU cooling time after the UO<sub>2</sub> fuel is discharged has a detrimental but acceptable impact on performance. However, the incineration of legacy stockpiles requires handling large cooling times, and the results of Chapters 2 and 5 suggest that the RMPWR will not be feasible if cooling times are more demanding.

### ***8.1.2. RMPWR Thermal-hydraulic Analysis***

Only a simple RMPWR LBLOCA analysis has been performed due to the lack of availability of a thermal-hydraulic code which can model RMPWRs. As this appears to be the limiting condition, a full LBLOCA analysis should be undertaken if possible. If thermal-hydraulic limits on clad temperature and oxidation are indeed exceeded for an LBLOCA scenario, this could motivate consideration of an alternative cladding material such as SiC (although stainless steel will almost certainly incur too high a reactivity penalty in this case). Coupled neutronic-thermal-hydraulic modelling is necessary to determine whether positive reactivity can occur during a LBLOCA. The results of this may guide further core analysis, e.g. of a non-retrofit core design. The transient response to other coolant-related accidents will also be affected by different kinetic properties (e.g. reduced neutron lifetime, reduced DNF) and lower coolant inventory and these should also be considered (e.g. main steam line break, anticipated transient without scram).

### ***8.1.3. RMPWR Full-core Modelling***

The neutronic methodology used here could be improved in further analysis, in particular to use more energy groups, and for the WATU concept use of assembly discontinuity factors is necessary to achieve accurate results. As the fuel assembly geometry and fuel management scheme have now been derived, it is recommended that the equilibrium cycle is re-analysed with a hyperfine group Monte Carlo lattice calculation and a multi-group core calculation. This is computationally expensive, but may be acceptable as now only a single lattice design needs to be analysed in this manner. Combined CRP/LP optimization is recommended to see if it is generally possible to achieve acceptable power peaking factors with use of mechanical shim. This must include the consideration of pin-level power peaking, especially given the complications introduced by heterogeneous fuel design and rod shadowing effects. Further analysis is needed on re-tuning of the control and safety systems. In particular, transient analysis is necessary to evaluate the performance with bank switching maneuvers over core life. The response of the core to accident scenarios needs to be evaluated, in particular due to the positive ZCR, and much lower DNF and neutron lifetime than in conventional PWRs.

### ***8.1.4. RBWR Full-core Modelling***

As with the RMPWR, it may be advisable to re-analyse the ‘optimal’ equilibrium core with a hyperfine energy group Monte Carlo lattice calculation. The thermal-hydraulic modeling could also be improved by using a steady state code rather than a ‘time marching’ code to improve convergence and reduce computational cost. Also, response of the reactor to transients and accidents needs to be investigated. Consideration of core dynamics and stability is also necessary, particularly as the core properties are somewhat different to U-Pu RBWR designs. Notably, the core height is higher in some considered designs, and the VC is expected to be somewhat more negative. This is likely to result in a higher positive reactivity in overcooling transients, and make it more difficult to control during cold shutdown. The likely solution is inclusion of a larger number of control rods, which appears feasible. Also as with the RMPWR, pin-level power peaking also needs to be considered, to confirm that it can be kept within the limits identified by the MCPR constraint.

### ***8.1.5. Time-dependent Fuel Cycle Analysis***

The models considered here are mostly ‘steady state’ scenarios, i.e. an assumption of equilibrium is made. While this is useful for a feasibility study, the fuel cycle takes a very long time to reach equilibrium. The evolution of neutronic and fuel cycle performance over time should be evaluated.

### **8.1.6. Fuel Performance Analysis**

The fuels proposed in this thesis are variably  $(\text{Th,U3})\text{O}_2$ ,  $(\text{Th,Pu})\text{O}_2$ ,  $(\text{Th,Pu,MA})\text{O}_2$  and  $(\text{Th,U3,MA})\text{O}_2$ . All of these represent a significant departure from currently used fuels. Moreover, different pellet sizes and high burn-up designs are also advocated. The fuel and cladding performance need to be investigated using a fuel performance code. The availability of codes which can model these fuels is currently limited or non-existent<sup>35</sup> but it should be considered for future work. Zircaloy cladding performance in a relatively hard neutron spectrum has been identified as a concern, and in the case of the RBWR this is exacerbated by the desire to extend the burn-up of the fuel to at least ~80 GWd/t. This may motivate future consideration of 310 stainless steel clad as an alternative. In the hard neutron spectrum of the RBWR, the reactivity penalty is ~2000 pcm. From the results of Chapter 6, a high discharge burn-up appears possible, even with the reactivity penalty.

### **8.1.7. UK-specific Study**

This thesis has outlined a multi-tier fuel cycle where the first stage is a single Th-Pu MOX pass in a conventional PWR, followed by full recycle in a RBWR. This is of particular relevance to the UK, which possesses a stockpile of separated plutonium (Pu) in excess of 100 tonnes. This represents a storage liability and a proliferation risk. Pu management options include continued long-term storage, disposal in a long-term repository, and reuse as nuclear fuel (NDA, 2011). (King, 2011) concluded that using the Pu in mixed-oxide fuel (MOX) was economically favourable, and that further UK nuclear fuel reprocessing could also be economically viable given the right conditions, although this increased commercial risk.

Much superior operational experience is available for U-MOX fuel, which means further materials tests are needed before Th-Pu MOX could be deployed (Kelly and Franceschini, 2013). Experimental programs on Th-based fuels are also described in (Thor Energy, 2010; Schram and Klaassen, 2007; IAEA, 2012). Th-Pu MOX is the most credible near-term use of Th fuel in the UK. NNL (2010) concluded that “The thorium fuel cycle does not currently have a role to play in the UK context, other than its potential application for plutonium management in the longer term.”

As discussed, Th-Pu MOX is a credible single-pass strategy, which allows a decision on full TRU recycle to be delayed. In the case of the UK, no further reprocessing is necessary to perform the first stage of the multi-tier recycle strategy outlined in this thesis.

---

<sup>35</sup> Private communication with Dr Glyn Rossiter, National Nuclear Laboratory, Mar 2013

## **References**

- Abram, T., Ion, S., 2008. Generation IV nuclear power: A review of the state of the science. *Energy Policy* 36 pp. 4323-4330.
- Ahmad, A., Sheehy, S. L., Parks, G. T., 2012. The effect of beam interruptions on the integrity of ADSR fuel pin cladding: a thermo-mechanical analysis. *Annals of Nuclear Energy* 46 pp. 97-105.
- ANS. American Nuclear Society Position Statement 74, 2005.  
<http://www.new.ans.org/pi/ps/docs/ps74.pdf> Accessed 28/2/12.
- Answers, 2001. MONK. A Monte Carlo program for nuclear criticality safety and reactor physics analyses. User Guide for Version 9, ANSWERS/MONK/REPORT/005, SERCO, Winfrith, United Kingdom.
- Answers, 2004. WIMS. A modular scheme for neutronics calculations. User Guide for Version 9,” ANSWERS/WIMS(99)9, SERCO, Winfrith, United Kingdom.
- Answers, 2007. FISPIN for Nuclide Inventory Calculations. Introductory Guide to Version 10. ANSWERS/FISPIN/REPORT/001.
- AREVA/EDF, 2012. UK EPR PCSR – Sub-chapter 14.5 – Analyses of the PCC-4 events. UKEPR-0002-145 Issue 08
- Ashley, S. F., Parks, G. T., Nuttall, W. J., Boxall, C., Grimes, R. W., 2012. Nuclear energy: thorium fuel has risks. *Nature* 492 pp. 31-33.
- Bae, Y., Jang, J., Kim, H., Yoon, H., Kang, H., Bae, K., 2007. Research activities on a supercritical pressure water reactor in Korea. *Nuclear Engineering and Technology* 39 pp. 273-286.
- Baker Jr, L., Just, L. C., 1962. Studies of Metal-Water Reactions at High Temperatures. III. Experimental and theoretical studies of the zirconium-water reaction. Report ANL-6548, Argonne National Laboratory, Argonne, Illinois.
- Baldi, S., Porta, J., 2001. Elements of comparison between different inert matrix fuel as regards plutonium utilisation and safety coefficients. *Progress in Nuclear Energy* 38 pp. 375-8.
- Basile, D., Chierici, R., Beghi M., Salina, S., Brega, E., 1987 (revised 1999). COBRA-EN: An upgraded version of the COBRA-3C/MIT code for thermal-hydraulic transient analysis of light water reactor fuel assemblies and cores. Report No. 1010/1, ENEL SpA, Milan, Italy.
- Behar, C., 2013. French R&D program on SFR and the ASTRID prototype. In: Proc. IAEA International conference on fast reactors and related fuel cycles: safe technologies and sustainable scenarios (FR13), Paris, France, Mar 4-7, 2013.

- Bjork, K. I., Fhager, V., Demaziere, C., 2011. Comparison of thorium-based fuels with different fissile components in existing boiling water reactors. *Progress in Nuclear Energy* 53 pp. 618-625.
- Bonnerot, J-M., Pillon, S., Bejaoui, S., D'Agata, E., Hania, R., Herlet, N., Jankowiak, A., Auclair, M., Bendotti, S., Lambert, T., Valentin, B., 2010. Development program on minor actinide bearing blankets at CEA. In: Proc. 11<sup>th</sup> International Exchange Meeting on Partition and Transmutation, IEMPT 11, San Francisco, California, USA, Nov 1-4, 2010.
- Brossard, P., Abram, T. J., Petti, D., Sawa, K., Lee, Y. W., Fuetterer, M. A., 2009. The VHTR fuel and fuel cycle project: status of ongoing research and results. In: Proc. GIF Symposium, Paris, France, 9-10 Sep 2009.
- Bunn, M., Fetter, S., Holdren, J. P., van der Zwaan, B., 2003. The economics of reprocessing vs direct disposal of spent nuclear fuel. Belfer Center for Science and International Affairs, John F Kennedy School of Government, Harvard University.
- Cao, L., Oka, Y., Ishiwatari, Y., 2008. Fuel, core design and subchannel analysis of a superfast reactor. *Journal of Nuclear Science and Technology* 45 pp. 128-148.
- Cardin, M-A., Steer, S. J., Nuttall, W. J., Parks, G. T., Goncalves, L. V. N., de Neufville, R., 2012. Minimizing the economic cost and risk to accelerator-driven subcritical reactor technology. Part 2: The case of designing for flexibility. *Nuclear Engineering and Design* 243 pp. 120-134.
- Chang, H., Yang, Y., Jing, X., Xu, Y., 2006. Thorium-based fuel cycles in the modular high temperature reactor. *Tsinghua Science & Technology* 11 pp. 731-738.
- Cheng, S-K., Todreas, N. E., 1986. Hydrodynamic models and correlations for bare and wire-wrapped hexagonal rod bundles – bundle friction factors, subchannel friction factors and mixing parameters. *Nuclear Engineering and Design* 92 pp. 227-251.
- Chun, T-H., Oh, D-S., 1998. A pressure drop model for spacer grids with and without flow mixing vanes, *Journal of Nuclear Science and Technology* 35 pp. 508-510.
- Coates, D. J., Parks, G. T., 2011. Actinide breeding and reactivity variations in a thermal spectrum ADSR- Part 2: Enhanced sustainability in the thermal spectrum. *Annals of Nuclear Energy* 38 pp. 2132-2139.
- Courtaud, M., Deruaz, R., D'Aillon, L. G., 1988. The French thermal hydraulic program addressing the requirements of future Pressurized Water Reactors. *Nuclear Technology* 80 pp. 73-82.
- Cozzo, C., Staicu, D., Somers, J., Fernandez, A., Konings, R. J. M., 2011. Thermal diffusivity and conductivity of thorium-plutonium mixed oxides. *Journal of Nuclear Materials* 416 pp. 135-141.

Crette J. P., 1998. Review of the Western European breeder programs. *Energy* 23 pp. 581-591.

Csom, G., Reiss, T., Feher, S., Czifrus, S., 2012. Thorium as an alternative fuel for SCWRs. *Annals of Nuclear Energy* 41 pp. 67-78.

Cummins, W. E., Corletti, M. M., Schulz, T. L., 2003. Westinghouse AP1000 Advanced Passive Plant. In: Proc. Int. Congress Advances in Nuclear Power Plants (ICAPP '03), Cordoba, Spain, May 4-7 2003.

Dalle Donne, M., Hame, W., 1985. Critical heat flux correlation for triangular arrays of rod bundles with tight lattices, including the spiral spacer effect. *Nuclear Technology* 71 pp. 111-124.

DECC. Department of Energy & Climate Change, 2011. Management of the UK's plutonium stocks. A consultation response on the long-term management of UK-owned separated civil plutonium.

Delene, J. G., Sheffield, K. A., Reid, R. L., Hadley, S., 1999. An assessment of the economics of future electric power generation options and the implications for fusion. Oak Ridge National Laboratory ORNL/TM-1999-243.

Denman, M., LaChance, J., Sofu, T., Flanagan, G., Wigeland, R., Bari, R., 2012. Sodium fast reactor safety and licensing research plan – Volume I. Sandia National Laboratories report SAND2012-4260.

Devictor, N., Varaine, F., Marsault, P., Chenaud, M-S., Bernardin, B., Conti, A., Sciora, P., Venard, C., Fontaine, B., Martin, L., Mignot, G., 2012. Pre-conceptual design study of ASTRID core. In: Proc. IAEA technical meeting on innovative fast reactor designs with enhanced negative reactivity feedback features, Vienna, Austria, Feb 27-29, 2012.

Diamond, D. J., Bromley, B. P., Aronson, A. L., 2002. Studies of the Rod Ejection Accident in a PWR. Brookhaven National Laboratory, W-6382.

Dobson, A., 2008. GNEP deployment studies. Preliminary conceptual design studies. Technical report, Volume IV – Advanced recycling reactor.

Downar, T. J., Xu, Y., 2001. The utilisation of thorium fuel in a Generation IV light water reactor. In: Proc. Advanced Reactors with Innovative Fuels Workshop, Chester, UK.

Downar, T., Seker, V., Ward, A., Xu, Y., Collins, B., 2008. Thorium fuel performance in a boiling water reactor. Thomas J. Downar LLC. Chicago, Illinois.

Downar, T., Hall, A., Jabaay, D., Ward, A., Greenspan, E., Ganda, F., Bartoloni, F., Bergmann, R., Varela, C., DiSanzo, C., Kazimi, M., Shwageraus, E., Feng, B., Herman, B., 2012. Technical

evaluation of the Hitachi Resource-Renewable BWR (RBWR) Design Concept. Report Number 1025086, Electrical Power Research Institute, Palo-Alto, California.

Dreier, J., Analtsis, G., Chawla, R., 1988. NEPTUM-III reflooding and boiloff experiments with an LWHCR fuel bundle simulator: Experimental results and initial code assessment efforts. *Nuclear Technology* 80 pp. 93-106.

Driscoll, M. J., Downar, T. J., Pilat, E. E., 1990. The linear reactivity model for nuclear fuel management. American Nuclear Society, La Grange Park, Illinois.

Dziadosz, D., Ake, T. N., Saglam, M., Sapyta, J. J., 2004. Weapons-grade plutonium-thorium PWR assembly design and core safety analysis. *Nuclear Technology* 147 pp. 69-83.

Erbacher, J., Wiehr, K., 1988. Experimental investigation of the reflooding and deformation behavior of an advanced pressurized water reactor tight lattice fuel rod bundle in a loss-of-coolant accident. *Nuclear Technology* 80 pp. 153-160.

Feng, B., Ganda, F., 2013. Reducing the void coefficient of reactivity in high conversion water reactors. In: Proc. ICAPP 2013, Jeju Island, Korea, Apr 14-18, 2013.

Fennern, L. E., 2007. ABWR Seminar – Reactor, core & neutronics. GE Energy/ Nuclear Apr 13, 2007.

Fiorina, C., Krepel, J., Cammi, A., Franceschini, F., Mikityuk, K., Ricotti, M. E., 2013a. Analysis of thorium and uranium fuel cycles in an iso-breeder lead fast reactor using extended-EQL3D procedure. *Annals of Nuclear Energy* 53 pp. 492-506.

Fiorina, C., Franceschini, F., Mammot, M., 2013b. Safety aspects of Th-use in FRs. In: Proc. Int. Conf. on Fast Reactors and Related Fuel Cycles (FR13) Paris, France, Mar 4-7, 2013.

Fiorina, C., Stauf, N. E., Franceschini, F., Wenner, M. T., Stanculescu, A., Kim, T. K., Cammi, A., Ricotti, M. E., Hill, R. N., Taiwo T. A., Salvatores, M., 2013c. Comparative analysis of thorium and uranium for transuranic recycle in a sodium cooled fast reactor. *Annals of Nuclear Energy* 62 pp. 26-39.

Forsberg, C. W., 2007. Thermal- and fast-spectrum molten salt reactors for actinide burning and fuel production. In: Proc. Global 2007, Boise, Idaho, USA, Sep 9-13, 2007.

Forschungszentrum Juelich, 2008. RED IMPACT. Impact of partitioning, transmutation and waste reduction technologies on the final nuclear waste disposal. Synthesis report. ISBN 978-3-89336-538-8.

Franceschini, F., Petrovic, B., 2008. Advanced operational strategy for the IRIS reactor: load follow through Mechanical SHIM (MSHIM). *Nuclear Engineering and Design* 238 pp. 3240-52.

- Franceschini, F., Petrovic, B., 2009. A soluble boron-free core design for the IRIS-50. In: Proc. Int. Conf. American Nuclear Society 2013 Annual Meeting, Atlanta, USA, June 14-18, 2009.
- Franceschini, F., Lahoda, E., Carelli, M., Wenner, M., Ferroni, P., Fiorina, C., Sartori, A., Ricotti, M., Petrovioc, B., 2011. A comprehensive approach to waste management with thorium. In: Proc. Technical Meeting on World Thorium Resources, Thiruvananthapuram, India, Oct 17-21, 2011.
- Franceschini, F., Fiorina, C., Huang, M., Petrovic, B., Wenner, M., Krepel, J., 2012. Radiotoxicity characterization of multi-recycled thorium fuel – 12394. In: Proc. Waste Management Conference, Phoenix, Arizona, USA, Feb 26 - Mar 1, 2012.
- Franceschini, F., Lindley, B. A., Fiorina, C., Lahoda, E., Wenner, M., 2013. Promises and challenges of thorium implementation for transuranic transmutation – 13550. In: Proc. Waste Management Conference, Phoenix, Arizona, USA, Feb 24-28, 2013.
- Franceschini, F., Fiorina, C., Lindley, B. A., 2014. Evaluation of actinide recycle and burn in a multi-tier reactor system. Collaborative Research Project – Near term and promising long term options for deployment of thorium energy system, Milan, Italy, Apr 8-11, 2014.
- Frepoli, C., Ohkawa, K., Kemper, R. M., 2004. Realistic large break LOCA Analysis of AP1000 with ASTRUM. In: Proc. 6th Int. Conf. Nuclear Thermal Hydraulics, Operations and Safety (NUTHOS-6), Nara, Japan, Oct 4-8, 2004.
- Fridman, E., Kliem, S., 2011. Pu recycling in a full Th-MOX PWR core. Part I: Steady state analysis. Nuclear Engineering and Design 241 pp. 193-202.
- Fukaya, Y., Okubo, T., Uchikawa, S., 2008. Investigation on spent fuel characteristics of reduced-moderation water reactor. Nuclear Engineering and Design 238 pp. 1601-1611.
- Fukaya, Y., Nakano, Y., Okubo, T., 2009a. Study on high conversion type core of innovative water reactor for flexible fuel cycle (FLWR) for minor actinide (MA) recycling. Annals of Nuclear Energy 26 pp. 1374-1381.
- Fukaya, Y., Nakano, Y., Okubo, T., 2009b. Study on characteristics of void reactivity coefficients for high-conversion-type core of FLWR for MA recycling. Journal of Nuclear Science and Technology 46 pp. 819-830.
- Fyfitich, S., 2003. Alloy 600 PWSCC mitigation: Past, present, and future. In: Proc. Conf. Vessel Penetration Inspection, Crack Growth and Repair, Gaithersburg, Maryland, USA, Sep 29 - Oct 2, 2003.
- Galperin, A., 1995. Utilization of light water reactors for plutonium incineration. Annals of Nuclear Energy 22 pp. 507-511.

Ganda, F., Milosevic, M., Greenspan, E., Taiwo, T., 2007. TRITON/NEWT calculation of the CORAIL assembly for plutonium recycling in PWR. In: Proc. Joint International Topical Meeting on Mathematics & Computation and Supercomputing in Nuclear Applications (M&C + SNA 2007), Monterey, California, USA, Apr 15-19, 2007.

Ganda, F., Vujic, J., Greenspan, E., 2011. Thorium self sustaining BWR cores. In: Proc. ICAPP 2011, Nice, France, May 2-5, 2011.

Ganda, F., Arias, F. J., Vujic, J., Greenspan, E., 2012. Self-sustaining thorium boiling water reactors. *Sustainability* 2012 4 pp. 2472-2497.

GE Nuclear Energy, 1997. ABWR Design Control Document. Chapter 1. Introduction and General Description of Plant. US NRC Issued Design Certification – Advanced Boiling-Water Reactor (ABWR).

GE, 2011. GE Hitachi Nuclear Energy proposed to turn world's biggest civilian plutonium stockpile into electricity. <http://www.gereports.com/ge-hitachi-nuclear-energy-proposed-to-turn-worlds-biggest-civilian-plutonium-stockpile-into-electricity/> Accessed 28/2/12.

Ghrayeb, S., Ivanov, K., Levine, S., Puente-Espel, F., Loewen, E. P., 2009. Improving burnup performance of fast sodium cooled reactor by utilizing thorium based fuels. In: Proc. Int. Conf. Mathematics, Computational Methods and Reactor Physics (M&C 2009), Saratoga Springs, New York, USA, May 3-7, 2009.

Gorman, P. M, Zhang, G., Seifried, J. E., Varela, C. R., Vujic, J. L., Greenspan, E., 2014. The fuel-self-sustaining RBWR-Th core concept and parametric studies. In: Proc. ICAPP 2014, Charlotte, North Carolina, USA, Apr 6-9, 2014.

Gregg, R., Hesketh, K., 2013. The benefits of a fast reactor closed fuel cycle in the UK. In: Proc. Global 2013, Salt Lake City, Utah, USA, Sep 29 - Oct 3, 2013.

Hall, A., Xu, Y., Ward, A., Downar, T., Shirvan, K., Kazimi, M., 2013. Advanced neutronics methods for analysis of the RBWR-AC. In: Proc. Int. Conf. American Nuclear Society 2013 Annual Meeting, Atlanta, Georgia, USA, June 16-20, 2013.

Hall, A., Downar, T., Ward, A., Jarrett, M., Wsyocki, A., Xu, Y., Shirvan, K., 2014. Advanced methods development for equilibrium cycle calculations of the RBWR. In: Proc. ICAPP 2014, Charlotte, North Carolina, USA, Apr 6-9, 2014.

Hallstadius, L., Johnson, S., Lahoda, E., 2012. Cladding for high performance fuel. *Progress in Nuclear Energy* 57 pp. 71-76.

Hamase, E., Damian, F., Poinot-salanon, C., Saito, M., Sagara, H., Han, C. Y., 2013. A feasibility study on long-life reduced-moderation water reactor with highly protected Pu breeding by doping with minor actinides. *Annals of Nuclear Energy* 54 pp. 76-84.

Harris, A.D.H., 2013. Heavy water as a thorium breeder reactor coolant. MEng report, University of Cambridge (available on request).

Hecker, H. C., 1979. Summary of the Nuclear Design and Performance of the Light Water Breeder Reactor (LWBR). DOE Research and Development Report, WAPD-TM-1326.

Hejzlar, P., Todreas, N. E., Shwageraus, E., Nikiforova, A., Petroski, R., Driscoll, M. J., 2009. Cross-comparison of fast reactor concepts with various coolants. *Nuclear Engineering and Design* 239 pp. 2672-2691.

Hetric, D. L., 1993. Dynamics of Nuclear Reactors. Chapter 5, pp. 164–170. American Nuclear Society, La Grange Park, Illinois.

Hibi, K., Shimada, S., Okubo, T., Iwamura, T., Wada, S., 2001 Conceptual designing of reduced-moderation water reactor with heavy water coolant. *Nuclear Engineering and Design* 210 pp. 9-19.

Hiruta, H., Youinou, G., 2013. Preliminary neutronic study of D<sub>2</sub>O-cooled high conversion PWRs. In: Proc. Global 2013, Salt Lake City, USA.

Hoffman, E. A., Yang, W. S., Hill R. N., 2006. Preliminary core design studies for the advanced burner reactor over a wide range of conversion ratios. Argonne National Laboratory, ANL-AFCI-177.

Hu, R., 2010. Stability analysis of the boiling water reactor: methods and advanced designs. Massachusetts Institute of Technology PhD thesis.

Hutt, P. K, Gaines, N., Halsall, M. J., McEllin, M., White, R. J., 1991. The UK core performance package. *Nuclear Energy* 30 pp. 291-298.

Hyland, B., Collins, E. D., Ellis, R. J., Del Cul, G., Magill, M., 2011. Transmutation of americium in a lanthanide matrix. In: Proc. Global 2011, Nagoya, Japan, Dec 11-16, 2011.

IAEA, 2003. Potential of thorium based fuel cycles to constrain plutonium and reduce long lived waste toxicity. IAEA-TECDOC-1349, International Atomic Energy Agency, Vienna, Austria.

IAEA, 2004. Status of advanced light water reactor designs. IAEA-TECDOC-1391, International Atomic Energy Agency, Vienna, Austria.

IAEA, 2005a. Country nuclear fuel cycle profiles. Second edition. Technical reports series no. 425, International Atomic Energy Agency, Vienna, Austria.

IAEA, 2005b. Thorium fuel cycle – potential benefits and challenges. IAEA-TECDOC-1450, International Atomic Energy Agency, Vienna, Austria.

IAEA, 2006. Fast reactor database, 2006 update, IAEA-TECDOC-1531, International Atomic Energy Agency, Vienna, Austria.

IAEA, 2008. Spent fuel reprocessing options. IAEA-TECDOC-1587, International Atomic Energy Agency, Vienna, Austria.

IAEA, 2009. Status of minor actinide fuel development. Technical reports series no. NF-T-4.6, International Atomic Energy Agency, Vienna, Austria.

IAEA, 2012. Role of thorium to supplement fuel cycles of future nuclear energy systems. Technical reports series no. NF-T-2.4, International Atomic Energy Agency, Vienna, Austria.

ICRP (International Commission on Radiological Protection), 1996. ICRP Publication 72: Age dependent doses to the members of the public from intake of radionuclides Part 5, compilation of ingestion and inhalation coefficients. Annals of the ICRP 26/1.

Ignatiev, V., Feynberg, O., Gnidoi, I., Merzlyakov, A., Smirnov, V., Surenkov, A., Tretiakov, I., Zakirov, R., 2007. Progress in development of Li,Be,Na/F molten salt actinide recycle & transmuter concept. In: Proc. ICAPP 2007, Nice, France, May 13-18, 2007.

Ishikawa, N., Okubo, T., 2009. Analytical evaluation on dynamical response characteristics of reduced-moderation water reactor with tight-lattice core under natural circulation core cooling. Annals of Nuclear Energy 36 pp. 650-658.

Ito, K., Haiwaka, K., Maruyama, H., 1998. Top technologies of ABWR Part 2: BWR core and fuel technologies. Hitachi Review 47 pp. 168-175.

Kang, J., von Hippel, F. N., 2001. U-232 and the proliferation-resistance of U-233 in spent fuel. Science & Global Security 9 pp. 1-32.

Kawashima, M., Suzuki, M., Hill, R. N., 1992. A core design study for “zero-sodium-void-worth” cores. In: Proc. Int. Conf. Design and Safety of Advanced Nuclear Power Plants (ANP'92), Tokyo, Japan, Oct 25-29, 1992.

Kazimi, M. S., et al., 2010. MIT study on the future of the nuclear fuel cycle. Massachusetts Institute of Technology, MIT report series 1: 5-9.

Kelly, J. F., Franceschini, F., 2013. Imminent: irradiation testing of (Th, Pu) O<sub>2</sub> Fuel – 13560. In: Proc. Waste Management Conference, Phoenix, Arizona, USA, Feb 24-28, 2013.

- Kim, T. K., 2002. Assessment of CORAIL-Pu multi-recycle in PWRs. Argonne National Laboratory, ANL-AAA-018 2/28/2002.
- Kim, T. K., Downar, T. J., 2002. Thorium fuel performance in a tight-pitch light water reactor lattice. *Nuclear Technology* 138 pp. 17-29.
- Kim, T. K., Stillman, J. A., Taiwo, T. A., Hill, R. N., Finck, P. J., Salvatores, M., 2002. Assessment of transuranics stabilization in PWRs. In: Proc. PHYSOR 2002, Seoul, Korea, Oct 7-10, 2002.
- Kim, T. K., Wilson, P. P. H., Hu, P., Jain, R., 2004. Feasibility and configuration of a mixed spectrum supercritical water reactor. In: Proc. PHYSOR 2004, Chicago, Illinois, USA, Apr 25-29, 2004.
- Kim, T. K., Yang, W. S., Grandy, C., Hill, R. N., 2009. Core design studies for a 1000 MWth advanced burner reactor. *Annals of Nuclear Energy* 36 pp. 331-336.
- King, D., 2011. A low carbon nuclear future: Economic assessment of nuclear materials and spent nuclear fuel management in the UK. Smith School of Enterprise and the Environment, University of Oxford.
- Kozlowski, T., Miller, R. M., Downar, T. J., Barber, D. A., Joo, H. G., 2004. Consistent comparison of the codes RELAP5/PARCS and TRAC-M/PARCS for the OECD MSLB coupled code benchmark. *Nuclear Technology* 146, pp. 15-28.
- Knight, M., Bryce, P., Hall, S., 2013. WIMS/PANTHER analysis of UO<sub>2</sub>/MOX cores using embedded supercells. *Nuclear Technology* 183 pp. 398–408.
- Krepel, J., Hombourger, B., Mikityuk, K., 2013. Dependence of the thorium closed fuel cycle parameters on the moderation level of the molten salt reactor. In: Proc. ICAPP 2013, Jeju Island, Korea, Apr 14-18, 2013.
- Lalieux, P., Boulanger, D., Van Geet, M., 2012. Back-end requirements that need to be taken into account in the fuel design phase. In: Proc. Top Fuel 2012, Manchester, UK, Sep. 2-6, 2012.
- Leppänen, J., 2007. Development of a New Monte Carlo Reactor Physics Code, Helsinki University of Technology DSc thesis, VTT Publications 640.
- Lindley, B. A., Franceschini, F., Parks, G. T., 2013a. Void reactivity feedback analysis for U-based and Th-based LWR incineration cycles. In: Proc. Global 2013, Salt Lake City, Utah, USA, Sep 29 - Oct 3, 2013.

- Lindley, B. A., Zainuddin, N. Z., Franceschini, F., Parks, G. T., 2013b. Analysis of advanced PWR loading schemes for transuranic incineration in thorium. In: Proc. ICONE21, Chengdu, China, July 29 - Aug 2, 2013.
- Lindley, B. A., Drera, S. S., Kelly, J. F., Ashley, S. F., Parks, G. T., 2013c. An open-cycle RBWR concept utilizing LEU-Th seed blanket fuel. In: Proc. ICAPP 2013, Jeju Island, Korea, Apr 14-18, 2013.
- Lindley, B. A., Zainuddin, N. Z., Ferroni, P., Hall, A., Franceschini, F., Parks, G. T., 2014a. On the use of reduced-moderation LWRs for transuranic isotope burning in thorium fuel – Part I: Assembly analysis. *Nuclear Technology* 185 pp. 127-146.
- Lindley, B. A., Zainuddin, N. Z., Ferroni, P., Hall, A., Franceschini, F., Parks, G. T., 2014b. On the use of reduced-moderation LWRs for transuranic isotope burning in thorium fuel – Part II: Core analysis. *Nuclear Technology* 185 pp. 147-173.
- Lindley, B. A., Ahmad, A., Zainuddin, N. Z., Franceschini, F., Parks, G. T., 2014c. Steady-state and transient core feasibility analysis for a thorium-fuelled reduced-moderation PWR performing full transuranic recycle. *Annals of Nuclear Energy* 72 pp 320 -337.
- Lindley, B. A., Parks, G. T., 2014d. Axially homogeneous thorium fuel designs for transuranic burning in reduced-moderation BWRs. To be presented at: PHYSOR 2014, Kyoto, Japan, Sep 28 - Oct 3, 2014.
- Lindley, B. A., Parks, G. T., 2014e. Axially heterogeneous thorium fuel designs for transuranic burning in reduced-moderation BWRs. To be presented at: PHYSOR 2014, Kyoto, Japan, Sep 28 - Oct 3, 2014.
- Lindley, B. A., Franceschini, F., Parks, G. T., 2014f. The closed thorium-transuranic fuel cycle in reduced-moderation PWRs and BWRs. *Annals of Nuclear Energy* 63 pp. 241-264.
- Lindley, B. A., Fiorina, C., Franceschini, F., Lahoda, E. J., Parks, G. T., 2014g. Thorium breeder and burner fuel cycles in reduced-moderation LWRs compared to fast reactors. *Progress in Nuclear Energy* 77 pp. 107-123.
- Liu, W., Kureta, M., Yoshida, H., Ohnuki A., Akimoto, H., 2007. An improved critical power correlation for tight-lattice rod bundles. *Journal of Nuclear Science and Technology* 44 pp. 558-571.
- Liu, W., Ohnuki, A., Yoshida, H., Kureta, M., Takase, K., Akimoto, H., 2008. Thermal feasibility analyses for the 1326MWe high conversion-type innovative water reactor for flexible fuel cycle. *Heat Transfer Engineering* 29 pp. 704-711.

- Long, Y., Siefken, L. J., Hejzlar, P., Loewen, E. P., Hohorst, J. K., MacDonald, P. E., Kazimi, M. S., 2004. The behaviour of ThO<sub>2</sub>-based fuel rods during normal operation and transient events in LWRs. *Nuclear Technology* 147 pp. 120-139.
- Maloney, M.T., Diaconu, O., 2003. Minatom export control behaviour: Economic factors & motivations. cost analyses and methodology related to nuclear electric generation. Clemson University, Second report to Lawrence Livermore National Laboratories.  
<http://myweb.clemson.edu/~maloney/download/RussianNucs/CU-LLNL-DOE-report2.doc>  
Accessed 23/7/2013.
- Mieloszyk, A., Kazimi, M., 2014. Fuel performance analysis of a (ThU)O<sub>2</sub> fueled reduced moderation boiling water reactor. In: Proc. ICAPP 2014, Charlotte, North Carolina, USA, Apr 6-9, 2014.
- Mittag, S., Kliem, S., 2011. Burning plutonium and minimizing radioactive waste in existing PWRs. *Annals of Nuclear Energy* 38 pp. 98-102.
- Morrison, A., 2003. PANTHER User Guide, E/REP/BBDB/0015/GEN/03 ED/PANTHER/UG/5.5, British Energy, Barnwood, United Kingdom.
- Mukohara, T., Koshizuk, S-I., Oka, Y., 1999. Core design of a high-temperature fast reactor cooled by supercritical light water. *Annals of Nuclear Energy* 26 pp. 1423-1436.
- Nagy, K., 2012. Dynamics and fuel cycle analysis of a moderated molten salt reactor. PhD thesis, Delft University of Technology, The Netherlands.
- Nakano, Y., Okubo, T., Uchikawa, S., 2007. Conceptual design study of a 180 MWt small-sized reduced-moderation water reactor core. *Journal of Nuclear Science and Technology* 43 pp. 1471-1480.
- NDA. Nuclear Decommissioning Authority, 2011. Plutonium strategy, Current position paper, Feb 2011.
- NERI, 2002. Advanced proliferation resistant, lower cost, uranium-thorium dioxide fuels for light water reactors. Nuclear Energy Research Initiative, INEEL/EXT-02-01411. Progress report for work through Sept 2002.
- Newton, T., Hosking, G., Hutton, L., Powney, D., Turland, B., Shuttleworth, E., 2008. Developments within WIMS10. In: Proc. PHYSOR 2008, Interlaken, Switzerland, Sep 14-19, 2008.
- Nifenecker, H., David, S., Loiseaux, J. M., Meplan, O., 2001. Basics of accelerator driven subcritical reactors. *Nuclear Instruments and Methods in Physics Research A* 463 pp. 428-467.

NNL National Nuclear Laboratory, 2010. The thorium fuel cycle: An independent assessment by the UK National Nuclear Laboratory. Position paper, Aug 2010.

NNSA National Nuclear Security Administration, 2011. Fact sheet. NNSA's MOX fuel fabrication facility and U.S. plutonium disposition program. Feb 14 2011.  
<http://nnsa.energy.gov/mediaroom/factsheets/mox> Accessed 10/4/13

NRC, 2013, US NRC Regulations (10 CFR) Part 50 – Domestic licensing of production and utilization facilities. Section 50.46 Acceptance criteria for emergency core cooling systems for light-water nuclear power reactors. Nuclear Regulatory Commission. <http://www.nrc.gov/reading-rm/doc-collections/cfr/part050/part050-0046.html> Accessed 23/2/13.

NSERC, 2011. Canada's national program on Generation IV energy technologies – Research and development priorities for 2012-16. National Sciences and Engineering Research Council of Canada. [http://www.nserc-crsng.gc.ca/professors-professeurs/rpp-pp/GENIV0809Priorities-GENIV0809Priorites\\_eng.asp](http://www.nserc-crsng.gc.ca/professors-professeurs/rpp-pp/GENIV0809Priorities-GENIV0809Priorites_eng.asp) Accessed 16/4/13.

Nuclear Decommissioning Authority, 2010. Geological disposal: generic post-closure safety assessment. NDA/RWMD/030.

Nuclear Engineering International, 2004. Fuel design data. Sep 2004, pp. 26-35.

NUREG/CR-4375, 1985. Theory, design, and operation of liquid metal fast breeder reactors, including operational health physics. Idaho National Engineering Laboratory, Idaho Falls.

Nuttin, A., Guillemain, P., Bidaud, A., Capellan, N., Chambon, R., David, S., Meplan, O., Wilson, J., 2012. Comparative analysis of high conversion achievable in thorium-fuelled slightly modified CANDU and PWR reactors. *Annals of Nuclear Energy* 40 pp. 171-189.

OECD Nuclear Energy Agency, 1994. The economics of the nuclear fuel cycle. Organisation for Economic Cooperation and Development, Paris, France.

OECD Nuclear Energy Agency, 1999a. Present status of minor actinide data. Organisation for Economic Cooperation and Development, Paris, France.

OECD Nuclear Energy Agency, 1999b. 1<sup>st</sup> phase P&T systems study: status and assessment report on actinide and fission production partitioning and transmutation. Organisation for Economic Cooperation and Development, Paris, France.

OECD Nuclear Energy Agency, 2002. Accelerator-driven systems (ADS) and fast reactors (FR) in advanced nuclear fuel cycles: a comparative study. Organisation for Economic Cooperation and Development, Paris, France.

OECD Nuclear Energy Agency, 2003. Plutonium management in the medium term: a review by the OECD/NEA working party on the physics of plutonium fuels and innovative fuel cycles (WPPR). Organisation for Economic Cooperation and Development, Paris, France.

OECD Nuclear Energy Agency, 2006a. Very high burn-ups in light water reactors. Organisation for Economic Cooperation and Development, Paris, France.

OECD Nuclear Energy Agency, 2006b. Physics and safety of transmutation systems: A status report. Technical report. NEA-6090. Organisation for Economic Cooperation and Development, Paris, France.

OECD Nuclear Energy Agency, 2013. Minor actinide burning in thermal reactors: a report by the working party on scientific issues of reactor systems. Organisation for Economic Cooperation and Development, Paris, France.

Office of Nuclear Reactor Regulation, 1994. Issuance of amendments for the Palo Verde Nuclear Generating Station Unit No. 2 (TAC No. M89800), <http://pbadupws.nrc.gov/docs/ML0223/ML022350416.pdf> Accessed 3/12/12.

Office of Nuclear Reactor Regulation, 1996. Issuance of amendments for the Palo Verde Nuclear Generating Station Unit No. 1 (TAC No. M94541), Unit No. 2 (TAC No. M94542) and Unit No. 3 (TAC No. M94543), <http://pbadupws.nrc.gov/docs/ML0217/ML021710572.pdf> Accessed 3/12/12.

Office for Nuclear Regulation, 2011. The storage of liquid high level waste at Sellafield: Revised regulatory strategy. TRIM: 2011/295603.

Onoue, M., Kawanishi, T., Carlson, W. R., Morita, T., 2003. Application of MSHIM core control strategy for Westinghouse AP1000 nuclear power plant. In: Proc. GENES4/ANP2003, Kyoto, Japan, Sep 15-19, 2003.

Parks, G.T., 1996. Multiobjective pressurized water reactor reload core design by nondominated genetic algorithm search. Nuclear Science and Engineering 124 pp. 178-187.

Pope, M. A., Lee, J. I., Hejzlar, P., Driscoll, M. J., 2009. Thermal hydraulic challenges of gas cooled fast reactors with passive safety features. Nuclear Engineering and Design 239 pp. 840-854.

Porta, J., Puill, A., 1998. U-free Pu fuels for LWRs: the CEA/DRN strategy. In: Proc. OECD/NEA Workshop on Advanced Reactors with innovative fuels, Villigen, Switzerland, Oct 21-23, 1998.

Powney, D. J., Newton, T. D., 2004. Overview of the WIMS 9 Resonance Treatment. ANSWERS/WIMS/TR.26, Issue 1, SERCO, Winfrith, United Kingdom.

Pugh, O., 1978. Introduction to nuclear technology: Fuel element reprocessing. Fast reactor training centre, Dounreay Nuclear Power Development Establishment.

- Puill, A., Bergeron, J., 1997. Advanced plutonium fuel assembly: An advanced concept for using plutonium, in pressurized water reactors, *Nuclear Technology* 119 pp. 123-140.
- Rahman, F. A., Franceschini, F., Wenner, M., Lee, J. C., 2012. Thorium fuel options for sustained transuranic burning in Pressurized Water Reactors – 12381. In: *Proc. Waste Management*, Phoenix, Arizona, USA, Feb 26 - Mar 1, 2012.
- Raitses, G., Todosow, M., 2010. Thorium-based fuel cycle options for PWRs. In: *Proc. ICAPP 2010*, San Diego, California, USA, June 13-17, 2010.
- Rehme, K., 1987. Handbook of single-phase convective heat transfer. Chapter 7 – Convective heat transfer over rod bundles, edited by S. Kakac, R. K. Shah, W. Aung, John Wiley & Sons.
- Rempe, N. T., 2007. Permanent underground repositories for radioactive waste. *Progress in Nuclear Energy* 49 pp. 365-374.
- Rimpault, G., Plisson, D., Tommasi, J., Jacqmin, R., Rieunier, J., Verrier, D., Biron, D., 2002. The ERANOS code and data system for fast reactor neutronic analyses. In: *Proc. PHYSOR 2002*, Seoul, Korea, Oct 7-10, 2002.
- Rouault, J., Serpantie, J. P., Verwaerde, D., 2009. French R&D program on SFR and the ASTRID prototype. In: *Proc. IAEA Int. Conf. Fast Reactors and Related Fuel Cycles: Challenges and Opportunities (FR09)*, Kyoto, Japan, Dec 7-11, 2009.
- Rubbia, C., Buono, S., Gonzalez, E., Kadi, Y., Rubio, J. A., 1995. A realistic plutonium elimination scheme with fast energy amplifiers and thorium-plutonium fuel. *European Organisation for Nuclear Research Technical Report CERN/AT/95-53(ET)*.
- Salvatores, M., 2005. Nuclear fuel cycle strategies including partitioning and transmutation. *Nuclear Engineering and Design* 235 pp. 805-816.
- Schram, R. P. C., Klaassen, F. C., 2007. Plutonium management with thorium-based fuels and inert matrix fuels in thermal reactor systems. *Progress in Nuclear Energy* 39 pp. 617-622.
- Sease, J. D., Pratt, R. B., Lotte, A. L., 1966. Remote fabrication of thorium fuels. ORNL-TM-201. For presentation at the Second International Thorium Fuel Cycle Symposium, Getlinburg, Tennessee, USA, May 3-6, 1966.
- Shaposhnik, Y., Shwageraus, E., Elias, E., 2013. Core design options for high conversion BWRs operating in Th-<sup>233</sup>U fuel cycle. *Nuclear Engineering and Design* 263 pp. 193–205.
- Shaposhnik, Y., Margulis, M., Kotlyar, D., Shwageraus, E., Elias, E., 2014. Assessment of shutdown margin requirements for high conversion BWR with Th-U233 fuel. In: *Proc. ICAPP 2014*. Charlotte, North Carolina, USA, Apr 6-9, 2014.

- Shirvan, K., Andrews, N., Kazimi, M. S., 2013. Best estimate void fraction and critical power correlations for tight lattice BWR bundles. In: Proc. ICAPP 2013, Jeju Island, Korea, Apr 14-18, 2013.
- Shirvan, K., Kazimi, M. S., Cheng, L., Todosow, M., Hall, A., Jarrett, M., Ward, A. M., Downar, T. J., 2014. Stability and safety analysis of tight lattice breeding LWR. In: Proc. ICAPP 2014, Charlotte, North Carolina, USA, Apr 6-9, 2014.
- Shwageraus, E., 2003. Rethinking the light water reactor fuel cycle. Massachusetts Institute of Technology PhD thesis.
- Shwageraus, E., Hejzlar, P., Kazimi, M. S., 2004. Use of thorium for transmutation of plutonium and minor actinides in PWRs. Nuclear Technology 147 pp. 53-68.
- Sinha, R. K., Kakodkar, A., 2006. Design and development of the AHWR – the Indian thorium fuelled innovative nuclear reactor. Nuclear Engineering and Design 236 pp. 683-700.
- Sorensen, R. T., Davis, J. C., Lee, J. C., 2006. Thorium-based fuels for enhancing plutonium transmutation in light water reactors. Transactions of the American Nuclear Society 94 pp. 87-88.
- Takaki, N., Mardiansah, D., 2012. Core design and deployment strategy of heavy water cooled sustainable thorium reactor. Sustainability 4, 1933-1945.
- Takeda, R., Miwa, J., Moriya, K., 2007. BWRs for long-term energy supply and for fissioning almost all transuraniums. In: Proc. Global 2007, Boise, Idaho, USA, Sep 9-13, 2007.
- Thor Energy, 2010. Thorium-Plutonium LWR fuel – activity summary. Oslo, Sept 2010. <http://www.thorenergy.no/~media/ThorEnergy/PDF/Thor%20Energy%20Activities%20-%20Web%20-%20ny.ashx> Accessed 28/2/12.
- Tobita, Y., 2013. Safety strategy of JSFR establishing in-vessel retention of core disruptive accident. In: Proc. Int. Conf. Fast Reactors and Related Fuel Cycles (FR13) Paris, France, Mar 4-7, 2013.
- Todosow, M., Kazimi, M., et al., 2004. Optimization of heterogeneous utilization of thorium in PWRs to enhance proliferation resistance and reduce waste,” BNL-73152-2004 MIT-NFC-065, Brookhaven National Laboratory.
- Todosow, M., Galperin, A., Herring, S., Kazimi, M., Downar, T., Morozov, A., 2005. Use of thorium in light water reactors. Nuclear Technology 151 pp. 168-176.
- Todosow, M., Galperin, A., 2009. Heterogeneous assembly design for utilization of thorium in VVER reactors, In: Proc. Advances in Nuclear Fuel Management IV (ANFM 2009), Hilton Head Island, South Carolina, USA, Apr 12–15, 2009.

Tong, L. S., 1967. Prediction of departure from nucleate boiling for an axially non-uniform heat flux distribution. *Journal of Nuclear Energy* 21 pp. 241-248.

Tsige-Tamirat, H., 2011. Neutronics assessment of the use of thorium fuels in current pressurized water reactors. *Progress in Nuclear Energy* 53 pp. 717-721.

Uchikawa, S., Okubo, T., Kugo, T., Akie, H., Takeda, R., Nakano, Y., Ohnuki, A., Iwamura, T., 2007. Conceptual design of innovative water reactor for flexible fuel cycle (FLWR) and its recycle characteristics. *Journal of Nuclear Science and Technology* 44 pp. 277-284.

Uematsu, S., Kashiro, K., Tobita, N., 2002. Dismantling of gloveboxes for MOX fuel fabrication by a glovebox dismantling facility. In: *Proc. Waste Management Conference, Tucson, Arizona, USA, Feb 24-28, 2002.*

UK Office of Nuclear Regulation, 2008. *Safety Assessment Principles – 2006 edition (Revision 1, February 2008).* Paragraphs 449, 451 and 474; *Engineering Principle for Criticality Safety 2 (ECR.2).* <http://www.hse.gov.uk/nuclear/saps/saps2006.pdf> Accessed 15/10/13

Vanhoenacker, L., 2009. Tractebel engineering experience in steam generator replacement and power uprate projects. *Proc. Int. Symposium on Nuclear Energy (ISNE-09), Amman, Jordan, Oct 26-28, 2009.*

Varaine, F., Buiron, L., Boucher, L., Verrier, D., 2010. Overview on homogeneous and heterogeneous transmutation in a French new SFR: Reactor and fuel cycle impact. In: *Proc. 11<sup>th</sup> International Exchange Meeting on Partition and Transmutation (IEMPT 11), San Francisco, California, USA, Nov 1-4, 2010.*

Veteau, J. M., Digonnet, A., Derauz, R., 1994. Reflooding of tight lattice bundles. *Nuclear Technology* 107 pp. 63-71.

Wade, D. C., Wigeland, R. A., Hill, D. J., 1997. The safety of the IFR. *Progress in Nuclear Energy*, 31, pp. 63-82.

Waltar, A. E., Todd, D. R., Tsvetkov, P. V., 2012. *Fast spectrum reactors*, Springer, New York.

Watts Bar, 2009. *Watts Bar Unit 2 final safety analysis report (FSAR) Amendment 93, Section 4.* Accessed through <http://adams.nrc.gov/wba/>. Added 2009. Accession number ML091400651.

Watts Bar, 2010a. *Watts Bar Nuclear Plant, Unit 2 – Amendment 99 to final safety analysis report (FSAR), Section 4 – Reactor.* Accessed through <http://adams.nrc.gov/wba/>. Added 2010. Accession number ML101610356.

Watts Bar, 2010b. Watts Bar Nuclear Plant, Unit 2 – Amendment 99 to final safety analysis report (FSAR), Section 5 – Reactor coolant system, pages 5.1-1 through 6.8-8. Accessed through <http://adams.nrc.gov/wba/>. Added 2010. Accession number ML101610357.

Weaver, K. D., MacDonald, P. E., 2002. A qualitative assessment of thorium-based fuels in supercritical pressure water cooled reactors. In: Proc. PHYSOR 2002, Seoul, Korea, Oct 7-10, 2002.

Weaver, K. D., Herring, J. S., 2003. Performance of thorium-based mixed-oxide fuels for the consumption of plutonium in current and advanced reactors. Nuclear Technology 143 pp. 22-36.

Wenner, M. T., Franceschini, F., Kulesza, J., 2012. Preliminary comparative shielding analysis for refabricating different fuel vectors. In: Trans. 2012 American Nuclear Society Winter Meeting, San Diego, California, USA, Nov 11-15, 2012.

Westinghouse Electric Company LLC, 2009. AP1000 European design control document Rev. 1. Chapter 4 Section 3 – Nuclear design. EPS-GW-GL-700. Westinghouse Electric Company LLC, Cranberry Township, Pennsylvania.

Westinghouse Electric Company LLC, 2010a. AP1000 Pre-Construction Safety Report. Chapter 4 Section 3 – Nuclear Design. UKP-GW-GL-732, Westinghouse Electric Company LLC, Cranberry Township, Pennsylvania.

Westinghouse Electric Company LLC, 2010b. AP1000 Pre-Construction Safety Report. Chapter 15 Section 6 – Nuclear Design. UKP-GW-GL-732, Westinghouse Electric Company LLC, Cranberry Township, Pennsylvania.

WNA, 2011. World Nuclear Association. Supply of uranium. <http://www.world-nuclear.org/info/inf75.html> Accessed 28/2/12.

WNA, 2013. World Nuclear Association. Nuclear power in India. <http://www.world-nuclear.org/info/Country-Profiles/Countries-G-N/India/> Accessed 11/4/13.

Worrall, A., 2013. Utilization of used nuclear fuel in a potential future US fuel cycle scenario – 13499. In: Proc. Waste Management Conference, Phoenix, Arizona, USA, Feb 24-28, 2013.

Wu, D., Yu, H., Yu, J., Yu, J., 2012. Reflooding characteristics investigation and predicted models improvement for the pressurized water reactor with the tight lattice core design. Nuclear Engineering and Design 249 pp. 335-347.

Xu, Y., Downar, T. J., Takahashi, H., 2002. Comparison of Th-232 and U-238 fuel performance in a tight lattice high conversion BWR. In: Proc. PHYSOR 2002, Seoul, Korea, Oct 7-10, 2002.

Xu, Y., Downar, T. J., 2006. GenPMAXS. Code for generating the PARCS cross section interface file PMAXS. Purdue University, West Lafayette, Indiana.

Yang, J. H., Kang, K. W., Song, K. W., Lee, C. B., Jung, Y. H., 2004. Fabrication and thermal conductivity of (Th,U)O<sub>2</sub> pellets. Nuclear Technology 147 pp. 113-119.

Yucca Mountain Project, 2007. EBS radionuclide transport abstraction. Yucca Mountain Project. DOC.20071004.0001. ANL-WIS-PA-000001 REV 03. Accessed through <http://adams.nrc.gov/wba/>. Accession number ML090720290.

Yun, D., Kim, T. K., Taiwo, T. A., 2010. Th/<sup>233</sup>U multi-recycle in pressurised water reactors: feasibility study of multiple homogeneous/heterogeneous assembly designs. In: Proc. 11<sup>th</sup> International Exchange Meeting on Partition and Transmutation (IEMPT 11), San Francisco, California, USA, Nov 1-4, 2010.

Zainuddin, N. Z., Lindley, B. A., Parks, G. T., 2013. Towards optimal in-core fuel management of thorium-plutonium-fuelled PWR cores. In: Proc. ICONE21, Chengdu, China, July 29 - Aug 2, 2013.

Zakova, J., Wallenius, J., 2013. Multirecycling of Pu, Am and Cm in BWR. Annals of Nuclear Energy 58 pp. 255-267.

Zhang, J., 2009. A review of steel corrosion by liquid lead and lead-bismuth. Corrosion Science 51 pp. 1207-1227.

Zhang, Y., 2001. Fertile free fuels for plutonium and minor actinides burning in LWRs. Massachusetts Institute of Technology MSc thesis.

Zhongsheng, X., Boczar, P. G., 1999. Paper 15 – Advanced CANDU fuel cycle vision. China Journal of Nuclear Power Engineering 20 pp. 560-565.